1137

TRANSPORTATION RESEARCH RECORD

Soil Mechanics Considerations in Arid and Semiarid Areas

TRANSPORTATION RESEARCH BOARD
NATIONAL RESEARCH COUNCIL
WASHINGTON, D.C. 1987

Transportation Research Record 1137
Price: $13.00
Editor: Alison Tobias
Typesetter: Lucinda Keeler

modes
1 highway transportation
4 air transportation

subject areas
61 soil exploration and classification
62 soil foundations
63 soil and rock mechanics
64 soil science

Transportation Research Board publications are available by ordering directly from TRB. They may also be obtained on a regular basis through organizational or individual affiliation with TRB; affiliates or library subscribers are eligible for substantial discounts. For further information, write to the Transportation Research Board, National Research Council, 2101 Constitution Avenue, N.W., Washington, D.C. 20418.

Printed in the United States of America

Library of Congress Cataloging-in-Publication Data
National Research Council. Transportation Research Board.

Soil mechanics considerations in arid and semiarid areas.

(Transportation research record, ISSN 0361–1981 ; 1137)
1. Road construction--Arid regions. 2. Roads--Arid regions--Design. 3. Soil mechanics--Arid regions. I. National Research Council (U.S.). Transportation Research Board. II. Series.
TE7.H5 no. 1137 380.5 s 88-4909
[TE175] [625.7'32]
ISBN 0-309-04513-4

Sponsorship of Transportation Research Record 1137

GROUP 2—DESIGN AND CONSTRUCTION OF TRANSPORTATION FACILITIES

Geology and Properties of Earth Materials Section
Wilbur M. Haas, Michigan Technological University, chairman

Committee on Soil and Rock Properties
James J. Schnabel, Schnabel Engineering Associates, chairman
Robert C. Bachus, S. S. Bandyopadhyay, Robert K. Barrett, Roy H. Borden, Timothy Bowen, Carl D. Ealy, William H. Highter, Robert D. Holtz, Richard H. Howe, Robert B. Johnson, Ernest Jonas, C. William Lovell, Priscilla P. Nelson, Gerald P. Raymond, Surendra K. Saxena, J. Allan Tice, Mehmet T. Tumay, John L. Walkinshaw, Gary C. Whited

Committee on Environmental Factors Except Frost
Malcolm L. Steinberg, Texas State Department of Highways & Public Transportation, chairman
S. S. Bandyopadhyay, Warren T. Bennett, Michael L. Bunting, Fu Hua Chen, Barry J. Dempsey, Donald G. Fohs, Donald J. Janssen, Badru M. Kiggundu, Amos Komornik, C. William Lovell, Robert L. Lytton, Said Ossama Mazen, R. Gordon McKeen, James B. Nevels, Jr., Zvi Ofer, Thomas M. Petry, Rogel H. Prysock, Albert C. Ruckman, Larry A. Scofield, Joe P. Sheffield, Shiraz D. Tayabji, T. Paul Teng, John L. Walkinshaw, William G. Weber, Jr., Gdalyah Wiseman

Neil F. Hawks, Transportation Research Board staff

The organizational units, officers, and members are as of December 31, 1986.

Sponsorship is indicated by a footnote at the end of each paper. The organizational units, officers, and members are as of December 31, 1986.

Transportation Research Record 1137

The **Transportation Research Record** series consists of collections of papers on a given subject. Most of the papers in a Transportation Research Record were originally prepared for presentation at a TRB Annual Meeting. All papers (both Annual Meeting papers and those submitted solely for publication) have been reviewed and accepted for publication by TRB's peer review process according to procedures approved by a Report Review Committee consisting of members of the National Academy of Sciences, the National Academy of Engineering, and the Institute of Medicine.

The views expressed in these papers are those of the authors and do not necessarily reflect those of the sponsoring committee, the Transportation Research Board, the National Research Council, or the sponsors of TRB activities.

Transportation Research Records are issued irregularly; approximately 50 are released each year. Each is classified according to the modes and subject areas dealt with in the individual papers it contains. TRB publications are available on direct order from TRB, or they may be obtained on a regular basis through organizational or individual affiliation with TRB. Affiliates or library subscribers are eligible for substantial discounts. For further information, write to the Transportation Research Board, National Research Council, 2101 Constitution Avenue, N.W., Washington, D.C. 20418.

Contents

Foreword

Arid zones make up a significant part of the earth's surface. Highway engineers in these areas have distinct problems. The nine papers included in this Record are on soil problems in arid and semiarid areas.

Fredlund and Rahardjo present a summary of unsaturated soil principles, theories relevant to highway design in arid regions, and application of these theories to highway engineering. They discuss techniques that are commonly used to measure soil suction, which is central to applying unsaturated soil theories.

Wray reports on the findings of a study of an on-grade slab model constructed on expansive clay soil in the dry climate of Texas. He determined seasonal changes in moisture content, soil suction, and surface elevations. These data showed a definite edge lift distortion of the slab.

P. van der Raadt et al. conducted a study in western Canada on in situ measurement of soil suction. Independent measurements were made using a thermal conductivity sensor, thermocouple psychrometers, and two filter paper techniques. The results of the study indicated that the thermal conductivity matric suction sensors show good potential for the in situ measurement of soil suction.

In Texas, Reed evaluated the performance of three pavements on expansive clay subgrade. Treatments of the subgrade to reduce warping included removal and replacement with lime-stabilized soils and inert fills, maintaining positive drainage, preswelling the subgrade, and modifications of pavement shoulders and base.

Pavements founded on expansive soils are damaged because of the seasonal wetting and drying of the foundation soils. Picornell and Lytton characterize the wettest and driest moisture content profiles that have the desired probability of occurrence during the lifetime of the pavement. They calculated the daily water balance using a consecutive series of annual events.

Uzan et al. describe the development and application of a method for estimating the response of a swelling soil profile to the percolation of surface water. The method is based on a model for the flow regime and a model for the swelling process under constrained conditions.

Greenstein reports on a method for nondestructive determination of elastic parameters of the existing subgrade and pavement, and its application in the rehabilitation program of airport runways. The existing pavement materials did not meet the standard specifications for plasticity, gradation, and CBR.

Roughness development and longitudinal cracking of pavements on expansive soils are due to seasonal wetting and drying. Picornell and Lytton report on the parameters of importance in the design of vertical moisture barriers used to isolate the subsoil from climatic changes.

Ismael reports on the relation of the vertical subgrade coefficient K to the standard penetration test values for desert sands based on analysis of field footing tests conducted in Kuwait. A comparison of the test results with other plate load tests on granular soils is included.

Soil Mechanics Principles for Highway Engineering in Arid Regions

D. G. FREDLUND AND H. RAHARDJO

Highway construction is commonly required in arid regions. Soils in these regions are generally unsaturated and are characterized by highly negative pore-water pressures. An extension of saturated soil mechanics principles is required to fully understand their behavior and to perform the necessary analyses for engineering purposes. In recent years there has been a rapid increase in understanding of the behavior of unsaturated soils. Conventional equations for shear strength, volume change, and seepage have been extended to embrace unsaturated soils. Presented in this paper is a summary of unsaturated soil principles and theories particularly relevant to highway design in arid regions. The application of these theories to highway engineering is outlined. In addition, several techniques commonly used to measure soil suction or negative pore-water pressure are discussed. The measurement of soil suction is central to applying unsaturated soil theories.

Significant areas of the earth's surface are classified as arid zones. The annual evaporation from the ground surface in these regions exceeds the annual precipitation. Figure 1 shows the climatic classification of the extremely arid, arid, and semiarid areas of the world. Meigs *(1)* used the Thornthwaite moisture index to map these zones. He excluded the cold deserts. Regions with a Thornthwaite index between –20 and –40 are classified as semiarid areas. A Thornthwaite index less than –40 indicate arid areas. About 33 percent of the earth's surface is considered arid and semiarid *(2)*. The distribution of extremely arid, arid, and semiarid areas in North America is given in Figure 2 *(1)*. These cover much of the area bounded by the Gulf of Mexico in the south to Canada in the north, and over to the west coast.

Arid and semiarid areas usually have a deep groundwater table. Soils located above the water table have negative pore-water pressures. The soils are generally unsaturated because of excessive evaporation and evapotranspiration. Climate changes highly influence the water content of the soil in the proximity of the ground surface. When the soil is wetted, the pore-water pressures increase, tending towards positive values. As a result, changes occur in the volume and shear strength of the soil. Many soils exhibit extreme swelling or expansion when wetted. Other soils show a significant loss of shear strength upon wetting. Changes in the negative pore-water pressures associated with heavy rainfalls are the cause of numerous slope failures. Reductions in the bearing capacity and resilient modulus of soils are also associated with increases in the negative pore-water pressure. These phenomena indicate the important role of negative pore-water pressures in controlling the mechanical behavior of unsaturated soils.

When the degree of saturation of a soil is greater than approximately 85 percent, saturated soil mechanics principles can be applied with reasonable success provided the negative pore-water pressures can be measured. However, when the degree of saturation is less than about 85 percent, it becomes necessary to extend saturated soil mechanics principles to embrace unsaturated soils. Soils used in the construction of highways fall into this latter category, particularly in arid areas. Therefore, it is important that unsaturated soil mechanics be incorporated into engineering associated with highway design.

STRESS STATE VARIABLES

The shear strength and volume change behavior of an unsaturated soil can best be described in terms of two independent stress state variables, namely $(\sigma - u_a)$ and $(u_a - u_w)$ *(3)*. The terms $(\sigma - u_a)$ and $(u_a - u_w)$ are referred to as net normal stress and matric suction, respectively,

where

σ = total normal stress,
u_a = pore-air pressure, and
u_w = pore-water pressure.

A complete description of the stress state can be represented by two independent stress tensors.

$$\begin{bmatrix} (\sigma_x - u_a) & \tau_{xy} & \tau_{xz} \\ \tau_{yx} & (\sigma_y - u_a) & \tau_{yz} \\ \tau_{zx} & \tau_{zy} & (\sigma_z - u_a) \end{bmatrix} \quad (1)$$

and

$$\begin{bmatrix} (u_a - u_w) & 0 & 0 \\ 0 & (u_a - u_w) & 0 \\ 0 & 0 & (u_a - u_w) \end{bmatrix} \quad (2)$$

where σ_x, σ_y, σ_z equal total normal stress in the x-, y-, and z-directions, respectively; and τ_{xy}, τ_{yx}, τ_{xz}, τ_{zx}, τ_{zy}, τ_{yz} equal shear stresses.

Department of Civil Engineering, University of Saskatchewan, Saskatoon, Saskatchewan S7N 0W0, Canada.

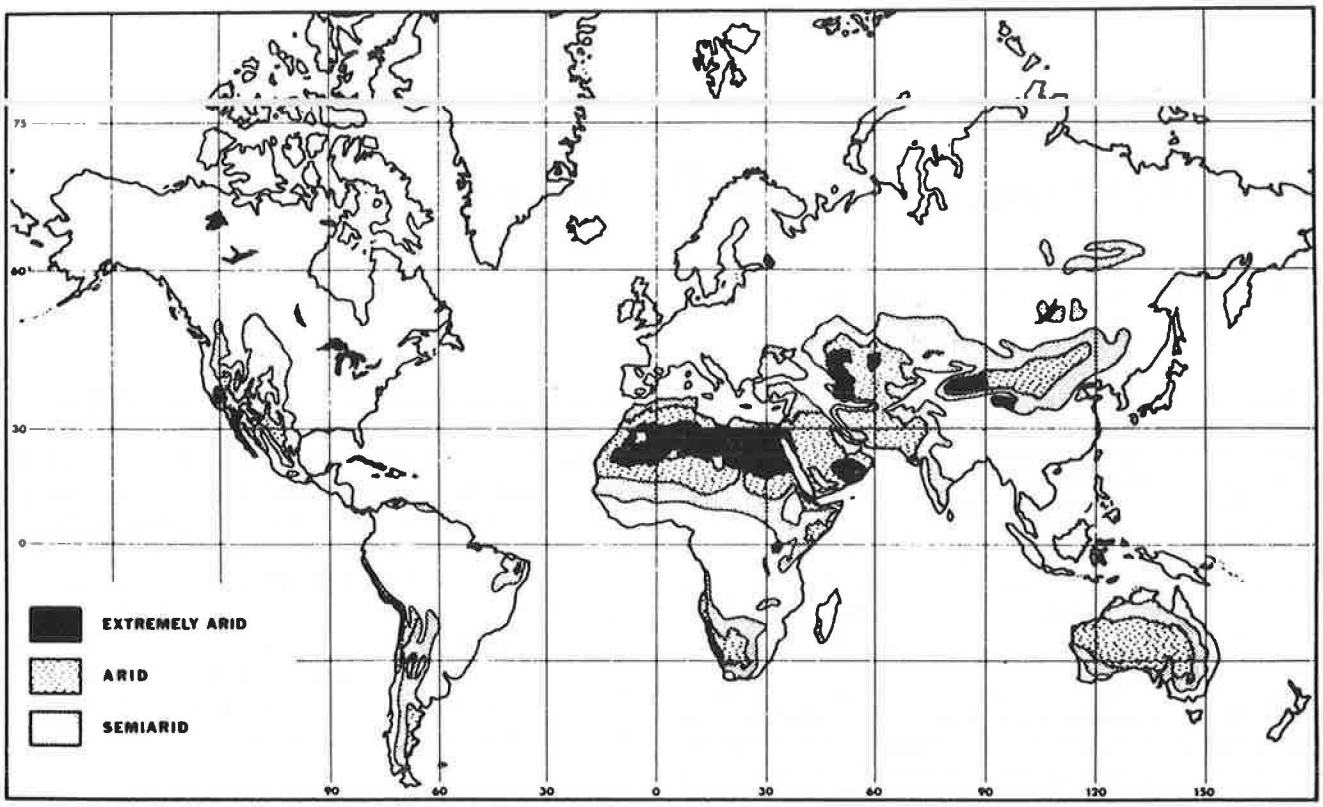

FIGURE 1 Extremely arid, arid, and semiarid areas of the world *(1, 2)*.

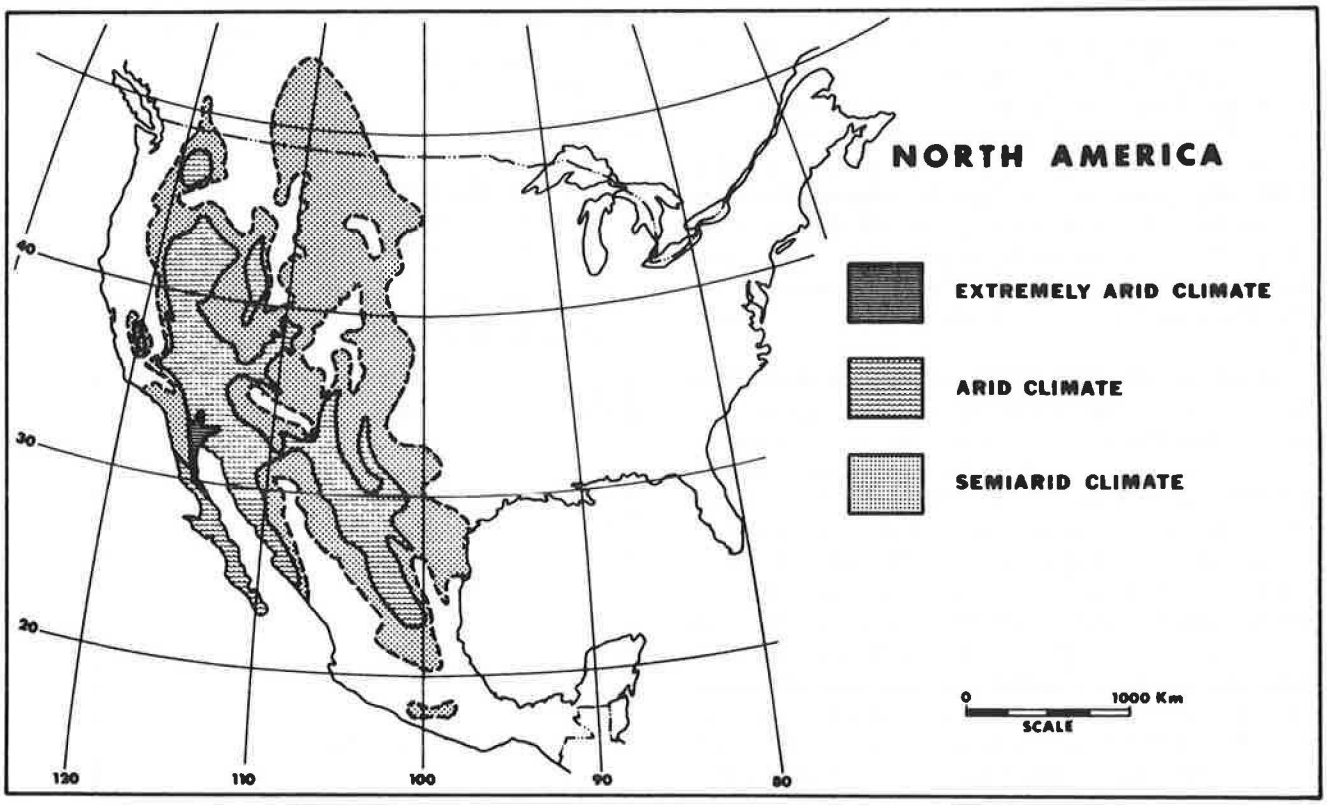

FIGURE 2 Extremely arid, arid, and semiarid areas of North America *(1)*.

The stress state variables can be shown to have smooth transition when going from an unsaturated soil condition to a saturated soil condition. As the degree of saturation approaches 100 percent, the pore-water pressure approaches the pore-air pressure. The matric suction term goes to zero. The net normal stress reverts to $(\sigma - u_w)$. The term, $(\sigma - u_w)$, is commonly referred to as effective stress in saturated soil mechanics.

The matric suction of a soil is a function of its water content. The relationship is referred to as the soil-water characteristic curve. The water content in the soil is predominantly influenced by the climatic environment. Therefore, the average matric suction in a region can be roughly correlated to the Thornthwaite moisture index. Both values become a reflection of the environment. In extremely arid, arid, and semiarid regions, the relative humidity in the soil pores can drop to as low as 30 to 40 percent (Blight, unpublished). This range of aridity corresponds to soil matric suctions as high as 165 MPa. In this environment, the role of the matric suction generally becomes more important than the role of the net normal stress for many practical problems.

MEASUREMENT OF SOIL SUCTION

From a thermodynamic standpoint, the total suction of a soil consists of two components, namely matric suction and osmotic suction.

$$\psi = (u_a - u_w) + \pi \qquad (3)$$

where ψ equals total suction and π equals osmotic suction.

Several devices commonly used for measuring soil suction and their range of measurement are listed in Table 1. Tensiometers directly measure the negative pore-water pressures. They consist of a porous ceramic, high air entry cup connected to a pressure measuring device. The entire device is filled with deaired water. The water in the tensiometer comes to equilibrium with the pore water in the soil during a measurement. In the field, the pore-air pressure is usually atmospheric (i.e., u_a is equal to 0). In this case, the matric suction is numerically equal to the absolute negative pore-water pressure. Therefore, the tensiometer reading is equivalent to the matric suction.

Tensiometers are limited to measuring pore-water pressures greater than approximately –90 kPa and <0 kPa. Highly negative water pressures cause cavitation of the pore fluid in the measuring system. The Quickdraw tensiometer from Soilmoisture Corporation has proven to be a useful tensiometer to rapidly measure negative pore-water pressures. The water in the tensiometer is subjected to tension for only a short period of time. As a result, the tensiometer can repeatedly measure pore-water pressures approaching one atmosphere in tension when it is properly serviced. In the laboratory, an axis translation technique can be used to impose matric suctions higher than one atmosphere (i.e., 101 kPa). The pore-air pressure becomes greater than atmospheric conditions when using this technique. The tensiometer reading can be added to the pore-air pressure reading to give the matric suction value. The matric suction value must not exceed the air entry value of the ceramic cup.

The thermal conductivity sensor for measuring matric suction consists of a porous ceramic block containing temperature-sensing elements and a miniature heater. Heat is generated at one point in the porous block and the temperature rise at a second point is measured after a period of time. The temperature rise is inversely proportional to the water content in the porous block. The water content of the porous block can be correlated with matric suction using a pressure plate technique. An indirect measurement of the matric suction in a soil is obtained when the sensor is allowed to come to equilibrium with the pore water in a soil. The MCS 6000 sensor from Moisture Control Systems, Inc., is of the thermal conductivity type and has been used in the laboratory (Figure 3) and in the field (Figure 4). The sensors appear to be quite suitable for field

TABLE 1 DEVICES FOR MEASURING SUCTION

Name of device	Suction component measured	Range (kPa)	Comments
Tensiometers	Negative pore-water pressures or matric suction when pore-air pressure is atmospheric	0 to ~ 90	Difficulties with cavitation and air diffusion through ceramic cup
Thermal conductivity sensors	Matric	0 to ~ 400+	Indirect measurement on a porous ceramic sensor
Psychrometers	Total	100* to ~ 8,000	Constant temperature environment required
Filter paper	Total	(Entire range)	May measure matric suction when in contact with moist soil
Pore fluid squeezer	Osmotic	(No limit)	Used in conjunction with a psychrometer or electrical conductivity measurement

*Controlled temperature environment to ± 0.001°C

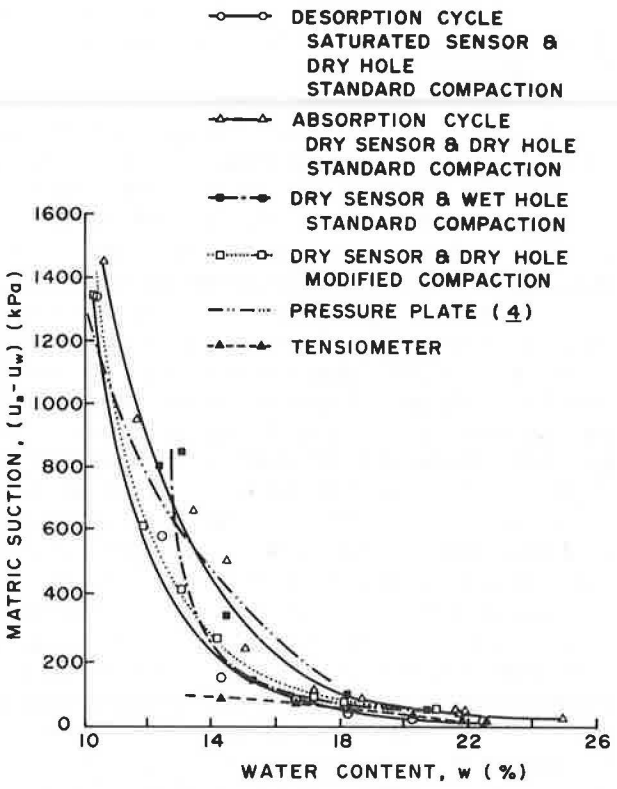

FIGURE 3 Laboratory measurements of matric suction on glacial till using thermal conductivity sensors (5).

use, being insensitive to temperature and salinity changes. Relatively accurate measurements of matric suctions below 300 kPa have been obtained *(4, 5)*. Poor contact between the porous block and the soil can cause the sensor to tend to measure total suction rather than matric suction *(6)*.

A psychrometer consists of a miniature chamber, covered with a fine screen or ceramic cup, containing a thermocouple. The psychrometer measures the relative humidity of the air. The relative humidity is inversely proportional to the total suction. Total suction can be computed when the air in the psychrometer is in equilibrium with the pore air of the soil. However, it is difficult to measure relative humidities approaching 100 percent. These humidities correspond to total suctions approaching zero. A controlled temperature environment of ±0.001°C is required to measure total suctions down to an accuracy of 10 kPa *(7)*. The lower limit of measurement for psychrometers is approximately 100 kPa under a controlled temperature environment. Psychrometers can be used for the in situ measurement of total suctions provided the magnitudes are greater than 300 kPa and the temperature fluctuations are small. Psychrometers are of most value for measuring high suctions in arid areas. Corrosion of the thermocouple wires may create a problem in measuring suction *(6)*.

The filter paper method can be used to estimate the total or matric suction of a soil *(8, 9)*. The filter paper is calibrated by establishing its water-characteristic curve. The water-characteristic curve relates the water content of the filter paper to its suction. When the water vapor in the filter paper is in equilibrium with the water vapor in a soil, the water content of the filter paper can be used to compute the total suction of the soil. On the other hand, the matric suction of the soil is measured when the filter paper is in contact and in equilibrium with the pore water in the soil *(9)*.

The osmotic suction of a soil can be determined from the electrical conductivity of the soil pore fluid. The pore fluid in the soil at a specific water content can be extracted using a pore-fluid squeezer or a pressure-plate apparatus.

CLASSIC PRINCIPLES AND EQUATIONS

Classic equations for describing the mechanical behavior of unsaturated soils can be presented as an extension of the equations commonly applied to saturated soils *(10)*. The extension

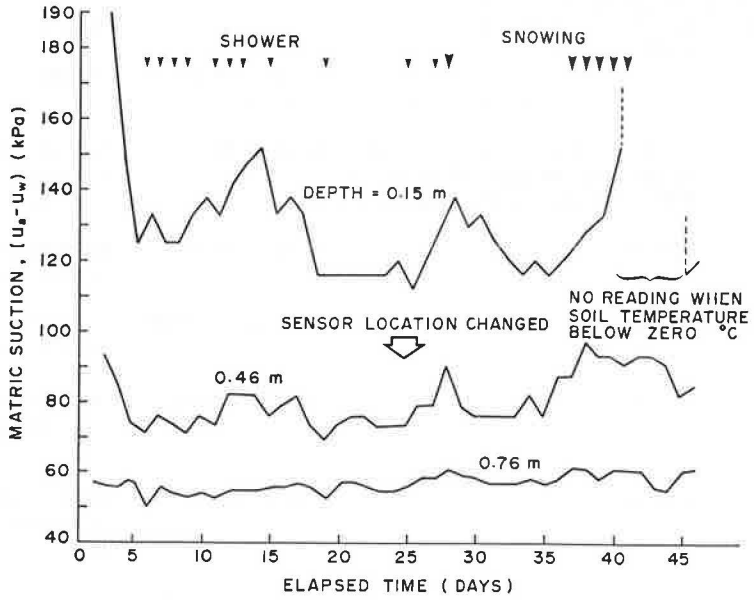

FIGURE 4 Field measurements of matric suction on glacial till using thermal conductivity sensors (from Lee, unpublished).

must be consistent with the number of stress state variables required for an unsaturated soil. Table 2 summarizes and compares some of the saturated and unsaturated soil mechanics equations. The variables used in these equations are described in the glossary. These equations are discussed in the next sections. When a soil approaches saturation, the unsaturated soil equations undergo a smooth transition to the saturated soil equations.

RESILIENT MODULUS

Fatigue prediction associated with pavement design requires the resilient modulus of the subgrade soil. The resilient modulus (i.e., analogous to an elastic modulus) can be obtained from a triaxial, repeated loading test on a soil specimen. Resilient modulus is computed as the ratio of the repeatedly applied deviator stress, $(\sigma_1 - \sigma_3)$, to the resilient (or elastic) strain in the major principal stress, σ_1, direction. The resilient modulus in a subgrade may vary in accordance with seasonal variations of matric suction in the subgrade soil. Pavement loading conditions also affect the subgrade resilient modulus. There have been numerous attempts to relate resilient modulus change to seasonal changes in the stress state *(11, 12)*. The stress state is related to the microclimatic environment.

The resilient modulus of an unsaturated soil can be a function of three stress variables, as shown in Equation 5 in Table 2. However, the net confining stress, $(\sigma_3 - u_a)$, is of relatively minor importance in comparison with the other two stress variables *(13)*. The influence of matric suction and deviator stress on the subgrade resilient modulus is illustrated in Figure 5. The resilient modulus increases as the matric suction increases or as the deviator stress decreases.

SHEAR STRENGTH

The Mohr-Coulomb failure criterion for a saturated soil is given by Equation 6. An extended form of the shear strength equation has been proposed for unsaturated soils [Equation 7 *(14)*]. The extended Mohr-Coulomb failure criterion can be represented as a three-dimensional surface, as shown in Figure 6. The failure surface is plotted using $(\sigma - u_a)$ and $(u_a - u_w)$ as abscissas. The intersection line between the failure surface and the front plane [i.e., τ versus $(\sigma - u_a)$ plane] represents the Mohr-Coulomb failure envelope for saturated conditions. On this plane the pore-air pressure is equal to the pore-water pressure or the matric suction is equal to 0. The failure envelope for a saturated soil has a slope and an intercept of ϕ' and c', respectively. The shear strength of the soil increases as the soil becomes unsaturated. The increase in the shear strength can be considered as an increase in the cohesion intercept because of an increase in matric suction (Equation 8). The increase in the cohesion intercept with respect to matric suction is defined by the intersection between the failure surface and the [τ versus $(u_a - u_w)$] plane. This line has a slope of ϕ^b, which can be

TABLE 2 SUMMARY OF CLASSIC SATURATED AND UNSATURATED SOIL MECHANICS PRINCIPLES AND EQUATIONS

Principle or equation	Saturated soil	Unsaturated soil
Stress state variables	$(\sigma - u_w)$	$(\sigma - u_a)$ and $(u_a - u_w)$
Resilient modulus	$E_r = f[(\sigma_3 - u_w), (\sigma_1 - \sigma_3)]$ (4)	$E_r = f[(\sigma_3 - u_a), (u_a - u_w), (\sigma_1 - \sigma_3)]$ (5)
Shear strength	$\tau = c' + (\sigma - u_w) \tan \phi'$ (6)	$\tau = c' + (u_a - u_w) \tan \phi^b + (\sigma - u_a) \tan \phi'$ (7)
		$c = c' + (u_a - u_w) \tan \phi^b$ (8)
Ultimate bearing capacity of clay	$q_{ult} = c N_c$ (9)	$q_{ult} = c N_c$ (10)
Constitutive equations for K_o loadings	Soil structure and water phase	Soil structure:
	$de = G_s\, dw = a_v\, d(\sigma_y - u_w)$ (11)	$de = a_t\, d(\sigma_y - u_a) + a_m\, d(u_a - u_w)$ (12)
		Water phase:
		$dw = b_t\, d(\sigma_y - u_a) + b_m\, d(u_a - u_w)$ (13)
Flow law for water (Darcy's law)	$v_w = - k_s\, \partial h_w / \partial y$ (14)	$v_w = - k_w (u_a - u_w)\, \partial h_w / \partial y$ (16)
	$h_w = y + u_w / \rho_w g$ (15)	$h_w = y + u_w / \rho_w g$ (17)
Steady state seepage	One-dimensional:	One-dimensional:
	$d^2 h_w / dy^2 = 0$ (18)	$k_w\, d^2 h_w / dy^2 + (dk_w / dy)\, dh_w / dy = 0$ (20)
	Two-dimensional:	Two-dimensional:
	$\partial^2 h_w / \partial x^2 + \partial^2 h_w / \partial y^2 = 0$ (19)	$k_w\, \partial^2 h_w / \partial x^2 + (\partial k_w / \partial x) \partial h_w / \partial x +$
		$k_w\, \partial^2 h_w / \partial y^2 + (\partial k_w / \partial y)\, \partial h_w / \partial y = 0$ (21)

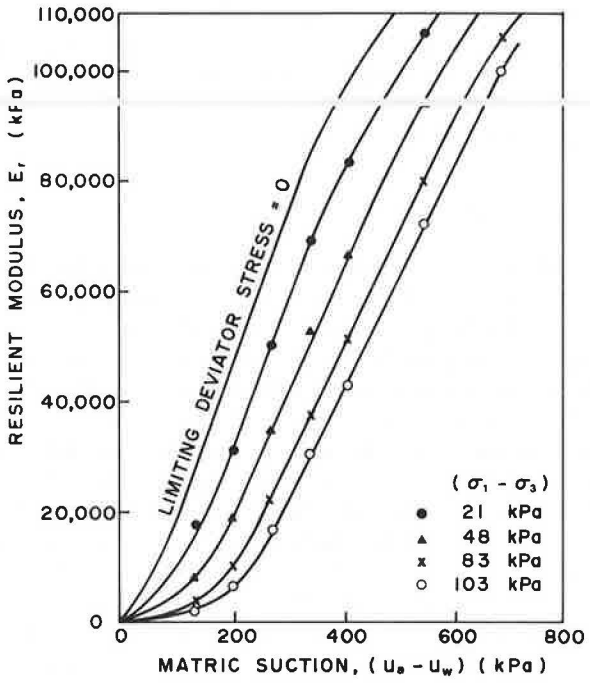

FIGURE 5 Influence of matric suction and deviator stress on the resilient modulus *(13)*.

measured experimentally (Figure 7). The value for ϕ^b is generally less than ϕ'.

Stability analyses for a saturated-unsaturated soil embankment can be performed using Equation 7 to define the shear strength of the soil. The factor of safety equations will be applicable to both the saturated and unsaturated zones. For the unsaturated zone, the cohesion is a function of matric suction (Equation 8). For the saturated zone, the matric suction goes to zero and the cohesion reduces to the effective cohesion intercept. Illustrated in Figure 8 is the effect of matric suction on increasing the stability of a simple slope. The increase in factor of safety due to soil suction has been demonstrated for unsaturated soil slopes in Hong Kong *(15)* and other regions *(16)*.

The ultimate bearing capacity of an unsaturated clay subgrade can be computed from Equation 10. The value of cohesion may be obtained from an unconfined compression test. The measured cohesion is a function of matric suction at failure (Equation 8). Excessive water infiltration into the subgrade soil can reduce the matric suction. This results in a reduction in shear strength that may, in turn, produce a subgrade failure. An understanding of unsaturated soil behavior is important in relation to the application of bearing capacity formulations in highway engineering.

VOLUME CHANGE

A change in the stress state of a soil produces a volume change. In a saturated soil, an effective stress increase results in settlement. In an unsaturated soil, a change in either the net normal stress or the matric suction can cause a volume change. However, heaves or settlements in unsaturated soils are most commonly caused by changes in matric suction. A net normal stress change of 10 to 1000 kPa commonly results from the construction of light-to-heavy structures. On the other hand, a desiccated soil in arid regions can undergo a change in matric suction ranging from 165 MPa to a practically zero suction. The matric suction changes are closely related to microclimatic changes.

Volume change in a saturated soil can be described using Equation 11. The equation relates void ratio and effective normal stress. In an unsaturated soil, two-volume change or constitutive relations are required. The constitutive equations for an unsaturated soil during K_o loading can be represented by Equations 12 and 13, respectively. Volume changes associated with the soil structure and the water phase are represented by changes in the void ratio and water content, respectively. These constitutive equations can be plotted as three-dimensional surfaces (Figure 9). Similar to saturated soils, volume changes in an unsaturated soil can be predicted from the void ratio constitutive surface. Water content change may be of interest for some problems. The water content constitutive surface helps

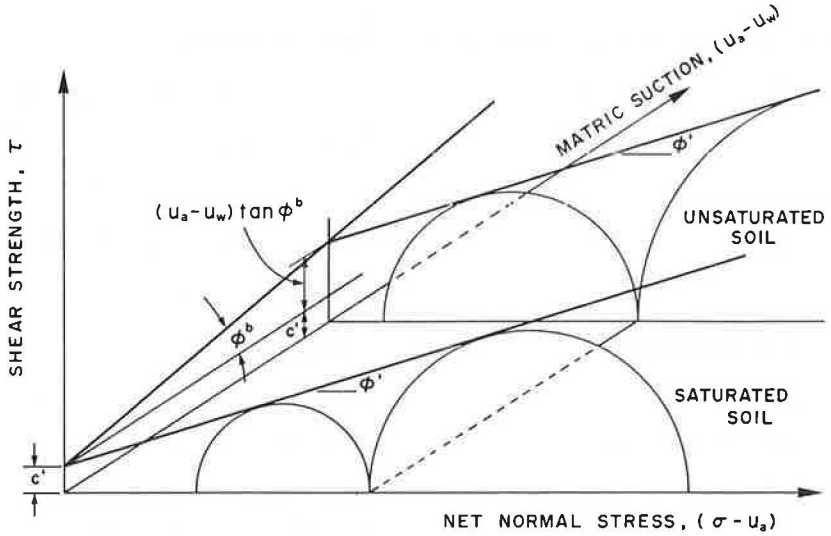

FIGURE 6 Three-dimensional failure surface for unsaturated soils.

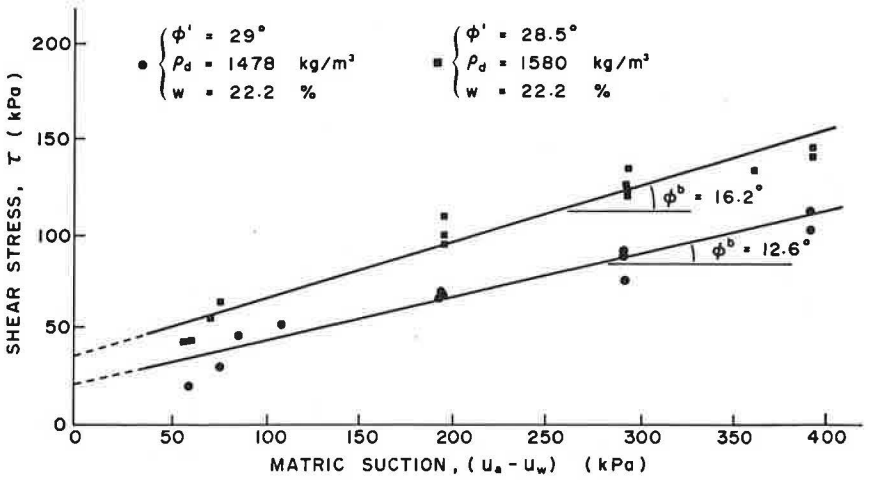

FIGURE 7 Experimental values of ϕ^b obtained from consolidated drained triaxial tests on Dhanauri clay (from Satija, unpublished).

understand the relationship among all the moduli for an unsaturated soil (i.e., a_t, a_m, b_t, and b_m).

Curve *A* in Figure 9 is essentially the one-dimensional consolidation curve for the soil in a saturated condition (Figure 10). The curve exhibits a linear relationship between void ratio and the logarithm of effective vertical stress, over a wide loading range. The coefficient of compressibility, a_t, is equal to a_v when the soil is saturated. The coefficient of water content change, b_t, can be computed as a_t multiplied by the specific gravity of the soil, G_s.

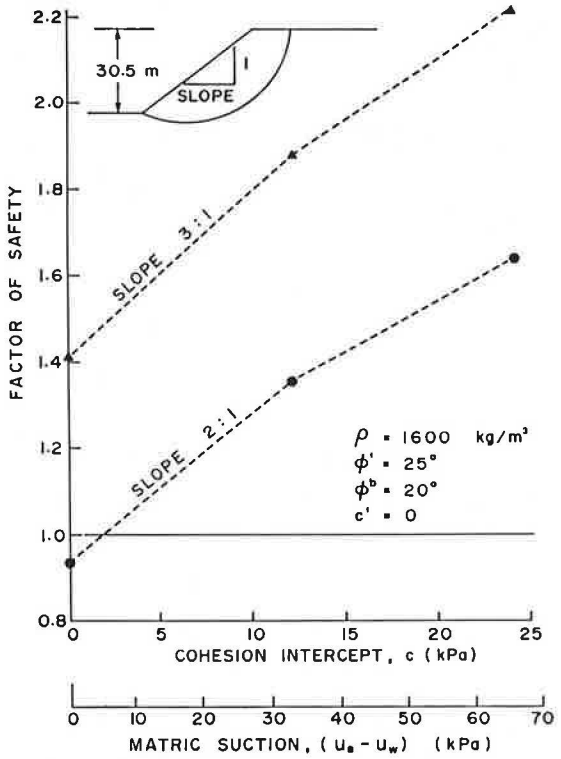

FIGURE 8 Increase in factor of safety due to an increase in matric suction *(18)*.

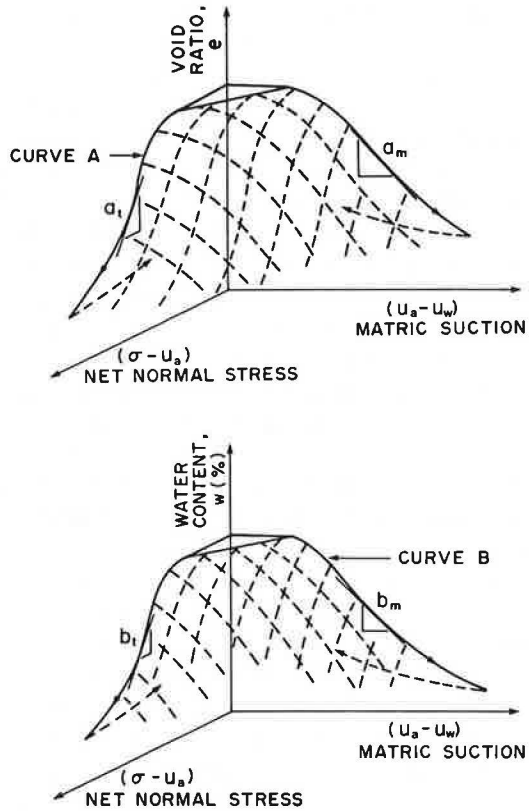

FIGURE 9 Three-dimensional void ratio and water content constitutive surfaces for an unsaturated soil.

Curve *B* in Figure 9 is a soil-water characteristic curve that can be obtained from a pressure plate test (Figure 11). The coefficient of water content change, b_m, can be computed from the soil-water characteristic curve. The shrinkage relationship for the soil relates the void ratio to the water content at various matric suctions (Figure 12). The slope of the shrinkage curve defines the ratio between the a_m and b_m coefficients of compressibility.

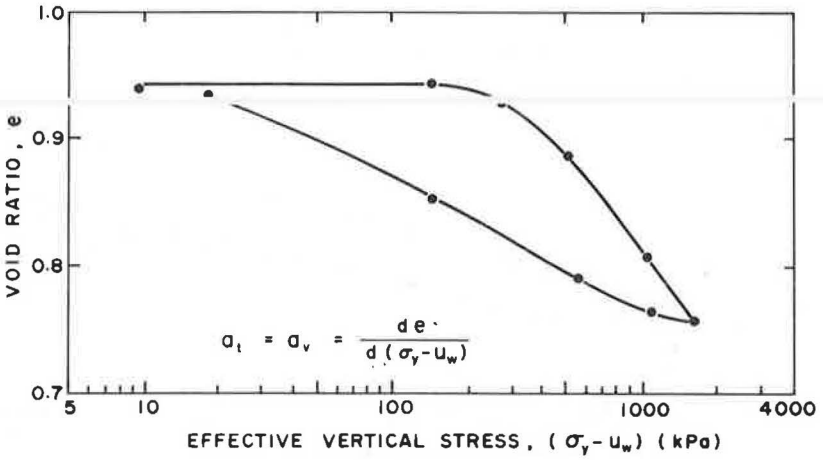

FIGURE 10 One-dimensional consolidation data for compacted Regina clay (from Gilchrist, unpublished).

The prediction of settlement or heave in a soil requires a knowledge of (a) the initial in situ state of stress, (b) the compression modulus or compressive index, C_c, or the swelling modulus or swelling index, C_s, and (c) the final state of stress. In a saturated soil, settlement is predicted using data from a one-dimensional consolidation test. The preconsolidation pressure and the compression index make up the essential data. The effective stress change between the initial and final conditions together with the compression index are used to predict the amount of settlement. The prediction of heave is an important application of the volume change theory in unsaturated soils. Heave is most commonly predicted based on a one-dimensional consolidation test. Either the constant volume or the free swell testing method can be used in order to obtain the swelling pressure and the swelling index of the soil. The stress state variable change between the initial and the final conditions together with the swelling index are used to predict the amount of heave.

Only the constant volume testing method will be discussed in this paper. In the constant volume consolidation test, the soil specimen is subjected to a token load and submerged in water. The specimen tends to swell because the negative pore-water pressure is released to atmospheric conditions. However, the specimen is maintained at a constant volume by increasing the applied load. The procedure is continued until the specimen exhibits no further tendency to swell. The applied load at this point is referred to as the uncorrected swelling pressure, P_s. Shown in Figure 13 is an average consolidation curve obtained from 34 constant volume consolidation tests performed on Regina clay. The deposit is proglacial lacustrine clay located in a semiarid region. The average uncorrected swelling pressure, P_s, for Regina clay was found to be 73.7 kPa.

The swelling pressure, P_s, must be corrected for sampling disturbance *(17)*. Sampling disturbance results in a reduction in the swelling pressure, P_s. A technique for correcting the swelling pressure is illustrated in Figure 13. This technique is a modified form of Casagrande's construction to estimate the preconsolidation pressure of a soil. The corrected swelling

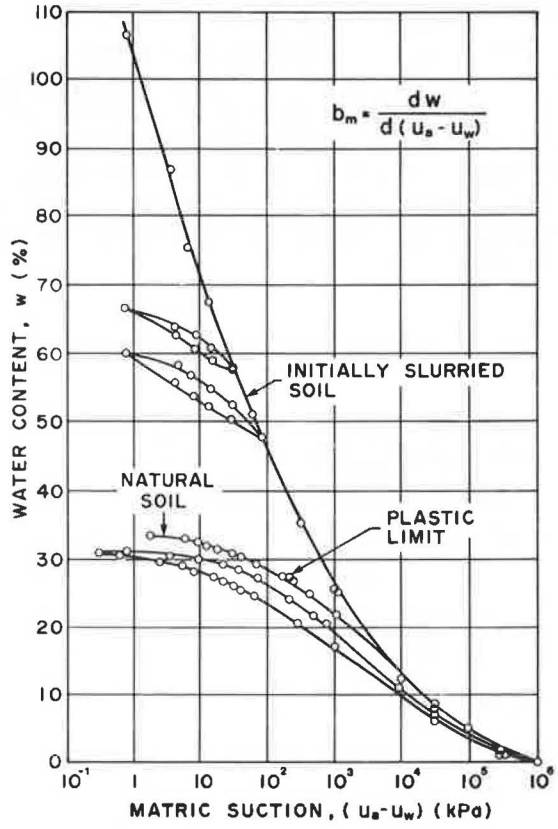

FIGURE 11 Soil-water characteristic curve for a heavy clay soil *(19)*.

pressure, P_s', for Regina clay is 134 kPa. The corrected swelling pressure represents the initial stress state of the soil. Swelling occurs from the corrected swelling pressure to the final stress state along the rebound curve (i.e., C_s). The final stress state can be estimated based on local experience. The swelling index for Regina clay is on the order of 0.065. Heave predictions using the corrected swelling pressure can be as much as

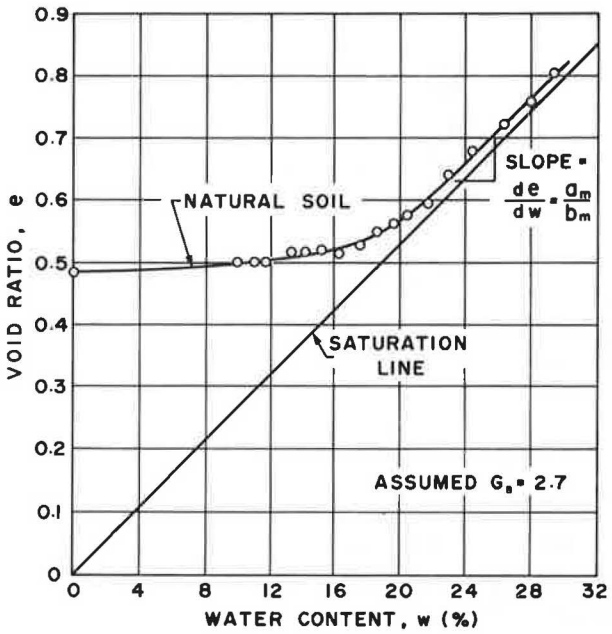

FIGURE 12 Shrinkage relationship for a heavy clay *(19)*.

two times the predictions using the uncorrected swelling pressure.

SEEPAGE AND MOISTURE MOVEMENT

Moisture movement in unsaturated soils results in numerous engineering problems. In an unsaturated soil, changes in microclimatic conditions cause the soil water to flow. Precipitation and evaporation generate moisture flows in and out of the soil. The rate of infiltration or evaporation can be used as a flux boundary condition in analyzing the flow of water in unsaturated soils. Temperature gradients also produce moisture and water vapor movements. However, thermally induced flows are not considered in this paper.

Water content and matric suction are directly affected by moisture movement. The pore-water pressure head (i.e., $u_w/\rho_w g$) distribution may vary from a static equilibrium condition to a steady state flow condition, as depicted in Figure 14. These variations also reflect variations of matric suction, as the pore-air pressure remains at atmospheric in the field. Changes in matric suction produce changes in the volume and shear strength of the soil.

Water flow in an unsaturated soil can be described using Darcy's law (Equation 16). The coefficient of permeability in an unsaturated soil is a function of the water content or matric suction of the soil. Hydraulic head gradients produce the driving potential for the flow of water in an unsaturated soil. The hydraulic head is the sum of the gravitational head (i.e., elevation) and the pore-water pressure head (Equation 17). In this case, the pore-water pressure head is negative. The use of the hydraulic head applies equally to both saturated and unsaturated soils. The water content should not be used as the driving potential for water flow.

The equations for the steady state seepage in one and two dimensions are presented as Equations 20 and 21, respectively. The equations describe the hydraulic head distribution in a soil during steady state water flow. The pore-water pressure head distribution (Figure 14) can be obtained by subtracting the elevation from the hydraulic head. The steady state equation for an unsaturated soil contains more terms than the equation for a saturated soil. The extra terms account for the variation in permeability with matric suctions at different locations in the soil.

PROSPECTS FOR THE FUTURE

A practical science for understanding the behavior of unsaturated soils is rapidly developing. The principles of unsaturated soil mechanics can be visualized as an extension of saturated soil mechanics. The understanding of unsaturated soil behavior

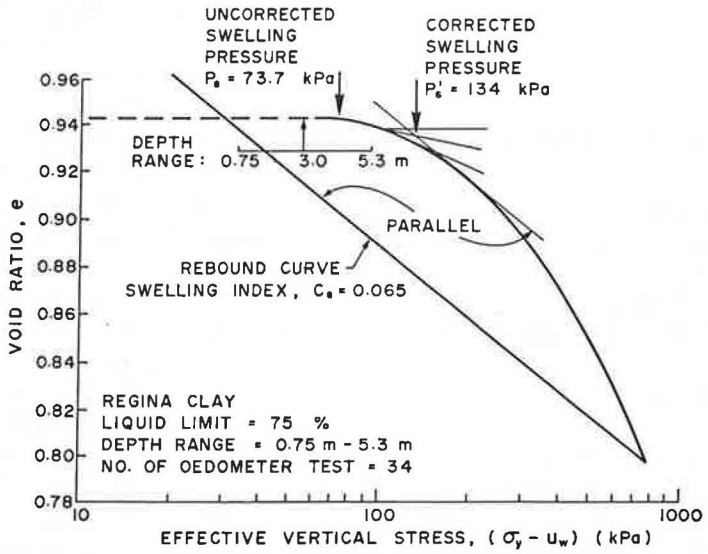

FIGURE 13 Average data from consolidation tests on Regina clay illustrating the swelling pressure correction *(20)*.

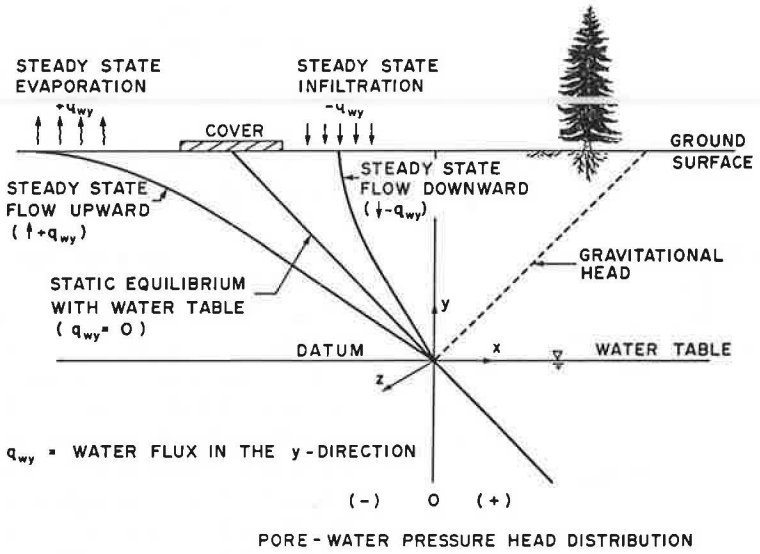

FIGURE 14 Pore-water pressure head distribution in the unsaturated zone during static equilibrium and steady state flow conditions.

is important to many problems relevant to highway engineering in arid and semiarid areas. Problems associated with volume change and shear strength can be analyzed and resolved with a consistent theoretical context. This eliminates the need for many empirical approximations that often depend on local practices.

Devices for measuring negative pore-water pressures or suctions have been developed and studies are required to ascertain their reliability and accuracy. Devices that measure total, matric, or osmotic suction are required. The measured quantities must be used in an appropriate manner in analyses.

Volume change and shear strength problems should be studied for changes that are taking place in the stress state variables. The end result will be the emergence of a technology that is more transferable from one region to another and from one climate to another.

GLOSSARY

Symbols and Variables Used in the Equations

E_r = Resilient modulus;
$(\sigma_3 - u_w)$ = Effective confining stress;
$(\sigma_1 - \sigma_3)$ = Deviator stress;
σ_1 = Major principal stress;
σ_3 = Minor principal stress (or total confining stress);
$(\sigma_3 - u_a)$ = Net confining stress;
τ = Shear stress;
c' = Effective cohesion intercept;
ϕ' = Effective angle of internal friction;
ϕ^b = Angle of shear strength increase with an increase in matric suction;
c = Cohesion intercept;
q_{ult} = Ultimate bearing capacity;
N_c = Bearing capacity factor for clay soils;
de = Change in void ratio;
e = Void ratio;
dw = Change in water content;
w = Water content;
a_v = Coefficient of compressibility;
$d(\sigma_y - u_w)$ = Change in effective vertical stress;
σ_y = Total vertical stress;
a_t = Coefficient of compressibility with respect to a change in $(\sigma_y - u_a)$;
$d(\sigma_y - u_a)$ = Change in net vertical normal stress;
a_m = Coefficient of compressibility with respect to a change in $(u_a - u_w)$;
$d(u_a - u_w)$ = Change in matric suction;
b_t = Coefficient of water content change with respect to a change in $(\sigma_y - u_a)$;
b_m = Coefficient of water content change with respect to a change in $(u_a - u_w)$;
v_w = Flow rate of water;
k_s = Water saturated coefficient of permeability;
$\partial h_w/\partial y$ = Hydraulic head gradient in the y-direction;
h_w = Hydraulic head;
y = Gravitational (or elevation) head;
$u_w/\rho_w g$ = Pore-water pressure head;
ρ_w = Water density;
g = Gravitational acceleration;
$k_w(u_a - u_w)$ = Unsaturated coefficient of permeability, which is a function of $(u_a - u_w)$;
$\partial k_w/\partial y$ = Change in water coefficient of permeability in the y-direction;
$\partial k_w/\partial x$ = Change in water coefficient of permeability in the x-direction;
$\partial h_w/\partial x$ = Hydraulic head gradient in the x-direction;
ρ = Total density of a soil;
ρ_d = Dry density of a soil; and
G_s = Specific gravity of a soil.

REFERENCES

1. P. Meigs. World Distribution of Arid and Semi-Arid Homoclimates. *UNESCO, Reviews of Research on Arid Zone Hydrology, Arid Zone Research,* Vol. I, New York, 1953, pp. 203–210.
2. H. E. Dregne. *Soils of Arid Regions.* American Elsevier Publishing Company, Inc., New York, 1976.
3. D. G. Fredlund and N. R. Morgenstern. Stress State Variables for Unsaturated Soils. *Journal of the Geotechnical Engineering Division, ASCE,* Vol. 103, 1977, pp. 447–466.
4. M. Picornell, R. L. Lytton, and M. Steinberg. Matrix Suction Instrumentation of a Vertical Moisture Barrier. In *Transportation Research Record 945,* TRB, National Research Council, Washington, D.C., 1983, pp. 16–21.
5. R. K. Lee and D. G. Fredlund. Measurement of Soil Suction Using the MCS6000 Gauge. *Proc., Fifth International Conference on Expansive Soils,* Adelaide, Australia, 1984, pp. 50–54.
6. B. G. Richards. Behavior of Unsaturated Soils. In *Soil Mechanics—New Horizons* (I. K. Lee, ed.), American Elsevier Publishing Company, Inc., New York, N.Y., 1974, pp. 112–157.
7. J. Krahn and D. G. Fredlund. On Total, Matric and Osmotic Suction. *Journal of Soil Science,* Vol. 114, No. 5, 1972, pp. 339–348.
8. I. S. McQueen and R. F. Miller. Calibration and Evaluation of a Wide-Range Gravimetric Method for Measuring Moisture Stress. *Soil Science,* Vol. 106, 1968, pp. 225–231.
9. S. Al-Khafaf and R. J. Hanks. Evaluation of the Filter Paper Method for Estimating Soil Water Potential. *Soil Science,* Vol. 117, 1974, pp. 194–199.
10. D. G. Fredlund. Soil Mechanics Principles That Embrace Unsaturated Soils. *Proc., 11th International Conference on Soil Mechanics and Foundation Engineering,* San Francisco, Calif., Vol. 1, 1985, pp. 465–472.
11. D. G. Fredlund, A. T. Bergan, and E. K. Sauer. Deformation Characterization of Subgrade Soils for Highways and Runaways in Northern Environments. *Canadian Geotechnical Journal,* Vol. 12, No. 2, 1975, pp. 213–223.
12. T. B. Edil and S. E. Motan. Soil-Water Potential and Resilient Behavior of Subgrade Soils. In *Transportation Research Record 705,* TRB, National Research Council, Washington, D.C., 1979, pp. 54–63.
13. D. G. Fredlund, A. T. Bergan, and P. K. Wong. Relation Between Resilient Modulus and Stress Conditions for Cohesive Subgrade Soils. In *Transportation Research Record 642,* TRB, National Research Council, Washington, D.C., 1977, pp. 73–81.
14. D. G. Fredlund, N. R. Morgenstern, and R. A. Widger. Shear Strength of Unsaturated Soils. *Canadian Geotechnical Journal,* Vol. 15, No. 3, 1978, pp. 313–321.
15. R. K. H. Ching, D. J. Sweeney, and D. G. Fredlund. Increase in Factor of Safety Due to Soil Suction for Two Hong Kong Slopes. *Proc., IV International Symposium on Landslides,* Toronto, Ontario, Canada, Vol. 1, 1984, pp. 617–623.
16. A. B. Fontoura, L. E. DeCompos, and L. M. Costa Filho. A Reanalysis of Some Slides in Gneissic Residual Soils. *Proc., IV International Symposium on Landslides,* Toronto, Ontario, Canada, Vol. 1, 1984, pp. 625–629.
17. D. G. Fredlund, J. U. Hasan and H. Filson. The Prediction of Total Heave. *Proc., Fourth International Conference on Expansive Soils,* Denver, Colo., American Society of Civil Engineers, Vol. 1, 1980, pp. 1–17.
18. D. G. Fredlund. Second Canadian Geotechnical Colloquium: Appropriate Concepts and Technology for Unsaturated Soils. *Canadian Geotechnical Journal,* Vol. 16, No. 1, 1979, pp. 121–139.
19. D. Croney and J. D. Coleman. Pore Pressure and Suction in Soil. *Proc., Conference on Pore Pressure and Suction in Soils,* Butterworths, London, 1961, pp. 31–37.
20. D. G. Fredlund. Prediction of Ground Movements in Swelling Clays. *Proc., 31st Annual Soil Mechanics and Foundation Engineering Conference,* Minneapolis, Minn., Feb. 1983.

Publication of this paper sponsored by Committee on Environmental Factors Except Frost.

The Effect of Climate on Expansive Soils Supporting On-Grade Structures in a Dry Climate

WARREN K. WRAY

An instrumented on-grade slab model was constructed on a site underlain by expansive clay soil located in a dry climate at Amarillo, Texas. The site was instrumented with moisture cells to measure changes in soil moisture content and thermocouple psychrometers to measure changes in soil suction as the seasons changed. The instrumentation was arranged so that changes in soil moisture and soil suction both vertically and horizontally could be measured, outside as well as beneath the covered surface. Surface elevation points were established at 3-ft centers over the entire site to measure changes in surface elevations and to relate the movements measured beneath the covered surface to those of the adjacent soil in response to the same climatological event. A series of deep bench marks at elevations of 2, 6.5, 9, and 14 ft was established to monitor the depths to which measurable soil shrink-swell occurred. All instrumentation and elevation measurements were recorded on a monthly basis. One complete year of measurements is reported. Surface and subsurface elevation changes and soil suction trends are presented, showing that the slab model at this dry climate site has developed into a well-defined edge lift distortion mode, heaving a maximum of more than 2 in. around the perimeter of the covered surface.

Almost all clay soils swell when they get wet or shrink when they dry. Those soils that do so to an excessive degree are termed expansive soils. Despite their expansive nature, that is, their tendency to change volume, these types of soil will seldom cause damage to on-grade structures supported on them if they are saturated. It is when they become only partly saturated that they become a problem for structures that are supported directly on the subgrade soil. From experience, the engineering community has found that expansive soils in geographical regions that are predominantly wet cause the most severe problems during extended periods of dryness or drought; conversely, expansive soils in regions that are predominantly dry usually cause more problems during periods of unusual wetness. For climate or environmental conditions that fall between these two extremes, it is known that expansive soils will swell following periods of wetness and will subsequently shrink when extended periods of dry weather follow the wet periods. This shrinking and swelling is cyclical in nature but usually not to the extremes described by the drought and excessively wet conditions previously noted. Thus, unlike other geotechnical engineering design problems, designing grade-supported structures to be constructed over expansive soils also requires a consideration of the climate, a nontraditional engineering design parameter.

Although swelling or shrinking of the soil beneath grade-supported structures could occur at almost any point—and often does—it has been observed that there are two predominant distortion modes *(1–6)*. The first of these is a concave upward shape, often described as dishing or edge lift because the soil is heaving around or near the edge of the grade-supported structure. The second distortion mode is a concave downward shape, often termed doming or center lift because the soil is swelling beneath the center of the grade-supported structure. This second distortion shape could also be caused by the soil around the edge drying out or shrinking, or could even be the result of a combination of both conditions, that is, shrinking around the edge and swelling in the center.

The shrinking or swelling of the soil in and by itself may not cause distress to the structure if the heave or shrink is uniform; in these instances, the structure is likely to ride up or down with the soil as it heaves or shrinks. The structure becomes distressed and suffers the most damage when it is subjected to differential shrinking or swelling such as that which occurs during the center lift or edge lift distortions previously described. Thus, a principal concern of the design professional (with the exception of exaggerated amounts of uniform shrink or swell) should be the differential movement to which the structure will be subjected as the soil on which it is supported moves in response to changes in climate.

In an effort to study the effect of climate on producing differential movements beneath an on-grade supported structure, two instrumented experimental sites were constructed. One site was located in College Station, Texas, and the second site was located in Amarillo, Texas. The College Station site was selected because of its relatively wet geographical location; Amarillo was chosen because of its principally dry climate. Each site was instrumented with thermocouple psychrometers to measure changes in soil temperature and changes in soil suction, and moisture cells to measure changes in soil moisture content. Changes in surface and near-surface elevations were also measured to determine the magnitude of shrink or swell that the slab model was experiencing and the depth to which this movement occurred. The purpose of this paper is to present some of the results obtained from the dry site at this intermediate point in the term of the project.

Department of Civil Engineering, Texas Tech University, P.O. Box 4089, Lubbock, Tex. 79409.

DESCRIPTION OF THE TEST SITE

Slab Model

The purpose of the field experiment was to measure the type and degree of distortion occurring beneath a covered surface as a result of differential swelling or shrinking of the soil under and adjacent to the covered surface. Thus, the slab needed to be flexible so that it would not impede or restrict differential soil movement. A conventional concrete slab would be too stiff to achieve this objective; consequently, a heavy plastic membrane was placed over the test site to represent the covered surface presented by a conventional concrete slab. Being impervious, the plastic would provide the same interruption in moisture flow into and out of the soil at the surface as would a concrete slab. To protect the membrane from wind and puncture, a 2-in. (50-mm) thick layer of clean sand was placed over it.

The dimensions of the slab were selected to be sufficiently long so that the distance over which the soil moisture change occurred could be captured and wide enough so that the instrumentation would be reasonably safe from being significantly influenced by moisture changes from the lateral direction. Based on published observations of this edge penetration or edge moisture variation distance *(1, 6–9)*, it was believed that a distance of 10 ft (3 m) would be a sufficient buffer for the lateral protection of the instrumentation. Thus, a width of 24 ft (7.3 m) and a length of 40 ft (12.2 m) were selected as the slab dimensions.

One subobjective of the project was to investigate the effect perimeter stiffening beams have on slabs-on-grade with respect to influencing the lateral loss or gain of soil moisture and the lateral distance over which this change occurs. To study this effect, an 18-in. (450-mm) deep grade beam was constructed around the east edge of the slab model. Thus, the 40-ft (12.2-m) length of the slab model would permit the 20 ft (6.1 m) making up the west end of the covered surface to respond to the climate-induced soil movements without being influenced by a perimeter grade beam while the eastern 20 ft would measure the grade beam effect.

Instrumentation

Two types of instrumentation were selected for use on the project: thermocouple psychrometers and soil moisture cells. However, the moisture cell results will not be presented in this paper. The psychrometers were individually calibrated using a wide range of NaCl solutions. The calibration procedure followed was that recommended by the manufacturer and used individual calibration chambers.

The instrumentation was placed beneath the covered surface in two identical parallel rows spaced 4 ft (1.2 m) apart with each row 10 ft (3.0 m) inward from the edge of the covered surface. The rows were aligned parallel to the longitudinal dimension of the slab model and were symmetrical about the transverse centerline. The plan view of the instrument locations is shown in Figure 1. Thermocouple psychrometers were placed in each location at depths of 1, 3, 5, 7, and 9 ft (0.3, 0.9, 1.5, 2.1, and 2.7 m) below the surface. All but the three centermost instrument locations in each row also had moisture cells installed at depths of 1, 3, and 5 ft below the surface. Figure 2 shows the vertical arrangement (termed a stack) of one row of the instrumentation.

Elevation Measurements

Upon completion of the surface cover installation, elevation points were established on a 3-ft (0.9-m) grid pattern to measure changes in surface elevation. The grid extended to a distance of 6 ft (1.8 m) outside the edge of the covered surface in order to monitor surface changes occurring in the uncovered soil adjacent to the slab model.

Five bench marks were established adjacent to the site. Each bench mark was set at a different depth: 2, 6.5, 9, 14, and 27.5 ft (0.6, 2.0, 2.7, 4.3, and 8.4 m). The groundwater table was determined to be well below 27.5 ft, at least 50 ft (15.2 m) and perhaps as much as 100 ft (30.5 m) deep according to local engineers and city officials. Thus, the deepest bench mark was believed to be sufficiently deep not to be affected by climate-

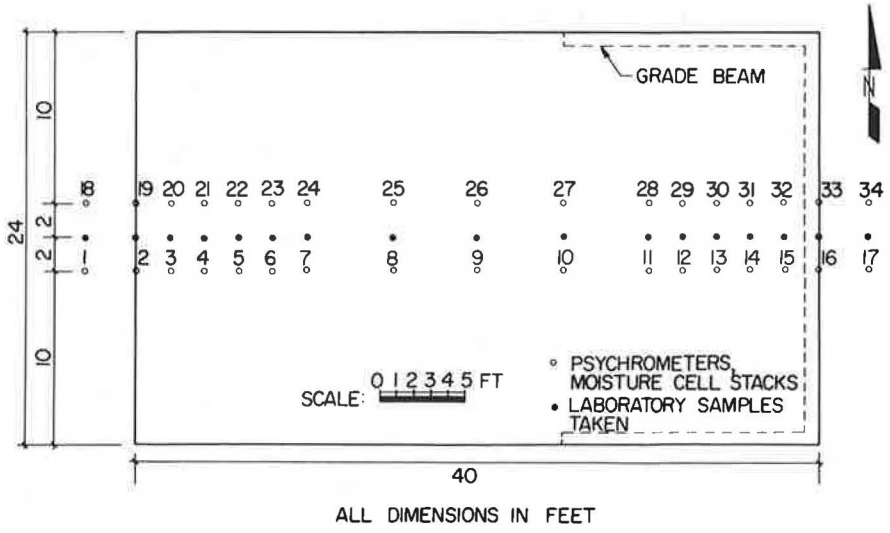

FIGURE 1 Plan view of slab model showing arrangement and location of the 17 twin instrument stacks (borings 1–34), location of borings taken for soil classification and laboratory testing, model dimensions, and location of perimeter grade beam.

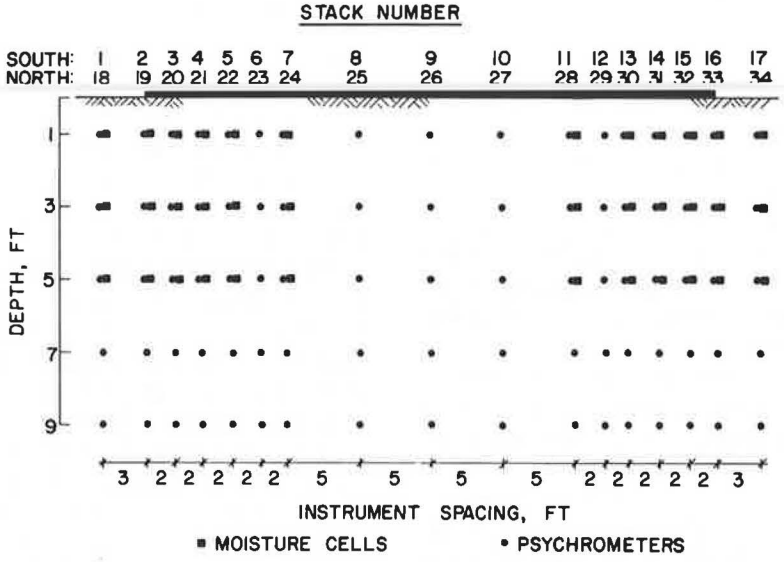

FIGURE 2 Elevation view of the arrangement and distribution of subsurface instrumentation along either of the lines of borings 1–17 or 18–34.

induced shrink/swell, but not so deep as to be influenced by a rising groundwater table. All elevation changes are referenced to the 27.5-ft deep bench mark.

Each bench mark was constructed of ¾-in. (20-mm) diameter steel pipe placed inside a 4-in. (100-mm) diameter polyvinyl chloride (PVC) liner pipe driven approximately 6 in. (150 mm) into the soil at the bottom of the boring. A slurry made up of bentonite and diesel oil, having a unit weight of approximately 100 lb/ft^3 (15.72 kN/m^3), was then poured into the annular space between the outside of the PVC pipe and the boring walls, completely filling the volume to the ground surface. Approximately 1 ft (0.3 m) of the slurry was also poured inside the PVC pipe. The purpose of the slurry was to prevent intrusion of water into the bottom of the boring as well as to prevent the bottom of the boring from drying out. Each PVC liner pipe extended above the ground surface and was capped to prevent direct intrusion of water, such as rain, for example.

PROPERTIES OF THE SITE SOIL

The site was located on the property of the Family Hospital Center in Amarillo. Four separate soil strata were identified at the site. The top 10 to 18 in. (250 to 450 mm) consisted of fill material that was partially topsoil and partially construction residue that had been graded over the site following completion of the hospital facility a number of years ago. This material consisted of a predominantly reddish brown silty clay. Underlying this top stratum was a dark gray silty clay that was approximately 2 ft (0.6 m) thick. Both of these upper strata were classified as CL in the Unified Soil Classification System and as A-6 in the AASHTO Soil Classification System. The third stratum was a light gray silty clay approximately 3 ft (0.9 m) thick that was underlain by another very similar light gray clay to at least 27.5 ft (8.4 m) that was slightly more sandy and slightly less plastic; both were classified as CH in the Unified system and A-7-5 in the AASHTO system. The mean Atterberg limit values as determined from multiple tests, and the ranges for the percentages passing the No. 200 sieve and the clay content as determined by the hydrometer test, are reported for each foot of depth in Figure 3.

Two in situ properties were determined from the soil recovered during sampling. The in situ moisture content was determined at each foot of depth for each of the 17 continuously sampled borings. The mean of the 17 moisture contents at each depth is shown in Figure 3. The moisture contents indicate that at the time of installation, the soil at the site was very dry near the surface but became progressively wetter to a depth of approximately 6 ft (1.8 m), whereupon the moisture content became a fairly constant value. With one exception, the in situ moisture content was found to be several percent below the plastic limit.

The second in situ property determined was soil suction. This was accomplished using the filter paper method suggested by McQueen and Miller *(10)*. The suction value was determined using S&S No. 589 White Ribbon filter paper and the McKeen calibration curve *(11)*. The means of the 17 soil suction values for each foot of sampling depth are also shown in Figure 3. X-ray diffraction analysis of each of the soil strata was also performed. This analysis indicated that the predominant clay mineral for each layer was smectite, with percentages ranging from 32 to 45 percent of the clay content.

Russam and Coleman *(8)* showed that there is a fundamental relationship between climate, as measured by the Thornthwaite Moisture Index (TMI), and soil suction. The TMI is a convenient measure to use because it is completely rational; that is, it requires only three pieces of data to calculate the index: total monthly precipitation, average monthly temperature, and north latitude of the location. Because of its convenience, the TMI was also selected to be used to measure climate in this investigation. Although Amarillo has an official National Oceanographic and Atmospheric Administration (NOAA) na-

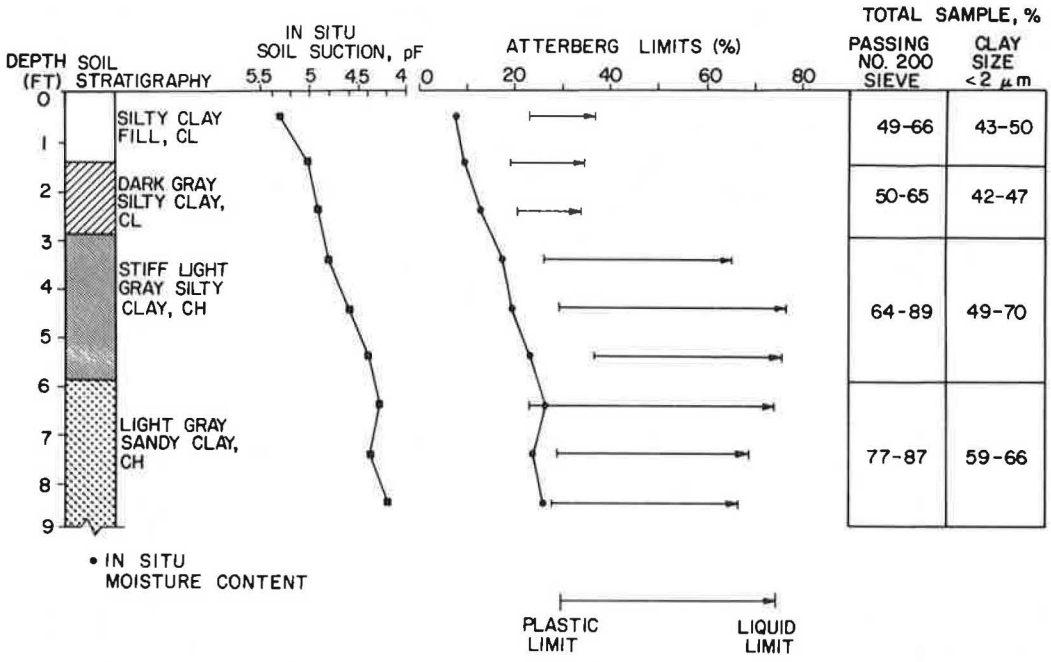

FIGURE 3 Site stratigraphy and in situ soil characteristics.

tional weather service measurement station, it is located at the Amarillo Airport, which is approximately 10 mi (16 km) from the experimental site. However, radio station KGNC in Amarillo, located approximately 1/4 mi (0.4 km) from the experimental site, maintains a small weather station for its newscasts. Its personnel kindly volunteered to record the temperature and precipitation for the project on a daily basis. Thus, the weather data used in calculating the TMI for the experimental site are considered to be site specific. KGNC began recording this data March 1, 1985. The precipitation that has fallen on the site is shown on a monthly basis in Figure 4. The precipitation amounts shown in Figure 4 before March 1985 were obtained from the NOAA weather station in Amarillo. The TMI for Amarillo was calculated using the NOAA records for the period 1941–1984. The mean TMI for this 44-yr period was found to be –21.9 in./yr (–56 cm/yr). The minus sign indicates that there is an annual water deficit (i.e., if there were an additional 21.9 in. of water available, the soil would give up that amount to the atmosphere each year through plant transpiration and evaporation). The annual TMIs ranged from the wettest value of +2.5 in./yr to the driest value of –41.8 in./yr (+6 cm/yr to –106 cm/yr). The TMI calculated for 1984, the year before the site installation, was –23.8 in./yr (–60 cm/yr) and for 1985 was –17.2 in./yr (–44 cm/yr), which suggests that

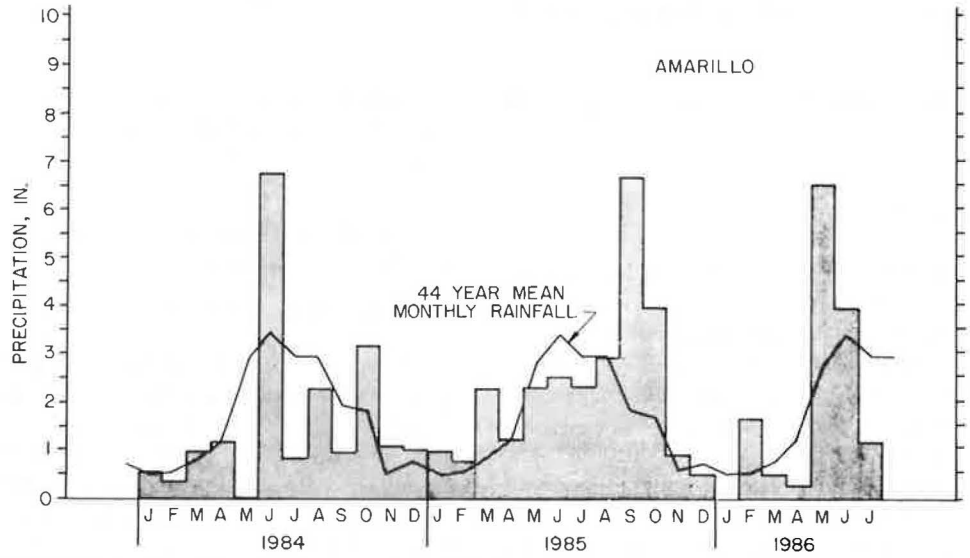

FIGURE 4 Monthly distribution of precipitation at the Amarillo site and the 44-yr monthly mean rainfall.

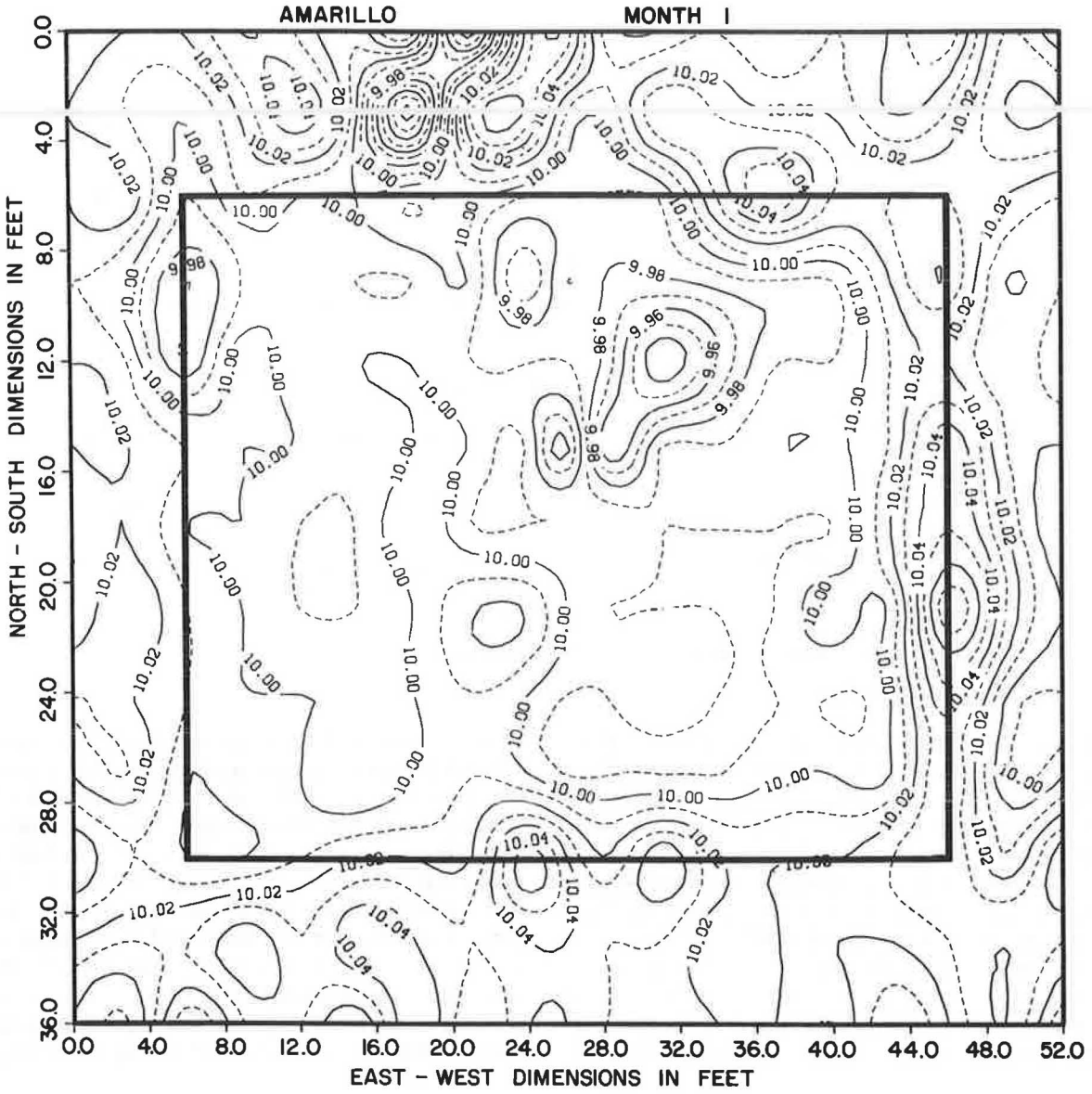

FIGURE 5 Contours of relative surface elevations at Amarillo showing changes in elevations with respect to the elevation at the time of site installation after 1 month.

1985, overall, was a wet year for Amarillo with respect to climate.

DATA MEASUREMENTS

All measurements were taken on a monthly basis. This frequency of measurement was selected with the intention of trying to capture soil suction and soil moisture content changes closer to the event that precipitated the change. Measurements taken during each monthly site visit included soil temperature, soil suction, soil moisture content, and surface and near-surface elevation measurements.

The elevation of each surface elevation point (a total of 247 points) was determined using conventional engineering surveying techniques with an engineer's level and a survey rod with 0.01-ft (3-mm) graduations. Also, the elevation of each deep bench mark, with respect to the 27.5-ft bench mark, was determined on each visit. Field data were converted into calibrated data in the laboratory during the days following each visit.

DISCUSSION OF MEASUREMENTS AND INDICATED TRENDS

Changes in Surface Elevations

The actual surface of the site slopes slightly (approximately 1 percent) from northwest to southeast. However, to make interpretation of the elevations more meaningful, each elevation point was normalized to an elevation of 10.00 ft. Thus, all elevations are actually relative elevations referenced to the elevation of the measurement point at the time of installation (July 1985). Figures 5–7 show elevation contours on a plan view of the instrumented site. The interior rectangle depicted by the heavy line represents the limits of the covered surface.

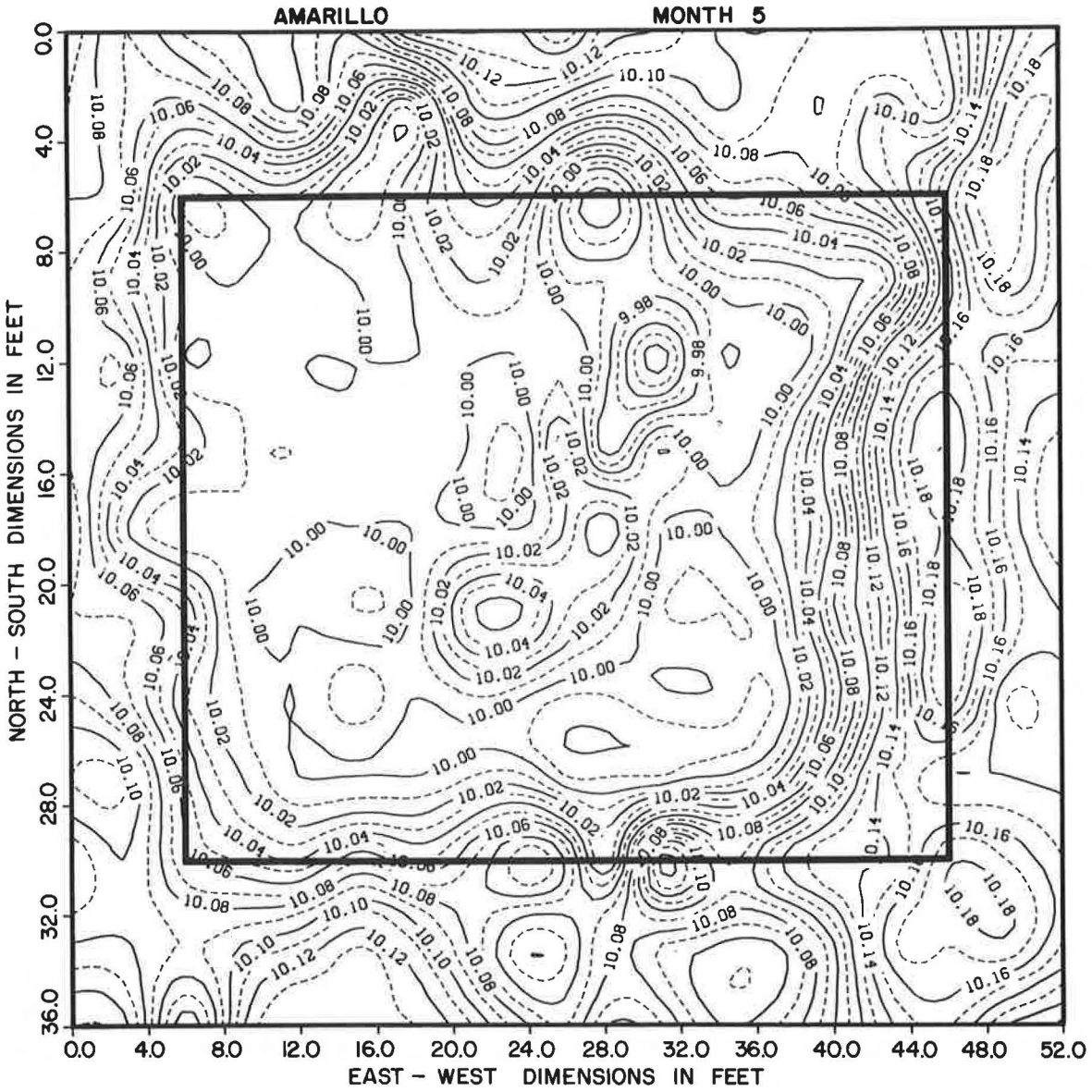

FIGURE 6 Contours of relative surface elevations at Amarillo showing changes in elevations with respect to the elevation at the time of site installation after 5 months.

Four days after installation, 1.53 in. (39 mm) of rainfall fell on the site and an additional 0.68 in. (17 mm) fell over the next 4 days. A total of 5.31 in. (135 mm) fell on the site during the 39 days between installation completion and the first measurement visit. That the dry soil had already begun to respond to this rainfall by the time of the first measurement visit is apparent in Figure 5. The months of September and October (Months 2 and 3, respectively) were very wet as indicated by comparing the rainfall for each of those months to the historic mean monthly rainfall. The site soil continued to respond to this period of wetness. Figure 6 shows the change in the elevation contours only 5 months after site installation (December 1985). This figure suggests that a definite edge lift (dishing) condition had begun to develop. However, beginning in November (Month 4), the heavy rainfall ceased and only nominal amounts of precipitation (either rainfall or snowmelt) occurred subsequently. Over the next 6 months, little change in the shape of the distortion occurred. Figure 7 shows the Month 12 (July 1986) elevation contours. Based on the historical mean monthly rainfall, it was expected that the edge heave so strongly shown in Figures 6 and 7 would begin to ameliorate in the late spring and early summer months. However, as can be seen from Figure 4, greater than average amounts of rain were received on the site during February, May, and June 1986 (Months 7, 10, and 11). Undoubtedly, this moisture has permitted the soil adjacent to the covered surface to retain sufficient moisture to avoid its expected reduction in elevation.

Inspection of Figures 5, 6, and 7 shows that the amount of heave that has occurred on the east end of the slab model—the grade beam end—is significantly greater than that which has occurred on the west end. A comparison of the edge heave magnitudes shows that the east end experienced a very rapid heaving, reaching a heave of 0.18 ft (2.2 in., 55 mm) by the

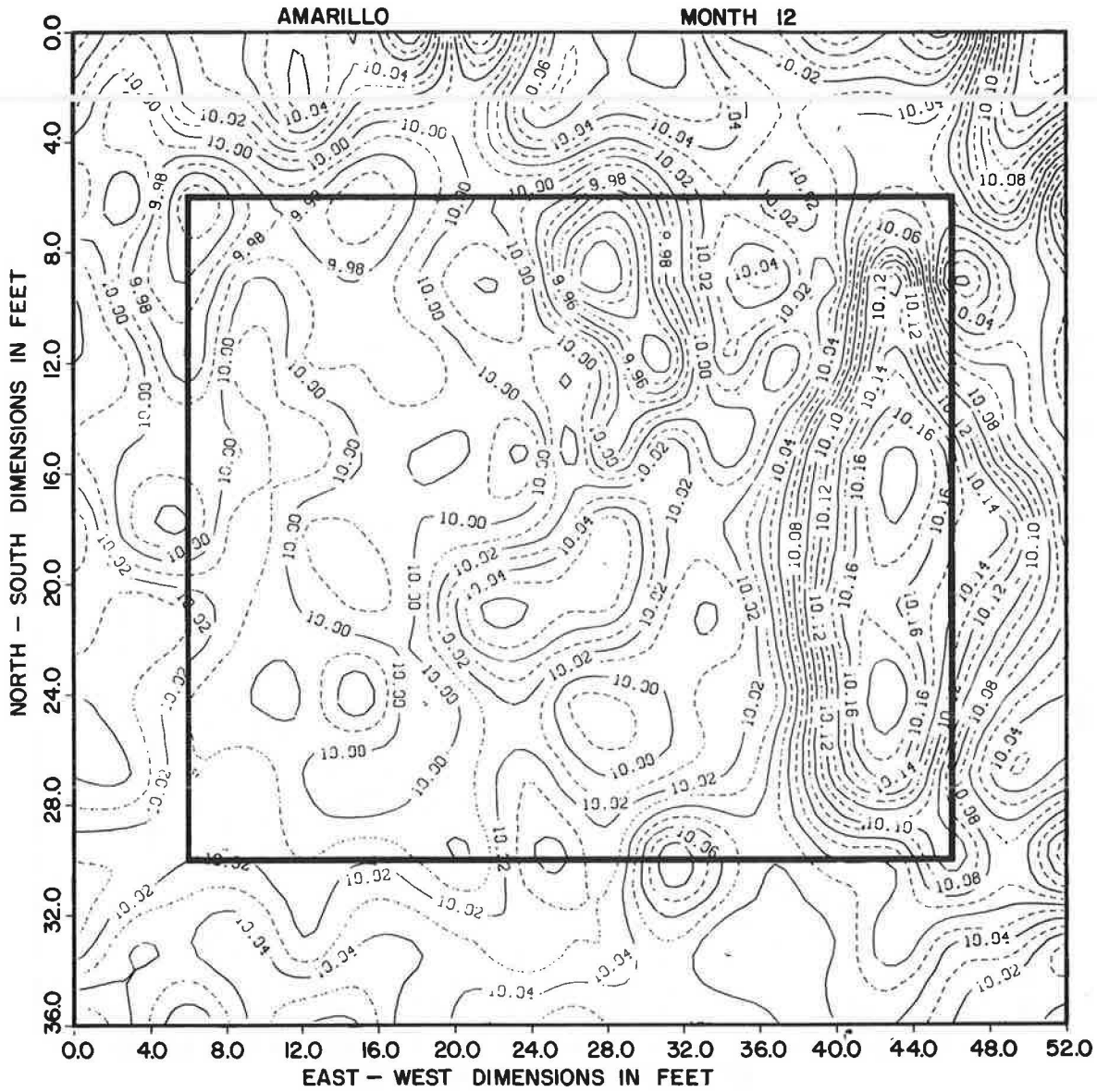

FIGURE 7 Contours of relative surface elevations at Amarillo showing changes in elevations with respect to the elevation at the time of site installation after 12 months.

time of the Month 3 measurement visit. The west end of the covered surface, however, experienced a heave of only 0.08 ft (1.0 in., 24 mm) during this same period. The heaving experienced on the east end was also projected back under the covered surface to some distance, suggesting that either the 18-in. (450-mm) deep grade beam has very little influence on the intrusion of water beneath the covered surface or that the depth of the intrusion extended much deeper than the 18 in. depth of the perimeter grade beam.

Figure 8 depicts the change in surface elevation on a month-by-month basis along the longitudinal centerline of the site. Points 7 and 20 are 6 ft and 3 ft (1.8 m, 0.9 m), respectively, outside the covered surface, whereas Point 33 is at the edge but on the covered surface. Points 241, 228, and 215 occupy similar positions, respectively, on the east end of the site. These figures show the rapid initial response of the uncovered soil, particularly at the east end, to the rainfall that occurred shortly after the installation of the site and the subsequent response to the period of wetness during Months 1, 2, and 3 (August–October 1985). These figures also show, with the exception of one point (Point 137), an inclination by the covered soil to remain fairly stable within the interior of the covered surface. The heave that showed immediately (Month 1) and then persisted at elevation point 137 cannot be satisfactorily explained, although, as can be seen in Figures 5, 6, and 7, it is localized. A careful inspection was made of the membrane in the vicinity of this point to see if a puncture could be contributing water to the soil beneath the cover in that location, but none was discovered.

There are two possible explanations for the substantial heave observed at the east end. One explanation is that despite the best efforts employed during construction to prevent it, surface water still managed to get between the wall of the footing excavation and the plastic membrane that formed the outside

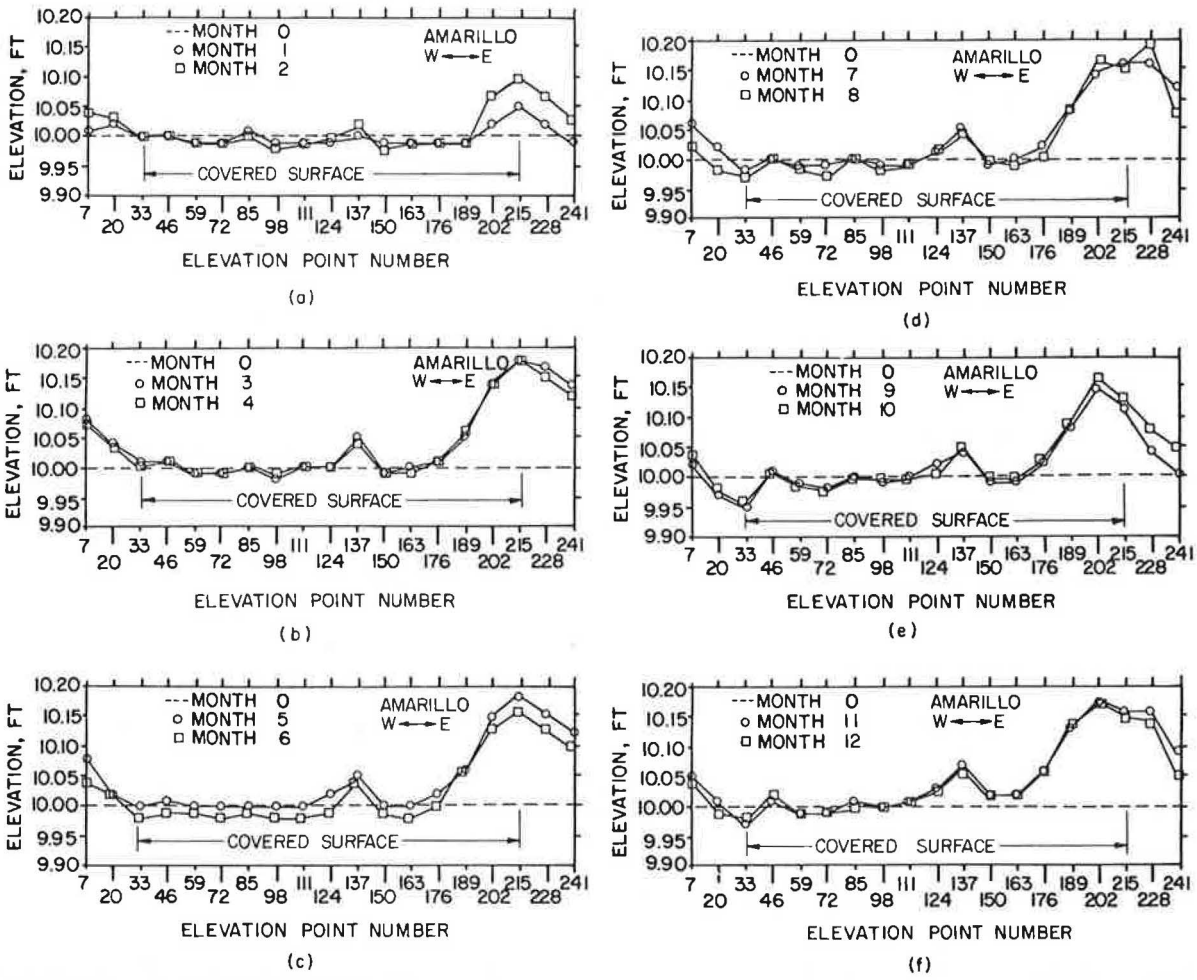

FIGURE 8 Monthly changes in relative surface elevations along the longitudinal centerline of the slab model for months 0–12.

wall of the grade beam and then under the grade beam. If so, then the entrapped water would have formed a reservoir and caused the observed heave. A second explanation is that one of the many surface fissures noted in the general area of the experimental site during installation, but not detected during the site layout despite a careful search, existed in the vicinity of this end of the covered surface and may have actually extended beneath the membrane. If so, this crack could have provided an access for surface runoff to penetrate below and beneath the covered surface and resulted in the observed heaving. A subsequent search for such a crack was made but none was found; however, due to the wet period of August–October 1985, most of the surface cracks noted in the area during the installation had either swelled shut or had contracted considerably. As of July 1986, many of these cracks had yet to open up to the widths and lengths observed in July 1985; thus, there is no certainty that such a crack near the east end of the covered surface does not actually exist.

A second observation that can be made about the month-by-month surface elevation changes concerns the distance measured inward from the edge of the covered surface over which change occurs. This observation can be accomplished by reviewing the month-by-month change in elevation of a specific point. Because of length limitations, only the points on the west end of the longitudinal centerline will be considered here. It can be seen from Figure 9 that the two points outside the covered area (Points 7 and 20) exhibit a fairly significant month-by-month change in elevation. Point 33, located at the edge of the covered surface, does not exhibit as dramatic a change in elevation as do the two uncovered points, but its trend follows that of the two outside points. The next innermost point, Point 46, is located 3 ft inside the edge of the covered surface. The month-by-month comparison of the elevation changes at this point shows little change, with the exception of a very slight heaving trend over the last few measurement months amounting to only 0.02 ft (6 mm). The next six elevation points (59, 72, 85, 98, 111, and 124), which extend 6, 9, 12, 15, 18, and 20 ft (1, 8, 3.6, 4.6, 5.5, and 6.1 m), respectively, from the west edge of the slab model, show only slight variations from the initial elevation. This might suggest that the edge penetration or edge moisture variation distance for this climate is between 3 and 6 ft (0.9 m, 1.8 m).

The trends are also fairly clear on the east half of the slab model. However, they are unquestionably influenced by the water that caused the rapid 0.19 ft (2.3 in., 58 mm) of total heave at the east edge of the covered surface.

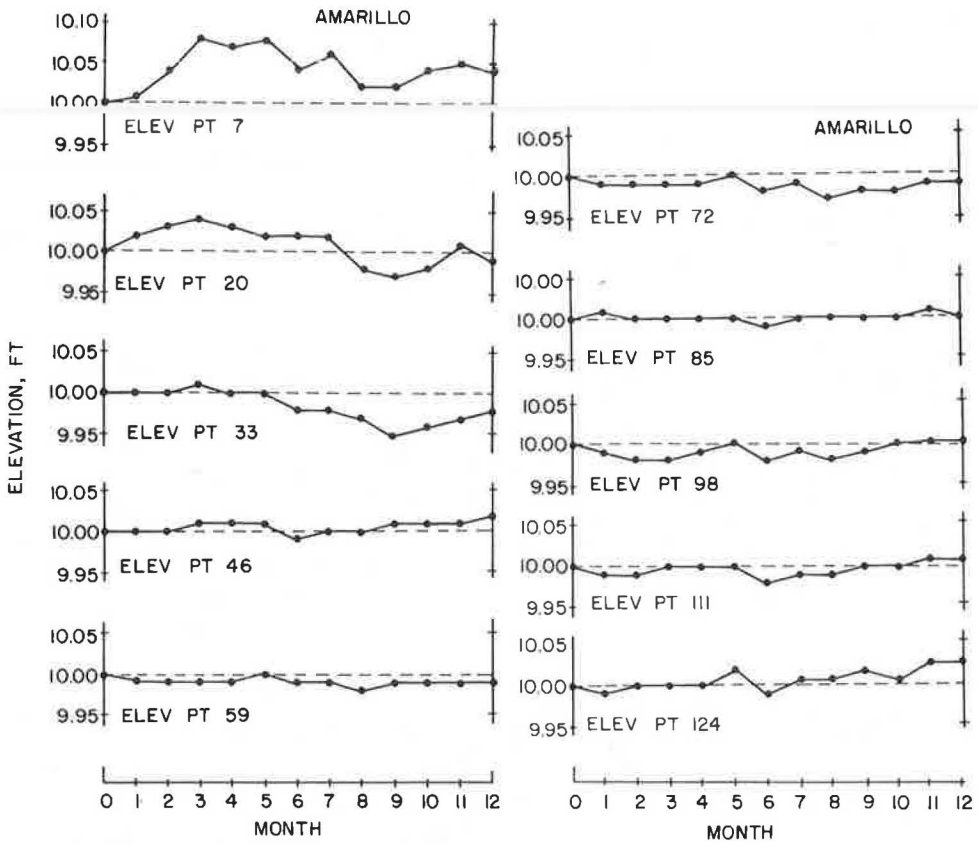

FIGURE 9 Month-by-month changes in surface elevation of individual points on the west half of the longitudinal centerline of the slab model.

Changes in Deep Bench-Mark Elevations

Although the deep bench marks were originally planned to be placed at depths of 2, 5, 9, and 15 ft (0.6, 1.5, 2.7, and 4.6 m), the depths obtained during construction resulted in actual depths of 2, 6.5, 9, and 14 ft (0.6, 2.0, 2.7, and 4.3 m). It was expected that the 2-ft bench mark would show both the greatest amount of movement and the greatest number of changes. Both the magnitude and the number of movements were expected to decrease as the depth of the bench mark increased. The changes actually recorded are shown in Figure 10. As expected, the shallowest 2-ft bench mark recorded the greatest total movement (0.10 ft, 1.2 in., 30 mm) but the 6.5-ft bench mark showed the most erratic movement. Although the movement exhibited by the 6.5-ft bench mark was substantially less than that experienced by the 2-ft bench mark, it was more than the nominal 0.01 ft (3 mm) of vertical heave experienced by the 9-ft bench mark.

The 14-ft bench mark showed a 0.01-ft heave in Month 5 (December 1985), immediately followed by a 0.02-ft (6-mm) shrink the next month, which, in turn, was followed by another heave of 0.01 ft in Month 7 (February 1986). A possible explanation for this rather rapid but brief change in elevation at this depth may be that the heave measured in Month 5 was a belated response to the wetness of Months 1–3, followed by a slight drying during Month 6. However, a roundoff inconsistency by the instrument man in reading the surveying rod may be a more reasonable explanation for the deviation of these two points which are, respectively, +0.01 ft and –0.01 ft below the apparent equilibrium elevation. The 0.01-ft shrink that was noted in the last 2 months of measurements may be a response to the period of low precipitation that occurred between November 1985 and May 1986 (Months 4–10), or it may again be a surveying roundoff error. The bench-mark elevations recorded over the first 12 months of the project certainly indicate that the depth of the active zone (depth of soil over which shrink/swell occurs) extends to a depth below 9 ft and may actually extend to at least 14 ft if the shrink indicated by the measurements made in Months 11 and 12 are actually changes in soil volume and not surveying roundoff inconsistencies.

Changes in Soil Suction

Plotting the in situ soil suction values as determined by the filter paper method at the time of installation (Figure 3) suggests that the equilibrium soil suction is below 9 ft (2.7 m). [Similar data from the companion wet-climate site suggest that the equilibrium soil suction occurs at a shallower depth of approximately 3.5 ft (1.1 m) at that location.] The month-by-month changes in the elevations of the deep bench marks also suggest the depth of the active zone to be greater than 9 ft. Thus, it is not surprising that the monthly psychrometer readings do not show a point at which equilibrium suction is

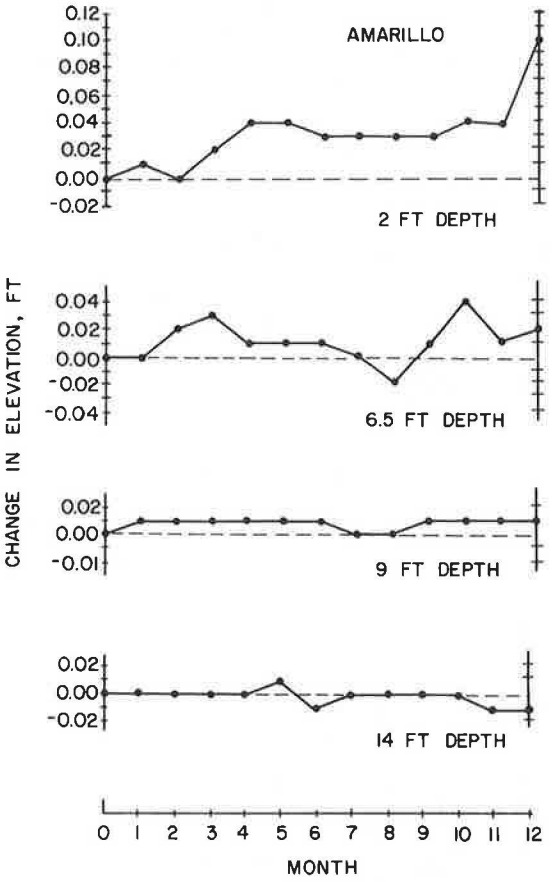

FIGURE 10 Month-by-month changes in elevation of the deep bench marks.

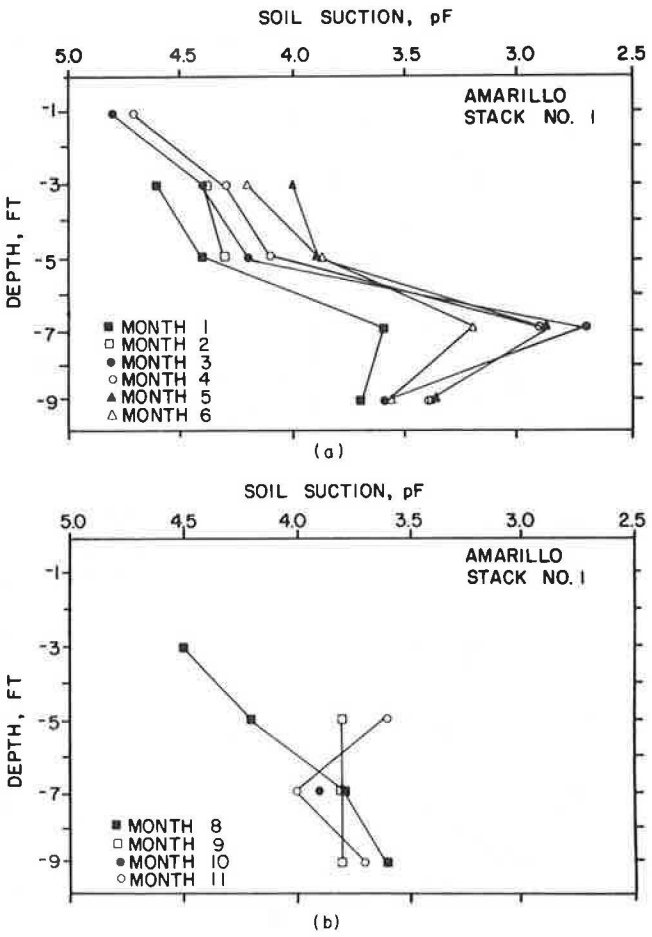

FIGURE 11 Monthly changes in soil suction with depth for instrument stack No. 1, located 3 ft outside the covered area.

present. However, plotting the monthly soil suction measurements versus depth presents some interesting trends.

Instrument stack No. 1 (Figure 1) is located 3 ft (0.9 m) outside the edge of the covered surface and is, therefore, measuring changes in the uncovered soil. The monthly psychrometer readings for this stack are depicted in Figure 11. The figure shows that a general wetting of the soil (a reduction in the soil suction) was measured from Month 1 through Month 5. However, beginning with Month 6, a gradual drying of the soil was noted through Month 8. Month 9 showed a rewetting occurring, but Months 10–12 suggest a new drying, at least at the lower depths of 7 to 9 ft (2.1 to 2.7 m). In reviewing the psychrometer results, it should be kept in mind that psychrometers are not reliable—and may not even produce a reading—in very wet soils. They are considered effective measuring devices for soil suction only if the water potential is at least 3.0 pF *(12)*. They also will not give results if the psychrometer tip becomes corroded; in these instances, the instrument essentially becomes dormant and will no longer respond. Thus, there are a number of months in the figures showing psychrometric measurements where there were no data to record. This condition is suggested in Figure 11, although it appears that the psychrometer at the 1-ft depth ceased functioning after Month 4. Figure 4 shows that an increase in precipitation occurred during the months of May and June 1986 (Months 10 and 11). Thus, the upper few feet of the soil may have still been wet enough from these rains to cause the soil suction to decrease to the point where infinity readings were measured for these instruments during the monthly readings. (Infinity readings imply that the soil conditions are too wet for a reading.) As can be noted from the figure, only one instrument provided a reading for Month 10 (May 1986) but the deeper instruments again gave readings during the Month 11 (June 1986) measurement visit. No psychrometric readings were obtained during the Month 7 measurement visit because of an equipment malfunction.

Figure 12 is representative of the west-end interior psychrometer readings. Instrument stack No. 20 is located 2 ft (0.6 m) inside the covered area. As was observed from the readings taken in the instrument stack outside the covered area (Figure 11), there is a general wetting of the soil from Month 1 through Month 5. At Month 5 this wetting trend is reversed, the soil begins to dry out, and the drying continues through Month 9. Month 10 shows a wetting of the soil had occurred but this reversed in Month 11 as Months 11 and 12 show a continued drying trend. However, the loss of instrumentation readings that occurred at Stack No. 1 due to the rains in Months 10 and 11 did not affect the covered instrumentation to the point that readings could not be made.

Instrument stack No. 26, located at the center of the covered area, has the same general shape as the other covered area stacks located beneath the west end of the slab model (Figure

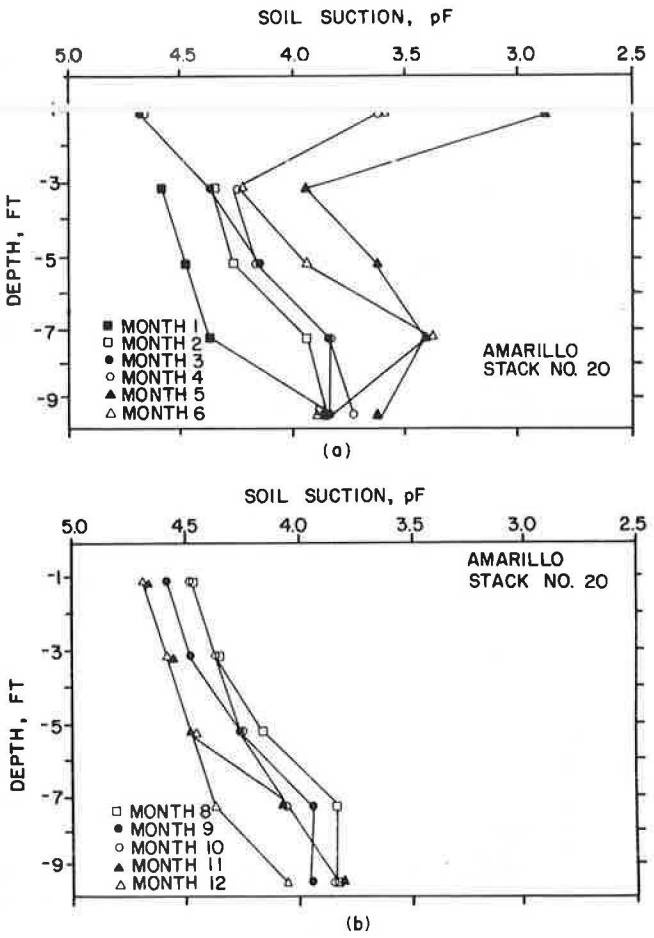

FIGURE 12 Monthly changes in soil suction with depth for instrument stack No. 20, located 2 ft inside the covered surface.

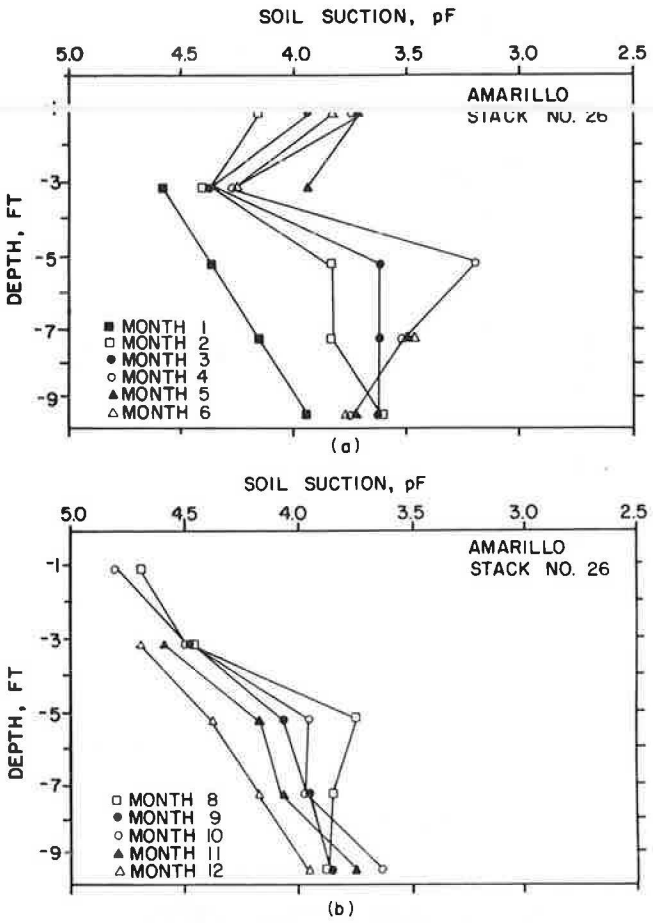

FIGURE 13 Monthly changes in soil suction with depth for instrument stack No. 26, located at the center of the covered surface.

13). It exhibits the same initial wetting followed by a general drying trend previously noted for the other instrument stacks. However, one observation to be made about each figure (Figures 11, 12, and 13) is that the slopes of the suction curves for Months 8–12 are all quite similar and all are within a fairly tight band, particularly for the covered instruments.

Similar soil suction versus depth curves could be plotted for each instrument stack as a function of time and analyzed in a similar fashion. Soil moisture content measurements could also be discussed similarly. However, such discussions would exceed the limits of this presentation and will be included in a future publication.

CONCLUSION

Twelve months of data are insufficient to form any definite conclusions from the measurements made and the trends developing from this field investigation. However, there are some observations that can be made at this time that may be of assistance to design professionals who must construct an on-grade structure over expansive soils in a dry climate.

1. The filter paper method of determining in situ soil suction is a simple and reasonably reliable method of determining the subsurface conditions with respect to potential for shrink or heave. It can apparently also provide an estimate of the depth to constant soil suction. The test is actually no more difficult to perform than the standard soil moisture content test, only requiring good laboratory technique.

2. The distance measured inward from the edge of a covered surface over which the soil moisture conditions change sufficiently to cause differential soil movement appears to be between 3 and 6 ft (0.9 to 1.8 m) for a location with a climate of about –22 in./yr (–56 cm/yr) as measured by the Thornthwaite Moisture Index.

3. An impervious surface, such as a structure or pavement slab, placed over an expansive soil when the soil is in a dry condition, can be expected to be subjected to edge heaving, at least initially.

4. Changes in the soil moisture conditions due only to changes in climate can apparently occur beneath a covered surface as far as 12 ft (3.7 m) inward from the edge of the surface. However, these induced changes may not result in significant amounts of shrink or swell in the supporting soil.

ACKNOWLEDGMENTS

The results reported in this paper were obtained under a National Science Foundation Grant. The field measurements and

laboratory testing were accomplished by Sydney Austin, Boon Lim, Jimmy Hawkins, C. H. Tsai, William Escajeda, and Norman McLeod. Wes Bratton and Dee Hardin prepared and drafted the figures.

The author is particularly indebted to the Family Hospital Center for providing the experimental site; Amarillo Engineering & Testing, Inc., Dyess Testing Laboratories, and KGNC radio, all of Amarillo, Texas; and N. L. Baroid Co., Lovington, New Mexico, which donated services and materials to the project.

REFERENCES

1. C. M. A. deBruijn. Moisture Redistribution of Soil Moisture Suction and Soil Moisture Density Beneath Two Different Surface Covers and the Associated Heaves at the Onderstepoort Test Site Near Pretoria. *Moisture Equilibria and Moisture Changes in Soils Beneath Covered Areas, A Symposium in Print*, Butterworths, Australia, 1965, pp. 122–134.
2. J. E. Holland, J. Washusen, and D. Cameron. *Seminar: Residential Raft Slabs*. Australian Engineering and Building Industries Research Association, Ltd., Swinburne College of Technology, Ltd., Hawthorn, Victoria, Australia, Sept. 1975.
3. R. L. Lytton and K. T. Meyer. Stiffened Mats on Expansive Clay. *Journal of the Soil Mechanics and Foundations Division*, ASCE, Vol. 97, No. SM7, Proceedings Paper 8265, July 1971, pp. 999–1019.
4. C. C. Mathewson, J. P. Castleberry II, and R. L. Lytton. Analysis and Modeling of the Performance of Home Foundations on Expansive Soils in Central Texas. *Bulletin of the Association of Engineering Geologists*, Vol. 12, No. 4, Fall 1975, pp. 275–302.
5. P. F. Walsh. The Design of Residential Slabs-on-Ground. *Division of Building Research Technical Paper No. 5*, Commonwealth Scientific and Industrial Research Organization, Highett, Victoria, Australia, 1974.
6. W. H. Ward. Soil Movement and Weather. *Proc., 3rd International Conference on Soil Mechanics and Foundation Engineering*, Zurich, Switzerland, 1953, pp. 477–482.
7. Statement of the Review Panel: Engineering Concepts of Moisture Equilibria and Moisture Changes in Soils. *Moisture Equilibria and Moisture Changes in Soils Beneath Covered Areas, A Symposium in Print* (J. E. Aitchison, ed.), Butterworths, Australia, 1965, pp. 7–21.
8. K. Russam and J. D. Coleman. The Effect of Climate Factors on Subgrade Moisture Conditions. *Geotechnique*, Vol. 11, No. 1, 1961, pp. 22–28.
9. J. A. Washusen. *The Behavior of Experimental Raft Slabs on Expansive Soils in the Melbourne Area*. Master's thesis, Victoria Institute of Colleges, Hawthorn, Victoria, Australia, 1977.
10. I. S. McQueen and R. F. Miller. Calibration and Evaluation of a Wide-Range Gravimetric Method for Measuring Moisture Stress. *Soil Science*, Vol. 106, No. 3, 1968, pp. 225–231.
11. R. G. McKeen. *Design of Airport Pavements for Expansive Soils*. Report DOT/FAA/RD-81/25, FAA, U.S. Department of Transportation, Washington, D.C., Jan. 1981.
12. W. K. Wray. The Principle of Soil Suction and Its Geotechnical Engineering Application. *Proc., Fifth International Conference on Expansive Soils*. Adelaide, Australia, May 21–23, 1984, pp. 114–118.

Publication of this paper sponsored by Committee on Environmental Factors Except Frost.

Soil Suction Measurements at Several Sites in Western Canada

P. VAN DER RAADT, D. G. FREDLUND, A. W. CLIFTON, M. J. KLASSEN, AND W. E. JUBIEN

Much of the difficulty in understanding the behavior of unsaturated soils comes from the lack of reliable means to measure the in situ soil suction, particularly when the suction is in excess of one atmosphere. In 1984, an extensive study was undertaken to investigate the use of the latest technology available for the measurement of soil suction. Several systems of measurement or devices were used in the study. The main objective of the study was to demonstrate how to measure soil suction in situ. The primary system used for the in situ measurement of matric suction was a commercially available thermal conductivity sensor. These sensors were selected because of the wide range of soil suctions that were anticipated in the in situ clays. Also, the installed sensors required no servicing and were easily adapted to electronic data acquisition for remote measurement. Other independent methods used included thermocouple psychrometers and two filter paper techniques. Five sites, located in western Canada, were selected for this study. A detailed subsurface investigation was conducted at each location. Representative disturbed and undisturbed samples were obtained for material characterization and for laboratory determinations of soil suction. All sites were instrumented by installing a culvert, 915 mm in diameter and 6 m in length. The culvert was installed vertically, off the edge of the railway ties. Six holes were cut through the culvert wall at predetermined depths below the top of the subgrade. Plastic sleeves were installed into the side of the excavation through these openings. The thermal conductivity matric suction sensors were then installed in undisturbed soil at the end of the sleeve. The sensors were connected to a data-acquisition system suspended within the culvert. Laboratory determinations of soil suction, using the psychrometer method, were conducted on undisturbed samples in order to establish a basis for comparison with the in situ measurements. The results of the study indicate that the thermal conductivity matric suction sensors show good potential for the in situ measurement of soil suction. Reasonable agreement was demonstrated between the field measurements and the laboratory results for the clay and fine-grained soils tested.

The behavior of compacted and natural unsaturated soils is strongly influenced by the state of stress in the pore water. The pore-water pressure is negative (relative to atmospheric pressure) and varies in response to the surrounding microclimate. A change in the negative pore-water pressure in turn produces a change in the volume and shear strength of the soil. An understanding of the effect of changing negative pore-water pressures is important from an engineering standpoint *(1, 2)*.

P. van der Raadt and A. W. Clifton, Clifton Associates Ltd., Regina, Saskatchewan S4N 5Y5, Canada. D. G. Fredlund, University of Saskatchewan, Saskatoon, Saskatchewan S7N 0W0, Canada. M. J. Klassen, CP Rail, Calgary, Alberta T2G 0P6, Canada. W. E. Jubien, CN Rail, Edmonton, Alberta T5J 0K2, Canada.

The negative pore-water pressure relative to the pore-air pressure (i.e., generally at atmospheric conditions) is referred to as matric suction. Another component of suction, called solute suction, is a function of the salt content of the pore fluid. The sum of the matric and solute suction is called total suction *(3–5)*.

The slowness in the development of a technology for understanding the behavior of unsaturated soils can be largely traced to the difficulties associated with measuring soil suction and in particular the negative pore-water pressure. Tensiometers have been used in soil science and other disciplines for several decades and have proven quite useful in measuring suctions less than approximately 0.9 atmosphere. The axis-translation technique has been used extensively in the laboratory. However, there has been a need for new devices and techniques that will provide reliable in situ measurements of soil suction, particularly in excess of one atmosphere of suction.

In 1984, a study was undertaken to investigate the latest technology available for the measurement of soil suction and an attempt to use this technology at several sites. The study was conducted by Clifton Associates Ltd., and was funded by Canadian Pacific Rail (CP), Canadian National Railways (CN), and the Transport Development Centre, Government of Canada (TDC). The main objectives of the study were

1. To measure soil suction in the field by using several methods;
2. To demonstrate the manner in which soil suction varies with the seasons in response to a changing microclimate; and
3. To assess the reliability of available devices for the measurement of soil suction. Particular attention was given to the use of the AGWA-II thermal conductivity sensor.

SYSTEMS TO MEASURE SOIL SUCTION

Three methods were used to measure suction in situ and in the laboratory. These were

1. The filter paper method,
2. The psychrometer, and
3. The AGWA-II thermal conductivity sensor.

Various types of tensiometers have been developed for measuring negative pore-water pressures. They have a limited range, require almost daily servicing, and are generally slow to equalize in highly plastic soils. It was decided not to use tensiometers in this study.

The Filter Paper Method

The filter paper method involves the placement of a filter paper either in direct contact with a soil specimen or in suspension above a soil suction specimen placed in a container *(6–8)*. Moisture equalization between the filter paper and the soil should take place in a relatively constant temperature environment. The filter papers are pretreated with a fungicide to inhibit bacterial growth.

The filter papers were allowed to equilibrate for at least 1 week before their water content was measured. The water content was then used along with the calibration curves to determine the suction of the soil. Considerable research has been done *(7, 9–12)* to establish calibration curves for the filter paper. Calibration curves established by McQueen and Miller *(7)* are shown in Figure 1.

Direct Contact Procedure

When dry filter paper is placed in contact with a soil sample, water will flow from the soil to the filter paper. Some water may enter the filter paper by vapor flow but equalization should be primarily through fluid flow as long as the soil is not extremely dry. Water movement should continue until the suction in the filter paper is equal to the suction of the soil. The filter paper is small in size when compared to the soil specimen and the amount of water movement from the soil is small. The filter paper is assumed to measure matric suction as there is a direct contact between the water in the soil and the filter paper.

Noncontact Procedure

When filter paper is suspended above a soil sample (i.e., no contact with the soil), the filter paper gains water from the soil through vapor movement. A potential difference exists between the soil pore water and the filter paper. The potential of the soil water is a function of matric suction and solute suction. Therefore, the equilibrium water content of the filter paper is a measure of the total suction of the soil.

Theoretically, it should be possible to measure both matric and total suction using slightly different filter paper procedures. A high degree of contact between the filter paper and the soil should result in the measurement of matric suction. No contact between the soil and the filter paper should result in the measurement of total suction.

Thermocouple Psychrometer Method

The thermocouple psychrometer measures total suction by using the Peltier effect to measure the relative humidity in the environment of a soil specimen placed in a sealed chamber *(13)*. The psychrometer is capable of measuring suctions ranging from approximately 100 to 8000 kPa. The accuracy of the suction measurement is a function of the constancy of the temperature environment in which the measurement is conducted *(14)*.

A psychrometer consists of a measuring junction of copper and constantan. A reference junction is also reused in measuring the sensor temperature. The construction of the 3-wire psychrometer and the chamber into which it is placed is shown in Figure 2.

A soil specimen is placed in the chamber with the psychrometer. Water evaporates from the soil into the sealed chamber. Evaporation ceases when the relative humidity in the chamber is equal to that of the air in the soil. A soil with a high total suction will have a depressed relative humidity, and vice versa.

Measurements of relative humidity must be made in a controlled temperature environment. Therefore, it is essentially imperative that these measurements be made in the laboratory *(15, 16)*. The temperature environment was maintained within ±0.01°C during this study.

The output from the psychrometer is in microvolts, which can be related to soil suction through use of a calibration curve. A calibration curve for each psychrometer is established by placing the psychrometer above an aqueous solution of NaCl *(17, 18)*. This procedure is repeated several times using various molar strengths of NaCl. A typical calibration curve is shown in Figure 2.

AGWA-II Thermal Conductivity Sensors

The AGWA-II sensor consists of a thermister and a 20-ohm heater embedded in a porous ceramic block *(19)*. The sensor gives an indirect measure of matric suction by using the heat dissipation characteristics of the ceramic block and the fluid in the pores *(20)*. The thermal conductivity of the ceramic block is much lower than that of water. As such, the amount of water in the pores greatly influences its thermal conductivity. As the suction in the soil reduces the water content of the ceramic block, its thermal conductivity is reduced. These sensors are

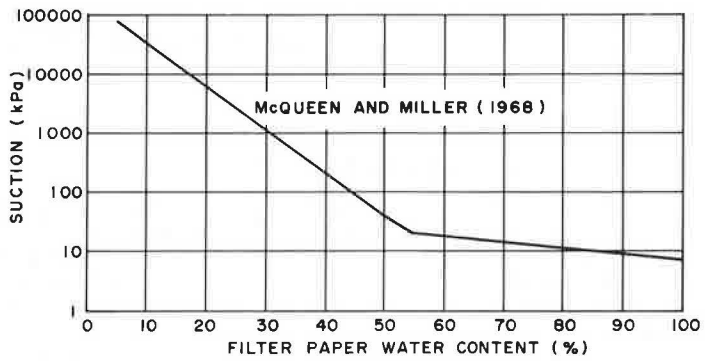

FIGURE 1 Calibration curve for filter paper versus suction.

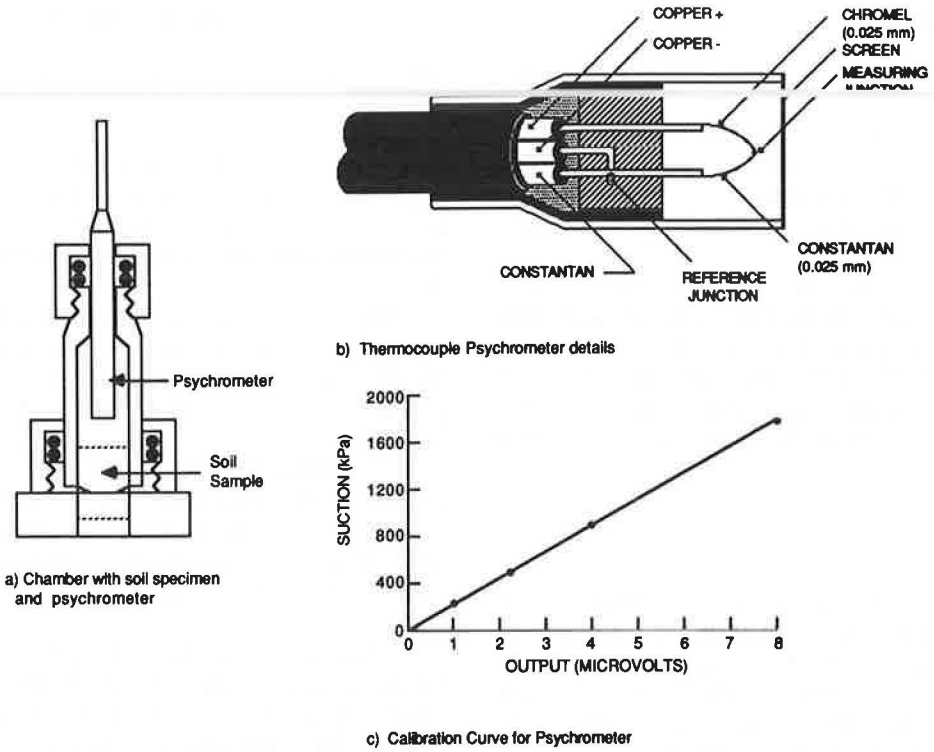

FIGURE 2 Details of the thermocouple psychrometer system to measure suction: (a) chamber with soil specimen and psychrometer, (b) thermocouple psychrometer details, and (c) calibration curves for psychrometer.

similar in principle to those manufactured previously by Moisture Control Systems of Findlay, Ohio *(21, 22)*.

The operation of the sensor can be described as follows. A controlled amount of heat (i.e., a constant current source for a specific time) is added to the center of the ceramic block. The temperature in the block is measured after a specified time interval. The rate at which heat dissipates is directly related to the water content of the ceramic block. The sensor is calibrated to give a fixed relationship between the rate of heat dissipation and the matric suction of the ceramic block.

Sensor calibrations were provided by the manufacturer. Their calibration procedure involved placing the sensors in a fine sand on a pressure plate apparatus. The sand and sensors were subjected to an applied suction until equilibration was established and their thermal conductivity was then measured. The sensors were read in the field using a hand-held meter. Some difficulties were encountered with the meter; these will be discussed later in this paper.

FIELD PROGRAM

Four sites located in western Canada were initially selected for the field program (see Table 1). A fifth site was subsequently added. The sites were selected on the basis of material type and proximity to major urban centers for ease of access. Sites Nos. 1, 2, and 3 are situated in highly plastic clay. Site No. 4 is situated in till and Site No. 5 is in a silty clay. Site No. 1 is located in an older subgrade that has not failed but is a continuing maintenance problem. Site No. 3 is located within a new subgrade, constructed within the last few years. Site No. 4 is located in a high-traffic section showing no distress. Site No. 5 is located in a large fill section that is currently performing well.

Sites Nos. 1, 2, 3, and 4 are all located within a 60-kilometer radius of Regina. Site No. 5 is located near Fort Saskatchewan, Alberta. The location of each site is indicated in Figure 3.

A subsurface investigation was carried out at each of the above site locations. The investigation included the gathering

TABLE 1 SITE LOCATION FOR TEST INSTALLATIONS

Site No.	Location	Rail System	Mileage and Subdivision
1	Belle Plain, Saskatchewan	CN	Mile 24.3 CB01
2	Bechard, Saskatchewan	CN	Mile 78.3 Lewvan Sub.
3	Regina, Saskatchewan	CN	New Lewvan Bypass
4	McLean, Saskatchewan	CP	Mile 67.2 Broadview Sub.
5	Fort Saskatchewan, Alberta	CN	Mile 2.14 Beamer Sub.

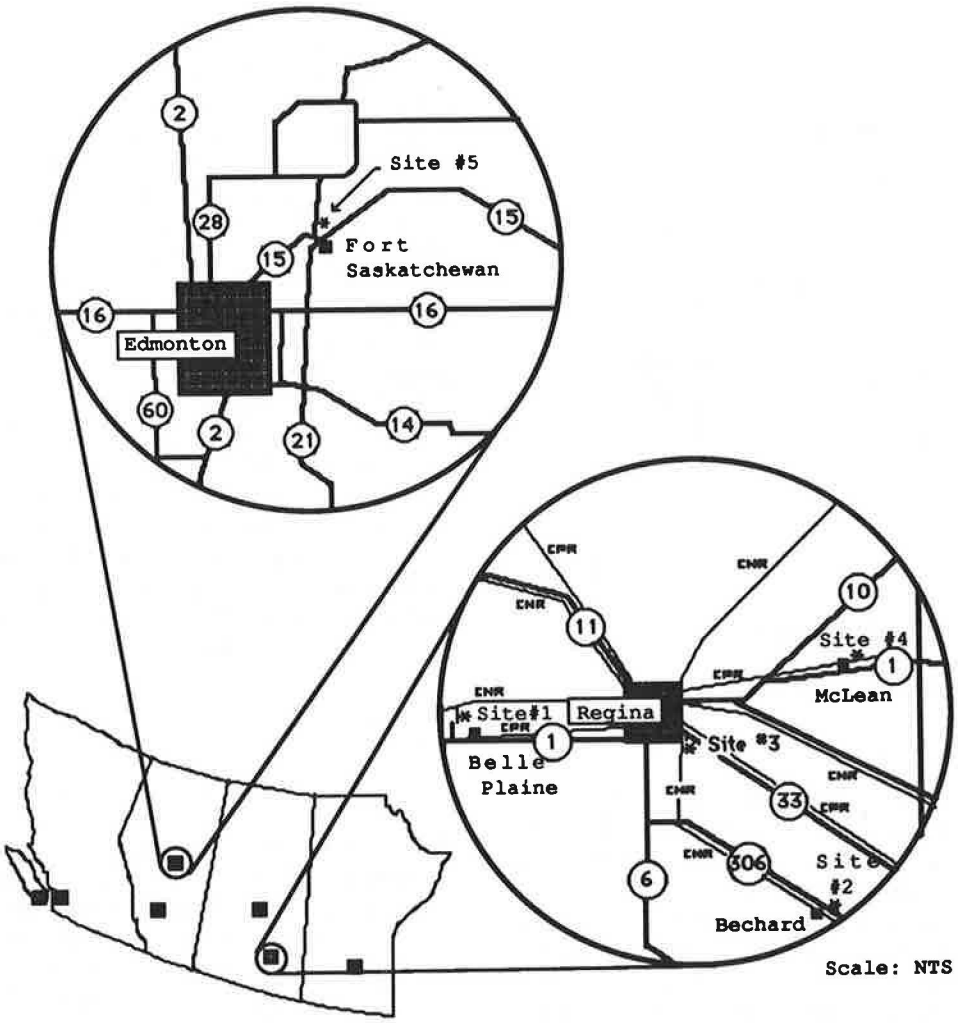

FIGURE 3 Plan showing location of sites in western Canada.

of representative disturbed and undisturbed samples for laboratory visual classification and index testing, followed by laboratory suction measurements. All sites were instrumented by installing a prefabricated 915-mm diameter culvert vertically, 6 m below the top of the tie elevation. The culvert was located directly off the end of the ties. AGWA-II sensors were installed at predetermined depths below the subgrade through the vertical wall of the culvert. A typical detail of this installation in illustrated in Figure 4. The location of the sensors for each site is indicated on the respective borehole logs. A standpipe piezometer was installed below the bottom of the culvert at each site to monitor the groundwater level.

The field monitoring of the AGWA-II sensors was initially performed with a hand-held readout device. In the early stages of the program, the sensors located within the Regina area were read every 1 to 3 days. The Edmonton site was read on a less frequent basis with the same readout device. Early in 1985, the frequency of readings was somewhat reduced. During the month of March an automated data acquisition system (i.e., data logger) was used. This method of data collection allowed the collection of data at an increased frequency. Initially, the data logger was used in a manual mode to read all of the sites in the Regina area. This was done to establish a correlation between the hand-held device and the data-acquisition system. The data-acquisition system was then installed at Site No. 1, where the performance of the system could be easily monitored. The data logger was initially set to read the sensors, on an hourly interval. The data presented in this paper cover only the results obtained using the hand-held readout device.

PRESENTATION OF DATA AND DISCUSSION OF RESULTS

Extensive data have been collected on suction measurements at the five sites. It is not possible to present and discuss all the data. Therefore, the data from Sites Nos. 1 and 3 have been selected for more detailed presentation and discussion. Only a brief summary of the findings from the other sites is included. Much of the interpretation of the data is based on previous research studies performed on similar materials *(4)*.

Site No. 1

Site No. 1 is located on CN trackage near Belle Plaine, Saskatchewan. The track condition at this location is poor and

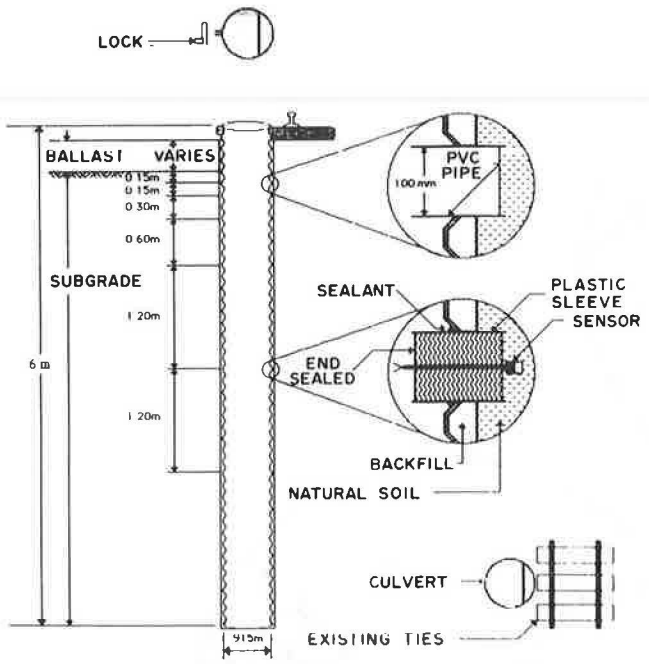

FIGURE 4 Typical culvert and sensor installation details.

much effort has been devoted annually to lifting and aligning the tracks. This is a spur line into a large potash mine and as such is subjected to heavy loading. The track has bearing capacity failures for most of its length.

The stratigraphy consists of 460 mm of gravel ballast and subballast overlying 5.6 m of stiff, highly plastic clay. The clay is underlain by a stiff-to-hard glacial till at the 6.1 m depth (Figure 5). A standpipe piezometer was installed with its tip at 9 m below grade. The piezometer remained dry for the duration of the project but a small amount of seepage entered the culvert during the spring breakup period.

AGWA-II sensors were installed on November 7, 1984. The sensors were saturated before installation. It is estimated that as much as 30 days were required to produce equilibration between the sensor and the soil (Figure 6). Most of the sensors appeared to have reached an equilibrium condition early in 1985. In late February 1985, the sensors began to freeze. During the equilibration time, the suction measurements climbed as the excess water within the sensor was drawn out by the suction of the soil. After some time, the sensors appeared to have stabilized with only a few departures from this trend. It is not known whether these periodic fluctuations are indeed variations in soil suction or whether they are related to the temperature influences on the hand-held readout device or possibly due to the temperature variations in the soil.

Based on the data collected to date, the AGWA-II sensors indicate matric suctions ranging from 75 to 250 kPa for the surficial clays. The suction profile was S shaped with respect to depth. Higher suctions were noted near the top of the subgrade just underlying the ballast. The suctions then varied slightly and finally decreased with depth (Figure 7). The suctions measuring using the AGWA-II sensors are in the range anticipated for Regina clay at the observed field water contents.

Both contact and noncontact filter paper measurements were made on undisturbed samples taken on November 7, 1984. The tests were performed in the laboratory. The filter paper was placed against the soil sample and double wrapped with Saran wrap and tinfoil and taped for the contact measurements. The samples were stored in a moist room at 22°C. The measured matric suctions ranged from 20 to 3000 kPa (Figure 8). The large scatter would indicate that possibly some of the filter papers did not have satisfactory contact with the soil and as a result measured total suction.

The results of two sets of data (i.e., two testholes) from filter papers not in contact with the soil are also shown in Figure 8. The total suctions ranged from 50 to 1800 kPa with a typical average of 545 kPa.

Total suction measurements using the psychrometer are shown in Figure 9. The results are relatively constant, ranging from 260 to 600 kPa. These values are also in the range of anticipated values for Regina clay at the observed water contents. Although the filter paper and psychrometer measurements are in the same order of magnitude, the filter paper results show considerable scatter. It appears that at low water contents it may be difficult to obtain a good contact between the soil and the filter paper.

Site No. 2

Site No. 2 is located on CN trackage south of Bechard, Saskatchewan. The track condition at this site is poor and requires periodic maintenance. This is a branch line with the principal commodity transported being grain.

The stratigraphy consists of 760 mm of gravel ballast and sand subballast overlying 1200 mm of stiff, highly plastic clay. This clay was strongly organic in nature. Underlying this clay is a stiff-to-hard, highly plastic clay that becomes less plastic just above the glacial till contact at the 7.9 m depth. The till was stiff to hard. A standpipe piezometer was initially dry but later indicated a water level 5.4 m below grade.

The AGWA-II sensors were installed on November 8, 1984. The measured matric suctions ranged from 130 to 225 kPa, with an average of 160 kPa. The contact filter paper measurements gave an average suction of 1075 kPa. This would indicate poor contact between the soil and the filter paper. The noncontact filter papers gave total suction ranging from 150 to 400 kPa, with an average of 240 kPa. These results could possibly be too low due to condensation droplets as a result of slight fluctuation in temperature. The psychrometer data gave total suctions ranging from 280 to 650 kPa, with an average of 490 kPa. The psychrometric data appear to be in the anticipated range for total suction.

Site No. 3

Site No. 3 is located on CN trackage near Regina, Saskatchewan. This line was recently moved to make way for the construction of the new Lewvan expressway in the city of Regina. The track condition is excellent. Recent construction and compaction were primary reasons for the selection of this site.

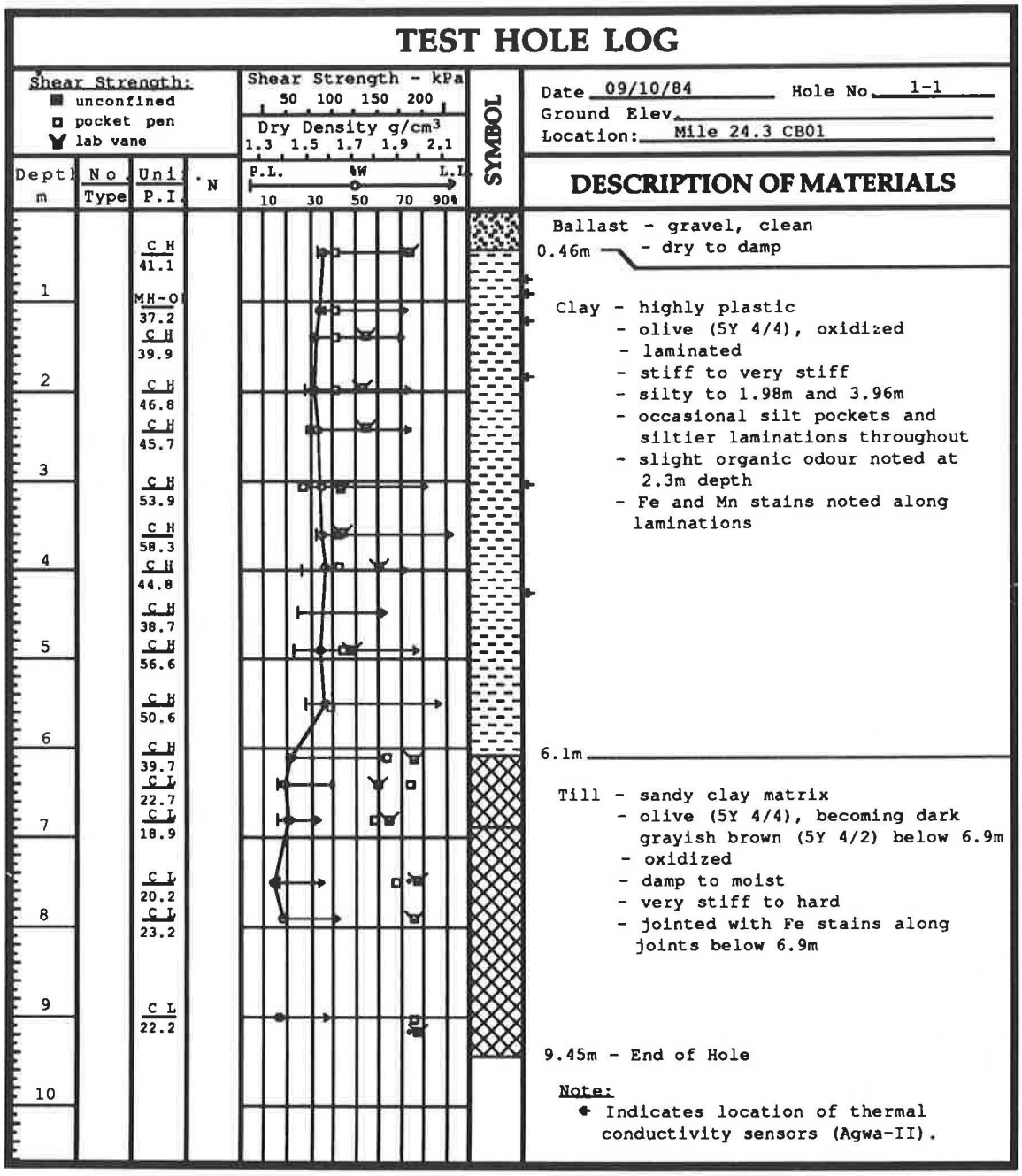

FIGURE 5 Test hole information from Site No. 1, Belle Plaine.

The stratigraphy consists of 460 mm of gravel ballast and subballast. Underlying the ballast is stiff-to-hard, highly plastic clay, which becomes less plastic just above the clayey silt contact at 5.8 m. The underlying silt has a thickness of 800 mm. Till was encountered below the silt and had a medium-to-stiff consistency (Figure 10). A piezometer was installed with its tip 9.1 m below the top of the tie. After the water levels stabilized in the standpipe piezometer, a water level of 4.7 m below grade was measured.

AGWA-II sensors were installed in the surficial clay at this site on November 8, 1984. By February 14, 1985, all sensors were responding well (Figure 11). The AGWA-II sensors were installed only within the surficial clays. The matric suction measured by the AGWA-II sensors indicated a range of from 60 to 275 kPa, with an average value of 160 kPa (Figure 12). The data show a typical S-shaped distribution of suction versus depth, rapidly decreasing to the water table.

The contact filter paper method indicated an average suction for the clay of 800 kPa with a range of from 400 to 5000 kPa (Figure 13). The noncontact filter paper method showed suctions ranging from 675 to 1500 kPa, with an average value of 1360 kPa. The above results would indicate that when an attempt is made to measure matric suction using filter paper, total suction is often inadvertently measured.

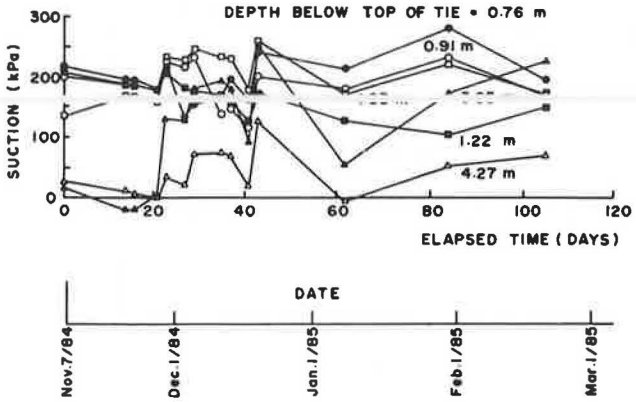

FIGURE 6 Plot of suction versus elapsed time for AGWA-II sensors at Site No. 1.

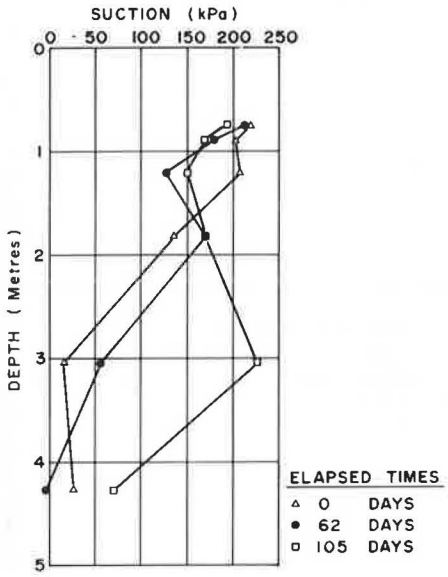

FIGURE 7 Plot of matric suction versus depth measured using AGWA-II sensors at Site No. 1.

The results from the psychrometer measurements are also shown in Figure 13. The psychrometer measurements indicate total suctions ranging from 575 to 1575 kPa, with an average of 920 kPa.

The subgrade at Site No. 3 was just recently constructed. The plot of shear strength versus depth, as illustrated on the testhole log (Figure 10), shows a correlation with the suction profile measured on February 14, 1985. The plot of shear strength by both the vane shear and pocket penetrometer methods indicates an undrained strength of 200 kPa near the top of the subgrade, dropping off rapidly to 100 kPa at the 3 m depth. The shear strength is maintained at this value and only slightly increases when the siltier material is encountered at the 5.8 m depth. The strength then increases slightly within the till. The reason for the increase in shear strength near the surface can be attributed to both the increased suction and possibly the compactive effort applied during construction.

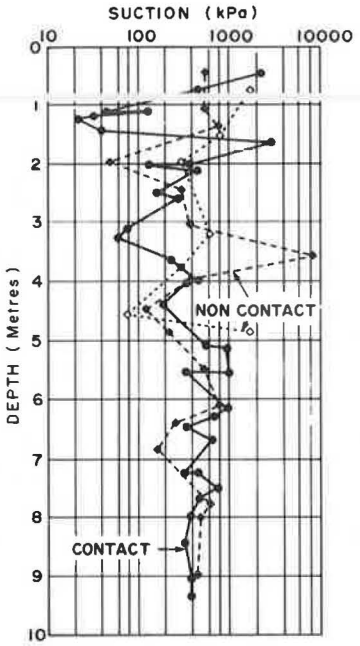

FIGURE 8 Suction versus depth for test hole No. 1 using the McQueen and Miller filter paper method.

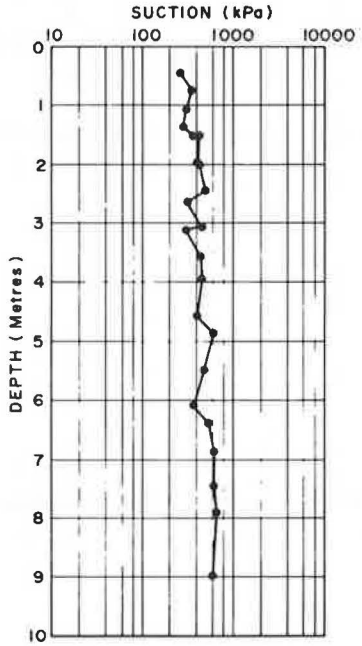

FIGURE 9 Plot of total suction versus depth for Site No. 1 using the psychrometric method.

Site No. 4

Site No. 4 is located on the CP main line 3.5-km east of McLean, Saskatchewan. The site, founded almost entirely on till, is subjected to large traffic volumes of various loadings and is performing well.

The stratigraphy at this site is relatively uniform. The surficial strata consist of 760 mm of gravel ballast and subballast.

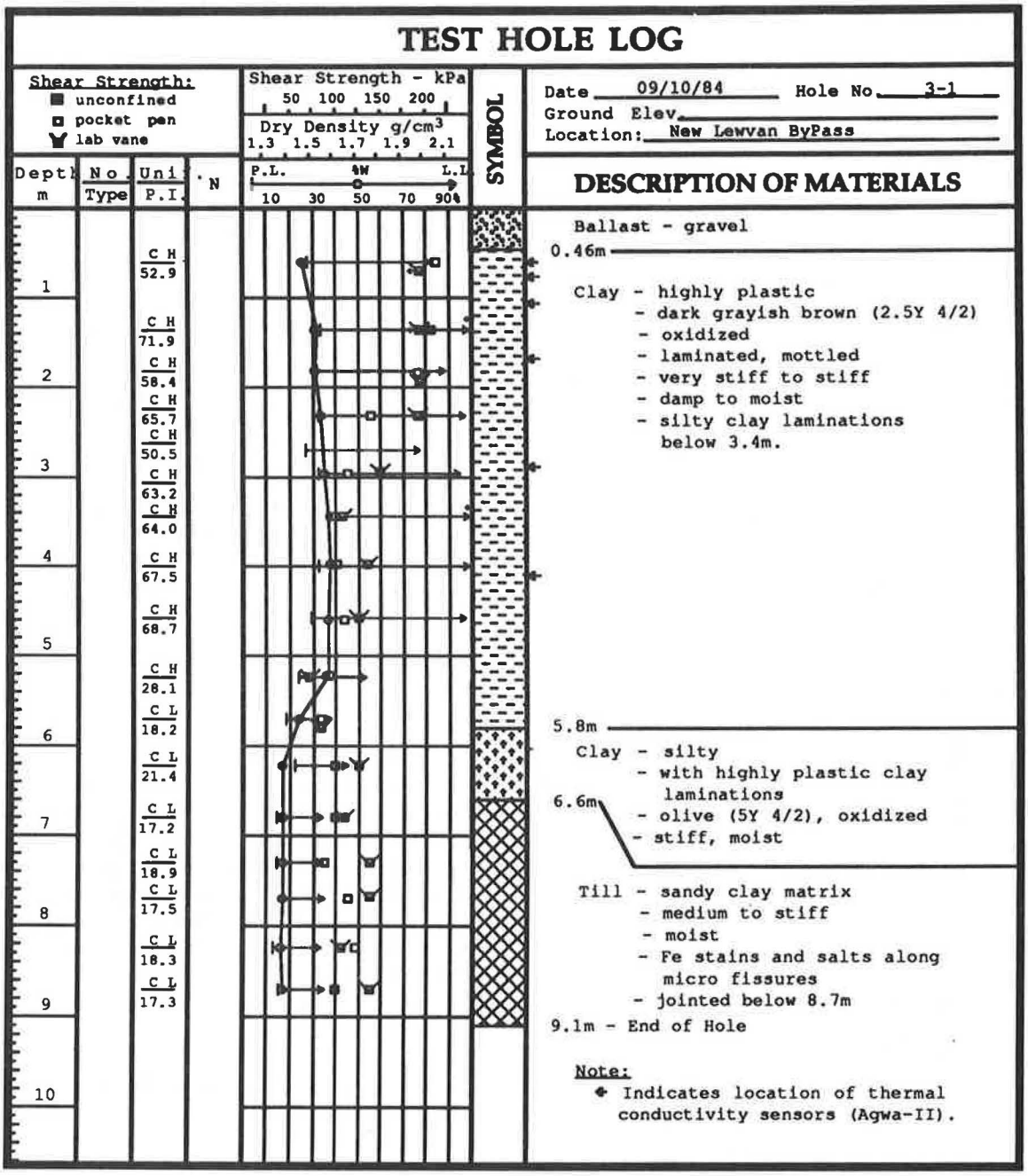

FIGURE 10 Test hole information from Site No. 3, Lewvan Expressway, Regina.

Underlying these strata are 740 mm of stiff-to-very-stiff silty clay. This material is believed to be fill. Stiff-to-hard till was encountered below the fill at the 1.5 m depth. A piezometer was installed with its tip 1.9 m below the top of the tie. The piezometer was initially dry but subsequently indicated a water level at 6.6 m below grade.

AGWA-II sensors were installed at this site on November 8, 1984. By February 15, 1985, all sensors were responding well. The first three sensors were installed within the fill. The bottom three sensors were installed in undisturbed till. The sensors measured suctions ranging from 60 to 160 kPa, with an average of 100 kPa.

The contact filter paper technique indicates suctions ranging from 225 to 575 kPa with an average of 370 kPa. The noncontact filter paper tests showed total suctions ranging from 650 to 1050 kPa, with an average of 900 kPa. These results are higher than would be anticipated. Possibly the air space around the specimens was too large relative to the size of the container.

The psychrometer measurements show total suctions ranging from 260 to 620 kPa, with an average of 425 kPa.

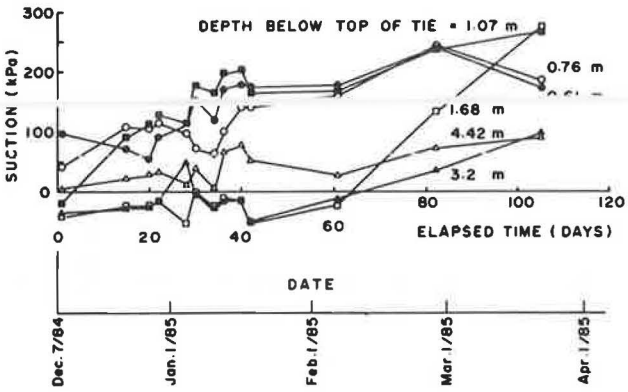

FIGURE 11 Plot of suction versus elapsed time for AGWA-II sensors at Site No. 3.

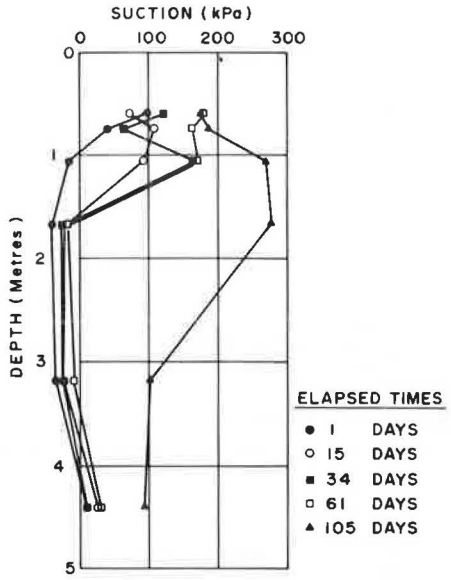

FIGURE 12 Plot of matric suction versus depth measured using AGWA-II sensors at Site No. 3.

Site No. 5

Site No. 5 is located on CN trackage near Fort Saskatchewan, Alberta. The site was selected because it was a large fill section and because the foundation materials were silty in nature.

The stratigraphy at this site was not uniform. It consisted of 1100 mm of gravel ballast and subballast. This stratum was frozen to 500 mm at the time of the investigation. Underlying this was 4.7 m of stiff-to-very-stiff silty clay fill material. A 300-mm-thick layer of organic topsoil and rubble was encountered at the 5.8 m depth. Stiff, silty clay was encountered below the organic layer at the 6.1 m depth. Fine- to medium-grained, water-bearing sand was encountered at 7.9 m. A piezometer indicated a water level at 6.1 m.

AGWA-II sensors were installed on October 30, 1984. All of the sensors were installed within the silty clay fill material. The matric suctions observed ranged from 0 to 200 kPa, with an average of 175 kPa. Possibly the sensor showing the lowest reading had not yet responded.

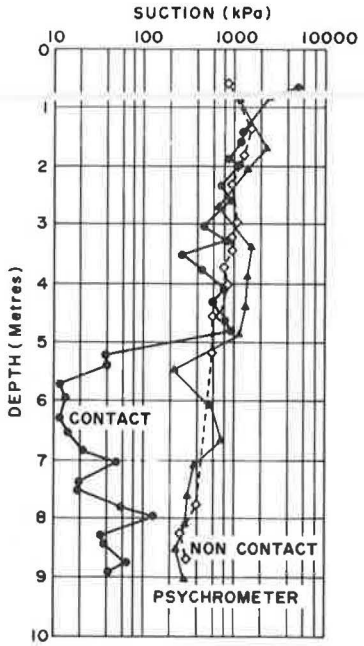

FIGURE 13 Filter paper and psychrometer results versus depth at Site No. 3.

The contact filter paper technique showed suctions ranging from 75 to 400 kPa, with an average of 175 kPa. The noncontact filter paper results showed suctions ranging from 325 to 450 kPa. The psychrometer results showed total suctions ranging from 125 to 365 kPa, with an average of 280 kPa.

The above results appear to be reasonable. The matric suction was 100 kPa near the surface, dropping off to zero at the 5 m depth. The total suction varies from a high of 300 kPa to a low of 200 kPa. The contact filter paper data appear to jump from a total suction measurement to a matric suction measurement as more water becomes available in the soil.

COMPARISON OF SUCTION MEASUREMENTS SYSTEMS

Filter Paper Method

The plots indicate varying trends of suction versus depth. Site No. 3 has high suctions near the surface, dropping off toward zero near the water table. On many of the plots from contact filter paper tests, there is an occasional spike showing a high suction. It appears that these spikes are not high matric suctions but are actually total suction measurements obtained while attempting to measure matric suction. This would indicate that when using the contact filter paper method, a given test may measure either matric or total suction. In almost all cases, the matric suctions measured were either close to the expected value or substantially greater. When greater, there was typically reasonable agreement with other measurements of total suction.

The measurements of total suction using the noncontact filter paper method seem to work reasonably well. However, there

were some difficulties relating the results of this method to the results obtained by the psychrometer method. It should be noted that when there was disagreement, the results of the filter paper method were usually higher than those from the psychrometer method.

The Psychrometer Method

The psychrometer method showed reasonably good correlation with the noncontact filter paper method for the measurement of total suction.

The AGWA-II Method

The results obtained using the AGWA-II sensors illustrate the variation of suction with depth and time. The variation of suction for a particular sensor with respect to time is attributed partly to the equilibration period for the sensor. Most of the profiles of suction versus depth indicate a high suction near the surface and then decrease with depth.

Some problems have been identified with the hand-held readout device. This was particularly true during the early stages of the study.

PROBLEMS IDENTIFIED AND RESOLVED TO DATE

Filter Paper Methods

There were several problems identified with this method during the study. One of the major problems associated with the contact filter paper method arises out of an inability to consistently measure matric suction. This problem became evident when attempts to measure matric suction resulted in the measurement of high suctions. It is speculated that this phenomenon occurs when matric suction determinations are attempted on samples with insufficient pore fluid to ensure fluid flow into the filter paper. The net result is that when matric suction measurements are attempted using the contact procedure, total suctions are frequently obtained.

There are numerous procedural problems experienced with the filter paper methods. These problems arise out of the extremely small measurements required for water content determinations. A filter paper will weigh approximately 0.25 g. Typical water contents will range from 30 to 60 percent. This requires the measurement of an extremely small quantity of water. After the filter paper has equilibrated it must be removed from the sample and its initial wet weight measured. The instant the filter paper is removed from the soil, evaporation begins. This results in the wet weight of the filter paper's changing constantly. This problem also occurs to a lesser extent after the filter paper is oven dried and the dry weight is being measured. The problem is directly related to the relative humidity of the ambient atmosphere. The humidity in the laboratory is virtually always different from that required for equilibrium in the filter paper. Therefore, a weight change in the filter paper always occurs. It was also noted that the tare containers used in water content determinations gained and lost water from the filter papers. The net effect of these difficulties is that this method is technique sensitive.

Various procedural techniques were employed in an attempt to minimize the effects of some of the difficulties discussed. Efforts were made to reduce the time of handling the wet filter papers before weighing to a matter of seconds. This reduced the total magnitude of loss. Similar procedures were invoked for the dry weight determinations.

The measurement of total suction worked well in almost all cases and it is possible that this method is better suited to this type of measurement.

Psychrometer Method

The procedures are somewhat involved and the equipment costs are significantly greater with this method compared with the filter paper method. There were no major difficulties associated with calibration or testing. The main difficulty is the high sensitivity of the psychrometer and the readout device to thermal gradients. To overcome this difficulty, the sample and the psychrometer were enclosed within a chamber. The chamber itself was then submerged in a multibuffered water bath. The bath temperature was maintained to within ±0.01°C.

After the psychrometers were calibrated, the time required for each suction measurement was approximately 2 to 3 days. For all sites except Site No. 4, the data collected agreed with expected values and with the values of total suction determined by the filter paper method.

The psychrometer equipment has been in use for several years, has proven reliability, and is readily obtainable. This, combined with the high repeatability of calibration and test results, would indicate that it is more reliable than the filter paper method.

AGWA-II Sensors

AGWA-II sensors have only recently been designed and built. The company is a small, specialized firm that must also do considerable development research. The hand-held readout device was designed and built by a third-party developer. The hand-held readout device, sensor interface, and power supply are new products but the sensors have been in use for several years. The sensors have been used primarily in irrigation to control automated irrigation systems *(23)*. The sensors appear to be proven devices with few difficulties.

The system was plagued with minor technical difficulties and setbacks throughout the project. The problems included electronic incompatibility of the hand-held readout device with the data logger as well as power supply difficulties. The electronic incompatibility of the hand-held device and the data-acquisition system resulted in a shift in the calibration of the original sensors. The net result was that a negative suction was measured for some of the sensors. This became less noticeable with time as the suctions increased. The offset difficulty was found to exist with the hand-held readout device and not with the data-acquisition system. The calibration equations for the sensors were also found to be incorrect for the hand-held readout device. The incorrect calibrations resulted in the entire calibration curve's being offset approximately 50 kPa. The sensors read by the hand-held device would indicate a suction of 50 kPa lower than the actual value. Some of the sensors were

recalibrated by the manufacturer and it was established that this was indeed the case. This difficulty was resolved in three ways. First, when the data-acquisition system was purchased, this problem no longer existed. Second, the supplier exchanged the hand-held device for an updated model with this problem rectified. Finally, the offset was established by running the original hand-held device and the new data logger in parallel to establish the correction for the data already collected. It should be noted that the data presented in this paper are not corrected for the calibration offset.

PRELIMINARY CONCLUSIONS

The results of this study would indicate that suction can be measured in the field. Reasonable agreement was demonstrated among the field measurements, laboratory results, and anticipated results. The major discrepancies were explainable. The manner in which soil suction in the subgrade varies throughout the season has only been partially addressed.

Our comments and conclusions regarding the measurement systems tested are as follows:

1. The filter paper method theoretically measures matric suction when there is sufficient contact between the filter paper and soil sample. However, it is difficult to ensure that there is sufficiently good contact between the filter paper and the soil. The filter paper method should not be used to determine matric suction.
2. The noncontact method appears to measure total suction, reasonably well. It is important to ensure reasonable temperature control during the equilibration period. The method agrees quite well with the psychrometer method but the results generally exhibit more scatter.
3. The psychrometer method, which measures total suction, is sensitive to the thermal environment in which the test is performed. The test is also operator sensitive. The measurement should only be performed in a laboratory.
4. The AGWA-II sensors and equipment had several difficulties related to supply of equipment and some minor technical difficulties. Most of the difficulties experienced with this equipment have been resolved. The AGWA-II method is the preferred method for measuring suction for several reasons. First, the method demonstrates relatively consistent and reasonable results. Second, this method measures matric suction. Third, the system lends itself to data acquisition and battery operation, which is essential for field measurement at remote locations.

ACKNOWLEDGMENTS

The data presented in this paper are the result of a study financed equally by Canadian Pacific Rail, Canadian National Railways, and the Transport Development Centre, Government of Canada. Their interest and financial support were appreciated.

R. Phene of AGWATRONICS, Merced, California, worked closely with the personnel from Clifton Associates Ltd. in an attempt to expedite the development of the AGWA-12 sensor and readout equipment. His assistance demonstrated that a combined effort is extremely useful in the development of new technology.

REFERENCES

1. D. Croney and J. D. Coleman. Pore Pressures and Suction in Soil. *Proc., Conference on Pore Pressures and Suction in Soils,* Butterworths, London, 1961, pp. 31–37.
2. D. G. Fredlund. Appropriate Concepts and Technology for Unsaturated Soils, Second Canadian Colloquium. *Canadian Geotechnical Journal,* Vol. 16, No. 1, 1979, pp. 121–139.
3. J. D. Oster, S. L. Rawlins, and R. D. Ingvalson. Independent Measurement of Matric and Osmotic Potential of Soil Water. *Proc., Soil Science Society of America,* Vol. 33, No. 2, April/May 1969, pp. 188–191.
4. J. Krahn and D. G. Fredlund. On Total, Matric and Osmotic Suction. *Soil Science,* Vol. 14, No. 5, 1972, pp. 339–348.
5. T. B. Edil and S. E. Motan. Laboratory Evaluation of Soil Suction Components. *Geotechnical Testing Journal,* Vol. 7, No. 4, Dec. 1984.
6. R. Gardner. A Method of Measuring the Capillary Tension of Soil Moisture Over a Wide Moisture Range. *Soil Science,* Vol. 43, No. 4, April 1937.
7. I. S. McQueen and R. F. Miller. Calibration and Evaluation of a Wide Range Method for Measuring Moisture Stress. *Soil Science,* Vol. 106, No. 3, 1968, pp. 225–231.
8. S. Al-Khafaf and R. J. Hanks. Evaluation of the Filter Paper Method for Estimating Soil Water Potential. *Soil Science,* Vol. 117, No. 4, 1972.
9. R. G. Fawcett and N. Collis-George. A Filter Paper Method for Determining the Moisture Characteristics of Soil. *Australian Journal of Experimental Agriculture and Animal Husbandry,* Vol. 7, April 1967.
10. A. P. Hamblin. Filter Paper Method for Routine Measurement of Field Water Potential. *Journal of Hydrology,* Vol. 53, 1981, pp. 355–360.
11. R. F. Miller, F. Reuben, and F. A. Branson. *Water Relations of Rangeland Ecosystems: I. Techniques for Defining Water Relations in Soils.* U.S. Geological Survey, Denver, Colo., 1982.
12. P. M. Gallen. *The Measurement of Soil Suction Using the Filter Paper Method.* M.Sc. thesis, University of Saskatchewan, Saskatoon, Canada, 1985.
13. R. W. Brown. *Measurement of Water Potential with Thermocouple Psychrometers: Construction and Applications.* U.S. Department of Agriculture Forest Service Research Paper, Int-80, Ogden, Utah, 1970.
14. D. E. Daniel, J. M. Hamilton, and R. E. Olson. *Suitability of Thermocouple Psychrometers for Studying Moisture Movement in Unsaturated Soils, Permeability and Groundwater Contaminant Transport.* ASTM STP 746, American Society for Testing and Materials, Philadelphia, Pa., 1979, pp. 84–100.
15. R. Gardner. Relation of Temperature to Moisture Tension in Soil. *Soil Science,* Vol. 79, 1955, pp. 257–265.
16. A. Klute and L. D. Richards. Effect of Temperature on Relative Vapour Pressure of Water in Soil: Apparatus and Preliminary Measurements. *Soil Science,* Vol. 93, 1962, pp. 391–396.
17. C. P. Hedlin and F. N. Trofimenkoff. *Relative Humidities Over Saturated Solutions of Nine Salts in the Temperature Range of 0 to 90°F.* 1963 International Symposium on Humidity and Moisture, Washington, D.C., May 1963.
18. R. L. Meyn and R. S. White. Calibration of Thermocouple Psychrometers: A Suggested Procedure for Developing a Reliable Predictive Model. *Psychrometry in Water Relations Research,* 1972, pp. 56–63.
19. C. J. Phene, G. J. Hoffman, and S. L. Rawlins. Measuring Soil Matric Potential In Situ by Sensing Heat Dissipation With a Porous Body: Theory and Sensor Construction. *Proc., Soil Science Society of America,* Vol. 35, Madison, Wis., 1971, pp. 27–32.

20. B. Shaw and L. D. Baver. Heat Conductivity as an Index of Soil Moisture. *Journal of the American Society of Agronomy,* Vol. 31, 1939, pp. 886–891.
21. M. Picornell, R. L. Lytton, and M. Steinberg. Matric Suction Instrumentation of a Vertical Moisture Barrier. *Journal of Transportation,* ASCE, 1983.
22. D. G. Fredlund and R. K. C. Lee. Measurements of Soil Suction Using the MCS 6000 Sensor. *Proc., Fifth International Conference on Expansive Soils,* Adelaide, South Australia, May 1984.
23. C. J. Phene, G. J. Hoffman, and R. S. Austin. *Controlling Automated Irrigation with Soil Matric Potential Sensor.* Transactions of the American Society of Agricultural Engineers, St. Joseph, Missouri, Vol. 16, 1973, pp. 773–776.

Publication of this paper sponsored by Committee on Environmental Factors Except Frost.

Roadway Performance in an Expansive Clay

RONALD F. REED

The performance of three pavement designs with expansive clay subgrade is presented. The pavements have been subjected to extensive warping attributed to differential swelling of the underlying soil. The purpose of this paper is to evaluate the effectiveness of the three designs in reducing warping, and to provide suggested alternative designs. The study focuses on pavements west of Dallas, Texas, situated over weathered shale of the Eagle Ford geologic formation. The weathered shale is highly expansive with heaving in excess of 12 in. being recorded. Postconstruction heave is attributed to increase in the soil moisture regime over time. Pavement warp occurs primarily in deep cut areas where the finished grade lies near or below the original zone at which soil moisture was stable and was not influenced by seasonal fluctuations. Data indicate that the overall movement of the pavements studied was upward. Differential vertical movements caused warping. The differential movement is attributed to the influence of: (a) underground utilities; (b) micro and macro soil structure features; (c) drainage; (d) patterns of water migration; and (e) stress release. The study evaluates the performance of three specific pavements. Subgrade treatments used to minimize potential movements included removal and replacement with lime stabilized soils and inert fills, and maintaining positive drainage. Alternative subgrade treatment by preswelling is discussed. Modification of pavement shoulders and base to account for shrinkage and loss of bearing support is a necessary component of preswelling design. Preswelling and suggested base and shoulder modifications are compared to current design techniques used in the area on an economical basis.

Warped pavements founded on expansive clays often result in maintenance costs that are experienced sooner in the pavement life than anticipated. Even if the effect of warping is not serious enough for repair, its effect on vehicle operations does little good for the reputation of pavement designers and highway contractors. Warped pavements founded on plastic clays present an opportunity for soils engineers. Warping as used in this paper is a term applied to a phenomenon caused by differential expansion of the pavement's underlying soils. Soil expansion causes a roller-coaster effect or series of successive waves that extend across the pavement section. By comparison, surface depressions caused by shrinkage are generally limited to the outside edges of the pavement and do not extend across the entire width, as is the case in the expansion of underlying joints. For relatively thin pavement sections, failure can occur in either case as a result of loss of continuous subgrade support. Shrinkage can be and has been effectively controlled by the addition of either vertical or horizontal barriers *(1–4)* or by the extension of the pavement shoulders *(2, 4)*, or both. Little attention has been given to controlling expansion with its resultant warping effect on pavement.

Rone Engineers, 11234 Goodnight Lane, Dallas, Tex. 75229.

Reviewed in this paper are pavement design and performance in a specific geologic formation, the Eagle Ford, the outcrop residual soils of which are prone to swelling. The paper is based on general observation of pavement performance throughout the local area and on the evaluation of three sites west of Dallas, Texas. An example of pavement movement in this formation due to heave is shown in Figure 1. The information and recommendations herein are considered to be applicable in varying degrees to other expansive soils derived from other parent geologic formations.

FIGURE 1 Observed pavement warp, Westbound, I-635 near MacArthur Blvd., Irving, Texas. Design section shown in Figure 4.

GEOLOGIC DESCRIPTION

The Eagle Ford Group is a marine-deposited montmorillonitic clay-shale of the Cretaceous Age. Weathering of the formation results in relatively dry, thick, deep, potentially expansive clays. Depth of weathering typically varies from 10 to 35 ft. Surface movements in excess of 12 in. have been documented by the author based on survey data *(5)*.

The weathered shale within the study area exhibits the horizontally bedded structure characteristic of the shale, and is moderately to highly jointed and fissured. The soil fabric is dense and relatively impermeable; however, the mass permeability is greater because of the joints and fissures.

The moisture content of the soil below the zone of seasonal moisture variation is generally 2 to 4 percentage points below the plastic limit and becomes drier with depth. Samples subjected to constant volume swell (CVS) tests exhibit swell pressures on the order of 10 to 15 ksf and volumetric swell of 10 to 15 percent. A typical soil moisture profile with pressure swell test results is shown in Figure 2. The zone of seasonal moisture variation is relatively shallow approximately 7 to 10 ft below the surface. The shallowness is attributed to the following causes, among others: rolling site topography, which enhances surface drainage, and the propensity of the surface soils

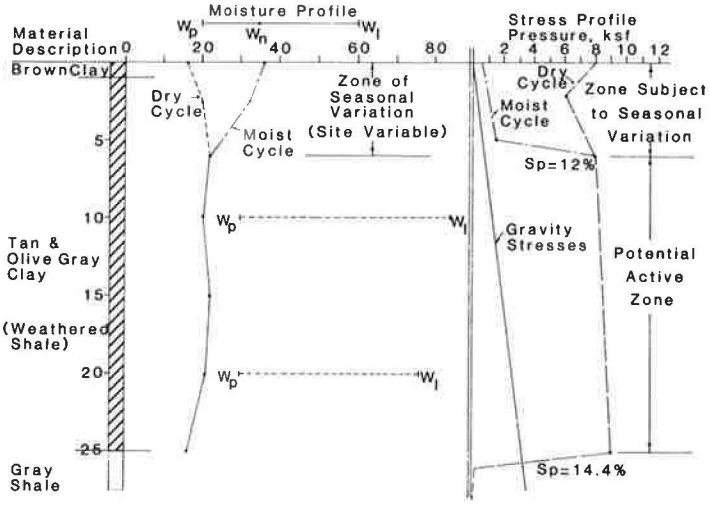

FIGURE 2 Active zone of movement.

to swell and decrease their permeability. The jointed and fissure structure may also contribute by inhibiting soil suction between adjacent soil blocks.

Perched groundwater is intermittently present in varying degrees along the weathered/unweathered interface. Perched groundwater is attributed to surface infiltration and gravity flow through joints and fissures and along weathered patterns. Subsurface channelization is not uncommon and, coupled with the intermittency of the perched groundwater, can make prediction of the hydrogeologic conditions difficult.

ACTIVE ZONE OF MOVEMENT

The active zone is defined as the soil column, measured from the surface, which is subject to potential movement. It extends well below the zone of seasonal moisture variation and frequently is in excess of 20 ft. This depth of active soils is considered to be a result of the high swell pressure and volumetric swell characteristics exhibited throughout the soil or weathered profile. An active zone to this depth is not unique to the Eagle Ford, with depths in excess of 20 ft reported by both Johnson *(6)* and Komornick *(7)* in other formations.

The concept of the deep active zone, and one which is subject to seasonal moisture variation, is shown in Figure 2. The swell pressure for the upper soils is seasonally variable dependent on soil moisture; whereas below the seasonal zone the swell pressures of clay shales can be above the available gravity stresses for significant depths.

An awareness of the full potential of the active zone is necessary if an accurate prediction of surface movement is to be made. The concept of a seasonal zone underlain by a deeper active zone is also important from a design aspect. For example, if free water is introduced relatively deep (15 to 20 ft) from a utility trench system, the resultant swelling will be reflected in pavement warping at the surface.

LITERATURE REVIEW

Several excellent sources are available that treat the general subject of roadway design over expansive clays *(1, 2, 8)*. Based on the literature, the following items appear to be common to clayey, shrink-swell formations:

1. An increase in soil moisture in unsaturated clays occurs immediately beneath the center of the pavement over time. Among the causes attributed to this rise are a reduction in evapotranspiration and changes in temperature and surface water ingress through joints and cracks in the pavement.
2. Shoulders and pavement edges, if unprotected, will reflect cyclic movement (shrink-swell) associated with seasonal variation in soil moisture.
3. Removal of a limited depth of expansive clay and replacement with inert fill in formations where the active zone extends to substantial depths is not effective if water is made available to the underlying clay *(1, 2, 8)*.
4. The use of permeable soil as backfill for utility lines can result in heave due to swelling of the underlying and adjacent clays as the permeable fills can become a conduit for free water to flow to the deeper or adjacent clays.
5. Altering the groundwater regime can initiate deep-seated movement.
6. The use of thick pavement sections to act as a surcharge is generally not effective over soils exhibiting high swell pressures *(2, 7)*. Thicker sections can, however, spread the movement over a greater distance.
7. Moisture barriers, either horizontal or vertical, are effective for stabilizing soil moisture, provided complete cutoff of water can be obtained *(3, 4)*.
8. Prewetting the subgrade has been effective in reducing postconstruction movement *(1, 2, 9–11)*.

This list is far from exclusive. However, it enumerates some of the common factors involved with roadway design over an expansive soil.

The methods for design in clays exhibiting high swell potential can be effectively divided into two views: wet or dry, dependent on the condition of the subgrade before placement of the pavement. The dry approach requires the postconstruction maintenance of moisture conditions existing at the time of placement; that is, the use of either horizontal or vertical barriers. The wet approach, alternatively termed preswelling,

attempts to elevate the subgrade moisture before placement of the pavement.

The amount of water needed to effectively preswell the clays is definable through evaluation of the soil properties. A technical explanation is beyond the scope of this paper. For general purposes, it can be assumed that the amount of water added will be the amount needed to bring the moisture content 2 to 4 percent above the clays' plastic limit.

Suggested preswelling techniques consist of delaying construction through the rainy season *(11)*, ponding *(1, 2, 10)*, and pressure injection *(9)*. Postconstruction heave control by lime slurry pressure injection was reported by Cothren *(9)*, although the pavement was only 2 years old at the time of the report.

CASE STUDIES

Pavements constructed by city, county, and state agencies and private developers within Dallas County, Texas, underlain by outcrops of the Eagle Ford Group, have experienced warping to varying degrees. These areas are generally limited to locations where cuts of varying amounts were required to establish finished grade.

Cursory examination of pavement performance at 12 locations indicated that the unaffected areas were situated in either deep fill sections, very deep cut sections, or were underlain by varying thicknesses of alluvial or terrace deposits. Lack of movement in the areas of very deep cut is attributed to the exposure of the unweathered shale as a subgrade soil.

In order to provide more exact information, three specific sites were chosen that incorporate different design sections. Each of the three locations was evaluated for exposed geologic conditions; the number of individual warps per length of roadway, drainage, cut or fill conditions; presence of underground utilities; and the design section. A summary of the evaluated items for each site is provided in Table 1. More detailed information on each site is provided in the following paragraphs.

Site 1: Farm to Market 1382, Cedar Hill

This section of Farm to Market (FM) 1382 studied consists of the relocation portion around the recently completed Joe Pool Lake, southwest of Dallas, Texas.

The design used for both cut and fill sections is shown in Figure 3. No utilities are shown on the plans in the affected area studies, nor were any observed on site. All of the warping occurred in cut sections. Good drainage of surface water appeared to have been established and maintained by the use of bar ditches.

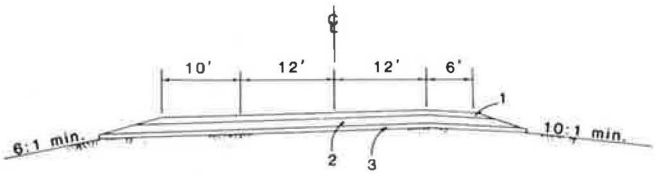

1. 7.5" Asphaltic surface and base.
2. 12" Foundation course, weathered Limestone with 2% lime.
3. 6" lime subgrade, 4% hydrated lime.

FIGURE 3 Design section, Site 1, F.M. 1382.

Individual warps in groups of two and three were observed. The ridge line of the warp extended transversely across the pavement, with the width of the warp as measured perpendicular to the ridge being 35 to 60 ft in length. Differential movement perpendicular to the ridge was observed to be 3 to 6 in. Typically, differential movement was greater toward the uphill side of the original grade. A transverse pavement crack was present along the center of the ridge of approximately one-half of the observed warps.

Based on the general transverse nature of the warp, subgrade heave at Site 1 is attributed to perched water traveling through the joints and fissures of the weathered shale or through the weathered limestone used as a base, or both. Where the design was concerned, no special precautions were taken to account for a swelling subgrade or the naturally complex hydrogeologic conditions compounded by construction operations.

Site 2: Westbound Interstate Highway 635, Immediately East of MacArthur Boulevard, Irving, Texas

The warping at this site consisted of 20 individual warps over a 1.5-mi length of roadway. The length of warps varied from approximately 50 to 100 ft, with differential vertical movement of 3 to 6 in. The roadway is approximately 7 years old and has

TABLE 1 OBSERVATION SITES AND ROADWAY PERFORMANCE

Site No.	No. of Warps/Length (mi)	Drainage Conditions	Cut or Fill	Utilities	Approximate Age (yr)	Comments
F.M. 1382	15/2.1 (southbound)	Drained away from pavement	Cut	None	6	Section presently being overlaid with asphalt
	17/1.3 (northbound)	Nonirrigated				
MacArthur Blvd.	6/0.20	Controlled construction grade/ surface drained to pavement	Cut	Numerous, with special backfill detail	4	Two panels replaced
		Irrigated				
I-635	10/0.50 (westbound)	Drained away from pavement	Cut	None	6–7	Section replaced and overlain
	20/1.50	Nonirrigated				

experienced distress at this location since construction. The design section is shown in Figure 4.

Project plans indicate that cuts of 12 to 27 ft were required to establish grade. Borings indicate that the top of the unweathered shale is at a depth of about 40 ft. Utility lines are not shown to be present under the roadway. Positive drainage of surface water away from the pavement was provided.

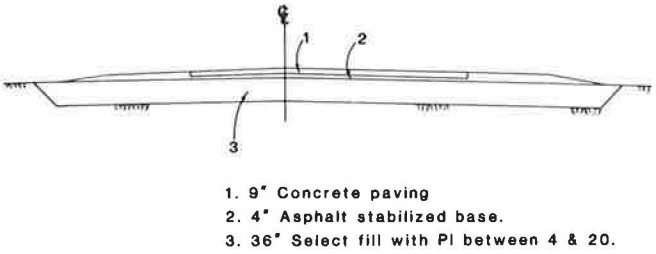

FIGURE 4 Design section, Site 2, Westbound I-635 at MacArthur Blvd.

As shown in Figure 4, special precautions in the form of overexcavation and replacement were taken in the design to account for the presence of expansive Eagle Ford clays. The existing soils were overexcavated to a depth of 36 in. and replaced with nonexpansive fill. Examination of Figure 4 shows that the nonexpansive fill extended beyond the surface of the roadway and shoulders.

Based on the design section, the soils encountered at a nearby outcrop, and the amount of cut required to establish grade, subsurface conditions at the completion of excavation consisted of varying thicknesses of weathered shale. Since construction, the clays (weathered shale) have expanded because of the availability of water. It is anticipated that water is made available both by surface runoff infiltrating the sandy subbase and by perched groundwater flowing along preexisting weathered channels.

The pavement warp here is attributed to moisture infiltration into the subgrade clays and subsequent differential expansion. The warping is not considered to be a result of the seasonal variation in moisture because of the relatively wide shoulders that provide a horizontal barrier and because the warping extends across the width of the pavement.

Site 3: MacArthur Boulevard, North of Interstate Highway 635, Irving, Texas

MacArthur Boulevard consists of an 8-in. concrete pavement over a modified subgrade. Subgrade modification consisted of a single, 3-ft-deep lime slurry injection, with scarification of the surficial lime into the upper 6 in. of subgrade. Utilities are present under the pavement. The utilities were encased in concrete, with native clay soils used as backfill. Utility lines parallel and adjacent to the eastside of the pavement were bedded in gravel and backfilled with a clayey sand. The design section is shown in Figure 5.

Movement of the pavement since project construction is shown in Figure 6. Within the portion of the roadway underlain by residual soils, measured movements have ranged from 2.0 to 11.5 in. Movements shown in Figure 6 were measured

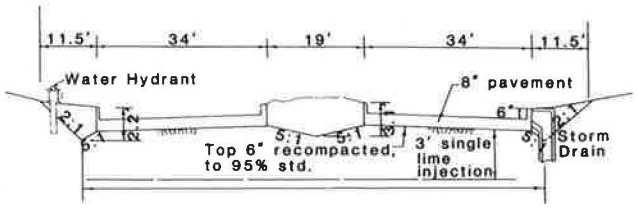

FIGURE 5 Design section, Site 3, MacArthur Blvd.

along the east gutter line, but similar movements were measured 11 ft west of the east gutter. As at Sites 1 and 2, the observed warping extended across the width of the pavement.

The proximity of the warps to existing utility lines is evident in Figure 6. Observations over the last 4 yr have shown a progressive extension of the warping from east to west.

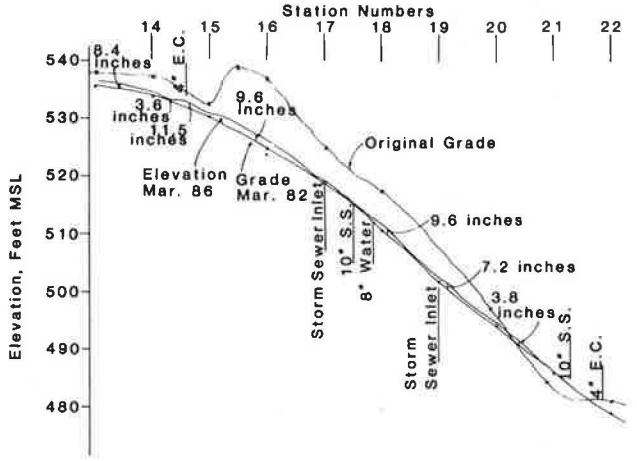

FIGURE 6 Natural finished grades along the east curb line, Site 3, MacArthur Blvd.

Two soil borings were made through the roadway at the location of a heave immediately underlain by a utility line. These borings encountered perched water in the backfill clays, and an elevated soil moisture in the adjacent natural soils. Based on the borings and subsequent utility excavation, it is believed that the native clay backfill was placed in a dry condition in the form of small clods. Water traveling in the gravel bedding and sand backfill of a nearby utility line adjacent to the uphill side of the pavement (east) flowed through the backfill of the utility line beneath the pavement and became accessible to the relatively dry natural clays both below and adjacent to the excavation.

ALTERNATIVE DESIGN CONSIDERATIONS

Alternative designs must answer two basic questions: Will the design perform acceptably? and Is the cost/benefit ratio acceptable? Cost/benefits were analyzed by comparing a typical section used in the Dallas area for a particular section versus the sections currently used in the Eagle Ford geologic formation.

Analysis of the costs associated with construction of a section of heavy highway were analyzed by comparing a section used for I-635 west of I-35E (Site 2) to another section of I-635 east of I-35E. The section of I-635 west of I-35E is shown in

Figure 4. The design section for I-635 east of I-35E consists of 8-in.-thick concrete, over a 6-in.-thick lime stabilized low Plasticity Index imported fill (PI 6 to 15) over a 6-in.-thick lime-stabilized (3 percent) subgrade. A comparison of the costs associated with construction of these two sections is presented in Table 2. The I-635 section west of I-35E costs approximately $41.75/yd^2 compared to $26.35 yd^2 east of I-35E, for a cost differential of $15.40/yd^2. Neglecting the cost of extraordinary maintenance for warped sections of alternative designs resulting in pavement costs less than $41.75 appears to be reasonable.

TABLE 2 SUMMARY OF COSTS, HEAVY HIGHWAY SECTIONS

Item	Cost/yd^2 ($)
9-in. concrete pavement	23.00
4-in. asphalt stabilized base	9.95
36 in. of imported fill, including excavation, Plasticity Index between 4 and 50	8.80
Total approximate cost I-635 section comparable to Figure 4	41.75
Section 2, I-635 east of I-35E	
8-in. concrete pavement	20.00
6-in. lime stabilized imported fill	3.90
6-in. lime stabilized subgrade	2.45
Total approximate cost, I-635 east of I-35E	26.35
Cost differential, Section 1 to 2	15.40

Costs associated with thinner sections were evaluated using a collector street of standard design, which consists of 8 in. of concrete over 6 in. of 6 percent lime stabilized subgrade as a base cost. This standard design section costs, in the Dallas market, approximately $22.45/yd^2. Removal of the pavement and replacement with an equal section, a typical method used to correct excessive warping, is estimated to cost $30.00/yd^2. Considering the replacement costs, some additional expenditure could be economically supported at the time of construction if it would preclude repair later in the form of pavement removal and replacement. Conservatively, approximately 10 percent of the concrete pavements in the Dallas area situated on the Eagle Ford formation are replaced over a 20-yr period.

As previously discussed, there are two design philosophies considered to be applicable in this geologic formation: wet or dry. The wet philosophy is to preswell a portion of the active zone before placement of the base and pavement. The dry approach consists of maintaining the existing soil moisture below the pavement structure. Due to the depth of the active zone and high volumetric swell, complete removal and replacement of the soil with less active or inert soils is not considered feasible.

If a dry approach is to be used, the barriers to subgrade water must account for the complex hydrogeology of the site as well as obvious manmade features and environmental changes imposed by development. Perched, intermittent groundwater is frequently encountered at the interface of the weathered/unweathered shale. Seepage occurs through both macro and micro discontinuities, and follows the pattern of weathering, which does not always follow surface topography. Intermittent groundwater made available to subgrade clays that have heretofore been dry, or that have reduced stress associated with cuts, will swell.

Utility lines backfilled with permeable soils provide an obvious source of water transmission. Use of impermeable backfill, while essential, may not stop the availability of water. Impermeable backfills perpendicular to the gradient of perched water can impede flow, building up higher gradients, or force the water to travel through other discontinuities, either of which provide water to relatively dry subgrades.

Alternatives such as clay backfill in utility lines under roadway sections, or incorporation of subsurface drain systems down the gradient of the roadway, or both, may be beneficial. The most important factor, if the dry approach is to be successful, is to account for all sources of potential water. As seen in the three study sites, and based on the author's experience with both paving and structures in this formation in the Dallas area, successful application of a dry approach is difficult.

Thicker pavement sections can reduce the effect of the warping by spreading the differential movement over a greater horizontal distance. As evidenced by pavement performance at Site 2, however, even relatively thick sections have not proven effective. Partial removal of the clays immediately under the pavement section and replacement with nonexpansive clayey sands is not recommended. Ponding of water in the more permeable clayey sands above an underlying clay must be prevented, or deeper movements will occur.

The wet approach consists of preswelling the subgrade before construction of the base or pavement. Preswelling by ponding has been effectively used in this and other formations *(1, 2, 10, 11)*. Postconstruction shrinkage can then be effectively controlled by installation of either horizontal or vertical barriers.

Difficulties associated with ponding consist of the time involved, the extremely wet surface at the completion of ponding, and the problem of getting deep penetration of the water. The use of the post holes in conjunction with ponding is a variation that can aid faster penetration of water to deeper depths. The post holes must, however, be sealed at the completion of ponding operations unless successful swelling throughout the active zone is accomplished, in order to control the availability of additional water to the deeper zone. Otherwise, available water can result in postconstruction heave at depths below previously swelled soils.

A suggested alternative to ponding consists of deep, multiple-pressure injections. The injections may consist of either water with surfactant coupled by a surface seal or a combination of lime slurry and water injections. The purpose of the lime injection is to provide a surface seal to maintain the injected moisture during the construction phase before placement of the base and wearing surface. Multiple water injections are necessary to provide free water in the joints, fissures, and hydraulic fractures for absorption by adjacent clays. Time between injections must be allowed for absorption and swelling to occur. The time interval is considered to be dependent upon the clay structure and the spacing of joints and fissures, but is generally 2 to 4 days. Three to five injections are typically necessary to sufficiently preswell these soils.

(The lime slurry pressure injection industry contends that an increased strength and a reduction in moisture migration is obtained by multiple lime slurry injections. This point is not

debated one way or the other. However, the main benefit of pressure injection in this geologic formation is considered to be one of preswelling by induced moisture.)

The depth of injection is dependent on the desired reduction in potential movement, but generally varies from 3 to 10 ft. The author personally prefers the deeper injections.

An alternative subgrade treatment for a city street (8-in. pavement) incorporating preswelling consists of one lime followed by three water injections to a depth of 8 ft. This subgrade treatment adds approximately \$2.00/yd^2 of pavement to the costs previously cited (\$22.45).

An alternative heavy highway design incorporating preswelling is shown in Figure 7. The savings of this section compared to the section used for I-635 (Site 2) amounts to \$7.86/yd^2.

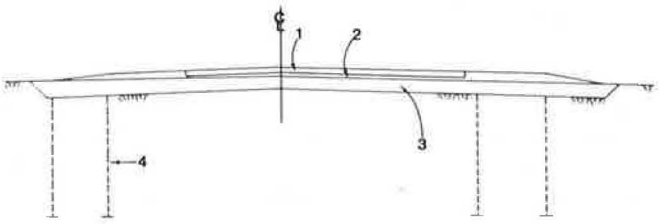

1. 9" Concrete paving.
2. 4" Asphalt stabilized base.
3. 20" Lime stabilized fill & subgrade.
4. 1 Lime - 3 Water injections to 8' depth.

FIGURE 7 Alternative highway design with preswelled subgrade.

Preswelling by injection under roadways has not been extensively addressed in the design community. Part of the lack of use of this technique is attributed to the mysticism associated with the injection process. Experience shows that the preswelling process has been used under building slabs in this formation for over 12 yr, with a high degree of success. The use of dry techniques, removal and replacement, or installation of horizontal or deep vertical barriers, or both, has not been successful, with results not unlike the roadways observed.

CONCLUSIONS

Based on the preceding case histories and discussions, the following conclusions are presented:

1. Soils of the Eagle Ford geologic formation within the Dallas area cause warps in pavement because of differential swell.
2. None of the pavement designs in the Dallas area reviewed effectively controlled pavement warp.
3. For the dry approach in design, all potential sources of water must be considered and positively controlled during and after construction.
4. Preswelling, based on previous work by others on roadways and by the author under buildings in this formation, appears to be a viable solution. Preswelling via post hole and ponding and by multiple injections has performed satisfactorily.

REFERENCES

1. D. R. Snethen et al. *A Review of Engineering Experiences with Expansive Soils in Highway Subgrades.* FHWA-RD-75-48, Federal Highway Administration, Washington, D.C., NTIS No. AD A020309, June 1975.
2. D. R. Snethen. *Technical Guidelines for Expansive Soils in Highway Subgrades.* FHWA-RD-79-51, Federal Highway Administration, Washington, D.C., NTIS No. PB 80-139550, June 1979.
3. M. L. Steinberg. Geomembranes Used to Control Expansive Soil. *Proc., International Conference on Geomembranes.* Industrial Fabrics Association International, New York, Vol. II, June 1984.
4. D. H. van der Merwe, F. Hugo, and A. P. Steyn. The Pretreatment of Clay Soils for Road Construction. *Proc., Fourth International Conference on Expansive Soils*, Denver, Colo., ASCE, Vol. I, June 1980.
5. R. F. Reed. Foundation Performance in an Expansive Clay. *Proc., 38th Canadian Geotechnical Conference.* Canadian Geotechnical Society, Rexdale, Ontario, Canada, Sept. 1985.
6. L. D. Johnson. *Overview for Design of Foundations on Expansive Soils.* Miscellaneous Paper GL-79-21, U.S. Army Engineer Waterways Experiment Station, Vicksburg, Miss., NTIS No. AD-A076, Sept. 1979.
7. A. Komornik, G. Wiseman, and Y. Ben-Yaacob. Studies of In Situ Moisture and Swelling Potential Profiles. *Proc., International Conference on Expansive Soils.* American Society of Civil Engineers, New York, Vol. I, 1969.
8. G. Wiseman, A. Komornik, and J. Greenstein. Experience with Roads and Buildings on Expansive Clays. Presented at the 64th Annual Meeting of the Transportation Research Board Session 157, Part 2, Jan. 1985.
9. S. M. Cothren. Roadbed Stabilization by Lime Slurry Injection Process. *Proc., Fifth International Conference on Expansive Soils,* Adelaide, Australia, June 1984.
10. R. L. McKinney, J. E. Kelly, C. McDowell. *The Waco Ponding Project.* Research Report 118-7, Center for Highway Research, University of Texas at Austin, Jan. 1974.
11. D. J. Weston. Expansive Roadbed Treatment for Southern Africa. *Proc., Fourth International Conference on Expansive Soils,* Denver, Colo., American Society of Civil Engineers, Vol. I, June 1980.

Publication of this paper sponsored by Committee on Environmental Factors Except Frost.

Characterization of the Meteorological Demand for the Design of Vertical Moisture Barriers

M. PICORNELL AND R. L. LYTTON

Pavements founded on expansive soils are damaged because of seasonal wetting and drying of the foundation soils. The magnitude of the damage is controlled by the wettest and driest moisture content profiles that occur at the site. The moisture profiles are altered with the removal or replenishment of soil moisture by the meteorological conditions. Because weather conditions cannot be predicted accurately, the extreme moisture content profiles are stochastic. The purpose of this study is to characterize the wettest and driest moisture content profiles that have the desired probability of occurrence during the lifetime of the pavement. The wettest and driest profiles are associated with the respective annual maximum and minimum depths of water stored in the soil profile. The stored depth of water in the soil profile is obtained by using a daily water balance to calculate the accumulation or depletion of water in the profile. The replenishment is due to rainfall and runoff from the adjacent pavement surface. The depletion of the profile is due to the actual evapotranspiration. The daily water balance is calculated using a consecutive series of annual events. Each year is characterized by the maximum and minimum water depths stored in the soil profile. The fact that both the maximum and minimum depths of stored water have distributions of their probability of occurrence makes it possible to define the probabilistic "design event." The design events are the maximum and minimum water depths that have the desired probability of not being exceeded in the lifetime of the pavement. Illustrated in this paper is this method for the climatic areas of Houston, Dallas-Fort Worth, and San Antonio, Texas.

Pavements founded on expansive soils are damaged because of the seasonal wetting and drying of the subsoil. The severity of the damage is determined by the magnitude of the subsoil moisture change from the wettest to the driest moisture profiles.

The subsoil moisture changes are determined by the climatic conditions at the site. Because weather conditions are unpredictable, the wettest and driest moisture profiles are stochastic. The design moisture profiles are the most extreme conditions that can reasonably be expected to occur during the lifetime of the pavement. These extremes can be evaluated based on the historical record of meteorological data for the site. This permits the determination of the probabilities of occurrence of the annual driest and wettest subsoil conditions. The annual extreme moisture profiles with a return period equal to the design life of the pavement are the design climatic conditions needed to select the minimum depth of the vertical moisture barrier.

M. Picornell, Civil Engineering Department, University of Texas at El Paso, El Paso, Tex. 79968. R. L. Lytton, Texas Transportation Institute, Texas A&M University, College Station, Tex. 77843.

This paper presents a semiempirical approach to evaluating the design intensities of the wettest and driest moisture conditions of the subsoil; describes the statistical analysis used to choose the design extremes; and presents a summary of the results obtained for the regional climatic conditions of San Antonio, Dallas-Fort Worth, and Houston, Texas. These three sites have broader implications for the United States because they are located in a moisture transition zone between wet and dry climates. Design events that are defined for these locations can probably be used for other sites in the wet and dry climatic zones.

CHARACTERIZATION OF THE SUBSOIL MOISTURE CONDITIONS

The aspect that has received most of the attention in the existing literature is the characterization of drought. In some disciplines, like hydrology, and for the earliest climatologists, drought is synonymous with a lack or deficit of rainfall. This aspect is discussed by Blumenstock *(1)*. He determines probabilities of runs of consecutive dry days for different sections of the United States using the criterion that the drought spell is over when a precipitation of 0.1 in. falls in a 48-hr period.

Thornthwaite *(2)* uses a precipitation-efficiency index to distinguish several types of climate. Based on this index, he prepared maps of the United States *(3)* and attached probabilities to the occurrence of drought during the growing season. This appears to have been the first attempt to tag a probability to the occurrence of drought *(4)*.

Rainfall is only the input into the soil profile, and a proper characterization of drought should also include how much is being taken out of the soil by evapotranspiration. The first and probably most well-known procedure including both components was proposed by Thornthwaite *(5)*. It considers the potential evapotranspiration (PET), which is determined from the average monthly air temperatures, and proposes a moisture index that compares PET and rainfall on a monthly basis.

All of these earlier procedures are assessed on a monthly basis and they neglect the influence of the soil profile as a moisture reservoir of varying capacity *(4)*. By way of contrast, on a daily basis it is possible to consider the inefficiencies of rainfall, losses as run-off, or evaporation as the soil is depleted and the PET cannot take place.

When the procedure is done on a daily basis, the soil profile is considered as a storage reservoir of soil water, characterized

by the maximum water depth available to plants, from maximum capacity to the point where insufficient water is available to the root system. However, two essentially different alternatives exist. The first one takes the drought as a relative condition *(6)*. Essentially, it considers, for example, that a given weather condition that might be considered a severe drought in the Northeast could be considered a wet period in west Texas. The method developed by Palmer *(7)* uses an accumulated severity index combined with the length of the dry period. The procedure measures variations from a normal or average condition, and the method can be used to characterize either dry or wet periods.

In the second alternative, proposed by van Bavel *(8)*, drought is considered to be an absolute condition, in which plant growth starts to be limited. In this approach, drought is characterized by the length of persistence of a certain condition or unit of measure: the "drought-day" *(4)*. This is defined as a 24-hr period in which the soil moisture stress exceeds a limit at which the conditions for plant wilting persist. As each growing season is characterized by the number of drought-days, it is possible to attach probabilities to the annual number of drought-days.

In this study, the moisture condition of the subsoil is characterized on the based of the soil water depth stored in the soil profile. At field capacity, the soil profile is at its maximum capacity. At the point of wilting of the vegetation, the soil profile is considered to be empty of available water; that is, there is no more soil water available for transpiration or soil evaportation. Probabilities are attached to the annual maximum and minimum water depths stored in the soil profile.

This approach requires the determination of the water depth stored in the soil profile on a daily basis. To perform the frequency analysis of drought intensity, it is necessary to analyze the variation of water depth stored in a soil profile through many years of data, whether historical or simulated stochastic data. The simulation is accomplished with a semiempirical procedure to establish the daily water balance. This requires knowledge of the maximum water storage capacity of the soil reservoir and how the water storage changes with the two possible meteorological conditions, rainfall and PET. The replenishment of water with rainfall is estimated with a proposed empirical procedure to assign runoff based on the depth of the rainfall and the status of the soil water at the beginning of the rainfall. The depletion of water is the result of the actual evapotranspiration. This is obtained from the daily PET with a semiempirical method that separates the PET into potential soil evaporation and potential plant transpiration. The actual rate of each component is estimated based on the status of the soil water stored in the profile and the cumulative soil evaporation and plant transpiration.

EXISTING RECORD OF WEATHER DATA

The meteorological data are available on magnetic tapes from the National Oceanographic and Atmospheric Administration (NOAA), National Climatic Center, Asheville, North Carolina. Two tape decks are used: TD-9750 from the Weather Bureau with the daily summary, and TD-1440 from the Airways Surface Observations, which includes hourly or every-third-hour observations.

The data extracted from these tapes are precipitation, percentage of possible sunshine, sky cover, mean daily temperature, mean relative humidity, and mean wind speed. The first task is to prepare a sequential file for each station with all the information organized in daily blocks for consecutive days. The data recorded hourly or every third hour are averaged out to obtain the daily average. The most relevant information missing from the records is the percentage of possible sunshine, which was not reported before January 1985.

TRANSPORTATIONS OF THE RAW METEOROLOGICAL DATA

All of the daily observations except precipitation are combined into a single variable, the PET, through Penman's formula. This expression is the most widely used to estimate daily evaporation and it is regarded as the most reliable *(9)*.

In the past, it was popular to use the method proposed by Thornthwaite *(5)*; however, this procedure calculates PET based only on incoming radiation and ignores the relative humidity of the air. In semiarid climates or in arid transitional zones *(10)* the relative humidity of the air is a factor as important as or even more important than radiation. Under these conditions, Penman's formula is particularly suitable. Penman's formula *(11)* estimates the potential evapotranspiration for a well-watered short grass, and it is as follows:

$$ET = \frac{\Delta}{\Delta + \gamma} (R_n - G) + \frac{\gamma}{\Delta + \gamma} 15.36 (1 + 0.0062 V) (e_s - e_d) \quad (1)$$

where

ET = potential evapotranspiration in cal cm^{-2} day^{-1};
Δ = slope of the saturation vapor pressure curve in mb/°C at the mean air temperature (mb = millibars);
γ = psychrometric constant in mb/°C;
R_n = incoming net radiant energy available at the evaporating surface in cal cm^{-2} day^{-1};
G = radiant energy lost into the soil mass by conduction in cal cm^{-2} day^{-1};
V = the daily average wind velocity in km day^{-1} at a height of 2 meters;
e_s = mean saturated vapor pressure in mb; and
e_d = actual vapor pressure in mb.

The term $R_n - G$ is the energy available at the evaporating surface. The energy lost into the soil, G, is usually neglected *(9)*, and Ritchie et al. *(12)* have shown that this is negligible until advanced stages of dessication are reached. In this study, G is considered to be zero.

The net radiant energy R_n *(13)* is calculated from

$$R_n = R_a (1 - r) [0.18 + 0.55(n/N)] - \sigma T_a^4 \left[0.56 - 0.08(e_d)^{1/2}\right][0.10 + 8.9 (n/N)] \quad (2)$$

where

R_a = mean extraterrestrial radiation in cal cm^{-2} day^{-1},
r = reflection coefficient taken as 0.2 for green crops,
n/N = percent of possible sunshine hours,
σ = Stefan-Boltzman constant 11.71 10^{-8} cal cm^{-2} day^{-1},
T_a = absolute air temperature (Kelvin), and
e_d = actual vapor pressure of the air in mb.

The mean extraterrestrial radiation R_a is a function of the latitude of the site and the day of the year. R_a is found by interpolating published extraterrestrial radiation data *(11)*.

The percentage of possible sunshine hours (n/N) was not reported before January 1965. However, this parameter has been satisfactorily related to mean daily cloud cover by many investigators *(14, 15)*. This relationship on a monthly basis is obtained by fitting a regression line to the simultaneous record of these two variables. In this manner, the recorded data before January 1965 can be included in the analysis.

The saturated vapor pressure is calculated from the mean absolute air temperature through the expression proposed by Richards *(16)*. The slope of the saturation pressure curve, Δ, is obtained by linear interpolation of the published data *(17)* of the variation on Δ/γ as a function of temperature.

The wind velocity in Penman's formula is the wind velocity at 2 m. The meteorological stations rarely report the wind speed at 2 m. The heights of the measuring instruments are available on the station's annual summaries *(16)*. The wind profile is approximated with a power law function. The exponent has been found to have a typical value of 1/7 in the lower atmosphere under neutral conditions *(17)*. With an exponent of 1/7, the other constant is backfigured from the measured mean wind velocity and the height of the station's measuring instruments.

STOCHASTIC SIMULATION

The design intensity of the subsoil moisture condition is selected based on the relative frequency of occurrence determined on a stochastically generated series of annual events, as it is believed to provide a better estimate of the probability of occurrence than if it is obtained from the frequency analysis based on the historical record alone *(18)*.

The two daily variables that are used to summarize moisture conditions are the rainfall depth and the PET. The stochastic generation used in this study follows in broad terms the procedure proposed by Larsen and Pense *(19)*. The main features are as follows:

1. It accounts for the seasonal periodicity of the climate by considering monthly distributions for the two variables.
2. The occurrence of precipitation is simulated with a first order Markov chain with two states: wet days and dry days.
3. The correlation between precipitation and PET is preserved through using different monthly distributions of Pet for wet and dry days.

A wet day is a day when there has been rain or a trace of rain; otherwise, it is a dry day. The state of one day is assumed to depend only on the state of the previous day through the monthly transition probabilities. These are experimentally determined probabilities of a wet day following a wet day, and of a dry day following a dry day. The division of days into wet and dry is somewhat arbitrary. Nevertheless, the PETs during wet and dry days are noticeably different at all three sites.

The first task consists of selecting the distributions that fit best to the observed monthly histograms of daily precipitation and PET on wet and dry days. This analysis is performed with the computer program "WEATHER". A FORTRAN listing of WEATHER is presented elsewhere *(20)*. This program examines the time sequence and forms the monthly histograms of precipitation and PET on wet and dry days. At the same time, the program counts the monthly totals of wet days, days with only a trace of rain, and the number of dry days preceded by a dry day and the number of dry days preceded by a wet day. The program also fits a number of theoretical distributions to the observed histograms and calculates the test statistic for a chi-square goodness-of-fit test.

The monthly distributions of precipitation are formed with precipitation amounts higher than a trace (higher than 0.005 in.). The occurrence of trace amounts is summarized by the probability of having trace amounts in wet days, which is determined as the ratio of the number of days with a trace of rain over the total number of wet days. This probability is defined on a monthly basis, and it is assumed to be constant within each month.

The transition probabilities are also assumed to be constant within each month. The monthly dry day transition probabilities were calculated as follows:

1. The dry-dry transition probability is the ratio of the number of dry days preceded by a dry day over the total number of dry previous days, and
2. The wet-dry transition probability is the ratio of the number of dry days preceded by a wet day over the total number of wet previous days.

The monthly wet day transition probabilities were obtained by subtracting the dry day transition probabilities from 1.

The theoretical distribution fitted to the more-than-trace-amount of rainfall is a gamma distribution with an exponent of less than 1, which results in a distribution asymptotic to both the x and y axes in the first quadrant. The parameters of these distributions are calculated using the approximate maximum likelihood estimators of Greenwood and Durand *(21)*.

The monthly distributions of PET are formed separately for dry days and wet days. A beta distribution of zero lower bound is fitted to these data. The upper bound is treated as an additional parameter of the distribution. This upper bound is obtained by successive iterations as the value that minimizes the test statistic. For each iteration, the moment estimators are used to determine the other two parameters.

The stochastic simulation consists of generating a specified number of 1-year events of 365 days. This involves the generation of random observations from gamma and beta distributions. The simulation process is dominated by the first-order Markov chain used to simulate the occurrence of precipitation.

The total number of annual events generated is decided based on the design life of the pavement. In this study, the time

length of the generated sequence is one order of magnitude longer than the return period of the design event. The data are generated with the computer code "STOCHAS", whose FORTRAN listing is presented elsewhere *(20)*.

SOIL-WATER BALANCE

The parameters that intervene in the soil-water balance are the actual infiltration, the actual evapotranspiration, and the maximum water storage capacity of the soil profile. Another variable with a marked effect is the rainfall multiplying factor (RMF), which, as described elsewhere *(20)*, takes into account the runoff from the pavement surface.

The RMF is a function of the cross section of the pavement. The maximum water storage capacity of the soil profile is also a site-related parameter. To cover all possible cases to be encountered in a climatic region, these two parameters are assumed to have a range of values; the RMF is assumed to range from 1 to 5, and the maximum water depth capacity of the soil profile is assumed to range from 20 to 65 cm of water depth. With this approach, the soil-water balance is only a function of the regional climatic conditions and is independent of site-related characteristics.

The rest of this section describes how to obtain the actual infiltration from the rainfall depth, and the actual evapotranspiration from the PET.

Calculation of Infiltration

To formulate the water balance, it is necessary to estimate the portion of the rainfall plus runoff from the pavement that is not used in replenishing the soil profile. A variety of empirical procedures exist *(22, 23)*; most of them assign an empirical rate of runoff based on an antecedent condition and the rainfall depth. The antecedent condition is usually related to the amount of rainfall in a period of several days immediately preceding the event.

In this particular study, the soil-water depth stored in the soil profile is known at all times, and, intuitively, it appears that this should be a much better choice for the antecedent condition than the immediately preceding rainfall. This aspect is evaluated based on hydrologic measurements obtained from a grassed watershed in Riesel, Texas. These data were provided by the U.S. Department of Agriculture, Blacklands Conservation Center, Temple, Texas.

The measurements correspond to the watershed SW-12. This watershed has a typical central Texas swelling clay profile that is covered with native Texas grass. The only cultivation is to mow the grass once a year. The data available include daily rainfall and runoff depths from 1977 through 1982, and approximately biweekly measurements of stored water depth in the profile since the middle of 1979.

The alternative considered is based on the fact that the infiltration is limited to some maximum, based on the water depth deficit of the soil profile at the start of the event. How fast this water deficit can be replenished is a function of the permeability and the sequence of events and rainfall rates. In the case of a swelling soil deposit, there is an additional feature: the shrinkage cracks, which provide some immediate storage of rainfall independent of soil porosity. Holmes *(24)* has shown that, upon drying, a soil ped shrinks but it remains essentially saturated down to water potentials of the order of pF 5. This implies that the volume of water lost is approximately equal to the volume change of the soil profile except under the driest conditions. By assuming that the shrinkage is isotropic and infinitesimal, the linear shrinkage is one-third of the volumetric strain. The shrinkage in the vertical direction does not generate storage volume: only the two-thirds in the two horizontal directions cause the shrinkage cracks that provide the storage for the rainfall. Therefore, the maximum storage volume immediately available is about two-thirds of the total volume of the water deficit. This is true for the first rainfall onto a soil profile with empty cracks. But, once the cracks are partially filled, the storage available is no longer the two-thirds of the water deficit but some smaller fraction.

The value of this fraction is estimated from the soil water depth measurements and hydrologic record of watershed SW-12. For this purpose, the soil water depth antecedent to each event is determined by interpolating between consecutive measurements. The rate of water evaporation is assumed constant in each interval. The rate applicable to each period is found by dividing the water loss (initial minus final soil water measured) plus the net precipitation (rainfall minus runoff during the interval) into the total number of days. The complete set of results is described elsewhere *(20)*. The main conclusion is that this fraction ranges from one-third to somewhat less than two-thirds.

The analyses are repeated for two assumptions of the value of this fraction of one-third and two-thirds. The case of one-third is the high runoff case. The case of two-thirds is the low runoff case. Whatever the value adopted, this fraction is considered to be a limit. Precipitation amounts smaller than this limit are assumed to cause no runoff. When the rainfall exceeds it, this limit is the maximum amount of water absorbed by the soil profile; the excess rainfall is runoff.

The total water depth available to replenish the soil profile is obtained by multiplying the rainfall depth by RMF. The need to include the RMF and the procedure to estimate its value are discussed elsewhere *(20)*. The rainfall depth of 0.05 in. is assumed to be a threshold. Below this threshold there is no runoff from the pavement, and thus the RMF is 1. Above this threshold rainfall, there is runoff from the pavement and the RMF is determined from the cross section of the pavement. If the total water depth available is larger than one-third (or two-thirds) of the water deficit of the soil profile, the excess water depth is considered runoff. If the total water depth available is smaller than one-third (or two-thirds) of the water deficit of the soil profile, all the water available is assumed to replenish the soil profile.

Determination of the Actual Evapotranspiration

The accounting of the water removed from the soil profile follows the semiempirical approach of Richardson and Ritchie *(9)*. This is a simplified method to estimate the actual evapotranspiration based on the PET and the stage of drying of the soil profile, accomplished by splitting the PET into a potential soil evaporation and a potential plant transpiration.

The effect of the stage of drying is then evaluated separately for each component.

The potential soil evaporation (E_{s0}) has been empirically related to the PET and the Leaf Area Index *(25)*.

How much of this potential can actually take place (E_s) depends on the moisture conditions at the soil surface and the moisture transmissivity of the soil matrix. Their effect has been considered *(26, 27)* to take place in two stages of soil evaporation, as follows:

1. The constant rate, or Stage I, when the actual soil evaporation matches the potential; and
2. The falling rate, or State II, when the actual evaporation rate lags behind the potential.

How long the profile remains in Stage I is determined by the cumulative soil evaporation that must remain smaller than a limiting value (U) typical of the soil profile. The cumulative evaporation in Stage I is adjusted on a daily basis adding the soil evaporation and subtracting the effective precipitation. The minimum of this cumulative evaporation is zero, and the effective rainfall in excess of U is not considered to affect it. Once the cumulative evaporation reaches the upper limit U, it remains constant at that value, and the soil profile enters into Stage II of evaporation.

In Stage II, the falling rate of evaporation is estimated following Black et al. *(28)*, who showed that the cumulative evaporation in Stage II is proportional to the square root of time elapsed since the evaporation started on an initially wet soil profile; the constant of proportionality, α, being a function of the hydraulic conditions of the soil matrix.

If the effective rainfall is higher than the cumulative Stage II evaporation, the profile is taken back to Stage I, and the excess rainfall is subtracted from the upper limit U to find the initial cumulative Stage I evaporation. If the rainfall is less than the cumulative Stage II evaporation, then the soil is kept in the Stage II drying, but the time origin is reestimated based on the new cumulative Stage II evaporation.

The values of the soil parameters (U = 6 mm) and [α = 3.5 mm/(day)$^{1/2}$] are adopted from Richardson and Ritchie *(9)* for a typical expansive soil profile in the Texas Blacklands.

Plant transpiration takes place in three distinctive stages of drying of the soil profile. In the first, the transpiration is determined by the atmospheric demand alone. The stage extends from field capacity (a soil water depth of UL), up to a threshold known as the lower limit for potential evaporation (a soil water depth of LLE_0) *(29)*. In the second stage, transpiration is limited by the soil water. This stage extends from LLE_0 to the lower limit of water availability (a soil water depth of LL). In the third stage, plant transpiration ceases altogether.

The actual plant transpiration in the first stage is equal to the potential transpiration. The potential plant transpiration (EP) has been found to depend on the PET and the Leaf Area Index *(30)*.

In the second drying stage, the drop of actual transpiration relative to the potential has been found to be proportional to the square root of time *(29, 31)*.

The last stage occurs when the soil water reaches the water depth LL. This is the minimum water depth attainable. Evaporation and transpiration are assumed to stop when the stored water depth falls to LL.

The actual evapotranspiration (E) is obtained by adding the actual soil evaporation (E_s) to the actual plant transpiration (E_p). If this sum (E) is larger than the PET, the actual evapotranspiration is considered to be the PET.

Formulation of the Water Balance

Soil water is accounted for on a daily basis. The soil water at the end of the day is found by adding the effective precipitation and subtracting the actual evapotranspiration to the soil water that had accumulated the previous day. The soil water depth is not allowed to fall below LL or above UL by neglecting any excess evapotranspiration or precipitation.

The procedure neglects the losses of soil water by deep percolation, or the upward flow from deeper layers. Nevertheless, the permeability of the soil matrix is extremely low, and the assumption of negligible water fluxes in the matrix seems quite appropriate.

The water balance is calculated with the computer program "DROUGHT", whose FORTRAN listing is presented elsewhere *(20)*. The program examines two possible runoff cases: high runoff and low runoff. The program analyzes a sequence of consecutive annual events of 365 days, each keeping an account of the maximum and minimum soil water depths that occurred during each year, and provides a distribution of the relative frequencies for each of the two extreme conditions.

DESIGN EVENTS FOR THREE TEXAS SITES

The design is based on the maximum and minimum soil water depth that is reasonable to expect in the lifetime of the pavement for a desired level of probability. The maximum capacity of the soil profile is treated as a parameter in this study, and the analyses have been performed for a range of soil capacities from 20 to 65 cm in 5 cm increments. The RMF is also treated as a parameter and all of the analyses are repeated for five different values of RMF from 1 to 5. Furthermore, each case considers two alternatives to assign runoff: in the high runoff case, the runoff is computed as all the rainfall exceeding one-third of the water deficit; in the low runoff case, all the rainfall that exceeds two-thirds of the water deficit is assigned to runoff. The low runoff case represents the limiting case; the events defined in this case are the least severe to be expected. The high runoff case is expected to be closer to the field conditions, that is, on the dry side.

The analyses at each site consist of about 25 runs of the program STOCHAS for each assumption of maximum water capacity and case of runoff. One thousand years are stochastically generated for each run. Each series is examined with the program DROUGHT to form the distributions of annual maximum and minimum water depths.

Annual Minimum Water Depths

The complete set of distributions for the three sites has been presented elsewhere *(20)*. These results indicate that the effect of the RMF is to increase the annual minimum water depths. This tendency is consistent for all of the cases studied. For

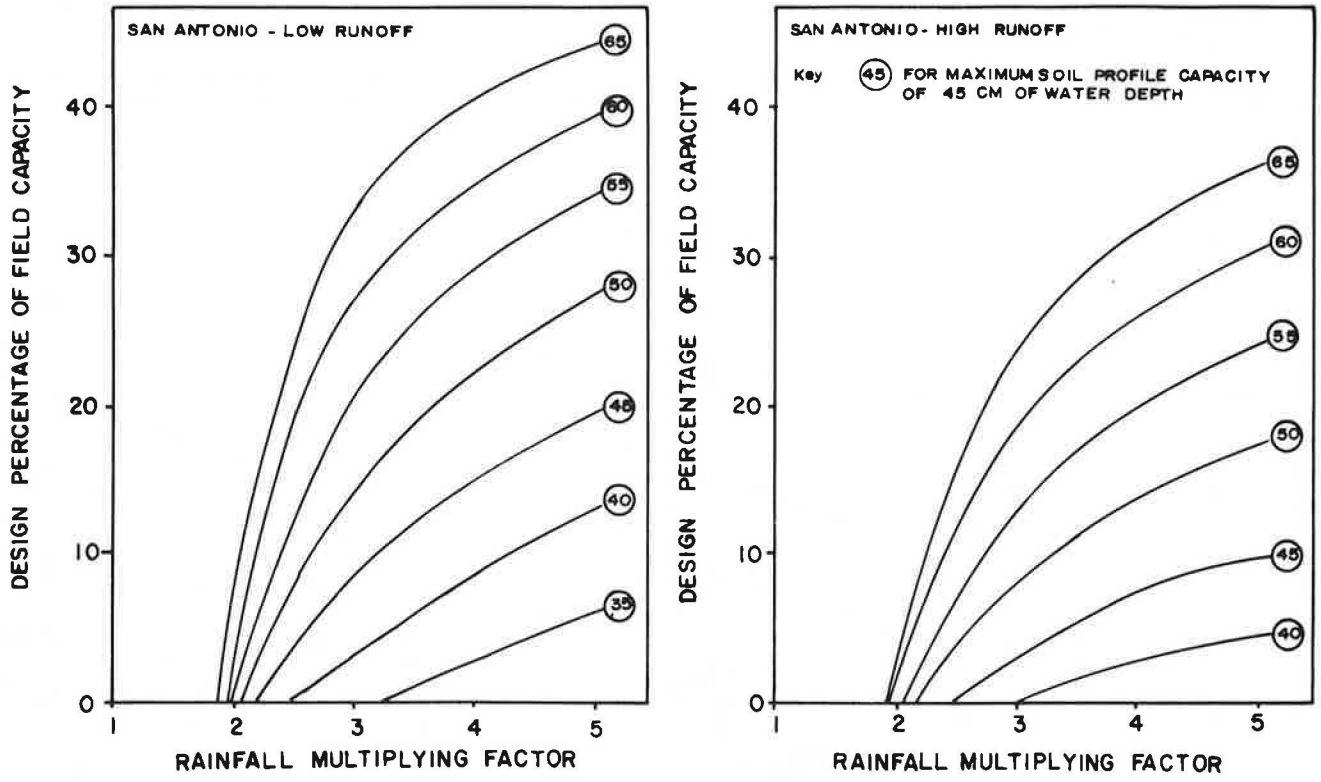

FIGURE 1 Twenty-five-year design events for San Antonio.

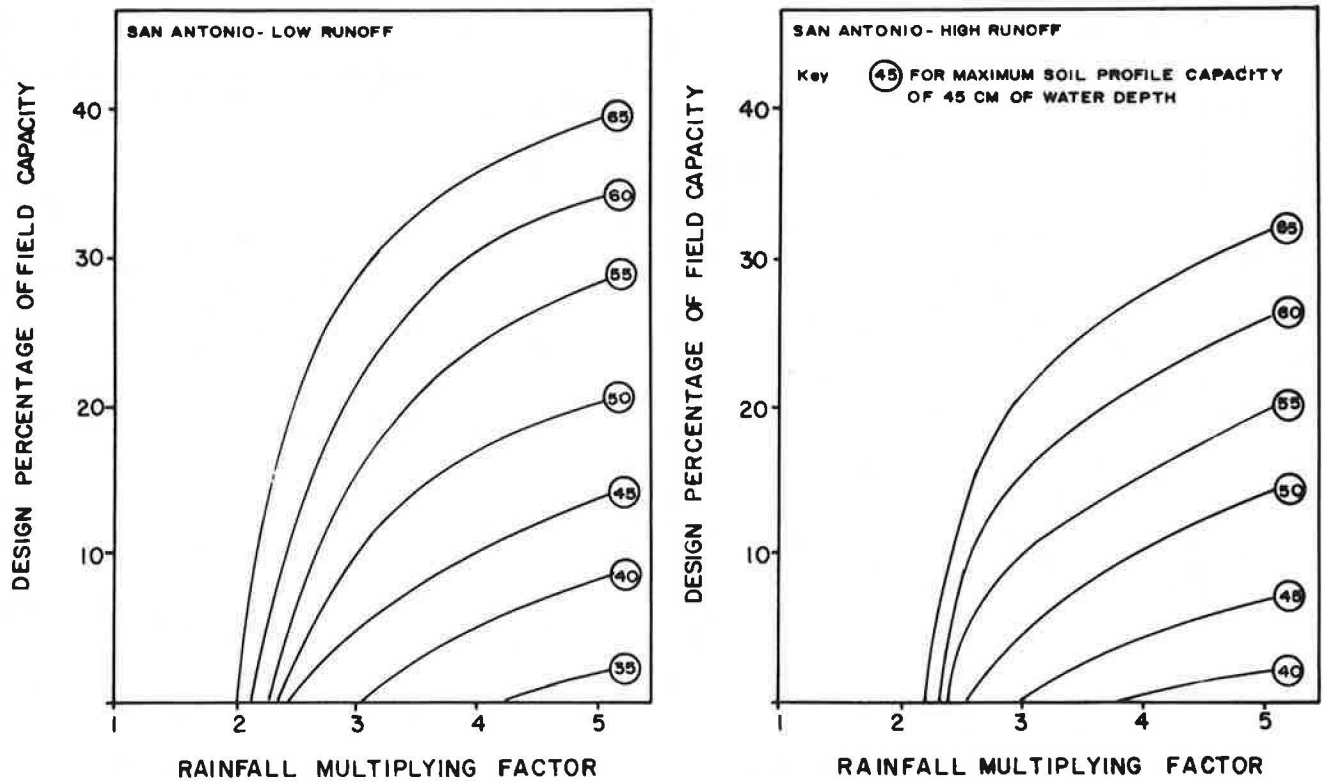

FIGURE 2 Fifty-year design events for San Antonio.

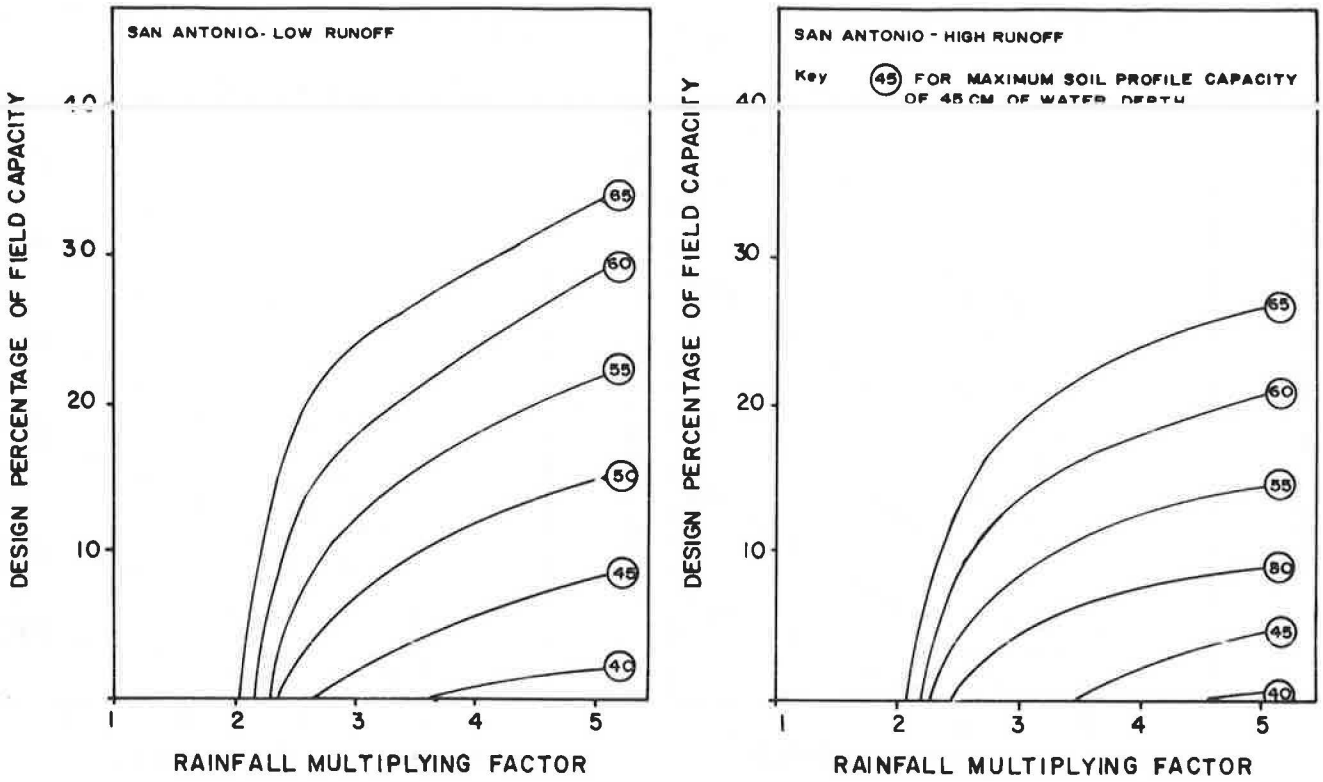

FIGURE 3 One-hundred-year design events for San Antonio.

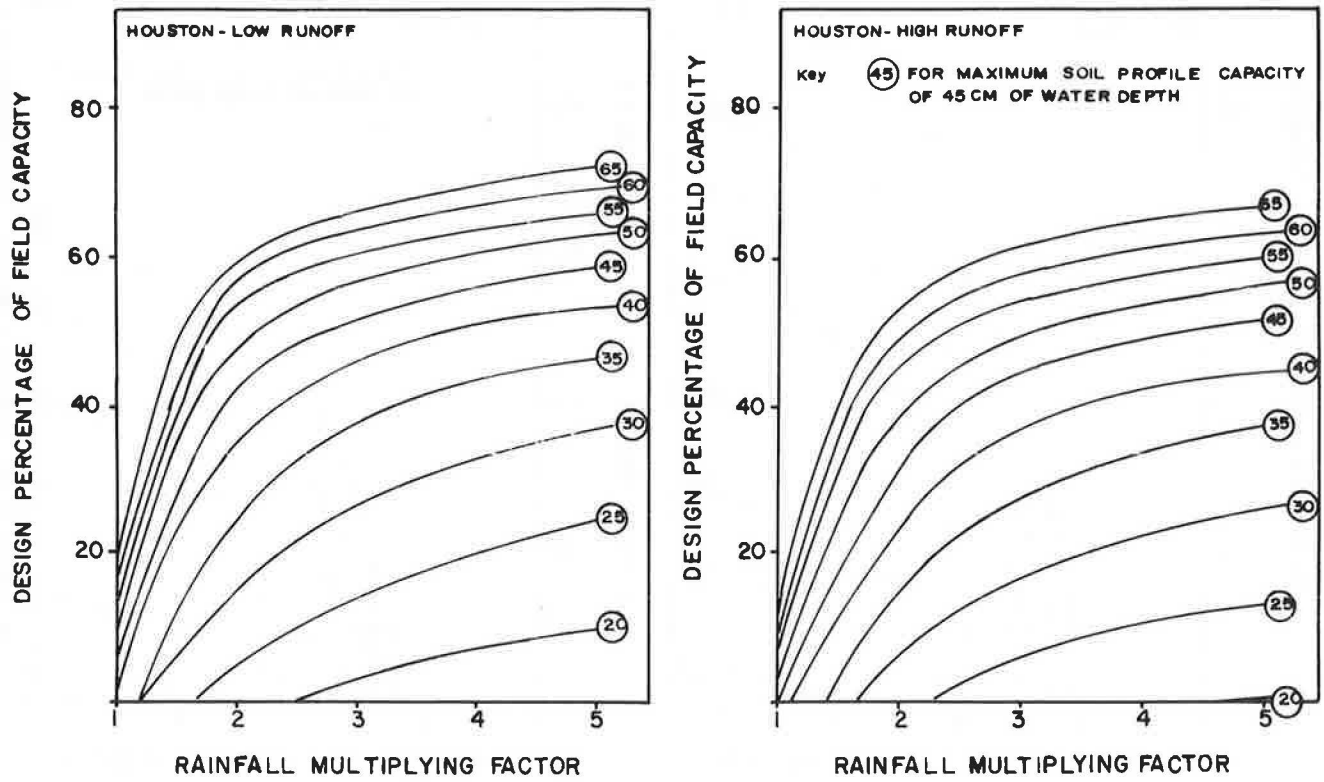

FIGURE 4 Twenty-five-year design events for Houston.

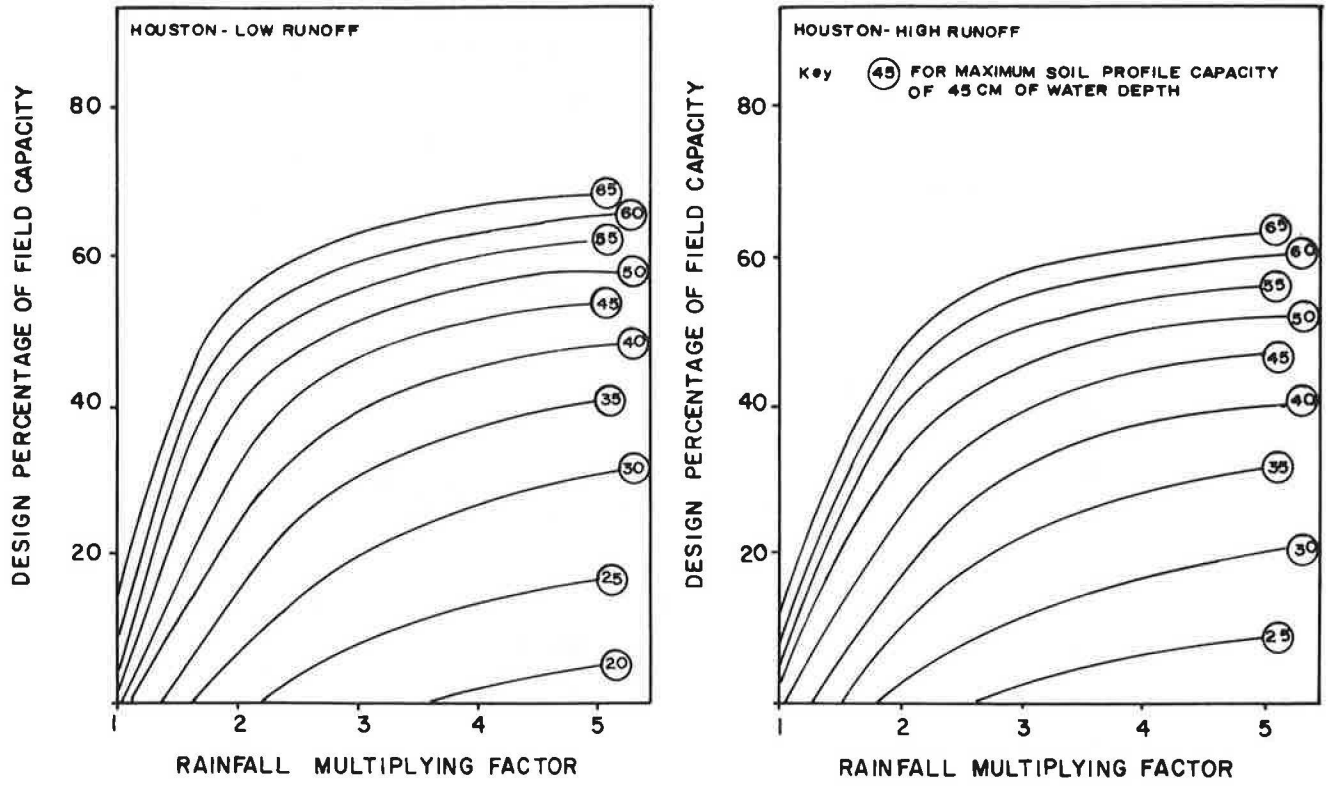

FIGURE 5 Fifty-year design events for Houston.

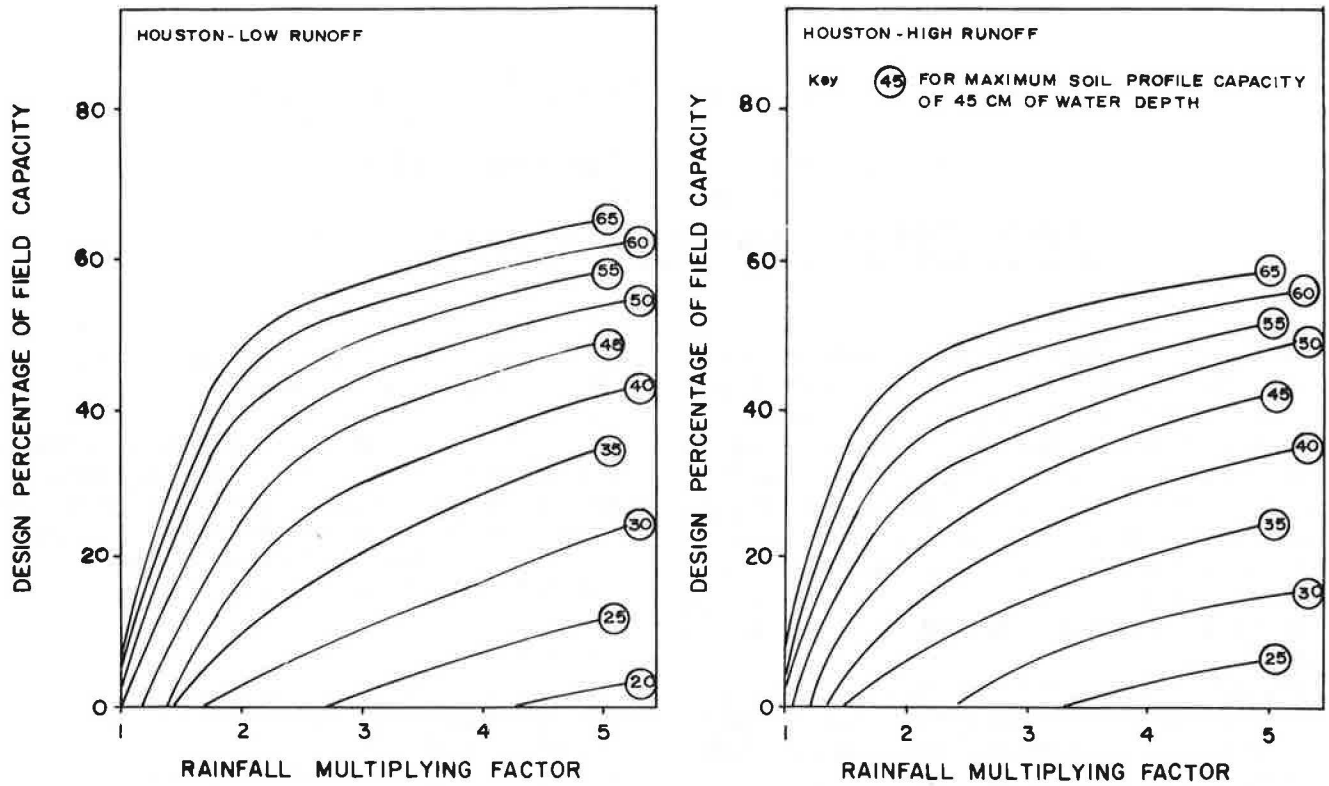

FIGURE 6 One-hundred-year design events for Houston.

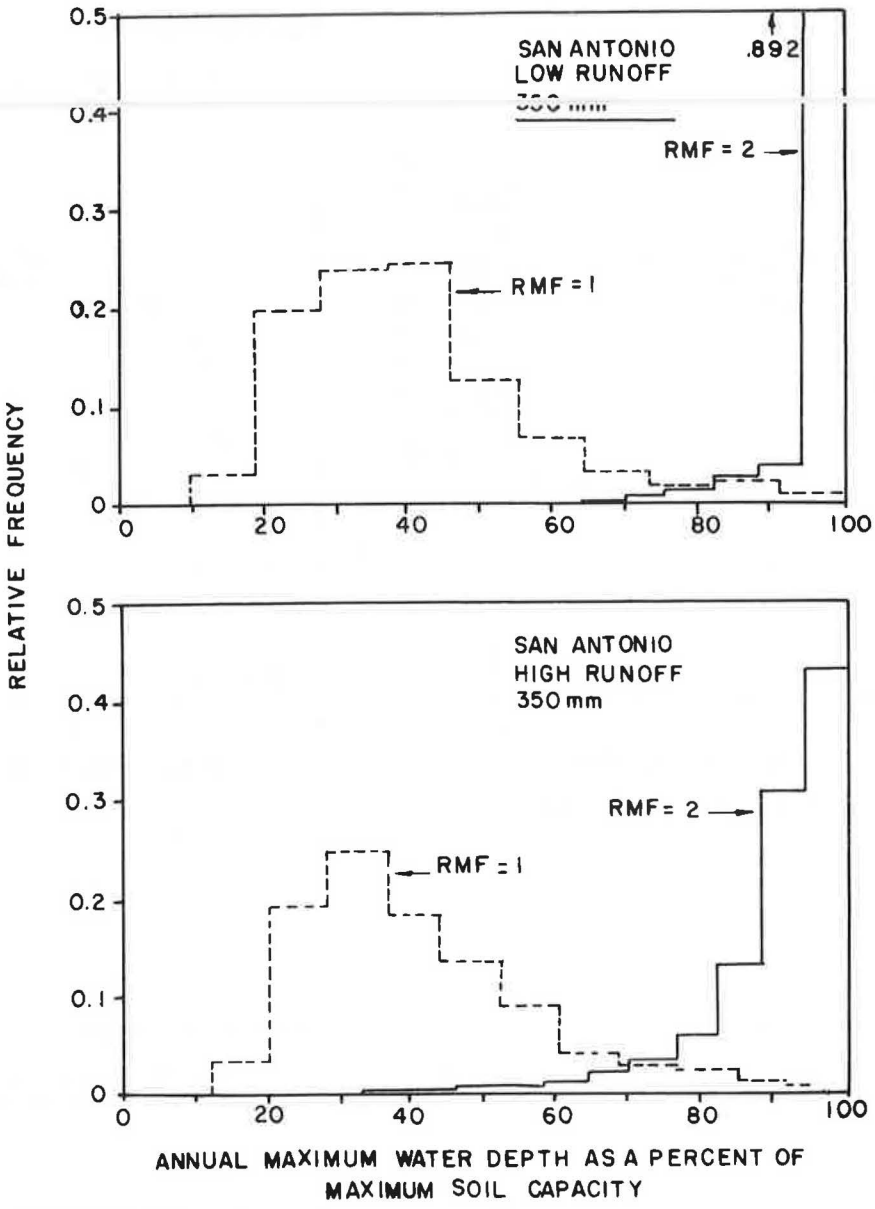

FIGURE 7 Effect of the rainfall multiplying factor on the distribution of annual maximum water depths in San Antonio.

an RMF of 1, the annual minimum water depth is 0 in more than 95 percent of the 1,000 events generated for San Antonio and Dallas-Fort Worth. There is a large increase of the minimum water depth when the RMF increases to 2 in these two areas. The changes associated with an RMF larger than 2 are smaller, though noticeable. The same general trend is also true for the Houston area, but here the changes introduced by increasing the RMF from 2 to 5 are minimal. The annual minimum water depth distribution for Houston with an RMF of 1 is quite similar to those for an RMF of 2 in the other two sites.

Intuitively, it seems that as the soil capacity decreases, the soil will be depleted more frequently. This trend is confirmed at all three sites. Again, the effects in San Antonio and Dallas-Fort Worth are similar; the bell-shaped distributions at high capacities become an exponentially decreasing distribution at the lower capacity range. The general trend is the same in Houston, but the distributions remain essentially bell shaped over the whole range of soil profile capacities.

The design events were chosen from the distributions of annual minimum soil water depths. Three design events were defined in each site for return periods of 25, 50, and 100 years. The results for San Antonio are shown in Figures 1–3 and for Houston in Figures 4–6. The distribution of annual maximum water depths at San Antonio is illustrated in Figure 7.

REFERENCES

1. G. Blumenstock. *Drought in the U.S. Analyzed by Means of the Theory of Probability.* Technical Bulletin 819, U.S. Department of Agriculture, 1942.
2. C. W. Thornthwaite. The Climate of North America According to a New Classification. *Geographical Review,* No. 21, 1931, pp. 633–655.

3. C. W. Thornthwaite. *Atlas of Climatic Types in the United States, 1900–1939.* Miscellaneous Publication 421, U.S. Department of Agriculture, 1941.
4. C. H. M. van Bavel and F. J. Verlinden. *Agricultural Drought in North Carolina.* Technical Bulletin 122, North Carolina Agricultural Experiment Station, Raleigh, N.C., 1956.
5. C. W. Thornthwaite. An Approach Towards a Rational Classification of Climate. *Geographical Review,* No. 38, 1948, pp. 55–94.
6. W. C. Palmer. Moisture Variability and Drought Severity. *Proc., Thirteenth Annual Meeting of the Agricultural Research Institute,* National Academy of Sciences, National Research Council, Washington, D.C., 1964, pp. 145–157.
7. W. C. Palmer. *Meteorological Drought.* Research Paper 45. Weather Bureau, U.S. Department of Commerce, 1965.
8. C. H. M. van Bavel. A Drought Criterion and Its Application in Evaluating Drought Incidence and Hazard. *Agronomy Journal,* No. 46, 1953, pp. 167–172.
9. C. W. Richardson and J. T. Ritchie. Soil Water Balance for Small Watersheds. *Transactions of the American Society of Agricultural Engineers,* 1973, pp. 12–77.
10. G. P. de Brimchambaut and C. C. Wallen. *Study of Agroclimatology in Semi-arid Zones of the Near East.* Technical Note 56. World Meteorological Organization, Geneva, Switzerland, 1963.
11. H. L. Penman. *Vegetation and Hydrology.* Technical Communication 53. Commonwealth Bureau of Soils, Harpenden, England, 1963.
12. J. T. Ritchie, E. Burnett, and R. C. Henderson. Dryland Evaporative Flux in a Subhumid Climate: III, Soil Water Influence. *Agronomy Journal,* Vol. 64, March–April 1972, pp. 168–173.
13. G. O. Schwab, R. K. Frevert, T. W. Edminster, and K. K. Barnes. *Soil and Water Conservation Engineering.* 3rd ed. John Wiley & Sons, New York, 1979, pp. 60–66.
14. D. A. De Vries. *Solar Radiation at Wageningen.* Mededeldelingen Land-bouwhogeschool, Wageningen, The Netherlands, 1955, pp. 277–304.
15. J. Kondo. Analysis of Solar Radiation and Downward Long-Wave Radiation Data in Japan. *Scientific Reports,* Tohokou University, Sendai, Japan, Series 5, No. 18, 1967, pp. 91–124.
16. *Local Climatological Data, Annual Summary with Comparative Data.* National Climatic Data Center, National Oceanic and Atmospheric Administration, Asheville, N.C., 1982.
17. W. H. Brutsaert and G. T. Yeh. A Power Wind Law for Turbulent Transfer Computations. *Water Resources Research,* No. 6, 1970, pp. 1387–1391.
18. C. T. Haan. *Statistical Methods in Hydrology.* The Iowa State University Press, Ames, 1979, pp. 289–291.
19. G. A. Larsen and R. B. Pense. Stochastic Simulation of Daily Climatic Data for Agronomic Models. *Agronomy Journal,* Vol. 74, 1982, pp. 510–514.
20. M. Picornell. *The Development of Design Criterion to Select the Depth of a Vertical Moisture Barrier.* Ph.D. dissertation. Texas A&M University, College Station, 1985.
21. J. A. Greenwood and D. Durand. Aid for Fitting the Gamma Distribution by Maximum Likelihood. *Technometrics,* No. 2, 1960, pp. 55–65.
22. *Hydrology.* National Engineering Handbook. U.S. Soil Conservation Service, 1972, Section 4.
23. H. F. Blaney and W. D. Criddle. *Determining Water Requirements in Irrigated Areas from Climatological and Irrigation Data.* Soil Conservation Service, U.S. Department of Agriculture, 1957.
24. J. W. Holmes. Water Sorption and Swelling of Clay Blocks. *Journal of Soil Science,* Vol. 6, No. 2, 1955, pp. 200–208.
25. J. T. Ritchie. A Model for Predicting Evaporation from a Row Crop with Incomplete Cover. *Water Resources Research,* Vol. 8, No. 5, 1972, pp. 1204–1213.
26. H. L. Penman. Estimating Evaporation. *Transactions,* American Geophysical Union, Vol. 37, No. 1, 1956, pp. 43–50.
27. J. R. Phillip. Evaporation and Moisture and Heat Fields in the Soil. *Journal of Meteorology,* No. 14, 1957, pp. 354–366.
28. T. A. Black, W. R. Gardner, and G. W. Thurtell. The Predication of Evaporation Drainage, and Soil Water Storage for a Bare Soil. *Proc., Soil Science Society of America,* Vol. 33, 1969, pp. 655–660.
29. C. H. M. van Bavel. Changes in Canopy Resistance to Water Loss from Alfalfa Induced by Soil Water Depletions. *Agricultural Meteorology,* No. 4, 1967, pp. 165–178.
30. J. T. Ritchie and E. Burnett. Dryland Evaporation Flux in a Subhumid Climate: III, Plant Influences. *Agronomy Journal,* Vol. 63, 1971, pp. 56–62.
31. J. T. Ritchie and W. R. Jordan. Dryland Evaporative Flux in a Subhumid Climate: IV, Relation to Plant Water Status. *Agronomy Journal,* No. 64, 1972, pp. 173–176.

Publication of this paper sponsored by Committee on Environmental Factors Except Frost.

Characterization of Constrained Swelling of Clay

JACOB UZAN, RAPHAEL BAKER, AND SAM FRYDMAN

Described in the paper are the development and application of a simple approach for estimating the response of a swelling soil profile to the percolation of surface water. The approach is made up of two parts: (a) A model for the flow regime, to predict the development of the wetted zone with time. It is used to predict the lateral extent and the vertical penetration of the wetting front for a surface wetting source of finite extent. (b) A model for the swelling process under constrained conditions. It is used to predict the surface heave of a swelling clay profile as a function of the extent of the wetted zone, and induced lateral and vertical constraints. The approach is illustrated by reference to the prediction of the development of heave with time in a swelling marl profile. The swelling parameters of the marl were obtained from laboratory tests in which radial as well as vertical stresses were measured. It is shown that the effect of confinement and limited extent of surface wetting source, often neglected in standard one-dimensional analysis, may be of major significance in limiting the heave that will develop in the field.

Evaluation of the response of swelling clay soils to the combined effects of wetting and mechanical constraints constitutes a formidable geotechnical problem. A complete solution of such a problem requires the study of saturated-unsaturated flow and its coupling with the swelling and stress-strain response of the material. The present state of knowledge does not allow such a comprehensive treatment but there exists, nevertheless, the need to estimate (even approximately) the expected response of a constrained clay layer to wetting.

The present paper describes the development of a model allowing the estimation of the combined effects of wetting from a surface source and mechanical constraint. The model is based on the following simplifying assumptions:

1. Decoupling of the flow and stress-strain problems. As a result of this decoupling, phenomena such as the effect of volume change on permeability, stress changes on suction, or suction changes on deformation moduli are not explicitly considered.
2. Representation of the continuous transition between the saturated and unsaturated flow regimes by a sharp wetting front advancing in time and space. As a result of this approximation, a volume element can exist only in one of two states: the initial (unwetted) state with degree of saturation S_o or a final saturated state with complete saturation, that is, $S_f = 1$.
3. Volume changes on wetting at constant stress and volume change due to stress change without wetting are assumed to be additive. Such an assumption is essentially a statement of a superposition principle between the free swell and stress-strain problems. This assumption results in a model that is similar to the one used in thermoelasticity, with volume changes due to wetting playing the role of thermal expansion.

On the basis of these assumptions, models for the flow regime and constrained wetting process are developed and used to illustrate the effect of extent of the wetted zone and of lateral constraint on the heave of a swelling marl profile covered by a nonswelling rock layer. The complete case study of feasibility of siting a nuclear power plant on such a profile is presented in a separate paper *(1)*.

A MODEL FOR THE FLOW REGIME

A comprehensive solution for the development of the wetted zone with time requires the solution of a complicated nonlinear partial differential equation describing saturated-unsaturated flow. Finite element programs for this purpose are available [e.g., Neuman *(2)* and Neuman et al. *(3)*], but these require parameter evaluation using nonroutine testing, and significant amounts of computer time. For the present simplified scheme, an approximate approach is used to obtain a solution for the development of the wetted zone. The solution contains two elements, one concerning the lateral extent of the wetted zone as a function of depth, and the other describing the vertical penetration of the wetting front with time. These two elements are discussed in the following paragraphs.

The Lateral Extent of the Wetted Zone

Use is made of an analytical solution for steady state flow of water from a ditch to a deep water table through homogeneous material, as presented by Harr *(4)* based on a derivation by Vedernikov *(5)*. Although this solution is for a two-dimensional case, it is also taken as a first approximation for axisymmetric conditions. A more complete discussion of Vedernikov's solution was presented by Baker et al. *(6)*. This solution may be expressed in the following form:

$$\frac{r - r_o}{H} = \left\{ \left(P_r\right)^{1/2} \left[1 - \exp\left(-\frac{\pi z}{2H}\right)\right]\right\} \quad (1)$$

where

r = lateral extent of wetted zone at depth z;
r_o = lateral extent of wetting source at surface;

Faculty of Civil Engineering, Technion-Israel Institute of Technology, Technion City, Mt. Carmel, Haifa 32000, Israel.

P_r = Permeability ratio; that is, ratio between horizontal and vertical coefficients of permeability; and
H = height of ponded water.

From Equation 1 it is seen that $(r - r_o)$ approaches a vertical asymptote at a radial distance equal to $H(P_r)^{1/2}$.

Vertical Penetration of the Wetting Front

The rate of penetration of the wetting front has been analyzed on the basis of one-dimensional vertical flow. In order to avoid the need for the solution of the nonlinear infiltration equation, the present approach is based on the assumption that the wetting process involves the advance of a sharp wetting front, that is, the material above the wetting front is assumed fully saturated and below the wetting front the degree of saturation equals its initial value. A similar assumption has been made by Bear *(7)*. Validity of this approximation was discussed by Baker et al. *(6)*.

Schematic profiles of degrees of saturation, S, and suction, ψ, as a function of depth, z, at a given time t, are shown in Figure 1. The full lines represent the complete infiltration solution, while the dashed lines correspond to the wetting front approximation used in the present analysis. As can be seen, the suction at the wetting front is not well defined, and a value of $\psi = \psi_o/2$ is used as a reasonable approximation. The profile is assumed homogeneous, with a constant value of ψ_o below the wetting front.

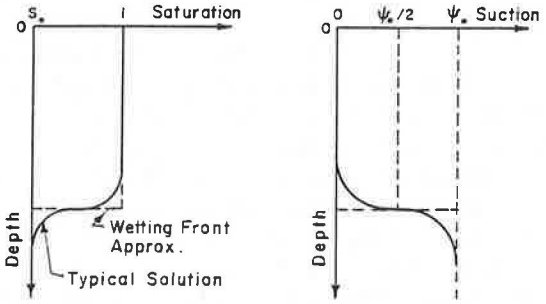

FIGURE 1 Degree of saturation and suction versus depth.

Following the analysis presented by Baker *(8)*, the following relation can be derived:

$$T = y - \ln(1 - y) \tag{2}$$

where y and T are nondimensional depth and time, respectively, defined as follows:

$$y = z/\overline{H} \tag{3a}$$

$$T = kt/n(1 - S_o)\overline{H} \tag{3b}$$

where

z = depth to the wetting front,
$\overline{H}$ = $h_c + \psi_o/2\gamma_w$,
h_c = thickness of the cracked zone,
ψ_o = initial suction in the unsaturated zone,
γ_w = unit weight of water,
k = the saturated coefficient of permeability,
t = time,
n = porosity, and
S_o = initial degree of saturation below the wetting front.

This solution applies to a homogeneous profile. An extension of the above approach to the case of a two-layered system has been developed using the concept of an equivalent coefficient of permeability. The solution is given by the expression

$$T = y - (B + 1)\ln(1 + y) + A \tag{4}$$

where

$$B = \overline{d}/\overline{H}\,(1 - k_2/k_1) \tag{5a}$$

$$A = \left[\left(\frac{n_1}{n_2}\right)\left(\frac{1 - S_1}{1 - S_2}\right)\left(\frac{k_2}{k_1}\right) - 1\right] \cdot \left[\frac{\overline{d}}{\overline{H}} - \ln\left(1 + \frac{\overline{d}}{\overline{H}}\right)\right] + B \ln\left(1 + \frac{\overline{d}}{\overline{H}}\right) \tag{5b}$$

where

$\overline{d}$ = thickness of upper layer,
k_1, n_1, S_1 = parameters of the upper layer, and
k_2, n_2, S_2 = parameters of the lower layer.

Equation 4 is valid for the case where the lower layer is less permeable than the upper one; otherwise there is no guarantee that the material in the bottom layer will be saturated.

Figure 2 shows the depth of the wetting front as a function of time for a particular choice of parameters. The shape of the wetted zone at different times is shown in Figure 3.

A MODEL FOR THE SWELLING PROCESS

The volume change of a soil element is a function of changes in the effective stress tensor acting on the element. This dependence may be expressed as a relationship between the void ratio e of the element, and the two components of the effective stress tensor: the mean effective normal stress, σ_m', and the deviational shear stress, τ_m [e.g., Newmark *(9)*]:

$$e = f_o(\sigma_m', \tau_m) \tag{6}$$

At levels of shear stress that are low relative to failure conditions, the void ratio change may be considered a function mainly of σ_m' [Henkel *(10)*, Frydman et al. *(11)*], and Equation 6 may be written approximately

$$e = f_1(\sigma_m') \tag{7}$$

It may be noted that Equation 7 describes the behavior of isotropic elastic materials in which volume change is dependent on changes in mean normal stress only. The effective normal stress, σ', in an unsaturated soil under drained conditions may be expressed in terms of the total stress, σ, and the water suction, ψ, as follows [see, for example, Bishop et al. *(12)*]:

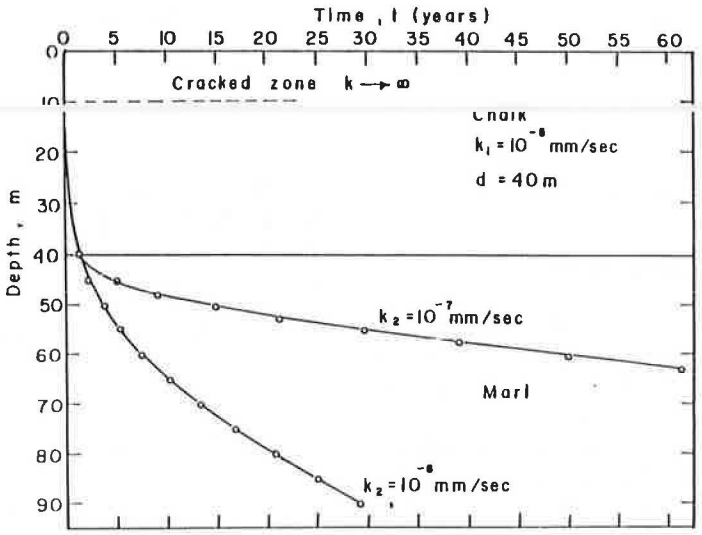

FIGURE 2 Position of wetting front as a function of time.

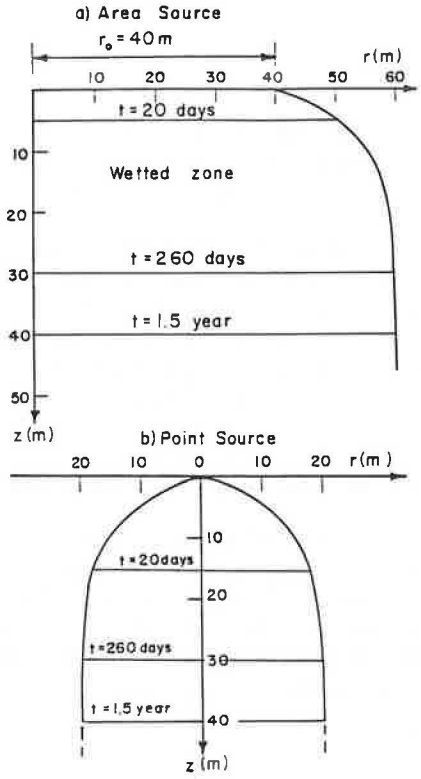

FIGURE 3 Shape of wetted zone at different times.

$$\sigma' = \sigma + \chi\psi \tag{8}$$

where χ is a soil parameter, dependent mainly on the degree of saturation of the soil, S. The suction, ψ, may also be assumed to be a function of the degree of saturation, S [Bear *(7)*]. Consequently, Equations 7 and 8 may be rewritten as

$$\sigma' = f_2(\sigma, S) \tag{9a}$$

$$e = f_3(\sigma_m, S) \tag{9b}$$

Therefore, the change in void ratio, de, may be expressed by

$$de = \frac{\partial e}{\partial \sigma_m} d\sigma_m + \frac{\partial e}{\partial S} dS = de_s + de_\sigma \tag{10}$$

that is, during a process that may involve wetting and change in applied stress, the total change in void ratio is the sum of two components—one due to the change in applied mean stress at constant degree of saturation (de_s), and the other due to change in the degree of saturation at constant mean stress (de_σ).

A similar approach has been presented by Picornell and Lytton *(13)*, except that they expressed de as a function of σ_m and ψ instead of σ_m and S; the approaches are equivalent. Justo et al. *(14)* also used a similar approach, but they applied to one-dimensional model and related void ratio changes to changes in vertical stress, σ_z, rather than mean normal stress, σ_m. It is, however, well accepted now that a three-dimensional approach is more representative of field conditions.

The wetting front approximation used for the analysis of the flow regime implies that a material element can exist only in one of two distinct saturation states. In the unwetted zone, $S = S_o$, the initial degree of saturation, and in the wetted zone, $S = 1$, and the material is fully saturated.

Figure 4 shows two curves representing the relationship between e and log σ_m for a clay soil element being compressed; curve *ABC* is for the soil at its natural moisture content, while curve *DEF* is for the saturated condition (i.e., $S = 100$ percent). The straight-line relationship for the saturated soil may be expressed as follows:

$$de_s = e_f - e_i = -\lambda \log [(\sigma_m)_f/(\sigma_m)_i] \tag{11}$$

where λ is a compression index, analogous to C_c or C_e, which relates e to σ_z in a one-dimensional process, and the subscripts f and i refer to final and initial conditions, respectively.

Point B represents the initial conditions of an unsaturated soil element that has a degree of saturation S_o and a void ratio e_o. If this element is wetted and allowed to swell under constant mean normal stress, a vertical path will be followed from point B; if the element becomes 100 percent saturated, it is assumed that it will reach point D and the change in void ratio is shown

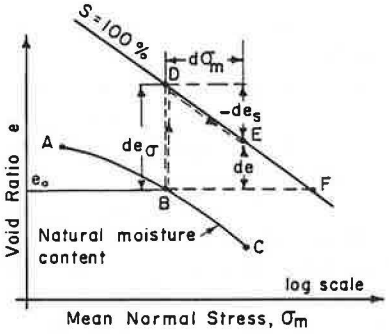

FIGURE 4 Void ratio: mean normal stress curves for wetted and unwetted marl.

on the figure as de_σ. If, on the other hand, the element is wetted under completely constrained conditions so that the volume cannot change, the state of the element will follow a horizontal path from point *B*; if full saturation is achieved, it is assumed that the element will reach point *F*, which defines the swelling pressure of the soil. Under field conditions, an element of soil will generally swell under partially confined conditions; in this case increase in void ratio will be accompanied by an increase in σ_m. If the element becomes fully saturated, it will reach the $S = 100$ percent curve at some point *E* between *D* and *F*. The void ratio change during such a process will be *de* and the stress increase $d\sigma_m$ as shown on the figure; this value is seen to be the sum of de_σ resulting from swell under constant σ_m and de_s resulting from compression at constant *S*, as expressed by Equation 10.

The analogy between the model already described for swelling of soils and that for a thermoelastic material is apparent. The void ratio change de_σ (path *BD*), which results from a change in the degree of saturation at constant stress, corresponds to volume change due to a change in temperature, *dT*. The void ratio change de_s (path *DE*), which results from a change in the state of stress at a constant degree of saturation ($S = 100$ percent), can be evaluated using conventional elastic stress analysis. Any arbitrary path *BE*, which is followed during a partially restrained process, may be considered as a superposition of paths *BD* and *DE*.

The model described previously is in the spirit of Jennings' *(15)* "double-oedometer" approach, with proper three-dimensional generalization. The formal correspondence between the swelling and thermal models is based on the expressions for volumetric strains in both models:

$$\text{Swelling model} \qquad \varepsilon_v = -\frac{1}{1+e_o}\, de_\sigma \tag{12a}$$

$$\text{Thermal model} \qquad \varepsilon_v = -3\alpha\, dT \tag{12b}$$

where α equals coefficient of linear thermal expansion, and ε_v equals volumetric strain (compression positive).

On the basis of Equations 12a and 12b, the following relation holds

$$\frac{de_\sigma}{1+e_o} = 3\alpha\, dT \tag{12c}$$

It is important to note that only the product *dT*, rather than the individual parameters α and *dT*, have a physical significance in terms of the present analogy; that is, any choice of α and *dT* which satisfies Equation 12c is equally valid. For convenience the following choice of parameters is made:

$$dT = de_\sigma \tag{13a}$$

$$\alpha = \frac{1}{3(1+e_o)} \tag{13b}$$

Equations 13a and 13b formalize the swelling-thermal analogy.

The second part of the model is based on the path *DE*; for this path, from Equation 11:

$$\varepsilon_v = -\frac{de_s}{1+e_o} = \frac{\lambda}{1+e_o}\log\left[1+\frac{d\sigma_m}{(\sigma_m)_i}\right] \tag{14}$$

Assuming an elastic model for compression at constant *S*, we have:

$$\varepsilon_v = \frac{d\sigma_m}{K} = \frac{3(1-2\mu)}{E}\, d\sigma_m \tag{15}$$

where *K* is the bulk modulus and *E* and μ are the modulus of elasticity and Poisson's ratio, respectively, of the saturated soil.

Combining Equations 14 and 15:

$$E = E(\sigma_m) = \left[\frac{3(1-2\mu)}{\lambda}\right](1+e_o)\left\{\frac{d\sigma_m}{\log[1+d\sigma_m/(\sigma_m)_i]}\right\} \tag{16}$$

If the Poisson's ratio is assumed to be constant, then the present model for the swelling of soils implies a nonlinear thermoelastic material with the modulus of elasticity, *E*, dependent on the mean normal stress (σ_m).

The complete swelling-elastic model is governed by the following system of equations for the axisymmetric case:

$$\varepsilon_z = \frac{1}{E}(d\sigma_z - 2\mu d\sigma_r) - \alpha de_\sigma \tag{17a}$$

$$\varepsilon_r = \varepsilon_\theta = \frac{1}{E}[d\sigma_r - \mu(d\sigma_r + d\sigma_z)] - \alpha de_\sigma \tag{17b}$$

The parameters μ, α, λ, and the function $de_\sigma = de_\sigma(\sigma_m)$ are evaluated on the basis of laboratory tests, as described in the following section.

EVALUATION OF GEOTECHNICAL PARAMETERS

In order to apply the procedure described previously, it is necessary to establish values for the following geotechnical parameters:

1. Flow Parameters: The coefficient of permeability *k*, porosity *n*, degree of saturation S_o, and in situ suction ψ_o in both the overlying layer and the swelling layer. A simplified analysis may be based on a constant ψ_o.
2. Heave Parameters: The elastic parameters *E* and μ for the overlying nonswelling material, and for the unwetted swelling soil. For the wetted swelling soil λ, μ, and e_o are needed for evaluation of the coefficient of linear expansion α (Equation

13b) and E = E (σ_m) (Equation 16). In addition, it is necessary to establish the function $dT = de_\sigma = de\ (\sigma_m)$ for the wetted swelling material.

The following presents an illustration of application of the model to the case of a swelling marl profile overlain by a 40-m-thick chalk layer.

Flow Parameters: Coefficients of permeability of the saturated marl were obtained from laboratory consolidation tests. These values were found to be in the range 10^{-7} to 10^{-9} mm/sec. In view of the possibility that fine crack patterns and foreign lenses within the marl would result in higher permeabilities for the en masse material, it was decided to carry out the analyses using values of $k = 10^{-7}$ mm/sec and 10^{-6} mm/sec; these values, on the high side, are conservative, as they will result in more rapid wetting and swell of the marl and consequent heave of the profile surface.

Values of n measured on core samples of the marl lay between 25 percent and 42 percent, and a value of n = 37.5 percent was adopted for the present analyses. The degree of saturation, S_o, of these cores varied between 75 percent and 95 percent, and a value of S_o = 85 percent was adopted.

Figure 5 shows laboratory suction curves obtained for two marl cores taken from within 3 m of the top of the marl layer. The in situ moisture content in this region was of the order of 20 percent; consequently, the value of ψ_o in the laboratory condition (without overburden pressure) was of the order of 2.0–2.5 MPa. The corresponding in situ value was obtained by subtracting the effect of overburden pressure [Croney et al. *(16)*], yielding a range of ψ_o = 0.4–1.5 MPa through the marl profile. A representative value of ψ_o = 1.0 MPa was chosen for the analysis.

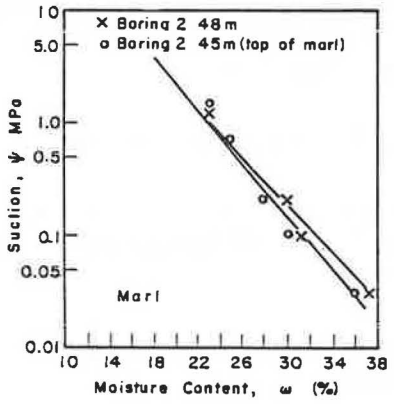

FIGURE 5 Suction curves from pressure plate tests for marl.

Elastic parameters of unwetted marl: Values of E and μ were obtained from the initial stages of one-dimensional confined compression tests in which samples were later wetted in order to study swelling. The tests were performed in special consolidometer rings instrumented with circumferential strain gauges [Komornik and Zeitlen *(17)*], enabling measurement of change in radial stress ($\Delta\sigma_r$) accompanying changes in vertical stress ($\Delta\sigma_z$) and swelling. Assuming linear elasticity, Equations 17, with $\alpha = 0$ and $\varepsilon_r = \varepsilon_o = 0$ may be used to evaluate parameters E and μ from results of these tests.

Tests were performed on specimens with dry densities varying from 15.2 kN/m^3 to 17.3 kN/m^3, and a wide range of E and μ values were obtained. Values of E = 300 kPa and μ = 0.35 (corresponding to a coefficient of earth pressure at rest, K_o of about 0.5) were chosen for the analysis.

Parameters of wetted marl: The elastic parameters E and μ and the swelling parameters and de_σ were obtained from one-dimensional confined swell and subsequent compression tests in which both vertical and radial stresses were measured. Figure 6 shows curves of e versus σ_m for four different marl samples in both the unwetted and the wetted states. Each curve is an average curve drawn through points obtained from tests on a number of specimens wetted after compression to different mean stresses; the wetted curves are drawn through points reached after swelling from the unwetted condition or after compression of previously wetted specimens.

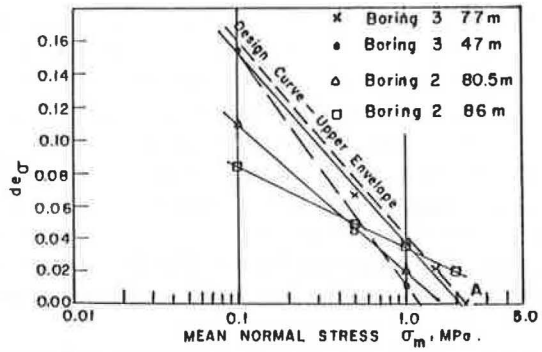

FIGURE 6 Laboratory $e - \sigma_m$ curves for marl samples.

For each set of curves, the vertical distance between the two curves represents de_σ for any particular σ_m. Figure 7 shows the relation $de_\sigma\ (\sigma_m)$ for the four samples. The upper envelope shown on the figure represents a conservative design curve.

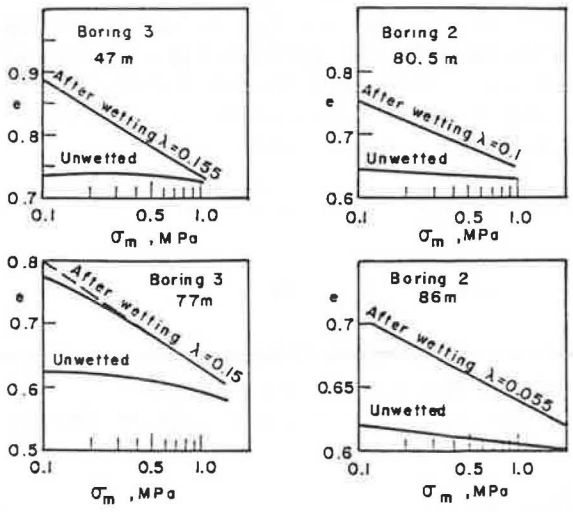

FIGURE 7 de_σ versus σ_m marl samples.

The sampling and testing program has indicated that values of e_o for the marl are consistently above 0.6 (see, for example, Figure 6). Because the swelling parameter α will be higher the lower the value of e_o, representing a more highly swelling material, a value of $e_o = 0.6$ is conservatively adopted for the present analyses, leading to $\alpha = 0.208$.

Results of swelling tests yielded values of μ between 0.1 and 0.3, and a value of 0.2 is adopted. E is assumed to be dependent on σ_m according to Equation 16, and is obtained from the wetted $e - \log \sigma_m$ curves in Figure 6. From these curves, λ was found to vary between 0.055 and 0.155. Adopting a value of $\lambda = 0.13$, and using the values of μ and e_o previously defined, E may be expressed as a function of $(\sigma_m)_i$ and $d\sigma_m$ through Equation 16. The depth corresponding to any value of $(\sigma_m)_i$ has been obtained by assuming an average profile total density γ of 18 kN/m^3 and a coefficient of earth pressure at rest, $K_o = 0.5$ in the unwetted marl.

NUMERICAL PROCEDURE

The models developed were used to study the effect of lateral restraint on heave. The profile analyzed consists of marl covered by a 40-m-thick chalk layer. The chalk layer is composed of an upper 10-m cracked (pervious) chalk and 30 m of sound chalk, with assumed coefficients of permeability 10^{-1} mm/sec and 10^{-5} mm/sec, respectively. A 40-mm diameter surface wetting source and a point source are considered.

Heave calculations are made using the finite element program SAP7 made available by the Israel Electric Co. Ltd. and developed by the Structural Mechanics Computer Laboratory, University of Southern California. Figure 8 shows a typical mesh. One run of the program involves calculation of the stress increments at the centers of the elements and the displacements at the nodes that result from wetting a particular depth of marl. For example, advance of the wetting front 10 m into the marl

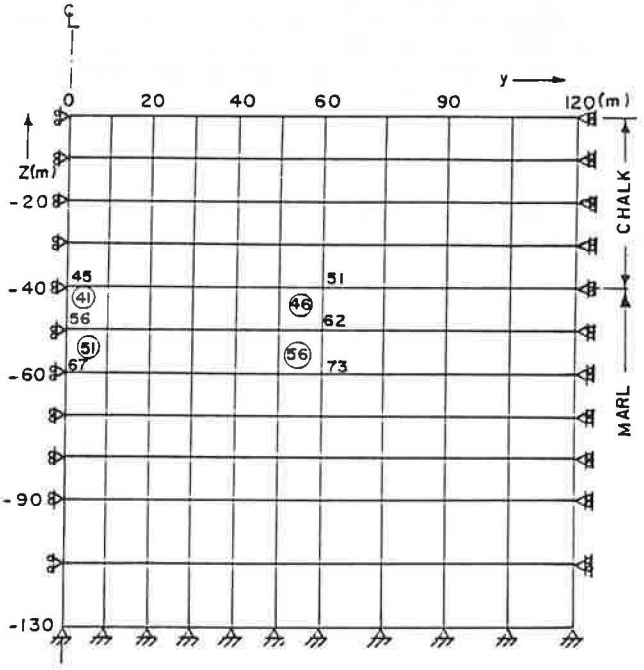

FIGURE 8 Typical finite element mesh—40-m chalk.

corresponds to wetting elements 41–46; this is input by specifying relevant values of de at nodes 45 to 51 and 56 to 62. If 20 m of marl are to be wet, values of de_σ are also specified at nodes 67 to 73, and so on. The input values of de_σ are a function of the initial mean stress, $(\sigma_m)_i$ at the node according to Figure 7, $(\sigma_m)_i$ being given by

$$(\sigma_m)_i = \frac{\sigma_z + 2\sigma_r}{3} = \frac{1 + 2K_o}{3}\gamma z \tag{18}$$

As the thermoelastic model employed here is nonlinear (the modulus of elasticity E depends on σ_m), it is necessary to use the finite element procedure iteratively. This was done in the following manner: as a result of a run, a value of $d\sigma_m$ is obtained at the center of each wetted marl element, a new E value is calculated and a new run carried out. The process is repeated until the change in E of all wetted marl elements is no greater than 5 percent; this usually requires two or three iterations.

RESULTS

A preliminary estimate of the expected surface heave, based on one-dimensional analysis (i.e., wetting extends to infinity in the horizontal direction and the constraining effect of the chalk because of its flexural rigidity is not considered), gave results of the order of 750 mm. This value represents an upper limit to the heave.

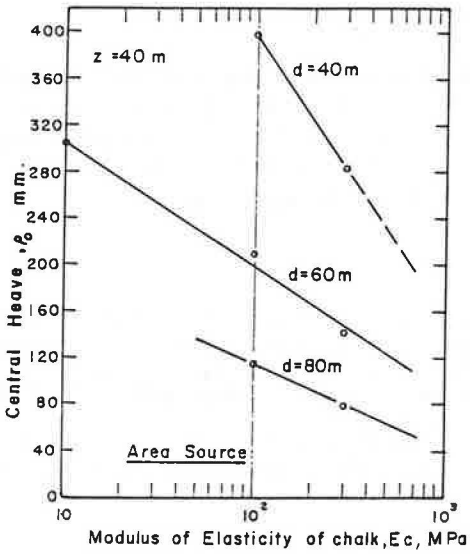

FIGURE 9 Influence of E_c on central heave.

Figure 9 shows the effect of chalk modulus of elasticity, E_c, on the central heave for a penetration of the wetting front 40 m into marl. The time for the wetting front to penetrate 40 m into the marl, resulting in the heave shown in Figure 9, may be obtained by reference to Figure 2. It is seen that for an assumed coefficient of permeability of marl $k_m = 10^{-7}$ mm/sec, infinite time is needed, while for $k_m = 10^{-6}$, the heave would develop after 20 years. In a similar way, values of central surface heaves may be obtained at various times (i.e., for different depths of

infiltration into the marl) following the start of wetting, for any values of chalk modulus of elasticity and chalk thickness; results of such a study are presented in an accompanying paper (7). Considering that a representative value of the in-mass modulus of elasticity of chalk would be expected to be of the order of 500 MPa (7), Figure 9 indicates that for $k_m = 10^{-7}$ mm/sec, a maximum heave of about 230 mm would be expected for a 40-m diameter surface wetting source—that is, about one-third of that estimated on the basis of one-dimensional swell analysis. In the case of a point wetting source, a central surface heave of only 23 mm would be predicted. This illustrates the extent of overestimation that may result from the one-dimensional analysis.

CONCLUSIONS

An approach has been developed and presented for the estimation of the surface heave to be expected at a swelling soil site. The approach is conservative in the it assumes the availability of an unlimited supply of water at the surface and the development of full saturation within the wetted zone.

The approach presented has been applied in the paper to the analysis of a particular profile, but it may be used to provide a conservative estimate of heave at any swelling soil site. It is shown that the effect of confinement and limited extent of surface wetting source, often neglected in standard one-dimensional analyses, may be of major significance in limiting the heave that will develop in the field.

ACKNOWLEDGMENT

The work described in this paper was carried out for the Israel Electric Co. Ltd., whose permission to publish the paper is gratefully acknowledged. The cooperation and encouragement of A. Kidron, I. Kiss, and S. Denekamp of the Israel Electric Co. Ltd. are particularly appreciated.

REFERENCES

1. S. Frydman, R. Baker, and J. Uzan. Constrained Swelling of Clay—A Case Study (in preparation).
2. S. P. Neuman. Saturated-Unsaturated Seepage by Finite Elements. *Journal of the Hydraulic Division*, ASCE, Vol. 99, No. HY12, 1973, pp. 2233–2250.
3. S. P. Neuman, R. A. Feddes, and E. Bresler. *Finite Element Simulation of Flow in Saturated-Unsaturated Soils Considering Water Uptake by Plants*. Third Annual Report, Project ALO-SWC-77. Technion-Israel Institute of Technology, Hydraulic Engineering Laboratory, 1974.
4. M. E. Harr. *Groundwater and Seepage*. McGraw Hill, New York, 1962.
5. V. V. Vedernikov. Seepage from Channels. *Wasserkraft and Wasserwirtschaft*, No. 11, 1934.
6. R. Baker, S. Frydman, and G. Wiseman. *Geotechnical Considerations in the Design and Construction of Earth Reservoirs*. Research Report, Technion-Israel Institute of Technology, Area of Geotechnical Engineering, 1984 (in Hebrew).
7. J. Bear. *Dynamics of Fluids in Porous Media*. Elsevier Science Publishers, Amsterdam, The Netherlands, 1972.
8. R. Baker. Seepage Losses from Small Irrigation Reservoirs. *Proc., 11th International Conference on Soil Mechanics Foundation Engineering*, San Francisco, Vol. III, 1985, pp. 1179–1182.
9. N. M. Newmark. Failure Hypotheses for Soils. *Proc., ASCE Research Conference on Shear Strength of Cohesive Soils*, Boulder, Colo., 1960, pp. 17–32.
10. D. J. Henkel. The Relationships Between the Effective Stresses and Water Content in Saturated Clay. *Geotechnique*, Vol. 1, 1960, pp. 41–54.
11. S. Frydman, J. G. Zeitlen, and I. Alpan. The Yielding Behaviour of Particulate Media. *Canadian Geotechnical Journal*, Vol. 10, No. 3, 1973, pp. 341–362.
12. A. W. Bishop, I. Alpan, E. E. Blight, and I. B. Donald. Factors Controlling the Strength of Partly Saturated Cohesive Soils. *Proc., ASCE Research Conference on Shear Strength of Cohesive Soils*, Boulder, Colo., 1960, pp. 503–532.
13. M. Picornell and R. L. Lytton. Modelling the Heave of a Heavily Loaded Foundation. *Proc., Fifth International Conference on Expansive Soils*, Adelaide, Australia, 1984, pp. 104–108.
14. J. L. Justo, J. Saura, J. E. Rodriguez, A. Delgado, and A. Jamarillo. A Finite Element Method to Design and Calculate Pier Foundations in Expansive-Collapsing Soils. *Proc., Fifth International Conference on Expansive Soils*, Adelaide, Australia, 1984, pp. 119–123.
15. J. E. Jennings. The Theory and Practice of Construction on Partly Saturated Soils as Applied to South African Conditions. *Proc., First International Conference on Expansive Soils*, 1965, pp. 345–363.
16. D. Croney, J. D. Coleman, and W. P. M. Black. Movement and Distribution of Water in Soil in Relation to Highway Design and Performance. In *HRB Special Report 40*, HRB, National Research Council, Washington, D.C., 1958, pp. 226–252.
17. A. Komornik and J. G. Zeitlen. An Apparatus for Measuring Lateral Soil Swelling Pressure in the Laboratory. *Proc., 6th International Conference on Soil Mechanics Foundation Engineering*, Vol. 1, 1965, pp. 278–281.

Publication of this paper sponsored by Committee on Environmental Factors Except Frost.

Using Nondestructive Testing in the Semi-Arid Zone of Peru

JACOB GREENSTEIN

Presented in this paper is a methodology for nondestructive pavement testing and its application in the rehabilitation program of the Talara and Piura Airports, located in the Pacific region of Peru approximately 1000 to 1100 km north of Lima. The area's water table is 2 to 8 m under the subgrade surface and the annual rainfall is less than 150 mm. Each airport has a 2500-m runway and is used mainly by medium-sized and small jet aircraft such as B-727s, B-737s, and F-28s. The existing pavement materials do not meet standard specifications for plasticity, gradation, and California bearing ratio, and the thickness is less than that recommended by the Federal Aviation Administration. Nevertheless, 15 years' experience generally indicates adequate pavement performance. It was concluded that the most practical way to interpret the actual performance of these marginal materials is to use nondestructive testing to determine the elastic parameters of the existing subgrade and pavement. The methodology used in Piura and Talara is based on the Hogg model of a thin plate on an elastic foundation. The subgrade modulus can be determined without prior knowledge of the thickness or the characteristics of the pavement layers. The pavement modulus can then be calculated for any given load and center deflection. The survey indicates that existing pavement materials in such arid zones can generate sufficient bearing capacity to support traffic loads of B-727s, B-737s, F-28s, and DC-8s. The test results were used to upgrade the existing airport so that they could carry 600 annual operations of B-727s with total gross weights of 160,000 lb for 20 years.

During 1985 and 1986, the Peruvian Air Transportation Authority started the rehabilitation program of Piura and Talara Airports. Both are located in the northern Pacific region of the country about 1000 to 1100 km north of the capital, Lima. These airports are mainly used inter alia as alternatives to the Pan-American Highway connecting the northern Pacific areas with the capital, because some sections of the highway are presently in poor condition. These airports are used mainly by medium-sized and small jet aircraft such as B-727s, B-737s, and F-28s. Occasionally, heavier aircraft, such as DC-8s, use Talara Airport. In both airports, the length of the runway is about 2500 m. Piura Airport is located at coordinates 05°12'S, 8°37'W and its elevation is 35 m above sea level. The airport pavement suffered severe failure in 1982 because of a combination of flooding—very rare in this area—and pavement overstress. The 1982 flash flooding was unusual with a return period of over 100 yr. This pavement failure has limited the effective length of the runway to 1700 m until completion of rehabilitation in November of 1986.

Louis Berger International, Inc., 100 Halsted Street, East Orange, N.J. 07019.

The Talara Airport is located about 150 km north of Piura and is used by passengers and to transport petroleum drilling and production equipment to the local on- and offshore oil fields. In addition, Talara Airport is also used as an emergency airport in case of bad weather in Lima or Guayaquil, Ecuador. Standard testing shows that the existing pavement materials do not meet FAA specifications for plasticity, gradation, and strength. Nevertheless, over 15 yr of experience have shown that even these marginal materials have performed adequately in the local arid conditions, with annual rainfall less than 150 mm and the water table 2 to 8 m under the subgrade surface. It was found that the most practical way to interpret the actual performance of the substandard material is to use nondestructive testing (NDT) to determine the in situ elastic parameters of the existing subgrade and pavement materials. NDT was used to minimize the cost of upgrading both airports.

METHODOLOGY

Nondestructive Testing

A rational methodology of pavement evaluation should be independent of the type of equipment used to test the materials. Although pavement materials are nonuniform and nonisotropic, and although their stress-strain relationships are not linear, one would expect to reach similar results using different NDT devices. Such a methodology has been successfully implemented worldwide *(1–4)*. Figure 1 presents a typical comparison of layer moduli for five different types of airport pavement tested with (a) the pavement profiler (PP), (b) a 16-kip vibrator (*V*), and (c) the falling weight deflectometer (FWD) *(4)*. Each NDT device was operated by a different operator on a different day and at randomly selected testing points for each one of the testing areas. The same subgrade modulus was obtained from the different NDT devices. Similar conclusions were obtained for the pavement modulus [see Figure 1 *(4)*]. Test Area 1 was 20 in. of portland cement concrete (PCC). Test Areas 2 and 3 were flexible pavement with 11.0 and 5.5 in. of asphalt concrete (AC), Test Area 4 was a composite section with 7 in. of AC on top of 6 in. of PCC, and Test Area 4 was 10.5 in. of PCC.

Dynamic NDT devices, such as the PP, FWD, or even the dynaflect are not available in Third World countries like Peru. In such countries the Benkelman beam is used for structural pavement evaluation. The rebound deflection basin is obtained under a dual-wheel axle load and is interpreted by a pocket computer with 8K of random access memory (RAM) to determine the elastic moduli of the subgrade and pavement.

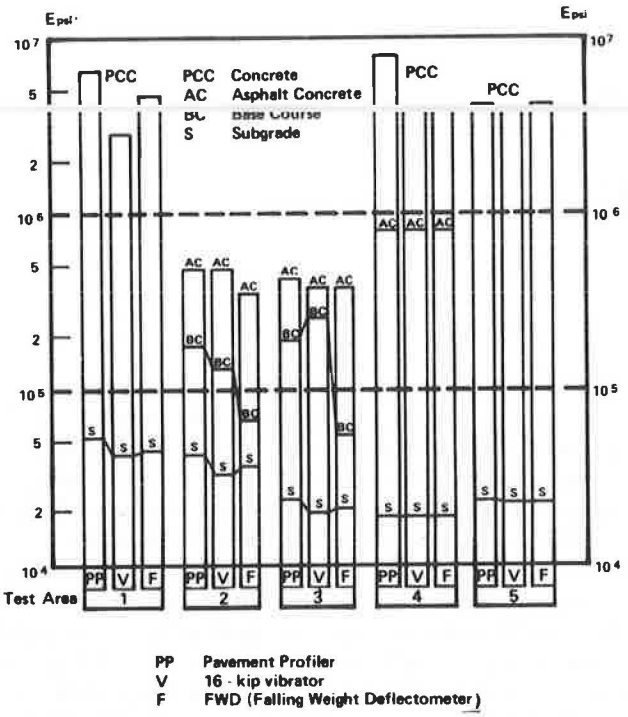

FIGURE 1 Comparison of lay moduli for five airport test areas determined by different NDT devices.

Demonstrated in Figure 2 is the use of the Benkelman beam for the rehabilitation study of Piura Airport. As shown in this figure, the beam operates on the lever principle. Every vertical movement of the tip of the beam generates a rotation of the beam through the pivot. A proportion of the tip movement is read with the dial gauge installed at the far end of the beam. The ratio of the rotating lengths of the beam is generally 1:4 (including the beam used in Piura); thus, the dial gauge at the end of the beam moves one-fourth of the vertical movement at the tip of the beam. Often the dial gauge is already calibrated to read the full tip movement (i.e., no multiplication by 4 is required).

The truck used in Peru had a single dual-wheel rear axle load (PP) weighing 8200 kg and a tire pressure of 4.9 kg/cm^2. Any value of PP can be used to determine the elastic parameters *(3)*. The truck moved away from the testing point at creep speed, and the rebound deflections were measured. This method was used to measure not only the maximum deflection under the rear axle ($D\phi$), but also to measure two additional deflections—D_{40} and D_{70}—at 40 and 70 cm away from the maximum, respectively. This nonroutine procedure was used to characterize the whole deflection basin needed in the structural evaluation methodology explained in the following sections. The choice of 40 and 70 cm was not arbitrary. The goal was to choose a distance at which the deflection would be about 50 percent of the maximum deflection. With little practice, it is possible to measure the offset deflections without having to stop the moving truck. A team composed of the truck driver and his assistant and an experienced engineer and his assistant was able to measure about 150 deflection basins in a typical working day.

Subgrade Modulus

In addition to being insensitive to the types of equipment used, the NDT methodology *(1–4)* has another advantage in that the subgrade modulus ($E\phi$) may be computed from the deflection bowl measurements without prior knowledge of the thickness or other characteristics of the pavement layers above the subgrade. The influence subgrade thickness is determined uniquely from the measured deflection basin *(1–4)*. This characteristic is extremely significant when pavement thickness is nonuniform, as in the case of Piura and Talara Airports. The Hogg model *(5, 6)* of a thin plate on an elastic foundation has been used to determine the subgrade modulus in the Peruvian airport projects. Extensive use of the Hogg model *(1–4, 7–9)* has shown it to yield satisfactory results for the modulus of elasticity of the subgrade ($E\phi$) or subgrade California bearing ratio (CBR) compared with values obtained from in situ testing. Figure 3, for example, presents the relationship between the measured and calculated deflection basin of flexible, rigid, and composite airport pavements *(4)*. This figure indicates agreement between the theoretical and the measured deflection basin. Another verification related to the subgrade strength is presented in Figures 4 and 5. These figures are taken from an NDT pavement evaluation study carried out in Thailand in 1984. Figures 4 and 5 indicate agreement between the in situ and the calculated CBR. The calculated subgrade CBR was determined by the following equation *(3, 9–12)*:

$$\text{CBR} = E\phi \text{ (in kg/cm}^2\text{)}/CE \quad (1)$$

where CE is an empirical factor that varies mainly between 100 and 150 for in situ CBR between 2 and 30. $CE = 130$ is usually used for pavement-strengthening design *(3, 9)*.

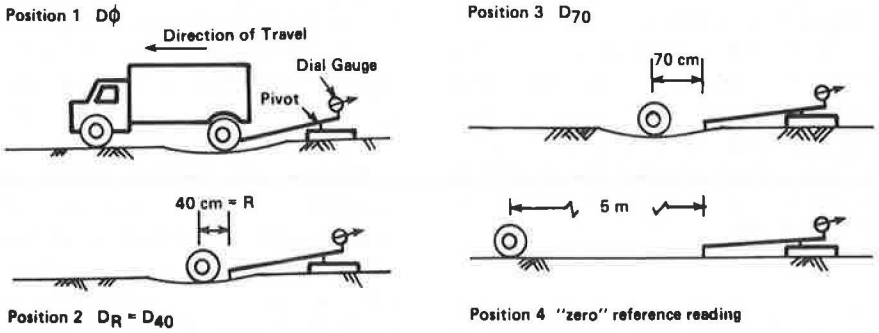

FIGURE 2 Schematic of Benkelman beam deflection procedure.

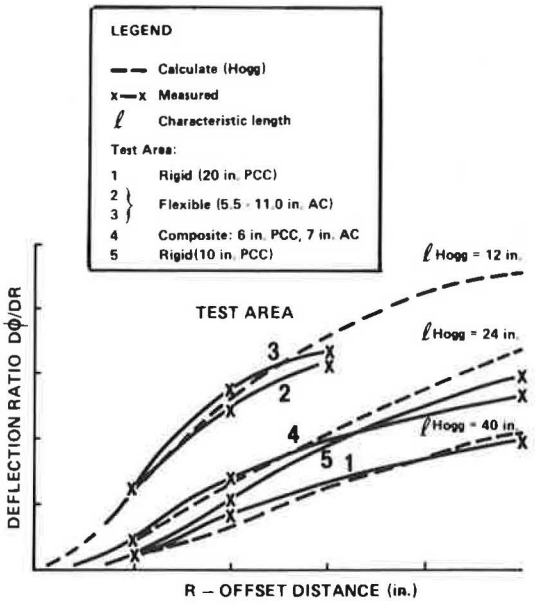

FIGURE 3 Comparison between measured and calculated deflection basin.

The use of the Hogg model for determining the subgrade modulus ($E\phi$) from the measured center deflection $D\phi$ and the deflection DR at an offset distance R are described in detail by Greenstein; Wiseman and Greenstein; Bergen and Greenstein; and Wiseman et al. *(1–4)*.

Determination of Pavement Modulus (E^*)

The combined modulus E^* of the AC and the base layers with a combined thickness of $HC = H_1 + H_2$ (see Figure 6) is determined by using the Odemark-Ullidtz equations *(13)* for equivalent thickness *(14)*. The equivalent thickness is determined according to the following equation:

$$HE = 0.9\, HC\, (E^*/E\phi)^{1/3} \tag{2}$$

The relationship between the center deflection $D\phi$ (between the dual wheels), the elastic modulus of the subgrade $E\phi$, and the pavement E^* is given in the following equation:

$$\begin{aligned} D\phi = {} & [(1+\mu)\,(PP)/2\pi]\,[(1/E^*)\,([2(1-\mu/r)] \\ & - [1/R(1)]\,\{2(1-\mu) + [Z(1)/R(1)]^2\}) \\ & + (1/E\phi)\,([1/R(2)]\,\{2(1-\mu) + [Z(2)/R(2)]^2\} \\ & - [1/R(3)]\,\{2(1-\mu) + [Z(3)/R(3)]^2\})] \end{aligned} \tag{3}$$

where

$$r = 1.5A = 1.5a, \tag{4}$$
$$Z(1) = HC + 0.6\,(A^2)/HC, \tag{4a}$$
$$R(1) = \{[Z(1)]^2 + (1.5A)^2\}^{1/2}, \tag{4b}$$
$$Z(2) = HE + 0.6\,(A^2)/HE, \tag{4c}$$
$$HE = 0.9HC\,(E^*/E\phi)^{1/3} \tag{4d}$$
$$R(2) = \{[Z(2)]^2 + (1.5\,A)^2\}^{1/2} \tag{4e}$$
$$Z(3) = (HE + NI) + 0.6\,(A^2)/(HE + NI), \tag{4f}$$

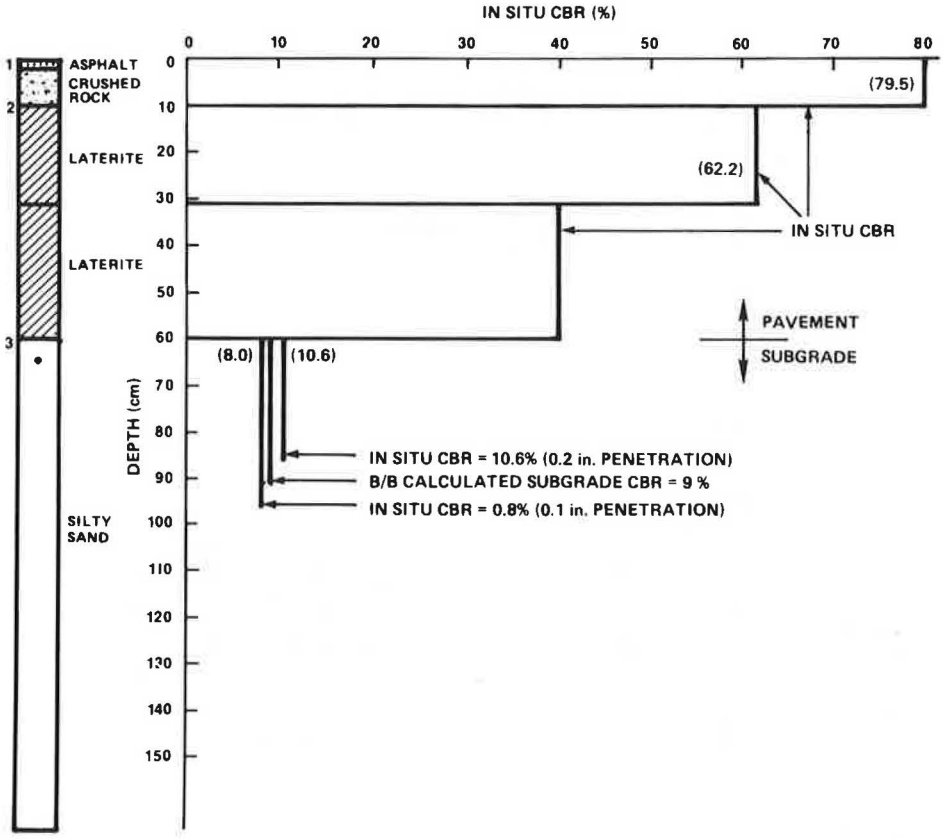

FIGURE 4 Relationship between calculated and in situ CBR (Thailand).

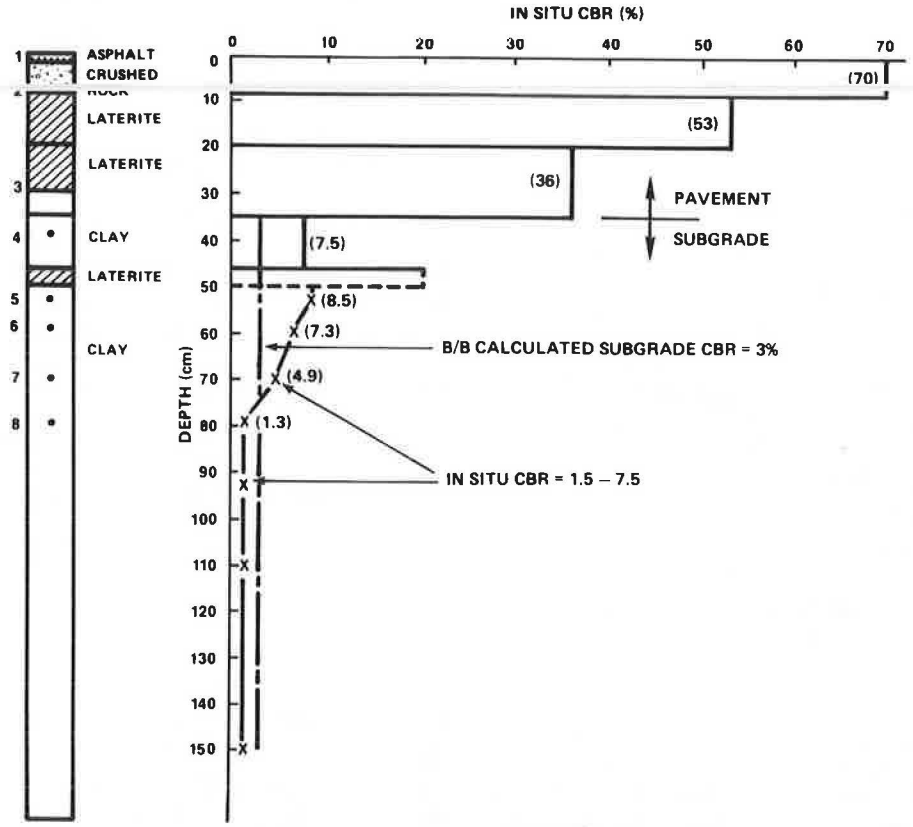

FIGURE 5 Relationship between calculated and in situ CBR (Thailand).

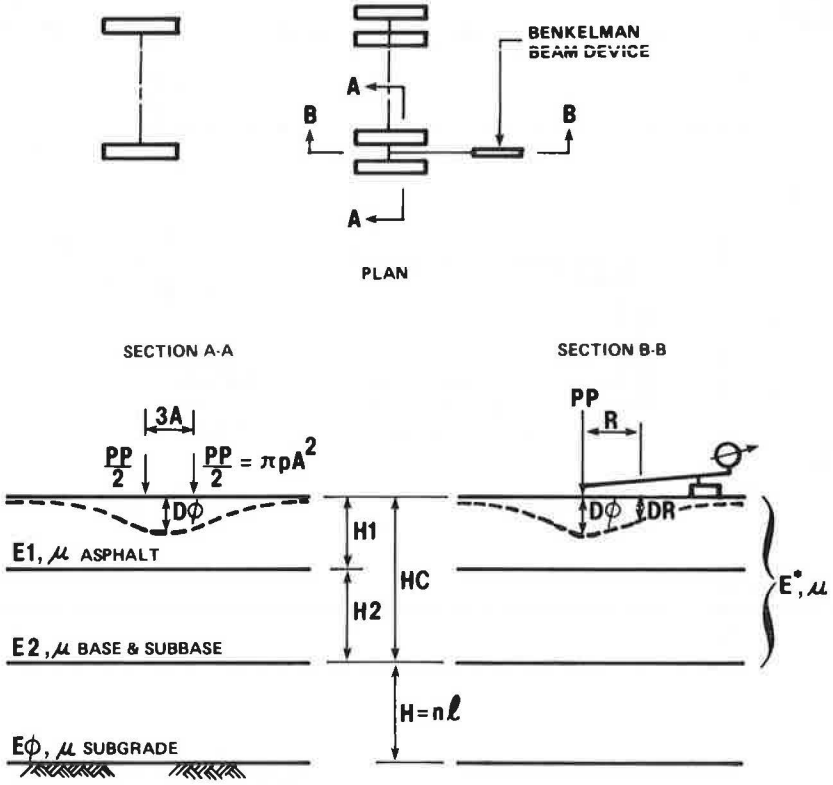

FIGURE 6 Subgrade pavement moduli parameters.

$$R(3) = \{[Z(3)]^2 + (1.5A)^2\}^{1/2}, \quad (4g)$$

N = 10 for rigid bottom at finite depth,
N = 100 for infinite subgrade,
PP = $\pi A^2 p$ (p = tire pressure), and
μ = Poisson factor.

Equations 2, 3, and 4–4g are used iteratively by pocket computer to determine the pavement modulus E^* for any given combination of subgrade modulus $E\phi$, pavement thickness HC, load PP, tire pressure p, and center deflection $D\phi$.

STRENGTHENING DESIGN OF PIURA AIRPORT

Destructive Testing Results

The test results of representative samples of subgrade, subbase, and base course materials are shown in Table 1. This investigation was carried out on six test pits, the locations along the pavement facilities of which are shown in Figure 7. The test results shown in Table 1 indicate that the pavement materials do not meet standard Federal Aviation Administration (FAA) specifications and are very sensitive to increased moisture. The increase in moisture analyzed in Table 1 was obtained by immersing the sample for 1 day. For example, in Pits 4 and 5 the base course material is classified as GC (clayey gravel or clayey sandy gravel) with plastic index PI = 9–19 and Passing Sieve 200 = 25–35. Standard specifications call for PI equal to or less than 6 and Passing Sieve 200 between 2 and 10. As is also shown in Table 1, the CBR of the GC material reduces from the 50–100 range to 2–9 after 1 day of immersion. Standard specifications call for minimum CBR = 80 after 4 days of immersion. Similar conclusions were obtained in other test pits.

Such routine destructive tests could not explain why the pavement of Piura Airport can accommodate medium-sized B-727, B-737, and F-28 jet aircraft. The only practical way to explain the past performance of the Piura pavement systems and to assign rational strength to the existing materials was to implement NDT techniques.

Analysis of NDT

The NDT survey and analysis determine the maximum deflection $D\phi$, offset deflection DR at an offset distance R, characteristic length $L\phi$, subgrade modulus $E\phi$, subgrade CBR, and pavement modulus E^*. Tables 2 and 3 present typical computerized results determined on Piura runway between Stations 1 + 375 and 1 + 975. The NDT was carried out each 25 m. The results in Tables 2 and 3 refer to offset deflection of R = 40 cm and R = 70 cm, respectively. These tables indicate that in both cases the distribution of CBR along the runway is similar. For both offset distances, the subgrade CBR is about 7 percent from Stations 1 + 375 to 1 + 575 and about 3 percent from Stations 1 + 575 to 1 + 975. This indicates that different deflections and

TABLE 1 INFLUENCE OF MOISTURE CHANGES ON MATERIAL STRENGTH (Piura Airport)

Pit No.	Type of Material	Classification	LL (%)	PI (%)	Passing Sieve 200 (%)	In Situ Moisture (%)	Laboratory CBR: In Situ Density (%)	
							In Situ Moisture	1 Day in Water
P-1	Subgrade	SC	30	12	44	3	73	2
P-2	Base	GM-GC	23	5	30	6	100	24
P-3	Subbase	SM	21	NP	20	2	100	9
P-3	Subgrade	SP-SM	–	NP	12	3	34	6
P-4	Base	GC	26	9	25	2	100	9
P-4	Subgrade	ML-CL	25	6	75	4	39	1
P-5	Base	GC	32	19	35	8	50	2
							100	3
P-6	Base	GP-GM	14	NP	10	1	82	8

NOTE: LL = liquid limit, PI = plastic index, CBR = California bearing ratio. SC = clayey sand or clayey gravelly sand; GM = silty gravel or silty sandy gravel; GC = clayey gravel or clayey sandy gravel; SM = silty sand or silty gravelly sand; SP = sand or gravelly sand, poorly graded; ML = silts, sandy silts, gravelly silts, or diatomaceous soils; CL = lean clays, sandy clays, or gravelly clays; and GP = gravel or sandy gravel, poorly graded.
SOURCE: Corps of Engineers.

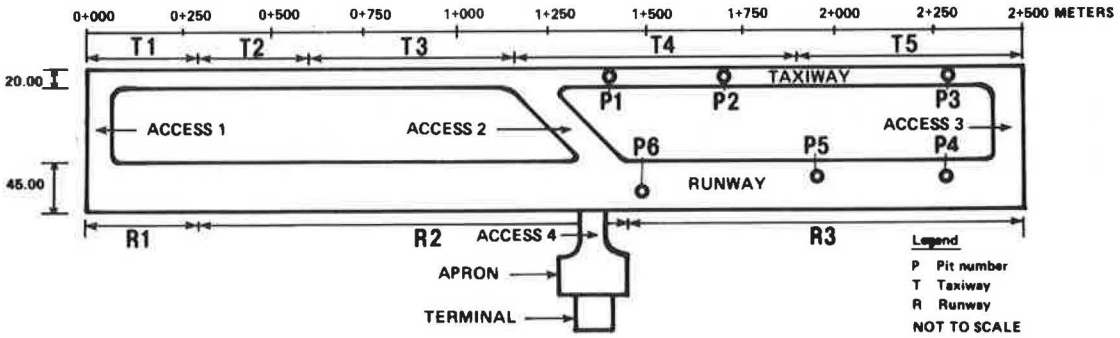

FIGURE 7 Schematic layout of Piura Airport.

TABLE 2 NDT TEST RESULTS OF PIURA RUNWAY (R = 40 cm)

Station	DØ .01 mm	DR .01 mm	LØ (cm)	EØ (kg/cm²)	CBR (%)	E* (kg/cm²)	E*/EØ	CBR Graphic
1+375	50.0	32.0	29.1	676.4	6.1	2526.5	3.7	******
1+400	58.0	30.0	20.0	747.2	6.8	1505.0	2.0	******
1+425	58.0	38.0	30.4	563.8	5.1	2298.9	4.1	*****
1+450	36.0	26.0	36.9	773.7	7.0	4797.8	6.2	******
1+475	38.0	30.0	46.0	605.7	5.5	6329.0	10.4	******
1+500	46.0	36.0	44.9	511.2	4.6	5041.9	9.9	*****
1+525	44.0	32.0	37.4	624.8	5.7	3996.5	6.4	**
1+550	66.0	56.0	58.3	282.2	2.6	5374.1	19.0	**
1+575	64.0	54.0	57.0	296.7	2.7	5360.2	18.1	**
1+600	76.0	54.0	35.6	377.5	3.4	2156.8	5.7	**
1+625	80.0	56.0	34.5	368.1	3.3	1959.2	5.3	**
1+650	58.0	54.0	96.7	200.6	1.8	14963.6	74.6	**
1+675	74.0	46.0	27.7	475.5	4.3	1613.6	3.4	** *
1+700	90.0	62.0	33.4	336.1	3.1	1690.4	5.0	**
1+725	82.0	50.0	26.8	440.0	4.0	1385.7	3.1	** *
1+750	104.0	68.0	30.3	315.4	2.9	1270.5	4.0	**
1+775	96.0	60.0	27.9	363.9	3.3	1252.7	3.4	**
1+800	114.0	68.0	25.9	325.3	3.0	961.0	3.0	**
1+825	130.0	58.0	17.1	379.6	3.5	560.7	1.5	**
1+850	184.0	128.0	34.1	161.8	1.5	845.1	5.2	*
1+875	124.0	82.0	30.9	260.1	2.4	1098.7	4.2	**
1+900	110.0	74.0	31.9	285.6	2.6	1290.2	4.5	**
1+925	104.0	68.0	30.3	315.4	2.9	1270.5	4.0	**
1+950	144.0	72.0	19.9	310.8	2.8	580.5	1.9	**
1+975	158.0	92.0	24.9	241.6	2.2	666.5	2.8	**

NOTE: $D\phi$ = maximum deflection under rear axle, DR = deflection at a distance R from $D\phi$ or rear axle, $L\phi$ = characteristic length (distance at which deflection is 50 percent of $D\phi$), $E\phi$ = subgrade modulus of elasticity, CBR = California bearing ratio, E^* = pavement modulus.

TABLE 3 NDT TEST RESULTS OF PIURA RUNWAY (R = 70 cm)

Station	DØ .01 mm	DR .01 mm	LØ (cm)	EØ kg/cm²	CBR (%)	E* kg/cm²	E*/EØ	CBR Graphic
1+375	50.0	14.0	22.7	816.8	7.4	1904.3	2.3	******
1+400	58.0	16.0	22.5	709.5	6.5	1619.6	2.3	******
1+425	58.0	12.0	18.6	808.9	7.4	1352.8	1.7	******
1+450	36.0	14.0	29.5	925.9	8.4	3560.4	3.8	******
1+475	38.0	18.0	36.0	748.2	6.8	4420.4	5.9	******
1+500	46.0	20.0	32.7	669.9	6.1	3189.3	4.8	******
1+525	44.0	18.0	30.9	731.8	6.7	3091.1	4.2	**
1+550	66.0	32.0	37.0	420.9	3.8	2651.4	6.3	**
1+575	64.0	40.0	52.1	322.0	2.9	4622.0	14.4	**
1+600	76.0	34.0	33.7	395.0	3.6	2025.3	5.1	** *
1+625	80.0	38.0	36.1	354.4	3.2	2094.0	5.9	**
1+650	58.0	34.0	47.3	387.0	3.5	4346.5	11.2	** *
1+675	74.0	22.0	23.7	534.6	4.9	1344.2	2.5	** **
1+700	90.0	34.0	28.8	379.3	3.4	1379.7	3.6	**
1+725	82.0	26.0	24.9	465.2	4.2	1283.5	2.8	** *
1+750	104.0	32.0	24.4	373.2	3.4	993.1	2.7	**
1+775	96.0	32.0	35.9	385.8	3.5	1139.6	3.0	** *
1+800	114.0	38.0	25.9	324.9	3.0	959.7	3.0	**
1+825	130.0	46.0	27.2	274.4	2.5	890.9	3.2	**
1+850	184.0	48.0	21.6	230.0	2.1	491.3	2.1	**
1+875	124.0	40.0	25.3	304.6	2.8	855.1	2.8	**
1+900	110.0	38.0	26.7	329.3	3.0	1037.1	3.1	**
1+925	104.0	32.0	24.4	373.2	3.4	993.1	2.7	**
1+950	144.0	40.0	22.6	284.8	2.6	657.0	2.3	**
1+975	158.0	42.0	21.9	265.-	2.4	579.8	2.2	**

NOTE: $D\phi$ = maximum deflection under rear axle, DR = deflection at a distance R from $D\phi$ or rear axle, $L\phi$ = characteristic length (distance at which deflection is 50 percent of $D\phi$), $E\phi$ = subgrade modulus of elasticity, CBR = California bearing ratio, E^* = pavement modulus.

offset distances can be used and still result in the same CBR or subgrade modulus. This can also be considered another verification of the NDT methodology used in this study. This verification is shown in more detail in Figure 8, which shows the relationship between the CBR calculated for both R = 40 cm and R = 70 cm. Up to CBR = 8, both calculated CBR values are practically the same. For higher CBR values, which are associated with strong subgrade and smaller deflections, the deflection measurement is more sensitive and therefore the correlation is, relatively, not as good. In conclusion, the subgrade CBR values calculated from the NDT vary between the upper and lower CBR values shown in Table 1 and seem to accurately represent the performance of the local subgrade materials of Piura Airport.

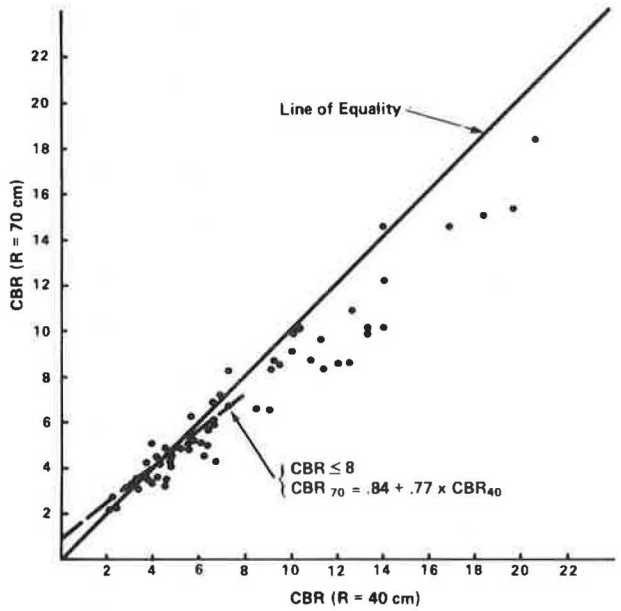

FIGURE 8 Distribution of subgrade CBR for R = 40 and R = 30 cm.

Pavement Evaluation and Strengthening Design

The total pavement thickness (*HC*, see Figure 6) is input to calculate the pavement modulus E^* (Equations 3 to 4g). Increasing the *HC* will reduce the value of E^* for a given subgrade modulus and deflection basin. The granular pavement modulus depends also on the subgrade strength *(15)*. In other words, $E_2/E\phi$ or $E^*/E\phi$ (see Figure 6) depends on $E\phi$. For a very strong subgrade E_2/E_1 tends to reach the Boussinesq uniform media where E_2/E_1 = 1. Experience with flexible pavement indicates that adequate performance is achieved when $E_2/E\phi$ varies between 2 and 5 *(2–4, 9, 15)*. This was also confirmed in the Piura study. No subgrade shear failure was observed when $E^*/E\phi$ was over 2 and subgrade CBR was over 6. The lower the subgrade CBR the higher the moduli ratio should be to prevent shearing failure and to achieve adequate pavement performance. Figure 9 presents a typical relationship between $E^*/E\phi$, *HC*, and subgrade CBR. This relationship was developed for the existing Piura Airport pavement sections that show adequate pavement performance. The main conclusion of Figure 9 is that for any given pavement thickness *HC*, an increase in the subgrade CBR reduces the required moduli ratio

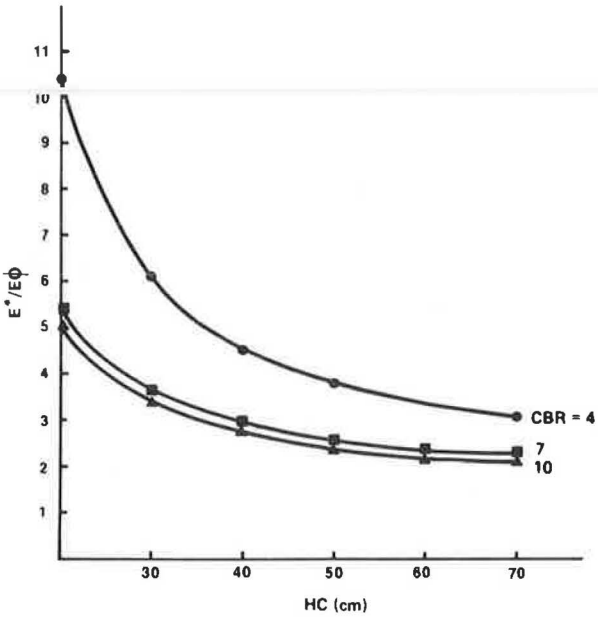

FIGURE 9 Typical relationship among $E^*/E\phi$, HC, and the subgrade CBR.

$E^*/E\phi$. Another interpretation of Figure 9 is that if the subgrade CBR and the moduli ratio $E^*/E\phi$ are known, the equivalent pavement thickness H_{EC} can be calculated. H_{EC} can be larger and smaller than the measured pavement thickness if $E^*/E\phi$ is greater than 5 and less than 2, respectively. The mechanism to determine the effective existing pavement thickness—H_{EC} in the Piura rehabilitation program—was carried out by means of the factor α defined in Equation 5:

$$\alpha = (\text{CBR}) \times (E^*)/(E\phi) \quad (5)$$

The higher the α factor, the higher the pavement rigidity or the better the existing pavement. Based on the conclusions shown in Figure 9 and the modulus ratio criteria of $E_2/E\phi$ = 2 – 5 *(2–4, 9, 15)*, the following relationship between α and the existing pavement thickness *HC* was developed:

1. When $\alpha \leq 10$ *HC* is reduced 10–20 percent, or H_{EQ} = (0.8–0.9) *HC*;
2. When $10 > \alpha > 15$, *HC* is not modified, or H_{EQ} = *HC*; and
3. When $\alpha \geq 15$, *HC* is increased 10–20 percent, or H_{EQ} = (1.1–1.2) *HC*.

HC denotes the existing pavement thickness, which was approximately 40 cm. H_{EQ} denotes the equivalent pavement thickness used to upgrade the existing pavement to carry 600 annual operations of B-727-100, with gross aircraft weight of 160,000 lb. The design parameters obtained from the NDT survey for the pavement strengthening are the subgrade CBR and α. The total thickness of a flexible pavement H_N needed to carry this traffic loading on a given subgrade CBR was determined according to the FAA standard guidelines *(16)*. The difference between the needed H_N and the existing equivalent thickness H_{EQ} is the required pavement strengthening. Table 4 summarizes the strengthening design of Piura Airport. The airport was divided into different sections with similar design parameters. For example, Section *R*2 is located on the runway between Stations 0 km + 300 m and 1 km + 450 m. The

subgrade CBR is equal to 7 and $\alpha = 20$. $H_N = 70$ cm *(16)*. The existing equivalent pavement thickness was increased from $HC = 40$ to 50 cm, because α is equal to 20. The $70 - 50 = 20$ cm of difference in pavement thickness is equivalent to 10 cm of asphalt concrete and 10 cm of granular base, which is equivalent to 5 cm of black base *(16)*. The Piura Airport pavement strengthening was completed in November 1986.

EVALUATION AND UPGRADING OF TALARA AIRPORT

This airport is located about 120 km north of Piura near the town of Talara. The altitude of the airport is about 100 m above sea level; the runway length is 2460 m; and the direction is 17/35. Takeoff and landing are done from north to south because of the strong southern wind. The climate conditions in Talara are similar to those in Piura with the water table 5–8 m beneath the subgrade surface. At Talara Airport, the use of marginal local materials has resulted in acceptable pavement performance. This airport is currently used for DC-8, B-727, and F-28 jet aircraft. The thickness of the upper layer of AC is 6 to 7 cm. The total airport pavement thickness varies between 45 and 60 cm, with an average total thickness of approximately $HC = 50$ cm. The pavement provided acceptable service during the last 10 yr. The base course is silty sand and gravel and its thickness is 15–30 cm. This base course has the following engineering properties (see Table 1 for classification description):

Classification: GC, GP-GM, and SP-SM;
Natural moisture: 4.5–5.5 percent;
Passing sieve 200: 19–25 percent (according to the FAA, it should be 2–10 percent); and
Plastic index: 7–14 (should be less than 7).

The laboratory CBR of the base course is very sensitive to moisture. An increase in humidity from 4.8 to 6.5 reduces the laboratory CBR from 80 to 10. The existing subbase material is sand clay or sandy silt classified as SC, SP-SM. The natural moisture content varies between 5 and 7 percent, passing Sieve 200 is 30 to 40 percent (should be less than 20 percent), and the plastic index is 7 to 15 percent (should be less than 8 percent). The local subgrade material is classified as CL, SP (see Table 1). Moisture content in the subgrade varies between 2 and 9 percent and the in situ CBR varies mainly between 5 and 8.

The preceding engineering information indicates that both the subbase and base-course materials do not meet standard FAA specifications and it is known that in tropical or even subtropical conditions this pavement is simply not adequate. Nevertheless, because of the arid conditions of Talara, good performance has been achieved. The NDT study carried out from December 1984 to January 1985 was analyzed and interpreted to better understand the performance of these marginal materials. The NDT survey was also used to determine the true strength parameters of the pavement materials. The conclusions of the NDT survey are presented in Figures 10 and 11. Figure 10 presents the CBR distribution and Figure 11 presents the distribution of α values defined in Equation 5.

Good correlation was obtained between the calculated CBR from the NDT survey and the in situ CBR determined on Pits 2 and 5 (see Figure 10). The in situ subgrade CBR was 6 and 11 in these two pits. Indicated in Figures 10 and 11 are the following three categories of subgrade CBR and three categories of α: $CBR \leq 5$; $5 < CBR \leq 8$, $CBR > 8$, and $\alpha \leq 10$, $10 < \alpha$

TABLE 4 STRENGTHENING PAVEMENT DESIGN: PIURA AIRPORT

Pavement Section[a]	Subgrade CBR (%)	α	H_N—Total Pavement Thickness Needed (cm)[b]	H_{EC}—Existing Pavement Thickness (cm)	Thickness of Strengthening Layers (cm)				Comments
					AC	Base	Subbase	Concrete Slab	
Runway Section									
(R1) 0 + 000 to 0 + 300	–	–	–	–	10	–	–		Concrete slab
(R2) 0 + 300 to 1 + 450	7	20	70	50	10	5[c]	–		
(R3) 1 + 450 to 2 + 500	4	8	90	30	10	20	30		
Taxiway									
(T1) 0 + 000 to 0 + 300	–	–	–	–	10	–	–		Concrete slab
(T2) 0 + 300 to 0 + 600	4	10	90	35	10	20	25		
(T3) 0 + 600 to 1 + 150	6	14	70	40	10	20	–		
(T4) 1 + 150 to 1 + 900	4	8	90	30	10	20	30		
(T5) 1 + 900 to 2 + 500	7	15	65	45	10	5[c]	–		
Access 1	9	20	60	50	10	–	–		
Access 2	7	15	65	45	10	5[c]	–		
Access 3	7	New	65	–	10	20	30		New pavement
Access 4	6	12	70	40	10	10[c]	–		
Apron	7	14	65	40	10	8[c]	–		

[a]See Figure 9 for location and layout.
[b]See *FAA Manual (16)*.
[c]Asphalt base.

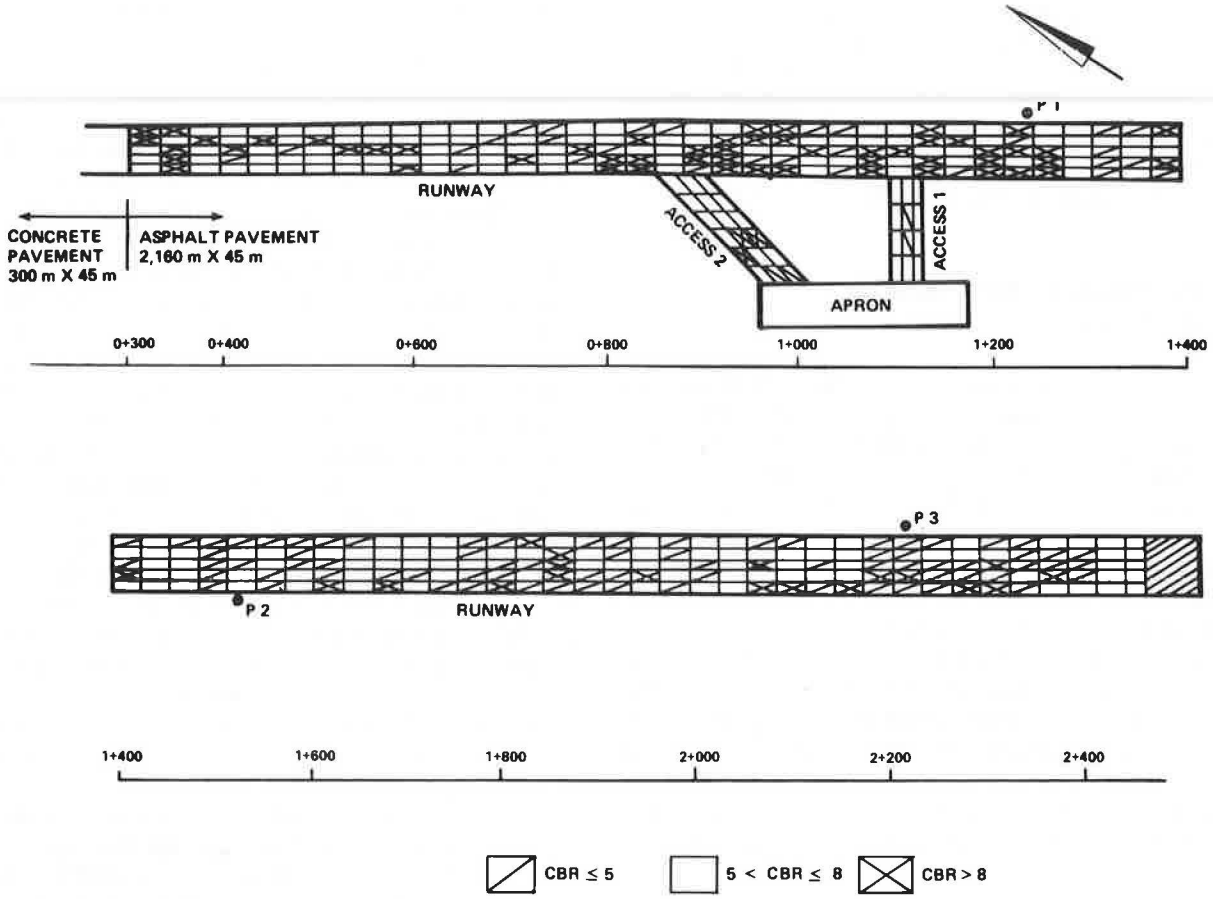

FIGURE 10 Distribution of the subgrade CBR in Talara Airport.

< 15, α ≥ 15. The average representative design parameters of the Talara Airport are CBR = 6–8 and α = 10–15. The average equivalent total pavement thickness design is H_{EC} = 50 cm.

Such an airport pavement can carry about 500 annual departures during 10 yr of a dual wheel gear aircraft with total gross weight of 100,000–120,000 lb *(16)*. This seems to be the weight of partially loaded B-727s, B-737s, and F-28s, mostly used for short distances of about 1100 km, which is the distance from Lima to Talara. In 1986, the Peruvian Transport Authority and the World Bank decided to implement the NDT survey to upgrade the airport pavement so that it could be used for B-727-100s with a gross weight of 160,000 lb and 600 annual departures. The strengthening design was based on (a) the previously mentioned traffic loading, (b) the distribution of CBR and α given in Figures 10 and 11, and (c) the FAA thickness design guidelines *(16)*.

The methodology used at Talara is identical to the strengthening design procedure used at Piura and is presented in Table 5. For example, in Station 0 km + 300 m to 1 km + 200 m, the subgrade CBR is 8 and α is 10. The total flexible pavement thickness needed is H_N = 60 cm *(16)*. As α = 10, the existing equivalent pavement thickness is reduced from 50 to 45 cm.

TABLE 5 STRENGTHENING PAVEMENT DESIGN: TALARA AIRPORT (600 annual operations—B-727)

Pavement Section	Subgrade CBR (%)	α	H_N—Total Pavement Thickness Needed (cm)[a]	H_{EC}—Existing Pavement Thickness (cm)	AC Overlay (cm)
Runway Section					
0 to 0 + 300	K = 150–250 PCI	Rigid	33	27	9
0 + 300 to 1 + 200	8	10	60	45	9
1 + 200 to 1 + 800	7	12	65	50	9
1 + 800 to 2 + 460	6	15	71	55	9
Accesses					
Access 1	7	15	65	55	6
Access 2	7	15	65	55	6

[a]See *FAA Manual (16)*.

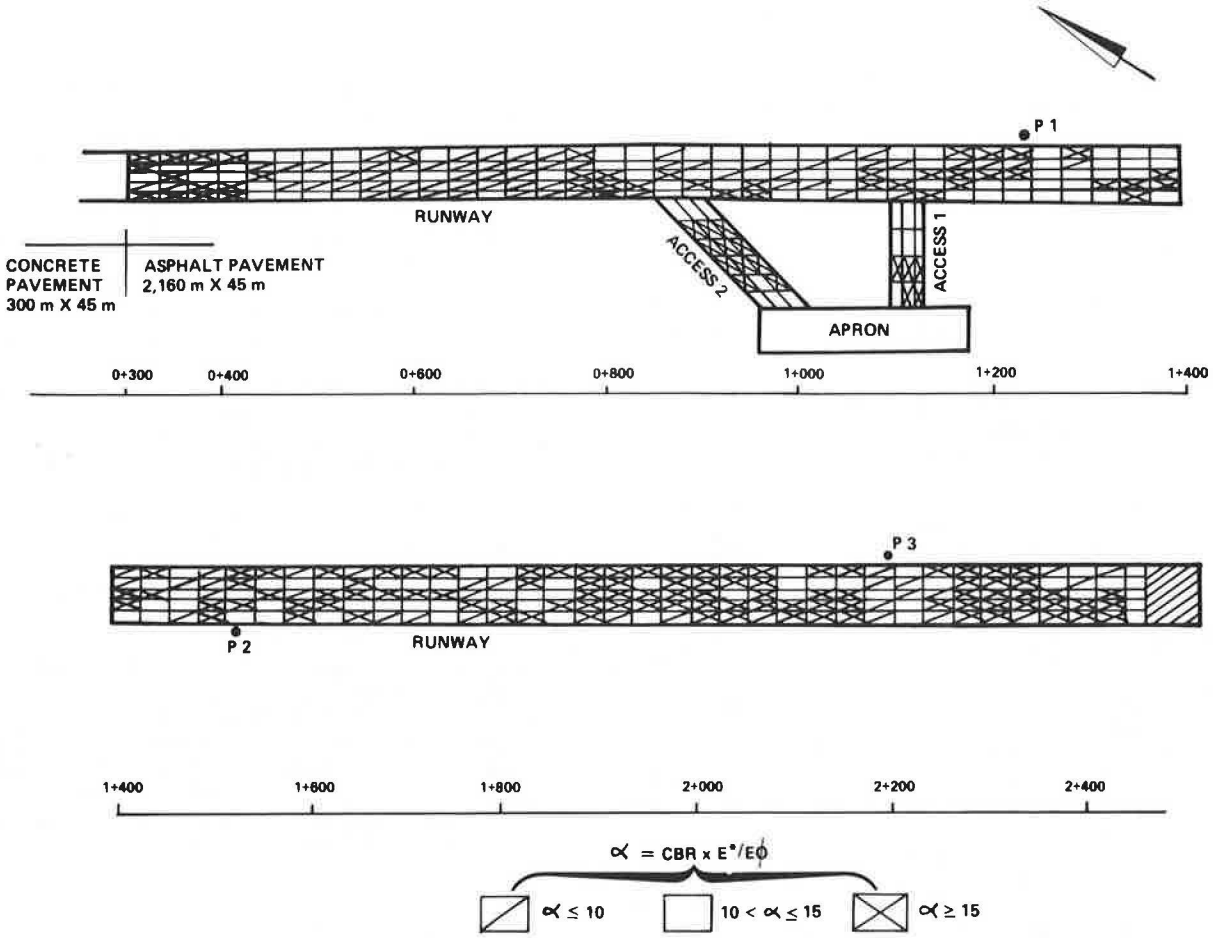

FIGURE 11 Distribution of α in Talara Airport.

The difference of pavement thicknesses is ($H_N = 60$) – ($H_{EC} = 45$) = 15 cm, which is equivalent in the semiarid region of Peru to 9 cm of asphalt overlay.

In a similar way, 9 cm of AC was designated to strengthen other sections of the runway and 6 cm of AC was needed to strengthen Accesses 1 and 2. The overlay thickness design of 9 cm of AC was also used to strengthen the rigid northern runway section *(16)* (see Table 5). This thickness might not be sufficient to prevent reflection of cracks. Nevertheless, it was decided to construct this AC overlay with two layers: the bottom AC layer of 6 cm with coarse gradation and a higher percentage of air voids of 6–8 percent to reduce refractions of cracks, and the upper layer of 3 cm with 3–5 percent air voids with smaller particles to improve riding quality. Monitoring of the new pavement performance is scheduled after construction is completed.

SUMMARY AND CONCLUSIONS

1. The Piura and Talara Airports have 2500-m-long runways and are located in the northern Pacific region of Peru, 1000–1100 km north of Lima. The water table is 2–8 m under the subgrade surface and the annual rainfall is less than 150 mm. Currently, B-727s, B-737s, and F-28s are using both airports and DC-8s are also used at Talara.

2. The existing pavement materials do not meet standard FAA specifications related to plasticity, gradation, and CBR-moisture relationships. Nevertheless, experience of about 15 yr generally indicates adequate pavement performance.

3. Local pavement failure occurred in 1982 in the southern edge of Piura Airport because of a combination of pavement overstress and rare flash flooding with a return period of over 100 yr.

4. It is concluded that the most practical way to interpret the actual performance of marginal pavement materials in the Peruvian arid zone is to use NDT to determine the elastic parameters of the existing subgrade and pavement materials.

5. The methodology used to evaluate and upgrade the Piura and Talara Airports is based on the Hogg model of a thin plate on an elastic foundation. The subgrade modulus can be determined without prior knowledge of the thickness or other characteristics of the pavement layers. Once the subgrade modulus is known, the pavement modulus can be calculated for any given load and center deflection.

6. The interpretation of the NDT survey indicates that the existing marginal pavement materials in the arid zone that do not meet standard specifications can generate sufficient bearing capacity to support traffic loads of B-727s, B-737s, F-28s, and DC-8s.

7. The subgrade modulus, CBR, and pavement modulus were determined each 25 m by an NDT survey carried out with a Benkelman beam. The pavement parameters were used to upgrade the existing airports so that they could carry 600 annual operations of B-727s with total gross weights of 160,000 lb.

REFERENCES

1. J. Greenstein. Use of NDT and Pocket Computers in Pavement Evaluation. *ASCE Journal of Transportation Engineering*, Vol. III, No. 3, May 1985.
2. G. Wiseman and J. Greenstein. Comparison of Methods of Determining Pavement Parameters from Deflection Bowl Measurements. *Proc., Seventh Asian Regional Conference on Soil Mechanics and Foundation Engineering*, Haifa, Israel, Aug. 1983, pp. 158–165.
3. L. Berger and J. Greenstein. Use of Pocket Computers for Rehabilitation of Rural Roads in Dominica. In *Transportation Research Record 997*, TRB, National Research Council, Washington, D.C., 1984, pp. 90–98.
4. G. Wiseman, J. Greenstein, and J. Uzan. Application of Simplified Layered Systems to NDT Pavement Evaluation. In *Transportation Research Record 1022*, TRB, National Research Council, Washington, D.C., 1985, pp. 29–36.
5. A. H. A. Hogg. Equilibrium of a Thin Plate, Symmetrically Loaded Resting on an Elastic Foundation of Infinite Depth. *Philosophic Magazine*, Vol. 25, No. 168, 1938.
6. A. H. A. Hogg. Equilibrium of a Thin Slab on an Elastic Foundation of Finite Depth. *Philosophic Magazine*, Vol. 35, No. 243, 1944.
7. W. T. Hoyinck, R. Van Den Ban, and W. Gerritsen. Lacroix Overlay Design by Three-Layer Analysis. *Proc., Fifth International Conference on the Structural Design of Asphalt Pavements*, Delft, The Netherlands, Vol. 1, Aug. 1982, pp. 410–420.
8. G. Wiseman and L. Berger. Evaluation of Airfield Pavements and Subgrades Based on Deflection Basin Measurements (NDT). *Report to TRB Task Force A2T56—Nondestructive Evaluation of Airfield Pavements*, TRB, National Research Council, Washington, D.C., 1981.
9. G. Wiseman, J. Uzan, M. S. Hoffman, I. Ishai, and M. Livneh. Simple Elastic Models for Pavement Evaluation Using Measured Surface Deflection Bowls. *Proc., Fourth International Conference on Structural Design of Asphalt Pavements*, Ann Arbor, Mich., Vol. 2, 1977, pp. 416–426.
10. J. L. Green and J. W. Hall, Jr. *Nondestructive Vibratory Testing of Airport Pavements*. Experimental Test Results and Development of Evaluation Methodology and Procedure. Report FAA-RD-205, Publication WES TR S-75-14. Vol. 1, Federal Aviation Administration, U.S. Department of Transportation, Sept. 1975.
11. W. Heukelom and A. F. G. Klomp. Dynamic Testing as a Means of Controlling Pavements During and After Construction. *Proc., Fifth International Conference on the Structural Design of Asphalt Pavements*, Delft, The Netherlands, 1982.
12. G. Wiseman. The Interpretation of Surface Deflection Measurements Using the Model of an Infinite Plate on an Elastic Foundation. *Symposium on Nondestructive Test and Evaluation of Airport Pavement*, U.S. Army Corps of Engineers Waterways Experiment Station, Vicksburg, Miss., Nov. 1975.
13. P. Ullidtz. Overlay and Stage-by-Stage Design. *Proc., Fourth International Conference on the Structural Design of Asphalt Pavements*, University of Michigan, Ann Arbor, 1977.
14. P. Ullidtz and K. R. Peattie. Pavement Analysis by Programmable Calculators. *Journal of the Transportation Engineering Division*, ASCE, Vol. 106, No. TE5, Sept. 1980, pp. 581–597.
15. A. I. M. Claessen, J. M. Edwards, P. Sommer, and P. Uge. Asphalt Pavement Design: The Shell Method. *Proc., Fourth International Conference on the Structural Design of Asphalt Pavements*, Vol. I, University of Michigan, Ann Arbor, 1977, pp. 39–44.
16. *FAA Manual*. AC-150/5320-6C, Federal Aviation Administration, U.S. Department of Transportation, 1978.

Publication of this paper sponsored by Committee on Environmental Factors Except Frost.

Behavior and Design of Vertical Moisture Barriers

M. PICORNELL AND R. L. LYTTON

Seasonal wetting and drying affect pavements on expansive soils with two main damage types: roughness development and longitudinal cracking. The purpose of the moisture barrier is to isolate the subsoil from these climatic changes. The predominant type of damage and the function of the barrier are found to depend on the initial moisture conditions of the subsoil. For desiccated soils, the barrier must prevent the infiltration of rainfall into the shrinkage cracks to stop the development of roughness. For wet soils, the barrier must prevent excessive drying under the edge of the pavement. The barrier depth is chosen based on the maximum crack depth and the shrinkage of the pavement edge that would occur under the most severe drought intensity expected during the lifetime of the pavement. The drought intensity is chosen based on a statistical analysis of meteorological data for the site. The driest matrix potential profile is obtained from the drought intensity through a simulation of unsaturated water flow. This profile is used to determine the maximum shrinkage. The accumulated shrinkage with depth is used to calculate the total edge shrinkage. A modified shrinkage, which includes the effect of multiple cracks, is used to simulate the propagation of the cracks. The rooting depth of native vegetation is identified as the controlling parameter on the barrier depth. A conservative estimate of the depth of grass roots is 8 ft. A successful moisture barrier must be placed to the depth of the roots in order to stop longitudinal cracking and about 25 percent deeper than the rooting depth to stop the development of roughness.

Two main types of damage affect pavements founded on expansive soils. One is the formation of mounds and depressions responsible for the development of roughness in the pavement and the resulting loss in riding quality and the other is the occurrence of longitudinal cracks near the edges of the pavement, which results in the progressive deterioration of the pavement.

The installation of a vertical moisture barrier enclosing the soils beneath the pavement is a measure that has been used to dampen the moisture variations of the subsoil to reduce the differential volume changes that the pavement must withstand *(1)*.

Described in this paper are the possible roles of the barrier, the design considerations needed to tailor the depth of the barrier to the specific conditions of a site, and a simplified procedure to select the depth of a vertical moisture barrier for practical applications.

M. Picornell, Civil Engineering Department, University of Texas at El Paso, El Paso, Tex. 79968. R. L. Lytton, Texas Transportation Institute, Texas A&M University, College Station, Tex. 77843.

ROLE OF A VERTICAL MOISTURE BARRIER

A vertical moisture barrier can play different roles depending on the moisture conditions of the subsoil at the time of installation of the barrier.

If the subsoil is initially very dry, the soil deposit exhibits a characteristic shrinkage crack fabric that splits the top of the soil deposit into blocks. These cracks permit the access of free water to the soils beneath the pavement. The soils of the crack walls have access to free water and, therefore, can swell. The inner parts of the soil blocks do not swell because they do not have access to water because of the extremely low permeability of the soil blocks. This differential swelling is responsible for the development of roughness *(2)*. The role of the moisture barrier for this condition is to prevent the access of free water to the crack fabric of the soils beneath the pavement. To achieve this goal, the barrier should be installed to the maximum possible depth of the shrinkage crack fabric for the conditions of the site.

If the subsoil is initially very wet, the crack fabric is closed or ineffective in transmitting free water. However, the subsoil beneath the edge of the pavement experiences seasonal moisture changes, whereas the moisture of the subsoil beneath the center of the pavement remains constant. This differential behavior is responsible for the formation of longitudinal cracks along the edges of the pavement *(3)*. In this case the role of the barrier should be to reduce the seasonal moisture changes of the soil under the pavement edges. The depth of the barrier should be chosen to reduce the settlements under the edge so that the angular deflection imposed on the pavement does not cause longitudinal cracks.

The two most frequent cases that are expected to occur in practice are the installation of the barrier with a new pavement or rehabilitation of an old pavement. A new pavement is normally built during the drier months of the year; the subsoil can therefore be expected to be in dry condition and the main role of the barrier in such a case is to prevent the development of roughness. As a contrast, if the barrier is used to rehabilitate an old pavement, the dominant consideration will usually be to mitigate edge drying because the subsoil would be normally expected to be very wet *(4)*.

PRELIMINARY DESIGN CONSIDERATIONS

The soils beneath the pavement are not in direct contact with the atmosphere. The water removed or the water that infiltrates beneath the pavement must pass through the soil profile adjacent to the edge of the pavement. This profile is exposed to the

atmosphere and extends from the edge of the pavement to the flow line of the side drainage ditch. The depth of the barrier must be chosen based on the deepest shrinkage cracks that can occur in this profile to prevent the free water from bypassing the barrier. Furthermore, the volume changes of the soils under the edge of the pavement and located below the depth of the barrier will be approximately the same as the volume changes of the soils at the same elevation but in the exposed soil profile. In summary, the design of the moisture barrier can be based on the volume changes and depth of shrinkage cracks estimated for this exposed soil profile.

The maximum shrinkage crack depth is a function of the driest moisture profile possible. The maximum volume changes are a function of the wettest and driest moisture profiles that are possible in the exposed soil profile. These moisture profiles are driven by the climatic conditions: rainfall and evapotranspiration. As the climatic conditions are stochastic in nature the wettest and driest moisture profiles are also stochastic. The pavement should be designed for the worst conditions that can reasonably be expected to occur during its lifetime. This implies the need for attaching probabilities to different stages of wetness and dryness of the soil profile. The design should be based on the extreme profiles that have the desired probability of not being exceeded in the life of the pavement.

This can be accomplished using the existing record of weather data. The details of this analysis have been described elsewhere *(5)*. The results of this study indicate that the wettest profile can be considered to be near saturation in semidesertic climates. The driest profile is characterized by the depletion percentage of the soil reservoir that has the desired probability of not being exceeded.

The next step is to relate the depletion percentage to the driest moisture content (or matrix suction) profile. This can be accomplished by numerical simulation of water flow through a one-dimensional soil profile. The water movement is driven by the climatic conditions at the exposed ground surface. The water is removed from the section by evaporation from the exposed soil surface and by transpiration of the native vegetation.

There is ample evidence that indicates that the evaporation from the soil surface is very small. This has been observed by Ritchie and Adams *(6)* from measurements in a lysimeter. The same conclusion can be obtained from the comparison of the heave measurements of de Bruijin *(7)* on a base soil surface treated with defoliant and on the same soil deposit covered with a glass-reinforced polyester sheet. The matrix suction profiles monitored by Ritchie et al. *(8)* and Richards *(9)* indicate that the effect of soil evaporation is confined to the uppermost foot of the soil deposit. The effect of the shrinkage in the upper foot on the maximum depth of the shrinkage cracks or on the volume changes of the soils under the edge is small compared to the total amount. Therefore, the driest profile can be obtained by simulation of the transpiration alone. This conclusion is in agreement with the observation of Williams and Pidgeon *(10)* that the vegetation controls the driest moisture profile.

An additional aspect relative to soil evaporation is that the presence of shrinkage cracks causes the exposure of more soil surface to the atmosphere and at wetter conditions than the ground surface. The question is whether, as suggested by Ravina *(11)*, the water removed from the crack faces can cause drying at the tip of the crack that could cause a progressive extension of the crack. The effect of wind drying has been found to decrease with depth inside the cracks *(12)*. The published data on moisture contents around cracks by Ritchie and Adams *(6)* and by Johnson and Hill *(13)* indicate that the removal of soil water from cracks deeper than 2 feet is unlikely. As the design crack depth is the maximum that is likely to occur in the desired return period, the crack depth sought will most likely be considerably larger than 2 feet. Therefore, it appears safe to conclude that crack propagation due to evaporation drying at the crack tip is negligible.

DETERMINATION OF THE DRIEST MOISTURE PROFILE

The driest matrix suction profile that corresponds to the depletion percentage chosen in the statistical analysis is obtained from the numerical simulation of the water flow driven by plant transpiration alone. The flow of water through the soil mass is assumed to obey an extension of Darcy's law proposed by Richards *(14)* for unsaturated soils with the inclusion of a sink term to account for the removal of pore water by the roots of the vegetation.

The approach adopted is to represent the roots by a sink term distributed uniformly within each elemental volume of soil. Molz et al. *(15)* have shown that this approximation is fairly close to reality. The extraction term used is a slight modification of the term proposed by Nimah and Hanks *(16)*. This model was satisfactorily tested under field conditions *(17)*.

A prerequisite to using this extraction term is knowing the root density distribution and rooting depth of the vegetative cover. The most frequent kinds of vegetation growing near pavements are native grasses. There is ample agreement in the literature *(10, 18–20)* about the rooting depths of native and sod-forming grasses, which are reported to be from 6 to 8 ft tall. Molz and Remson *(21)* have proposed a dimensionless root density distribution, which is shown in Figure 1, for rooting depths of 6 and 8 ft. Also shown in Figure 1 are root density distributions obtained from field surveys of soil monoliths by Weaver and Darland *(20)* and Laird *(18)* for typical Texas grasses. Molz's distribution for an 8-ft rooting depth is an envelope enclosing most of the available field data. This is the root density distribution adopted in this study.

The numerical simulation is approached through a finite element technique to discretize the space coordinates and to evaluate the space derivatives, and a finite difference scheme to discretize the time domain. The numerical algorithm used is an expanded version of the algorithm proposed by Nieber *(22)*. The simulation is performed with the program "CRKFLOW", whose FORTRAN deck is listed by Picornell *(5)*. The simulation is carried out with material properties of expansive soils typical of Texas. The permeability function used was fitted through the measurements presented by Ritchie et al. *(8)*. The desorption curve was obtained from laboratory tests on samples from I-37 in San Antonio, Texas *(5)*.

The matrix potential profile at several degrees of depletion of the soil reservoir is obtained from field capacity by imposing a constant transpiration rate of 0.00005 cm/sec. This simulation

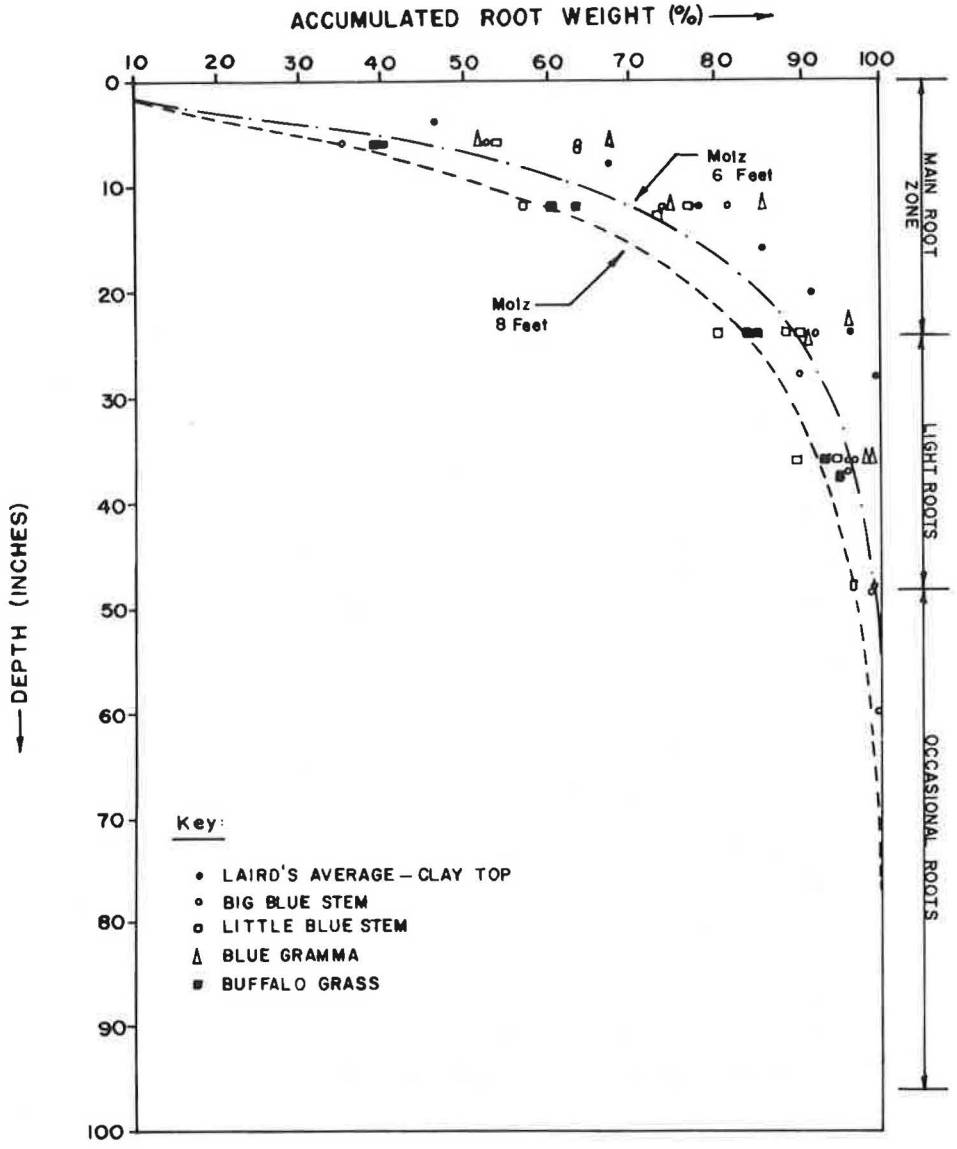

FIGURE 1 Summary of root density distributions for native grasses.

does not include any interruption due to rainy periods or soil water redistribution. The results of the simulation include nine intermediate steps of depletion plus the profile that corresponds to the wilting of the vegetative cover. These results are presented in Figure 2.

Although these results were obtained with a specific combination of permeability function and desorption curve, the resulting matrix potential profiles are considered to be representative for other expansive soils provided that their permeability functions are similar. The desorption curve is relevant when the matrix potential profiles must be related to the degree of water depletion in the soil profile.

These potential profiles were obtained assuming a rooting depth of 8 ft. The extension of these results to slightly different rooting depths can be obtained by scaling the depths. Figure 3 shows a comparison of a field matrix potential profile at the lower limit of water availability (8) for a crop with an observed rooting depth of 5 ft and the results of the simulation at the lower limit of water availability scaled for a rooting depth of 5 ft. This scaled profile compares favorably with Ritchie's field measurements.

DETERMINATION OF SETTLEMENTS AND CRACK DEPTH

The driving mechanism causing the edge settlements or the propagation of the shrinkage cracks is the volumetric strains experienced by the soil upon a change of matrix potential. The volumetric strains are determined with existing methods *(23)*. The linear shrinkage is obtained as one-third of the volumetric strain.

The material properties to apply this model can be obtained from laboratory tests on undisturbed samples *(24)*. However, the expenses involved are seldom justifiable in a routine design. This limitation can be avoided by finding these properties from published correlations *(25)* based on index soil properties.

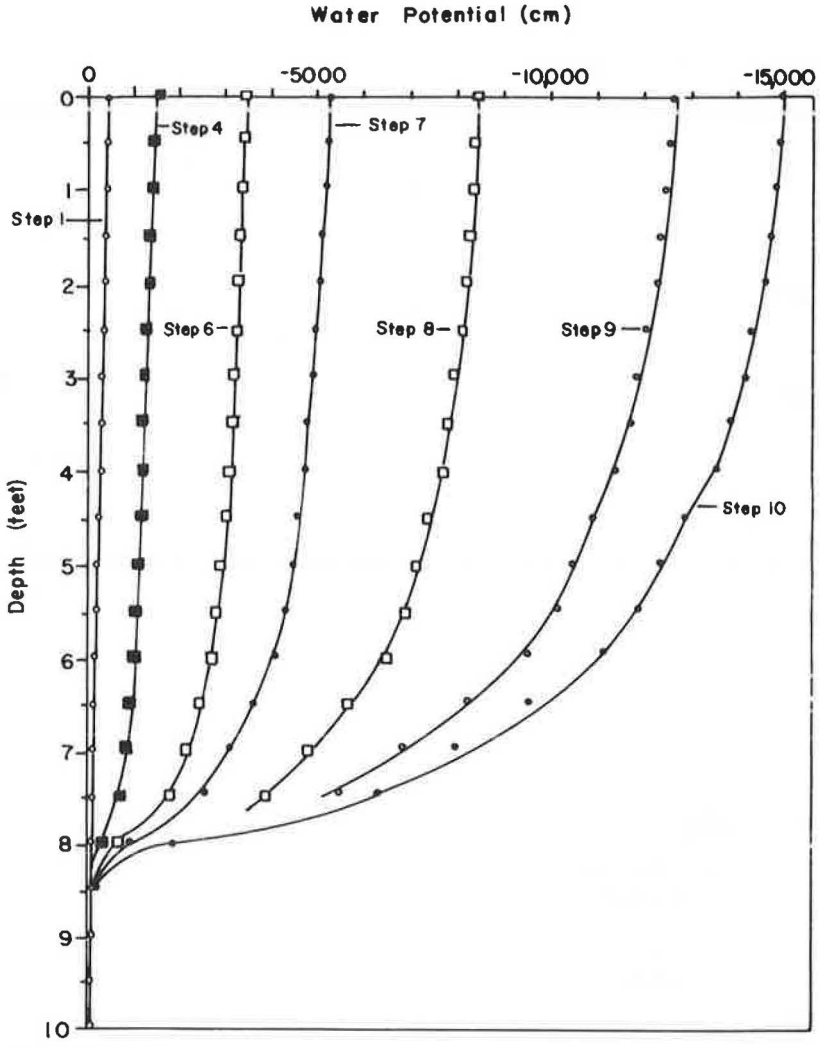

FIGURE 2 Design profiles of matrix potential versus depth.

The shrinkage of the soils under the pavement are estimated by the shrinkage of the exposed soil profile adjacent to the barrier. In this manner, the soils below the bottom of the barrier, the depth interval A–C in Figure 4, are assumed to experience the same movements as those experienced by the soils at the same elevation but outside the barrier. The soils enclosed by the barrier and located above the bottom tip of the barrier, the depth interval B–A in Figure 4, are assumed to remain at constant volume at all times.

From this point of view, the barrier depth is chosen as the smaller depth that would maintain an angular distortion of the pavement edge (ratio of edge settlement to the length of the edge moisture variation) at less than 1/360 on the occurrence of the design meteorological event. The edge moisture variation, E_m in Figure 4, is different depending on the depth of the barrier. A conservative estimate for E_m is the distance A–C between the bottom of the barrier and the bottom of the soil layer affected by the event.

The shrinkage crack propagation is a consequence of the differential shrinkage of the soils at different depths. There is an assortment of cracks with different depths in the soil mass. There is ample evidence *(26, 27)* that the number of shrinkage cracks in a section, their geometric configuration, and the distribution of crack depths are imposed by the type of vegetative cover and the predominant environmental conditions. A shrinkage crack depth distribution that is believed to be representative of roadside conditions in Texas corresponds to the site GRF in the experimental data published by El Abedine and Robinson *(26)*.

To estimate the maximum crack depth, it is necessary to study the behavior of a soil region extending between two consecutive major cracks. A typical spacing between major cracks is 16 ft (488 cm) *(2)*. The linear shrinkage that occurs at each depth translates into displacements imposed on the crack faces of all shrinkage cracks reaching each depth. Therefore, only part of the total shrinkage at each depth goes into increasing the width of the two major cracks. This part of shrinkage is estimated from the average crack spacing at each depth assuming that all cracks are evenly spaced. The distribution of crack depths used is shown in Figure 5. The analysis forces the distribution of cracks always to follow the relationship shown in Figure 5 independently of the size of the maximum crack depth. The average spacing is obtained by dividing the 16-

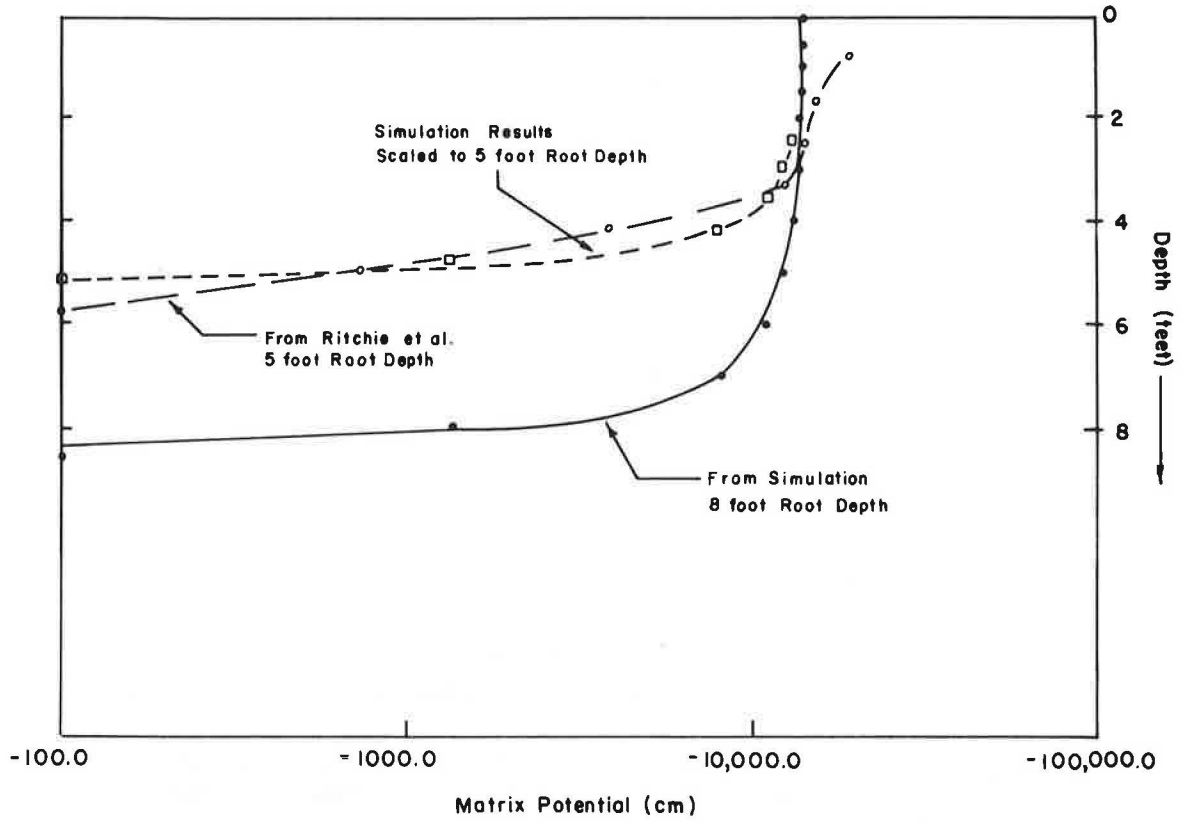

FIGURE 3 Water potential versus depth at the wilting point.

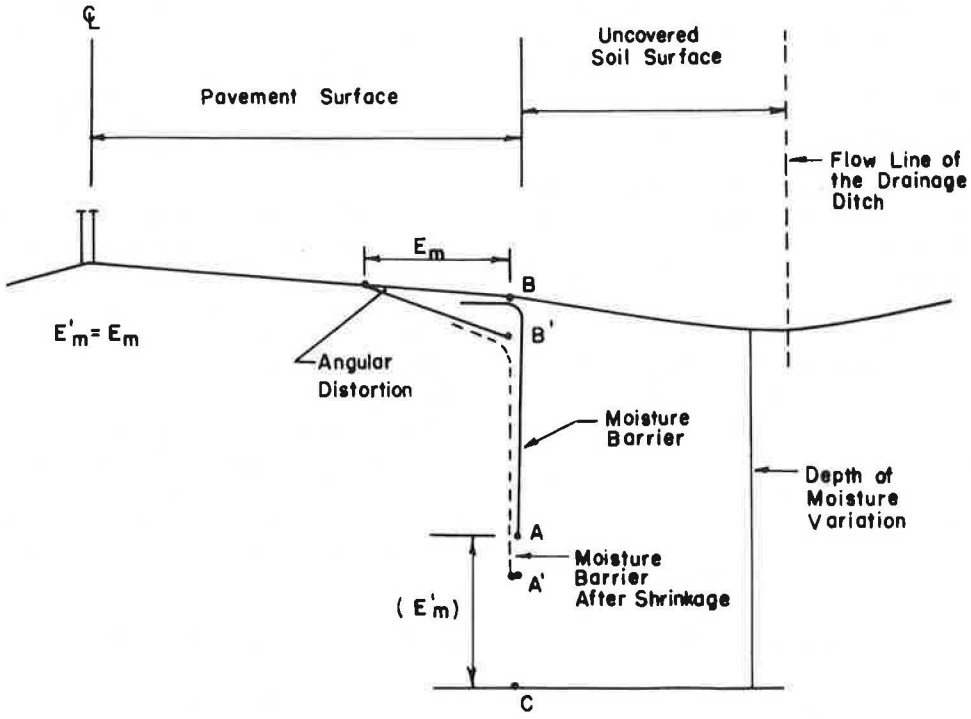

FIGURE 4 Illustration of the differential drying conditions under the pavement edge.

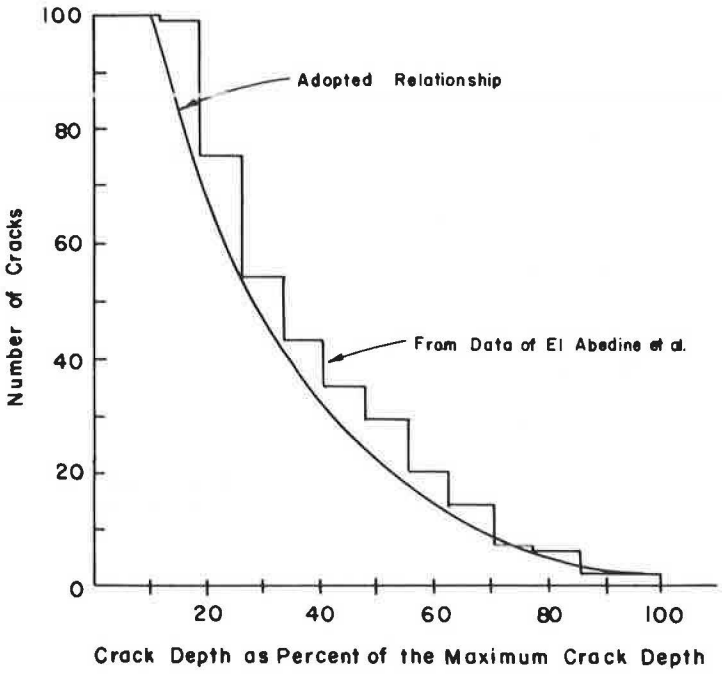

FIGURE 5 Distribution of number of cracks with depth.

ft (488-cm) spacing between major cracks into the number of cracks (n_c) minus 1 that reach the depth in question. Because the depth included in Figure 5 is relative to the maximum crack depth, n_c is found at each depth by trial and error. Because each soil column is bounded by two shrinkage cracks, this implies that the displacement (d_i) imposed on each crack face is the result of the linear shrinkage (ε_i) acting only on one-half of the average crack spacing.

Neglecting the Poisson's effect, the shrinkage crack must extend at least to the deepest point in the profile that will experience any volumetric strains in the change from the wettest to the driest profile. The question is how much the crack will propagate beyond this point imposed by the displacements that occur above this same point.

Besides the imposed displacements, the factor controlling this extra crack propagation is the predominant soil modulus in the area where the propagation takes place. The area into which the crack will extend will be essentially unaffected by the root extraction, as the change from wettest to driest conditions will not impose any volumetric strains at this level. Therefore, it is reasonable to assume that the soil in this area will behave very nearly as if it were saturated. Under these conditions, the extension of the crack may be analyzed assuming that the soil near the crack tip is elastic, with the elastic modulus being a function of the confining stress. The dependence of the elastic modulus on the confining stress is assumed to follow the model proposed by Janbu *(28)*. The material parameters of this model are adopted from typical values proposed for highly plastic soils *(29)*.

The effect of the soil modulus on the final crack depth is small. Therefore, it is believed that the crack depth for most expansive soils can be found, to a good approximation, using an elastic modulus of 1,400 psi (100 kg/cm^2) at 5 psi (0.3 kg/cm^2) confining pressure; that is, the crack depth can be found using the set of curves presented in Figure 6.

PROPOSED DESIGN PROCEDURE FOR DEPTH OF MOISTURE BARRIERS

The first step to determine the depth of a moisture barrier is to select the appropriate parameters for the particular site being considered. These include parameters related to the geometrical design of the cross section and others related to site conditions. The rainfall multiplying factor (RMF) is in the first category. The second category includes the rooting depth and the maximum water capacity of the soil profile.

The next step is to use these data and the design life chosen for the pavement to determine the minimum water depth associated with the design event as described elsewhere *(5)*. From this minimum, the driest matrix potential profile to be expected is defined. The driest and wettest profiles determine the total linear shrinkage that can take place at each depth within the root zone.

The total shrinkage at each depth is modified to take into account the presence of multiple shrinkage cracks. The maximum crack depth is obtained by trial and error. The criterion to prevent the development of pavement roughness is based on the maximum crack depth. The criterion to prevent excessive edge drying is derived from the expected profile of total shrinkage.

The evaluation of these parameters and a summary of all of the steps for the design are discussed in detail in the rest of this section. The design procedure is illustrated for a section of I-37 in San Antonio, Texas. The site investigation and the monitoring of this section have been described elsewhere *(30)*.

Rainfall Multiplying Factor (RMF)

The RMF embodies the effects of several phenomena that modify the availability of water to a soil profile adjacent to an

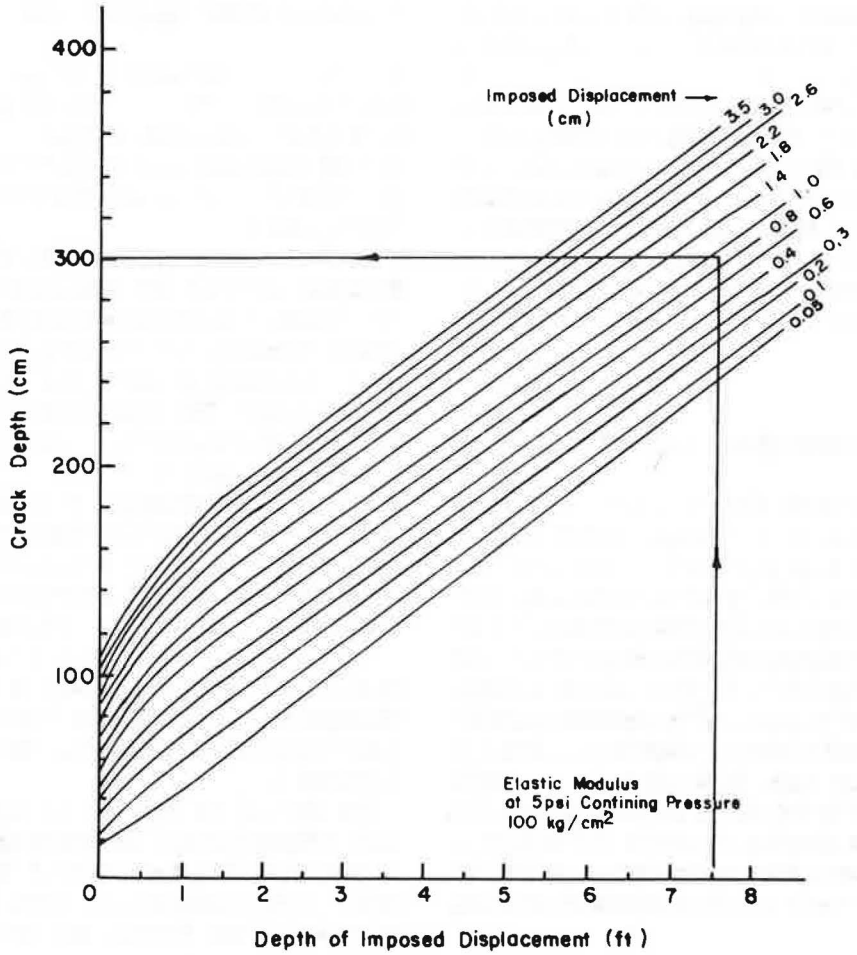

FIGURE 6 Design curves of crack depth versus imposed displacement and depth of imposed displacement for an elastic modulus of 100 kg/cm^2.

impermeable structure like a pavement. The first of these effects is due to the runoff from the pavement if it drains toward the side drainage ditch. This runoff is an extra supply of water for these soils above the normal rainfall for the area. The second effect is due to the shape of the general ground surface surrounding the pavement. If the ground surface slopes down away from the pavement, the free water within the crack fabric might flow away from the structure; by way of contrast, if the highway is in a cut, part of the rainfall on the slope will flow toward the drainage ditch and will provide an extra supply of water for the soils adjacent to the pavement. Thus, the depth of the moisture barrier may not be uniform within a section. The depth of the barrier must be defined for the conditions prevailing at the edge of the pavement where it is to be installed.

The RMF is equal to 1 when the pavement edge does not receive any runoff. When there is runoff from the pavement, the effect is estimated assuming that all the rainfall on the pavement is available to the edge soils. The total water available is obtained by multiplying the rainfall by the ratio of the width of the pavement draining to the side plus the width of the edge soils over the width of the edge soils. This relative width ratio is believed to be a reasonable estimate of the RMF for the case of a highway on flat ground; however, this value must be modified somewhat if the section runs in a cut or an embankment. When the highway is in a cut, the RMF is expected to be somewhat larger than the relative width. Similarly, it is expected that the RMF is smaller than the relative width ratio in the case of an embankment.

The section of I-37 that is used in the example runs in a cut about 15 ft deep. The roadway has three lanes with a shoulder in each direction separated by an impermeable median. The cross section is symmetrical with respect to the median, and, therefore, the moisture barriers on both edges of the pavement may be designed for identical conditions. The total width of each roadway is about 65 ft; the width of the exposed soil surface at the edge of the pavement is from 5 to 15 ft. Therefore, the relative width ratio is at least 5, even without including any contribution of water from the cut slope surface. In this case, an RMF of 5 seems reasonable.

Rooting Depth

There is ample agreement in the literature that the root system of native and sod grasses extends to maximum depths of 6 ft (180 cm) to 8 ft (240 cm). A root depth of 8 ft (240 cm) means that the barrier will be designed for the worst possible case. This assumption appears reasonable for the case of a well-developed homogeneous soil profile. However, under many conditions root development is impaired and the above assumption may be excessively conservative. Root growth is

controlled by water availability, soil compaction, and the availability of oxygen. But the main factor that limits root growth is oxygen availability *(27)*.

If the soil is depleted of water frequently, it seems reasonable to expect root depths of 8 ft (240 cm). However, if the profile is rarely emptied of water, the lower part of the root system will remain in anaerobic conditions most of the time, and therefore it will progressively die. If the root system is confined to shallower depths, the effect on the design can be very important. However, at the present time, until this aspect can be confirmed, the conservative approach is to use a root depth of 8 ft (240 cm).

Determination of the Driest Matrix Potential Profile

The root depth selected for the site is used to scale the design matrix potential profiles shown in Figure 2. The next step is to determine the minimum water depth for the design event. This is accomplished using the results of the statistical analysis *(5)* with the maximum soil capacity, life of the pavement, and the RMF. For I-37, a profile capacity of 22 in. (56 cm) of water, an RMF of 5, and a design life of 25 years indicate a design minimum water depth of 35 percent of the maximum capacity.

This percentage is used to identify which intermediate drying step yields a stored water depth closest to the design minimum. This is done by calculating the water depth stored for each step and then choosing the profile that contains a stored water depth closest to the design minimum. For I-37, the driest potential profile matrix possible corresponds to drying step No. 6.

Calculation of Shrinkage and Crack Depth

The first step is to calculate the linear shrinkage associated from saturation to the driest possible profile. Then the experimental crack distribution of Figure 5 is used to estimate the imposed displacements on the potential crack face. This process can be arranged in a table as illustrated for the pavement of I-37 in Table 1.

The final matrix potential at each node shown in column 3 is the drying step No. 6. The vertical stresses shown in column 4 are calculated with the unit weight of the soils at I-37. The soil parameters used are $\gamma_h = 0.08$ and γ_σ 0.10 and thresholds of –50 cm for the matrix potentials and 0.097 kg/cm^2 for the octahedral stresses. The linear shrinkage at each node is calculated by substituting the final potentials in column 3 and stress, column 4, into Equation 2.

From the linear shrinkage, the crack depth is calculated by trial and error. In Table 1, the first guess is a maximum crack depth of 9 ft (270 cm). The relative depth is found by dividing each node depth, column 2, into the 9 ft (270 cm). The number of shrinkage cracks that reach each node is read from Figure 5 as the ordinate of the continuous curve corresponding to the depth of the node. The number of cracks and the linear shrinkage are used in Equation 3 to determine the displacements imposed on the crack's face. These are listed under Trial 1, column 7.

The depth of the node and the imposed displacement are used in Figure 6 to read the corresponding crack depth, which is listed under Trial 1 of column 8. The largest value in this column is the maximum crack depth. In this case, the largest value is 325 cm. Because this crack depth is noticeably

TABLE 1 SAMPLE OF CALCULATION OF CRACK DEPTH FOR I-37 IN SAN ANTONIO, TEXAS

Mode No.	Depth (cm)	Matrix Potential (cm)	Vertical Stress (kg/cm)	Linear Shrinkage (%)	Angular Deflection	Imposed Displacement (cm) Trial 1	Trial 2	Trial 3	Imposed Crack Depth (cm) Trial 1	Trial 2	Trial 3
1	0	3256	*	*	*						
2	15	3242	0.073	4.83	0.034						
3	30	3216	0.047	4.82	0.033						
4	45	3185	0.093	4.81	0.032						
5	60	3158	0.100	4.76	0.031						
6	76	3123	0.130	4.36	0.029						
7	91	3085	0.160	4.05	0.028						
8	106	3049	0.190	3.79	0.027						
9	121	3008	0.223	3.54	0.025						
10	137	2919	0.260	3.28	0.024						
11	152	2848	0.290	3.10	0.023						
12	167	2769	0.320	2.92	0.021	0.594					
13	182	2663	0.353	2.73	0.020	0.740					
14	198	2377	0.387	2.47	0.018	0.927	0.603				
15	213	2085	0.420	2.20	0.016	1.193	0.716		275	261	
16	228	1750	0.453	1.89	0.013	1.537	0.838		298	288	
17	243	677	0.481	0.68	0.007	0.830	0.415		325	300	
18	258	131	0.513	0.00	0.000	0.000	0.000		312	292	
						Assumed Crack Depth			Resulting Crack Depth		
						270	300		325	300	

different from the initially assumed crack depth (270 cm), a new trial is necessary. The new guess is 10 ft (300 cm), which is the average of the two crack depths of the previous iteration.

The same process is repeated for the second guess. Now the resulting crack depth at the end of the iteration is 10 ft (300 cm), which is the same value as was assumed. Therefore, the maximum crack depth at I-37 for a 25-yr return period is 10 ft (300 cm).

The angular deflections shown in column 6 are intended to provide the basis on which to choose the criteria to prevent excessive edge drying. This column has been calculated assuming that the linear shrinkage obtained for each node is a representative average for a one-half-foot slice centered on the node. The settlement at the edge of the pavement is assumed to be the accumulated shrinkage of the soils deeper than the tip of the barrier. The angular deflection is estimated by dividing the edge settlement into the distance from the tip of the barrier to the first node with no shrinkage. The angular deflections shown in column 6 are the results for the depths of different barriers. The depth of the barrier that corresponds to a specific value of angular deflection, column 6, is the midpoint between the corresponding node and the node above it.

Design Criteria

When the moisture barrier is intended to prevent the development of pavement roughness, the barrier should extend to the maximum crack depth expected with the hydrologic regime imposed by the pavement, or to the crack depth existing at the time of construction, whichever is larger. For the case of I-37, this criterion would require a barrier 10 ft (300 cm) deep.

The second function of the moisture barrier is to prevent excessive drying of the soils under the pavement edges in order to prevent the formation of longitudinal cracks along the edges of the pavement. The size of the deformation that would cause the pavement to crack depends on the pavement itself. A concrete pavement would be expected to crack when the angular deflection exceeds 1/360. The asphalt concrete in a flexible pavement can take larger angular deflections. However, as the asphalt ages, the material becomes brittle. Because this aging process is very fast compared with the design life of the pavement, it is probably reasonable to use the same criteria for asphalt as for concrete.

For the case of I-37, to find the barrier depth that reduces the angular deflection to 1/360, it is necessary to interpolate the angular deflection data included in column 6. The interpolation was done assuming that the variation is linear. The resulting barrier depth is found to be 8 ft (240 cm).

The two criteria require barrier depths that differ by about 2 ft (60 cm) in the case of I-37. The question now is which of the two criteria should be used. The selection should be made on a case-by-case basis and should be based mainly on the initial status of the soil mass under the pavement. A vertical barrier for a new pavement would usually be designed to prevent the development of roughness. However, if there is evidence that the soil beneath the new pavement is not cracked, there is no need to design for this condition. It would be enough to design the barrier to prevent longitudinal cracking.

When a vertical barrier is to be placed at the time of repairing an old pavement, it is not clear which of the two alternatives should be used. The choice should be made depending on whether the subsoil under the old pavement has already reached the equilibrium profile. If this is the case, the barrier should be designed to prevent longitudinal cracking. Otherwise, it seems that the wise choice is to design the barrier to prevent the development of roughness.

In the case of I-37, a vertical moisture barrier was installed at a time of a major rehabilitation of that pavement section. The old pavement had been in place for more than 10 years at the time of the rehabilitation. This appears to be enough time for the soils under the old pavement to have reached their equilibrium profile. Thus, the existence of a shrinkage crack network in the soils beneath the pavement is unlikely. Therefore, the barrier depth at this site should be selected to prevent longitudinal cracking; that is, the barrier depth should be 8 ft (240 cm).

Sensitivity of Design Criteria to the Site Conditions

This section presents a comparison of the required barrier depths for a range of design events and different material parameters of the soil profile. This is intended to provide a basis on which to determine the accuracy required in evaluating the design parameters for a particular site. This comparison has been worked out for the section of I-37 in San Antonio.

The extreme design events possible for the San Antonio area are 100 percent depletion of soil water (i.e., the drying step No. 10), and the least demanding corresponds to a 65 percent soil water deficit (i.e., the drying step No. 6) *(5)*. The most relevant material property is the swelling coefficient. The comparisons were based on two extreme values of the swelling coefficient: one for a high swell material ($\gamma_h = 0.08$) and the other a typical swelling coefficient for a medium swelling soil ($\gamma_h = 0.04$). In both cases, the compressibility coefficient was assumed to be 20 percent larger than the corresponding swelling coefficient. The third parameter considered is related to the wettest condition that is reasonable to expect at a site. The two extremes considered are the matrix potential threshold −50 cm and the lowest limit usually accepted as the field wettest condition at a matrix potential of −1000 cm.

The effect of the change of these parameters on the required barrier depth is described in detail elsewhere *(5)*. For the longitudinal cracking criterion, the maximum difference in barrier depth for the two extreme combinations of the above parameters is only a few inches. Considering the accuracy of this simulation, it is believed that this difference is not significant. In summary, neither the design event nor the material properties have any significant bearing on the depth of the barrier required to prevent longitudinal cracking. In this case, the barrier must be placed to the depth of the root zone, independently of the design event or the properties of the subsurface soils.

The barrier depths required by the roughness criterion are always about 2 ft (61 cm) deeper than the depth required by the longitudinal cracking criterion. For the roughness criterion, the maximum difference in barrier depth for the two extreme combinations of parameters is about 1½ ft (45 cm). Although the effect is larger than for the other criterion, the effect of the design event and the material properties remains quite moderate.

In summary, the effect of the material properties and the design event on the required barrier depth seems to be very

small. The dominant factor by far is the depth of the root zone that the native vegetation will establish in the soil profile in question. As was discussed earlier, there is not enough information to determine whether the design event (or maybe the annual minimum water depth in an average year) has an effect on the root system that the plants establish in the soil. If this is so, the design event has an indirect effect on the barrier depth through the changes it might impose on the root depth or root distribution.

CONCLUSIONS AND RECOMMENDATIONS

The placement of a vertical moisture barrier enclosing the soils around an impermeable structure has as its main purpose the isolation of the subsoils from the climatic changes in the area. The barrier performs different roles depending on the initial state of the subsoil at the time of the installation. If the soil profile is at an advanced stage of desiccation, the role of the moisture barrier is to prevent the access of free water to the shrinkage crack fabric. If the subsoil is initially very wet, the role of the moisture barrier is to prevent excessive drying of the soil under the edges of the pavements.

From both points of view, the worst condition that governs the design is associated with the worst drought intensity that seems possible at the site. Drought severity is characterized based on the water deficit caused in the subsoil. This is evaluated by formulating the daily water balance using approximate methods to estimate the water going in and coming out of the soil as dictated by the meteorological conditions. The water that replenishes the subsoil originates from direct rainfall and runoff from the pavement. The extra supply of water because of runoff is included in the analysis by multiplying the rainfall by the RMF.

Drought severity is then related to the direct matrix potential profile. This relationship is obtained by numerical simulation of the water flow. This is assumed to conform to the extension of Darcy's law for unsaturated flow. The water extracted through the roots of the native vegetation is included in a sink term in the flow equation.

The analyses of the maximum crack depth of the maximum shrinkage that occurs at the edge of the pavement are found from the change of matrix potential from field capacity to the driest potential profile imposed by the design event. The shrinkage at any depth is found by accumulating all linear strains that occur below it. To find the depth of the crack, the strains imposed are modified to account for the presence of multiple cracks.

The displacement imposed at several depths within the root zone causes the propagation of the crack beyond it. Because this propagation takes place within a soil mass in which matrix potential changes are small, the soil behavior is assumed to be linearly elastic with moduli corresponding to a nearly saturated soil. The crack extension is determined with finite elements by imposing the set of displacements at each node of the root zone. The crack tip is chosen as the first node that is in compression when all the nodes above have two displacement freedoms.

A sensitivity analysis of the design parameters indicates that the edge shrinkage criterion is quite insensitive to any of the variables, whether the design event or the soil properties. The conclusion is that when a barrier is used to prevent excessive drying under the edge of the pavement, the barrier should reach the root depth. The barrier required by the roughness criterion is more affected by the variables considered. Nevertheless, the most extreme combinations of variables resulted in a 15 percent change in barrier depth. The barrier depth required by this criterion is about 25 percent larger than the root depth.

The parameter that is believed to have the most effect on the barrier depth is the rooting depth of the vegetation. A conservative rooting depth is 8 ft (240 cm). One potentially important aspect is the effect that the extra availability of water might have on the root system developed by the roadside vegetation. To determine the influence of this factor on the rooting depth, more research would be needed to clarify the rooting habits of native vegetation at roadsides, and how they are influenced by the runoff from the pavement.

It appears likely that this information could be developed with field studies that include the determination of root distribution in soil profiles taken from roadsides. The sites to study should be selected in several climatic regions and should also include several pavement widths. The need for more research in other aspects is contingent upon the results of the recommended research on root depth and root distribution. In this sense, if the native grasses develop root depths of about 8 ft (240 cm) under all circumstances, further research in other aspects is not warranted. However, if the root system established by the vegetation is dependent on the water availability, the influence of the design water depths will no longer be negligible and a better definition of the design event can result in significant savings in barrier depth.

REFERENCES

1. M. L. Steinberg. Deep Vertical Fabric Moisture Seals. *Proc., Fourth International Conference on Expansive Soils*, Denver, Colo., ASCE, pp. 383–400, 1980.
2. R. L. Lytton, R. L. Boggess, and J. W. Spotts. Characteristics of Expansive Clay Roughness of Pavements. In *Transportation Research Record 568*, TRB, National Research Council, Washington, D.C., 1976, pp. 9–23.
3. M. Dagg and K. Russam. The Relations Between Soil Shrinkage and the Development of Surface Cracks in an Experimental Road in Kenya. *African Soils 13*, 1968, pp. 5–25.
4. M. Picornell, R. L. Lytton, and M. Steinberg. Matrix Suction Instrumentation of a Vertical Moisture Barrier. In *Transportation Research Record 945*, TRB, National Research Council, Washington, D.C., 1983, pp. 16–21.
5. M. Picornell. *The Development of Design Criteria to Select the Depths of a Vertical Moisture Barrier.* Ph.D. dissertation, Texas A&M University, College Station, Dec. 1985.
6. J. L. Ritchie and J. E. Adams. Field Measurements of Evaporation from Soil Shrinkage Cracks. *Proc., Soil Science Society of America*, Madison, Wis., Vol. 38, 1974, pp. 131–134.
7. C. M. A. de Bruijin. Moisture Redistribution in Southern African Soils. *Proc., Eighth International Conference on Soil Mechanics*, Moscow, USSR, Vol. 2, 1973, pp. 37–44.
8. J. T. Ritchie, E. Burnett, and R. C. Henderson. Dryland Evaporative Flux in a Subhumid Climate: Soil Water Influence. *Agronomy Journal*, Vol. 64, March–April 1972, pp. 168–173.
9. B. G. Richards. Moisture Flow and Equilbria in Unsaturated Soils for Shallow Foundations. *Permeability and Capillarity of Soils*, ASTM STP 417, American Society for Testing and Materials, 1967, pp. 4–34.
10. A. A. B. Williams and J. T. Pidgeon. Evapo-Transpiration and Heaving Clays in South Africa. *Geotechnique*, Vol. 23, No. 2, 1983, pp. 141–150.

11. I. Ravina. The Influence of Vegetation on Moisture and Volume Changes. *Geotechnique,* Vol. XXXIII, No. 2, 1983, pp. 151–157.
12. J. E. Adams and R. J. Hanks. Evaporation From Soil Shrinkage Cracks. *Proc., Soil Science Society of America,* Madison, Wis., Vol. 28, 1964, pp. 281–284.
13. J. R. Johnson and H. O. Hill. A Study of the Shrinking and Swelling Properties of Rendzina Soils. *Proc., Soil Science Society of America,* Madison, Wis., Vol. 9, 1944, pp. 24–29.
14. L. A. Richards. Capillary Conduction of Liquids Through Porous Systems. *Physics 1,* 1931, pp. 318–333.
15. F. J. Molz, I. Remson, A. A. Fungaroli, and R. L. Drake. Soil Moisture Availability for Transpiration. *Water Resources Research,* Vol. 4, No. 6, 1968, pp. 1161–1169.
16. M. N. Nimah and R. J. Hanks. Model for Estimating Soil Water, Plant, and Atmospheric Interrelations: I. Description and Sensitivity. *Proc., Soil Science Society of America,* Madison, Wis., Vol. 37, 1973, pp. 522–527.
17. M. N. Nimah and R. J. Hanks. Model for Estimating Soil Water, Plant, and Atmospheric Interrelations: II. Field Test of Model. *Proc., Soil Science Society of America,* Madison, Wis., Vol. 37, 1973, pp. 528–532.
18. A. S. Laird. *A Study of the Root Systems of Some Important Sod Forming Grasses.* Florida Agricultural Experiment Station, Bulletin 211, 1930.
19. R. Driscoll. The Influence of Vegetation on the Swelling and Shrinking of Clay Soils in Britain. *Geotechnique,* Vol. 33, No. 2, 1983, pp. 93–105.
20. J. E. Weaver and R. W. Darland. Soil-Root Relationships of Certain Native Grasses in Various Soil Types. Ecology Monographs 19, 1949, pp. 303–338.
21. F. J. Molz and I. Remson. Extraction Term Models of Soil Moisture Use by Transpiring Plants. *Water Resources Research,* Vol. 6, No. 5, 1970, pp. 1346–1356.
22. J. L. Nieber. Simulation of Infiltration Into Cracked Soils. Presented at the 1981 Summer Meeting American Society of Agricultural Engineers, Orlando, Fla., June 21–24, 1981.
23. R. L. Lytton. The Characterization of Expansive Soils in Engineering. Presentation at the Symposium on Water Movements and Equilibria in Swelling Soils, American Geophysical Union, San Francisco, Calif., 1977.
24. M. Picornell and R. L. Lytton. Modeling the Heave of a Heavily Loaded Foundation. *Proc., Fifth International Conference on Expansive Soils,* Adelaide, Australia, 1984.
25. R. G. McKeen. Field Studies of Airport Pavements on Expansive Clays. *Proc., Fourth International Conference on Expansive Soils,* Denver Colo., ASCE, Vol. 1, 1980, pp. 242–261.
26. A. Z. El Abedine and G. H. Robinson. A Study on Cracking in Some Vertisols of the Sudan. *Geoderma 5,* 1971, pp. 229–241.
27. S. A. Taylor and G. L. Ashcroft. *Physical Edaphology.* W. H. Freeman & Co., San Francisco, Calif., 1972, pp. 355–356.
28. N. Janbu. Soil Compressibility as Determined by Odometer and Triaxial Tests. *Proc., European Conference on Soil Mechanics and Foundation Engineering,* Wiesbaden, Federal Republic of Germany, Vol. 1, 1963, pp. 19–25.
29. J. M. Duncan, P. Bryne, K. S. Wong, and P. Mabry. *Strength, Stress-Strain, and Bulk Modulus Parameters for Finite Element Analyses of Stresses and Movements in Soil Masses.* Report UBC/GT/80-01, University of California, Berkeley, Aug. 1980.
30. M. Picornell, R. L. Lytton, and M. L. Steinberg. Assessment of the Effectiveness of a Vertical Moisture Barrier. *Proc., Fifth International Conference on Expansive Soils,* Adelaide, South Australia, May 1984.

Publication of this paper sponsored by Committee on Environmental Factors Except Frost.

Coefficient of Subgrade Reaction for Footings on Desert Sands

NABIL F. ISMAEL

The selection of the coefficient of subgrade reaction *K* for the design of rafts, beams, and rigid pavements is not satisfactory because of the wide range of values recommended in the literature for each soil type and density. The results of recently conducted field footing tests at seven sites in Kuwait are analyzed for the purpose of relating the vertical subgrade coefficient *K* to the standard penetration test values for desert sands. The footings were square plain concrete, cast directly on the ground surface and ranged in size from 0.25 m to 1 m. Several variables were investigated including footing size, soil properties, footing depth, and material. A simple relationship was found between *K* and the standard penetration test values that takes into account the effect of the footing size or the width of the loaded area. Test results are compared with other plate load tests on granular soils in different areas around the world, to establish confidence in the derived correlation and to explain the causes of variation in different granular deposits.

Continuous beams, raft foundations, and rigid pavements are frequently analyzed by the elementary theory of beams on elastic foundations *(1)*. This theory is based on the Winkler's hypothesis that the contact pressure, q, at any point is proportional to the deflection, S, at the same point. The constant of proportionality, K, is called the coefficient of subgrade reaction. This coefficient is not actually constant but depends on the type of soil, the stress level, and the shape, dimensions, and rigidity of the footing. Theoretical investigations *(2)* indicate, however, that with proper selection of the values of the coefficient of subgrade reaction, reasonable accuracy may be expected with the use of the Winkler model.

For design purposes, the choice falls between this approach, followed by relatively simple computations, or the assessment of more fundamental material properties such as the soil modulus E and Poisson's ratio υ, accompanied by finite element calculations applied to the continuum representation of the problem *(3)*. Because of the cost of the latter approach and its present unsuitability for design processes, many design engineers choose the former method, with, however, an increasing use of computers to perform the detailed calculations.

Since the comprehensive work undertaken by Terzaghi *(4)*, little has been done to determine the coefficient of vertical subgrade reaction on a rational basis. The range of vlues recommended by Terzaghi for a square plate 0.3 m * 0.3 m (1 ft * 1 ft) resting on dry or moist sand are 6–18 MN/m^3 (20–60 ton/ft^3 for loose sand, 18-90 MN/m^3 (60–300 ton/ft^3) for medium sand, and 90–300 MN/m^3 (300–1,000 ton/ft^3 for dense sand. Terzaghi further proposed using values of 12, 39, and 150 MN/m^3 (40, 130, and 500 ton/ft^3) for loose, medium, and dense sand, respectively, with the corresponding reduced values of 7.5, 24, and 90 MN/m^3 (25, 80, and 300 ton/ft^3) for submerged sand. Scott *(3)* found that these values could be obtained from the relationship $K = 4\ N$ ton/ft^3, where N is the standard penetration test (SPT) value, and recommended that they be increased by 50 percent since the Terzaghi values based on bearing plate data are conservative.

Bazaraa and Howeedy *(1)* analyzed the results of 83 plate load tests on dry, medium-to-fine compacted sand fill at Brownville, Nebraska, and correlated the coefficient of subgrade reaction with the corresponding values of the relative density, D_r, determined for the sand at both sides of the plate. The same workers analyzed the results of 60 plate load tests at different sites in the United States, the United Kingdom, Australia, Czechoslovakia, Jamaica, and Hong Kong, where granular deposits were encountered. The value of the coefficient of subgrade reaction for these tests was correlated with SPT N values for each deposit. This was the first attempt to provide a simple and rational method for the selection of the coefficient of subgrade reaction.

Analyzed in this paper are the results of a recent field footing testing program carried out by Allison *(5)* at seven sites in Kuwait. The aim is to establish a simple correlation between the coefficient of vertical subgrade reaction and the SPT N values for foundations on calcareous desert sand. This is to provide accurate values for easy and convenient use by design engineers. Several variables are investigated herein including the effect of footing size, footing depth, and material. The results are compared with the preceding work *(1)* on different granular deposits around the world.

TESTING PROGRAM

The program carried out by Allison *(5)* included four series of tests conducted to establish the following: I, effect of footing size; II, effect of footing depth; III, influence of footing material; and IV, effect of soil properties.

Test series I–III were conducted at one site called KISR. Series IV was performed at the same site and at six others. Figure 1 shows the locations of test sites in Kuwait, which is situated at the tip of the Persian Gulf. SPTs were performed at each site and soil samples were taken for identification and analysis. An evaluation of the soil properties was made in the same locality.

Kuwait University, P.O. Box 5969, Safat 13060, Kuwait.

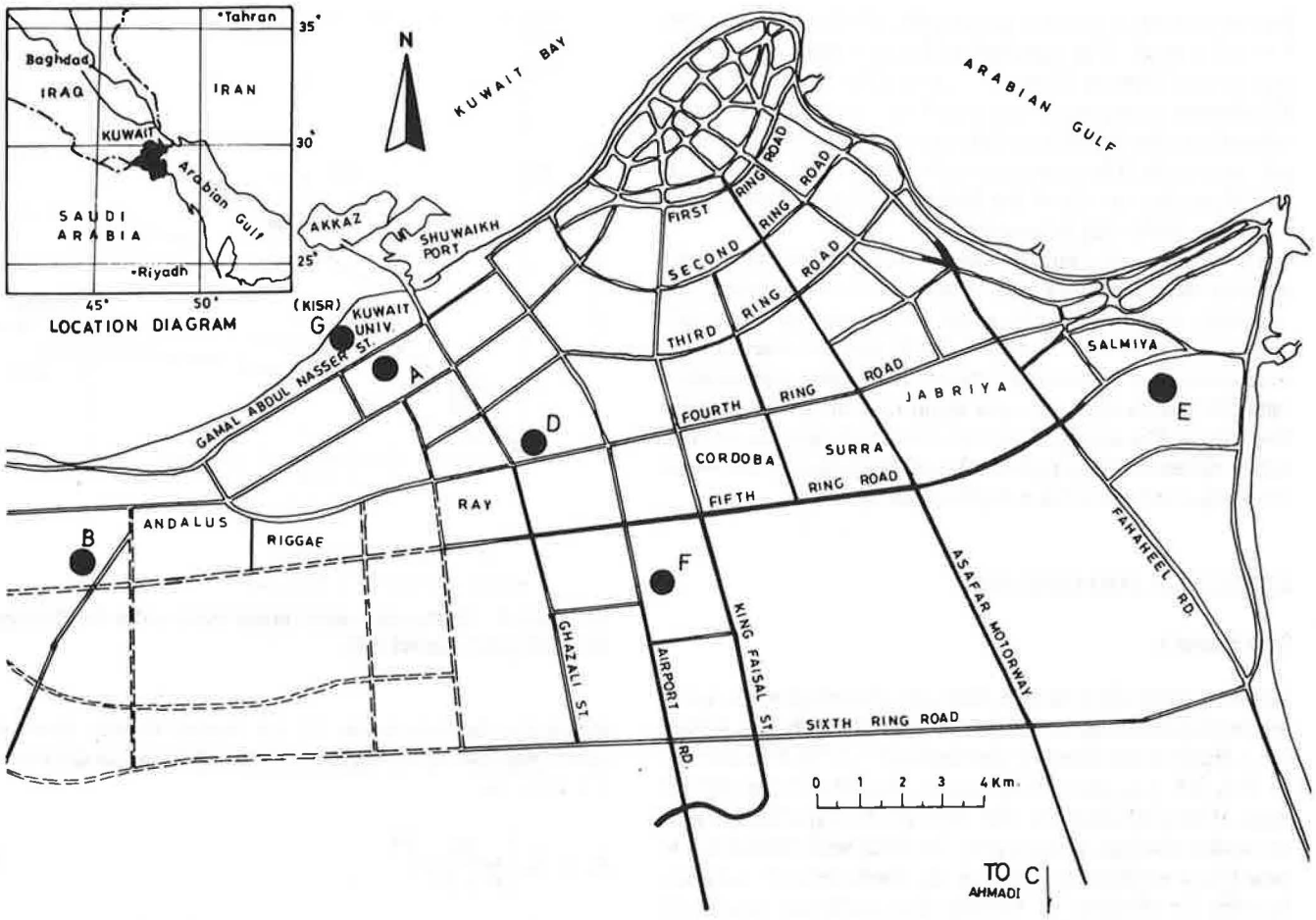

FIGURE 1 Location plan showing test sites.

The tests were carried out using a loaded tank transporter to provide 445 kN (50 ton) of load. The test procedure was in accordance with ASTM standard D1194-72. Loads were applied to each footing in cumulative equal increments of 45 kN (5 ton) using a 445-kN (50-ton) hydraulic jack acting through a series of machined steel plates of gradually increasing diameter. This is to spread the load evenly onto the footings, which were of concrete cast directly on the ground surface. Each load increment was maintained for a time interval of not less than 15 min and until the vertical movement had ceased. The loads were not cycled during the tests.

Settlement measurements were made using mechanical dial gauges bearing on a plate fixed to the base of the jack. Failure was not reached in any of the tests because the ultimate bearing capacity was not investigated herein; however, tests were carried out beyond the permissible settlement of footings under load.

SOIL CONDITIONS

Borings at the test sites revealed similar soil stratification. The soil profile consists of an upper surface layer of compact, relatively dry, fine-to-medium nonplastic, cohesionless, windblown sand with little silt. This is underlain by a more competent marine-deposited, slightly plastic, dense-to-very-dense, lightly-to-moderately cemented calcareous silty sand known locally as gatch. The upper layer, in which all the tests were carried out, extends well below the significant zone under the footings, and is classified as poorly graded sands, *SP*, or well-graded sands, *SW*, according to the Unified Soil Classification System. The limits of the grain size distribution curves for 20 selected samples from this layer, at a depth of 0–3 m (10 ft) taken from the test sites, are shown in Figure 2. They indicate

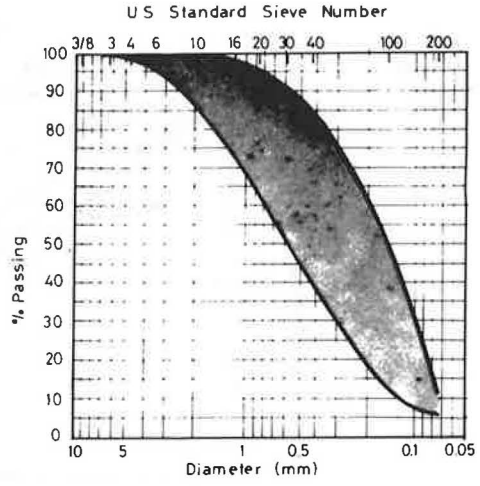

FIGURE 2 Limits of the grading curves for the upper layer [after Ismael *(7)*].

that the percentage of fines passing No. 200 sieve ranges from 5 to 12 percent. The standard penetration resistance in this layer ranges between 10 and 35 blows/0.3 m and these generally increase in magnitude with depth *(6)*. Chemical analysis on selected samples *(6)* indicated that quartz constitutes the principal component. The amount of carbonates varies between 10 and 20 percent, mostly in the form of calcite (calcium carbonate), thus indicating calcareous soils.

The lower layer contains between 5 and 35 percent of silt and clay and extends to a great depth over limestone bedrock. It is usually classified as silty sands, *SM*, or clayey sands, *SC*.

Soil conditions at the first site, KISR, where test series I–III were conducted, indicated a compact well-graded cohesionless sand (*SW*), with little silt, to a depth of 4 m (13 ft) over the lower layer. The average SPT value within the significant zone below the test footings (0.5–2 m) is 20 blows/0.3 m. The water level was encountered at a depth of 2.8 m (9.2 ft).

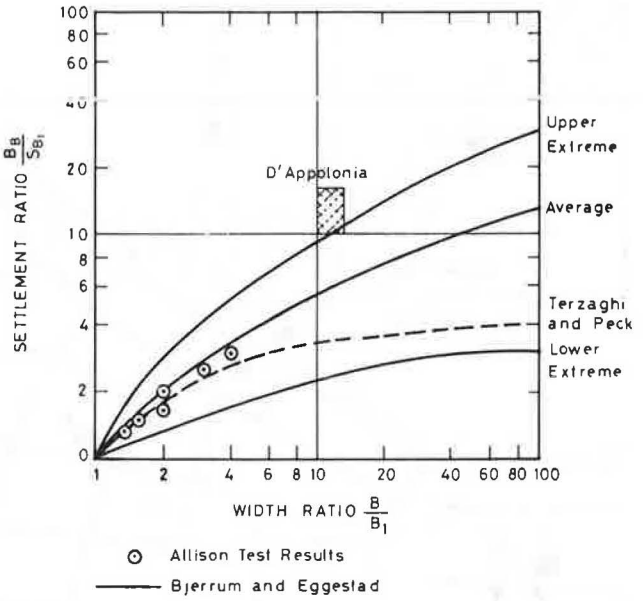

FIGURE 4 Settlement ratio versus width ratio for footings on sand [after Ismael *(7)*].

EFFECT OF FOOTING SIZE

Test Series I

To establish the effect of size, three sets of footings were cast in prepared excavations at a depth of 1 m (3.3 ft) below ground level. Each set consisted of four footings: 1, 0.75, 0.5, and 0.25 m (3.3, 2.5, 1.6, and 0.8 ft) square, located in three parallel lines, 10 m (32.8 ft) apart, with 10 m (32.8 ft) spacing between successive footings in each row. The tests were carried out to establish a relationship between the coefficients of subgrade reaction for footings of varying size under the same load intensity. If this is done, further work can be carried out more easily using footings of one size and the results related to larger-size footings.

The test results of this series are shown in Figure 3 in the form of pressure-settlement curves. Each curve represents the average results from three tests. From these curves the settlements corresponding to several load intensities were obtained for all footing sizes. A comparison was made between the average measured and predicted values of the settlement ratio, S_B/S_{B_1} for the different width ratios B/B_1. Figure 4 shows that the data points *(7)* are located slightly above the curve proposed by Terzaghi and Peck *(8)* based on the following formula:

$$S_B = S_1 \left(\frac{2B}{B + 0.3} \right)^2 \quad (1)$$

where S_B is the settlement of a footing of width B m, and S_1 is the settlement of a 0.3-m (1-ft) square plate loaded to the same intensity. The 0.3 in the denominator becomes 1 when B is expressed in feet.

The validity of this relationship was investigated by Bjerrum and Eggestad *(9)*. Their study of case records indicated that the increase in settlement with the dimension of the loaded area could not be represented by a single curve, and they defined an upper- and a lower-limit curve, and a curve giving an average correlation. Shown in Figure 4 are these curves and the results

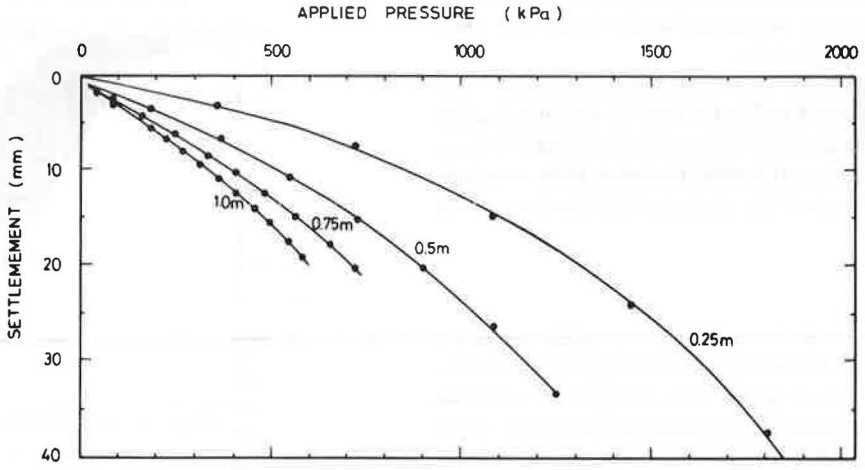

FIGURE 3 Load-settlement diagrams of footings of various size [after Allison *(5)*; depth = 1 m].

of D'Appolonia et al. *(10)*, who have reported an appreciable scatter.

The foregoing results, showing excellent correlation with the Terzaghi and Peck relationship *(8)* for desert sands, are not surprising. Parry *(11)* has proved the dependence of the settlement ratios on soil conditions by assuming four soil conditions and calculating the settlement ratios on the basis of a direct relationship between measured SPT N values and elastic modulus E. The results indicated that for soils showing improved relative density with depth, as in the case here, the calculated settlement ratios were in close agreement with Equation 1.

Because

$$K_B = \frac{q}{S_B},\ K_1 = \frac{q}{S_1}$$

therefore

$$\frac{K_B}{K_1} = \frac{S_1}{S_B} = \left(\frac{B + 0.3}{2B}\right)^2$$

therefore

$$K_B = K_1\left(\frac{B + 0.3}{2B}\right)^2 \tag{2}$$

where K_B and K_1 are the coefficient of subgrade reaction for square footings of width B m and 0.3 m (1 ft), respectively. The 0.3 in the numerator becomes 1 when B is expressed in feet.

The implication of Equation 2, which was proposed by Terzaghi *(4)*, is that the coefficient K_B for a footing of any size decreases, with increasing width to a minimum value of 25 percent, the coefficient K_1 for a 0.3-m (1-ft) square plate. The present tests confirmed the validity of this relationship for desert sands. The analysis by Parry *(11)*, however, indicated that this relationship cannot be used for all soil conditions, particularly those with constant N with depth, implying a decreasing relative density with depth.

Upon completion of the above tests, it was decided to carry out further testing at the other sites using 0.5-m (1.6-ft) square footings and to employ Equation 2 to calculate K_B of larger-size footings.

COEFFICIENT OF SUBGRADE REACTION

Test Series I and IV

After the effect of size was established, a series of tests was conducted at six other sites *(5)*, whose locations are shown in Figure 1. Three footings were cast on each site, each 0.5 m (1.6 ft) square at a depth of 1.0 m (3.3 ft). The results were compared with standard penetration tests carried out adjacent to the foundation pits. The results of the loading tests are shown in Figure 5. Results of other laboratory and in situ soil tests performed in connection with these experiments are listed in Table 1.

From the pressure-settlement diagrams of Figure 5, the coefficient of subgrade reaction was obtained. Because the curves are nonlinear, coordinates must be chosen arbitrarily. In the

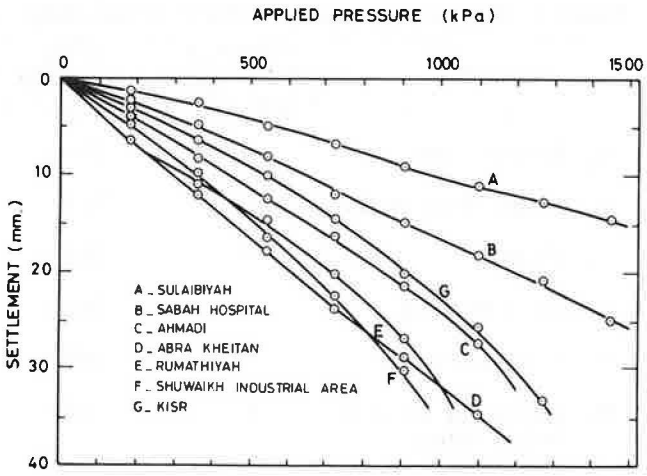

FIGURE 5 Load-settlement diagrams of 0.5-m footings at seven selected sites [after Allison *(5)*; depth = 1 m].

present study the coefficient corresponding to an applied pressure of 300 kPa (3 ton/ft^2) was employed in a similar way to the analysis made by Bazaraa and Howeedy *(1)*. The U.S. Corps of Engineers has used the deformation corresponding to 70 kPa (10 psi) for evaluation of subgrades for airfields *(12)*. A comparison made between the two methods with respect to present test results revealed that the difference in the magnitude of K did not exceed on average 5 percent.

The relationship between the coefficient of subgrade reaction and the measured SPT N value below the footing is plotted in Figure 6. As shown, test results on the 0.5-m (1.6-ft) footings are represented by the linear relationship

$$\begin{aligned} K_{0.5m} &= 2.7\,N \quad \text{MN/m}^3 \\ &= 9\,N \quad \text{ton/ft}^3 \end{aligned} \tag{3}$$

Extrapolating the results to those of a 0.3-m (1-ft) square plate by employing Equation 2,

therefore

$$\begin{aligned} K_1 &= 4.2\,N \quad \text{MN/m}^3 \\ &= 14\,N \quad \text{ton/ft}^3 \end{aligned} \tag{4}$$

For a square footing of width B m, the coefficient of subgrade reaction will be given by

$$K_B = 4.2\,N\left(\frac{B + 0.3}{2B}\right)^2 \quad \text{MN/m}^3$$

or

$$K_B = 14\,N\left(\frac{B + 0.3}{2B}\right)^2 \quad \text{ton/ft}^3 \tag{5}$$

For rectangular foundations having dimensions of $B*L$, Terzaghi *(4)* and Vesic *(2)* proposed correcting K_B for length to width effects *(13)*, thus:

$$K_{B*L} = K_B\left(\frac{1 + 0.5\frac{B}{L}}{1.5}\right) \tag{6}$$

TABLE 1 SOIL PROPERTIES ON EACH OF SEVEN LOAD TEST SITES [after Allison *(5)*]

Location	Average N Value (blows/0.3m)	Bulk Density (kg/m^3)	Moisture Content %	Water Table Level (m)	Grading of Sand
A. Sulaibiyah	30	1710	1.5	-	Medium, well graded
B. Sabah Hospital	25	1630	2.6	10.0	Medium, well graded
C. Ahmadi	15	1480	3.5	-	Coarse, well graded
D. Abra Kheitan	12	1520	2.4	-	Fine, poorly graded
E. Rumaithiyah	10	1630	4.9	2.6	Fine, poorly graded
F. Shuwaikh Industrial Area	10	1495	6.3	2.0	Silty, fine
G. KISR	20	1625	3.0	2.8	Medium, well graded

Values for the zone 0.5-2.0 meters below ground level

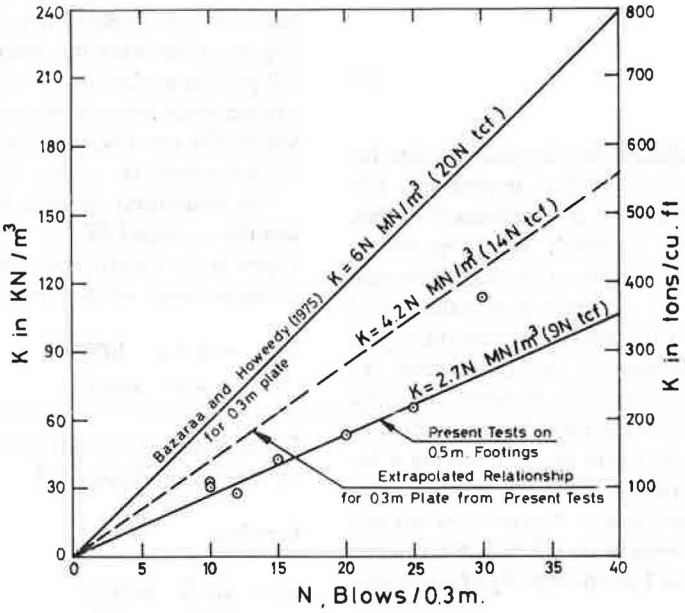

FIGURE 6 Relationship between standard penetration *N* values and the coefficient of subgrade reaction for desert sands.

The preceding equation indicates that the value of K of a very long foundation with a width B is approximately equal to 0.67 K_B.

Because it is much easier and less expensive to perform a standard penetration test than to perform a standard plate load test, a correlation such as that given by Equations 4 and 5 can be useful to the practicing design engineers who pick up values recommended in textbooks *(14)* for various soil conditions. Such values are not accurate, and vary over a wide range for each soil type. Bazaraa and Howeedy *(1)* analyzed the results of 60 plate load tests at different sites in the United States, the United Kingdom, Australia, Czechoslovakia, Jamaica, and Hong Kong, together with the corresponding N values. The soils at these sites are different and include clayey silty sand, fine-to-coarse sand, sandy gravel, gravel, and decomposed granite. Figure 7, reproduced from Bazaraa and Howeedy *(1)*, gives the relationship between the standard penetration N-value and the coefficient of subgrade reaction, K. There is considerable scatter in this relationship as may be expected in view of the different soil conditions. However, about 90 percent of the data fall within the range $K = 2.25\,N$–$15\,N$ MN/m^3 ($7.5\,N$–$50\,N$ ton/ft^3). Based on a statistical analysis of the data Bazaraa and Howeedy *(1)* suggested, the following relationship between K and N for a 0.3-m (1-ft) square plate is shown:

$$K_1 = 6\,N \quad MN/m^3$$
$$= 20\,N \quad ton/ft^3 \qquad (7)$$

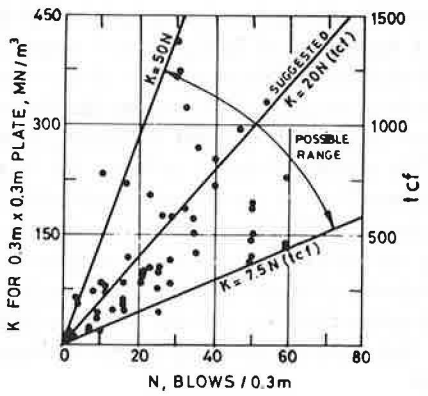

FIGURE 7 Relationship between standard penetration N values and coefficient of subgrade reaction for standard plate load tests on dry cohesionless soils at various sites [after Bazaraa and Howeedy *(1)*].

The values for K_1 given by Equation 7 are superimposed on Figure 6 along with present test results on desert sands. The values measured herein are nearly 70 percent of those based on Equation 7. However, they are within the range of values found *(1)* for granular soils as shown in Figure 7. This wide range of values is attributed to the different compressibilities of the soils tested that possess different classifications.

The results of the present tests and those reported by Bazaraa and Howeedy *(1)* indicate much higher values than those recommended by Terzaghi *(4)*, which were based on some limited bearing-plate data. In examining the Terzaghi values, Scott *(3)* observed that they can be given roughly by $K_1 = 1.2\,N$ MN/m^3 ($4\,N$ ton/ft^3) and recommended increasing them by 50 percent, thus

$$K_1 = 1.8\,N \quad \text{MN/m}^3$$
$$= 6\,N \quad \text{ton/ft}^3 \tag{8}$$

In examining the above recommendations relative to present test results (Equation 4), it is evident that they are very conservative in underestimating the coefficient of subgrade reaction by 2 to 3.5 times. They are even more conservative with respect to the recently reported field data (Equation 7) from different sites around the world *(1)*.

It should be emphasized that the standard penetration test N values employed in the analysis presented herein are the measured values with no correction applied. Recent tests and research indicated that the correction for the overburden pressure proposed by Peck et al. *(15)* is reasonable with respect to desert sands. Accordingly, for the shallow depth range employed herein, the corrected N value '$\overline{N}$' ranges from 1.44 to 1.5 N, averaging 1.47 N for the seven test sites. If the corrected N values are used, Equations 4 and 5 will be modified to

$$K_1 = 2.85\ \overline{N} \quad \text{MN/m}^3$$
$$= 9.5\ \overline{N} \tag{9}$$

$$K_B = 2.85\ \overline{N}\left(\frac{B+0.3}{2B}\right)^2 \quad \text{MN/m}^3$$

$$= 9.5\ \overline{N}\left(\frac{B+0.3}{2B}\right)^2 \quad \text{ton/ft}^3 \tag{10}$$

It is recommended that the corrected N values ($\overline{N}$) be used particularly for large footings and basement slabs. The N value used in the selection of the coefficient of subgrade reaction should be the average value within the significant zone of depth B below the footing. If the water level occurs and will remain at or below a depth $D_f + B$ beneath the ground surface where D_f is the depth of footing, no correction for water table may be applied. However, if the water table rises to a depth D_w measured from ground surface, a correction for the coefficient K_B calculated from Equation 5 or Equation 10 should be applied. The reduction factor proposed by Peck et al. *(15)* for the allowable solid pressure is recommended herein, thus

$$C_w = 0.5 + 0.5\,\frac{D_w}{D_f + B} \tag{11}$$

Another simple correlation reported *(1)* is the one between the coefficient of subgrade reaction and that of relative density. From an analysis of the results of 83 standard plate load tests on sand fill at Brownville, Nebraska, where the relative density, D_r, was determined at both sides of the plate, it was found that K_1 is exponentially related to the relative density D_r. Two curves are drawn to define a range that includes about 80 percent of the available field data. These curves, reproduced in Figure 8 *(1)*, are given approximately by the equations

$$K_1 = 300\,D_r^{1.7} \ \text{MN/m}^3 \ (1{,}000\,D_r^{1.7} \ \text{ton/ft}^3)$$

or

$$K_1 = 600\,D_r^{1.7} \ \text{MN/m}^3 \ (2{,}000\,D_r^{1.7} \ \text{ton/ft}^3) \tag{12}$$

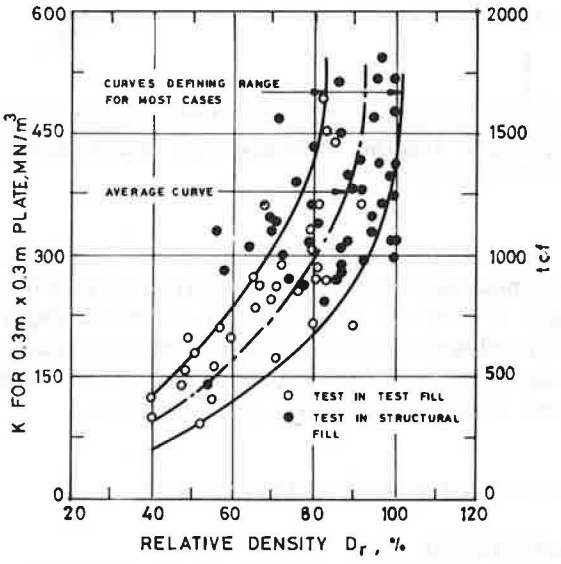

FIGURE 8 Relationship between relative density and coefficient of subgrade reaction for 0.3 m * 0.3 m standard plate load tests at Brownville, Nebraska [after Bazaraa and Howeedy *(1)*].

A reasonable average relationship *(1)* between K_1 and D_r is given approximately by

$$K_1 = 450\ D_r^{1.7}\ \text{MN/m}^3$$
$$= 1{,}500\ D_r^{1.7}\ \text{ton/ft}^3 \quad (13)$$

Although measurements of the relative density were not made at the sites of the present tests, the above correlation was mentioned because of its relevance and the similarity of the soil conditions. The soil conditions at the Brownville site consist of light brown, poorly graded medium-to-fine sand with a uniformity coefficient of close to 2 and a percentage passing No. 200 sieve of less than 10 percent.

INFLUENCE OF FOOTING DEPTH AND MATERIAL

Test series II was carried out to determine the influence of depth of shallow footings on the coefficient of subgrade reaction. For this purpose 24 footings were constructed at the first site, KISR; 12 of these of 1 m (3.3 ft) square, the remainder 0.5 m (1.6 ft) square. Three of each size were placed at depths of 0.5, 1, 1.5, and 2 m (1.6, 3.3, 4.9, and 6.5 ft). The footings were loaded in the same way as before and the results are shown in Figure 9.

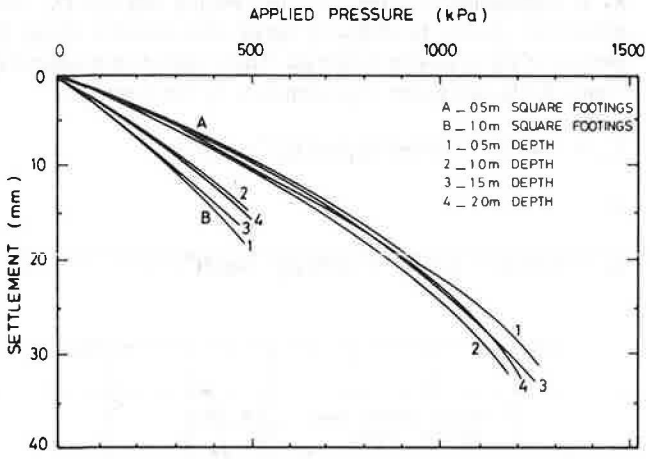

FIGURE 9 Influence of footing depth on settlement under load [after Allison *(5)*].

Unlike the previous tests showing the effect of size and soil properties, these tests show little difference between the coefficients of subgrade reaction within the shallow depth range employed herein. It is likely, however, that deeper footings will have a larger coefficient of subgrade reaction and an increased factor of safety against bearing capacity failure.

EFFECT OF FOOTING MATERIAL

Test Series III

Many loading tests are performed by applying the load to a steel plate instead of a concrete slab. To find out the difference between the coefficient of subgrade reaction as determined by the two methods, the load-settlement behavior of the three 0.5-m (1.6-ft) footings used in the second series of tests was compared with that of three steel plates of the same size placed on soil at the same depth. The concrete footings and the steel plates were rigid, with uniform settlement recorded during loading. The results are shown in Figure 10. Analysis of this data indicates that the coefficient of subgrade reaction for concrete footing is 20 percent larger than that for a steel plate. This may be attributed to the fact that there is clearly less friction between sand and smooth steel than there is between sand and rough concrete, and the loss of confinement may therefore be significant, resulting in more settlement under the steel plate.

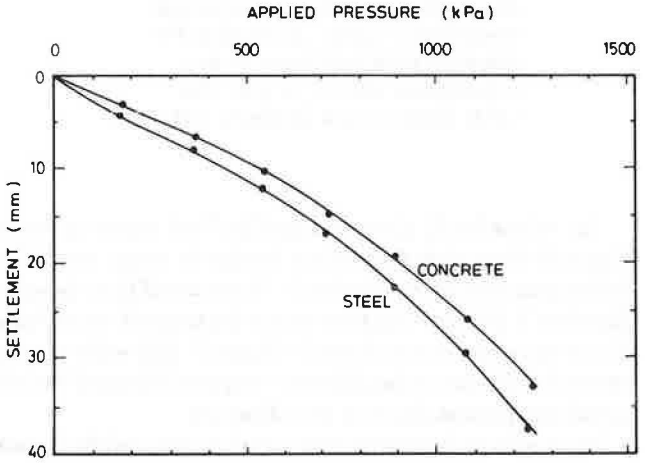

FIGURE 10 Comparison of settlement of concrete and steel footings under load [after Allison *(5)*].

CONCLUSIONS

The results of recent field loading tests on shallow square footings at seven sites in Kuwait were analyzed to establish a simple correlation for the determination of the coefficient of subgrade reaction. Several variables were investigated, including the effect of footing size, footing material, overburden pressure, and soil properties. Based on test results, the following conclusions have been reached:

1. The footing size greatly influences the coefficient of subgrade reaction. Test results on 1-, 0.75-, 0.5-, and 0.25-m (3.3-, 2.4-, 1.6-, and 0.8-ft) concrete footings indicated close agreement with the Terzaghi formula *(2)*.
2. The effect of footing depth in the shallow range up to 2 m (6.5 ft) on the coefficient of subgrade reaction is insignificant.
3. For the same depth and soil conditions, the coefficient of subgrade reaction for concrete footings is approximately 20 percent greater than that of a similarly rigid steel plate. This is due to a larger friction and a closer contact with soil for the concrete footings.
4. From test results, a simple correlation was established between the coefficient of subgrade reaction and the SPT (Equations 5 and 10) for desert sands. The coefficient of subgrade reaction obtained from this relationship is nearly three times larger than the recommended Terzaghi values.

5. The simple correlation developed herein for desert sands falls within the range found by Bazaraa and Howeedy *(1)* from analysis of standard plate test data on granular soils in different areas around the world.

ACKNOWLEDGMENT

The author is grateful to T. R. Allison, formerly with the Kuwait Institute for Scientific Research, for providing the field test data employed in the paper.

REFERENCES

1. A. R. Bazaraa and M. F. Howeedy. Coefficient of Subgrade Reaction for Footings on Cohesionless Soils. *Proc., Sixth Regional Conference for Africa on Soil Mechanics and Foundation Engineering*, Durban, South Africa; A. A. Balkema, Vol. V, Sept. 1975, pp. 51–55.
2. A. S. Vesic. Bending of Beams Resting on Isotropic Elastic Solid. *Journal of the Engineering Mechanics Division*, ASCE, Vol. 87, No. EM2, April 1961, pp. 35–53.
3. R. F. Scott. *Foundation Analysis*. Prentice-Hall, Inc., Englewood Cliffs, N.J., 1981.
4. K. Terzaghi. Evaluation of Coefficients of Subgrade Reaction. *Geotechnique*, London, England, Vol. 5, No. 4, 1955, pp. 297–326.
5. T. R. Allison. *Upgrading of Buildings*. Final Report, Project No. BM-8, Kuwait Institute for Scientific Research, Safat, Kuwait, 1981, pp. 47–73.
6. N. F. Ismael, A. Jeragh, M. Mollah, and O. Khalidi. A Study of the Properties of Surface Soils in Kuwait. *Journal of Southeast Asian Geotechnical Society*. Bangkok, Thailand, Vol. 17, No. 1, 1986, pp. 67–87.
7. N. F. Ismael. Allowable Pressure from Loading Tests on Kuwaiti Soils. *Canadian Geotechnical Journal*. Vol. 22, No. 2, 1985, pp. 151–157.
8. K. Terzaghi and R. B. Peck. *Soil Mechanics in Engineering Practice*. 2nd ed., John Wiley and Sons, New York, 1967.
9. L. Bjerrum and A. Eggestad. Interpretation of Loading Tests on Sand. *Proc., European Conference on Soil Mechanics and Foundation Engineering*. Wiesbaden, Federal Republic of Germany, Vol. 1, 1963, pp. 199–204.
10. D. J. D'Appolonia, E. D'Appolonia, and R. F. Brisette. Settlement of Spread Footings on Sand. *Journal of the Soil Mechanics and Foundations Division*, ASCE, SM3, 1968, pp. 735–760.
11. R. H. G. Parry. Estimating Foundation Settlements in Sand From Plate Bearing Tests. *Geotechnique*, Vol. 28, No. 1, 1978, pp. 107–118.
12. J. E. Bowles. *Analytical and Computer Methods in Foundation Engineering*. McGraw-Hill Book Co., New York, 1974, pp. 54–62.
13. B. M. Das. *Principles of Foundation Engineering*. Prindle, Weber & Schmidt 'PWS' Publishers, Boston, Mass., 1984.
14. J. E. Bowles. *Foundation Analysis and Design*. 2nd ed., McGraw-Hill Book Co., New York, 1977.
15. R. B. Peck, W. E. Hanson, and T. H. Thornburn. *Foundation Engineering*. 2nd ed., John Wiley and Sons, New York, 1977.

Publication of this paper sponsored by Committee on Soil and Rock Properties.